博士論文

ヒッグスセクターの構造に関する理論的研究

Theoretical Studies on the Structure of the Higgs sector

平成28年3月

富山大学大学院理工学教育部新エネルギー科学専攻
理論物理学研究室

菊地 真吏子

博士論文

Theoretical Studies on the Structure of the Higgs sector

Mariko Kikuchi

Department of Physics, University of Toyama,
3190 Gofuku, Toyama 930-8555, Japan

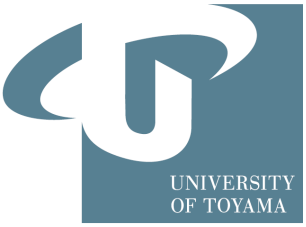

菊地 真吏子

富山大学大学院理工学教育部新エネルギー科学専攻
理論物理学研究室

2016年3月

To my parents.

ACKNOWLEDGMENTS

I would like to really express my heartfelt appreciation to my supervisor, Prof. Shinya Kanemura for courteously guiding me various things beyond the research for five years. I am very grateful to Dr. Kei Yagyu, Dr. Hiroshi Yokoya, Prof. Mayumi Aoki, Prof. Mitsuru Kakizaki, and Mr. Toshinori Matsui for the wonderful collaborations. I am also grateful to other faculty members of the laboratory, Prof. Takeshi Kurimoto for valuable discussions. I appreciate Prof. Mihoko Nojiri, Prof. Tomohiko Kuwai and Prof. Katsunari Enomoto for carefully reading my manuscript. I would also like to thank all the members of Theoretical Physics Group, the University of Toyama, Dr. Hiroaki Sugiyama, Dr. Makoto Nakamura, Mr. Naoki Machida, Mr. Akiteru Santa, Mr. Ryo Amai, Mr. Katsuya Hashino, Mr. Syota Nakatani, Mr. Shinya Odori, Mr. Koudai Sakurai, Mr. Kouichi Ishida and Mr. Yoshiaki Ishigure. Finally, I would also like to thank the secretary of our laboratory, Mrs. Asami Takagi.

Abstract

Although the standard model (SM) was completed by the discovery of the Higgs boson at the LHC in 2012, it is not the end of particle physics. Predictions of the SM are certainly consistent with the results of the LHC data within uncertainties, but some phenomena beyond the SM have been observed by other experiments; i.e. neutrino oscillation, dark matter and baryon asymmetry of the Universe. In addition, there are some theoretical problems in the SM such as the hierarchy problem. Such a situation means that the SM must be replaced by a new theory which is a more completed form so that the above problems can be solved.

Even though the Higgs boson was discovered, the structure of the Higgs sector has not been determined yet. In fact, there remain many questions for the Higgs sector. "What is the origin of the negative mass term in the Higgs potential ?" "Which is the nature of the Higgs field: is it an elementary field or a composite field ?" "How many Higgs fields are there in the true model ?" Because no theoretical principle requires the Higgs sector to be the minimal one, there is a possibility that the true Higgs sector is extended from that of the SM. Notice that most of extended Higgs sectors have not been excluded at all by the data of the LHC.

Furthermore, we can say that the structure of the Higgs sector is strongly related to a scenario of the new physics beyond the SM, because various models based on those scenarios introduce extended Higgs sectors. Each new physics model has a characteristic Higgs sector. Namely, determining the structure of the Higgs sector by the bottom-up approach is one of the most effective procedures to establish the new physics. Therefore, in this thesis, we discuss studies to determine the structure of the Higgs sector by testing various extended Higgs sectors at future collider experiments such as the LHC and the International Linear Collider (ILC).

There are roughly two kinds of the approaches for the Higgs search. One is to directly search the second Higgs boson at the collider experiments. The other is the indirect tests through detecting deviations from the SM predictions in observables such as electroweak oblique corrections and couplings of the discovered Higgs boson. In particular, it is time to study properties of the couplings of the discovered Higgs boson as precisely as possible, Coupling measurements of the Higgs boson have just started and the measurement accuracies will be improved at the LHC Run-II and future collider experiments such as the high luminosity LHC and the ILC. In order to compare the theory predictions with future precision data of Higgs boson coupling measurements which are expected to be at $\mathcal{O}(1)$ % level, we should evaluate these couplings with higher order corrections not only in the minimal Higgs sector but also in various extended Higgs sectors.

In this thesis, we investigate how extended Higgs sectors can be distinguished and identified by comparing precise calculations of the Higgs boson couplings including one-loop corrections with precision measurements of the Higgs boson couplings at future collider experiments. In particular, we focus on four types of two Higgs doublet models (THDMs) with the soft breaking Z_2 symmetry to avoid flavour changing neutral currents, the model with an additional real Higgs field (HSM) and that with an additional complex triplet Higgs field (HTM). In non-minimal Higgs sectors, the Higgs boson coupling constants can deviate from the predictions in the SM by effects of additional scalar bosons. Patterns of the deviations in various Higgs boson couplings largely depend on the structure of extended Higgs sectors. Therefore, the patterns are useful to discriminate Higgs sectors when they are detected at future colliders. Moreover, we may able to determine the true Higgs sector by fingerprinting the predictions on the Higgs boson

couplings in each model with the future precision data. We calculate various couplings of the discovered Higgs boson at the one-loop level by on shell renormalization in those models.

In the study of the THDMs, we perform renormalization calculations in the modified on shell scheme, in which the gauge dependence in the mixing parameter is consistently avoided. We present a complete set of the analytic formulae of the renormalized couplings in four types of THDMs. It is known that different characteristic patterns of deviations in Yukawa couplings ($hf\bar{f}$) can be allowed depending on four types of THDMs. We investigate how the pattern can be modified from the prediction at the tree level by including one-loop contributions under constraints from perturbative unitarity and vacuum stability, and current experimental data. We then numerically demonstrate how the inner parameters of the model can be extracted by future precision measurements of these couplings at the high luminosity LHC and the ILC. We found that the mixing parameters can be determined more precisely by using measurement uncertainties at the ILC. Furthermore, there are possibilities to obtain the upper bound for the mass of extra Higgs bosons without their direct discoveries and also to get information of the decoupling property.

In study of the HSM, we calculate renormalized Higgs boson couplings with gauge bosons and fermions at the one-loop level by the on-shell renormalization scheme. We investigate how they can be significant under the theoretical constraints from perturbative unitarity, vacuum stability and also the condition of avoiding the wrong vacuum. Furthermore, comparing with the predictions in the Type-I THDM which is one of four types of THDMs, we numerically demonstrate how the singlet extension model can be distinguished and identified by using precision measurements of the Higgs boson couplings at future collider experiments. We found that the HSM may be able to discriminated from the Type-I THDM by comparing hZZ, $hb\bar{b}$ and $h\gamma\gamma$ couplings and corresponding measured values in most of parameter regions.

In studies of the HTM, we also calculate renormalized electroweak parameters Δr and the renormalized W mass $m_W^{\rm reno}$ by two kinds of renormalization schemes in addition to renormalized Higgs boson couplings. We numerically evaluate how the hWW, hZZ and hhh couplings deviate from those of the SM at the one-loop level under the constraints from perturbative unitarity and vacuum stability, and current experimental data. We find that one-loop contributions to these couplings are substantial as compared to their expected measurement accuracies at the ILC. Therefore the HTM has a possibility to be distinguished from the other models by comparing the pattern of deviations in the Higgs boson couplings.

Contents

1 Introduction **1**

1.1 Overview . . . 1

1.2 Standard Model . . . 2

1.3 Higgs boson searches and discovery . . . 2

1.4 Problems with the Higgs sector of the Standard Model . . . 4

1.5 Hierarchy problem of the Higgs boson mass . . . 4

1.6 Phenomena beyond the standard model . . . 5

1.6.1 Neutrino masses . . . 5

1.6.2 Dark matter . . . 5

1.6.3 Baryon asymmetry of the Universe . . . 6

1.7 Physics of extended Higgs sectors . . . 6

1.7.1 Two Higgs doublet models . . . 7

1.7.2 Supersymmetric standard models . . . 7

1.7.3 Composite Higgs models . . . 7

1.7.4 Higgs singlet model . . . 8

1.7.5 Higgs triplet model . . . 8

1.7.6 Exotic Higgs models with $\rho = 1$ at tree level . . . 8

1.8 In this thesis . . . 9

1.9 Organization . . . 9

2 Review of the Standard Model **11**

2.1 Lagrangian . . . 11

2.2 Custodial symmetry . . . 14

2.3 Electroweak rho parameter ρ . . . 14

2.4 Theoretical Constraints on the Higgs boson mass . . . 15

2.4.1 Perturbative unitarity . . . 15

2.4.2 Triviality and vacuum stability . . . 16

2.5 Decay of the Higgs boson . . . 17
2.6 Radiative corrections in the SM . . . 17
2.6.1 Renormalization in the SM . . . 17
Renormalization in gauge and Higgs sector in the SM . . . 18
Renormalization in fermion sector in the SM . . . 19
2.7 One-loop level corrected electroweak observables . . . 20
2.7.1 Renormalized electroweak parameters . . . 20
2.7.2 Renormalized Higgs couplings . . . 21
Effective potential method . . . 22

3 Review of extended Higgs sectors **25**
3.1 Review of four types of the THDMs . . . 25
3.1.1 Lagrangian of the the THDMs . . . 25
Perturbative unitarity and vacuum stability . . . 29
Decay branching rations of Higgs bosons . . . 30
3.1.2 Electroweak S, T and U parameters . . . 34
3.1.3 Constraints from current experiments . . . 35
3.2 Review of the HSM . . . 36
3.2.1 Lagrangian of the HSM . . . 36
Lagrangian . . . 36
Perturbative unitarity, vacuum stability and wrong vacuum condition . . . 38
3.2.2 Constraints from an extra Higgs boson searches . . . 39
3.2.3 Electroweak S, T and U parameters . . . 39
3.3 Review of the HTM . . . 40
3.3.1 Lagrangian of the HTM . . . 40
3.3.2 Perturbative unitarity and vacuum stability . . . 43
3.3.3 Constraints from collider experiments . . . 44

4 Future experiments **45**
4.1 Second Higgs boson searches at collider experiments . . . 45
4.1.1 Direct search at the LHC . . . 45
4.1.2 Direct search at the ILC . . . 45
4.2 Fingerprints of the Higgs boson couplings . . . 46
4.2.1 Pattern of deviations in the Higgs boson couplings . . . 46
4.2.2 Future precision measurements of the Higgs boson couplings . . . 49

5 Radiative corrections to the Higgs boson couplings in the THDMs **51**

5.1 Renormalization in the THDMs . . . 51
5.2 Renormalized Higgs boson couplings in the THDMs . . . 55
5.2.1 Analytic expressions . . . 55
5.2.2 Deviations in the Higgs boson couplings at the one-loop level in the THDMs . 58
5.3 Discriminating four types of the THDMs . . . 58
5.4 Determination of inner parameters from the Higgs boson coupling measurements . 63
5.5 Summary . . . 67

6 Radiative corrections to the Higgs boson couplings in the HSM 71
6.1 Renormalization in the HSM . . . 71
6.2 Renormalized Higgs couplings in the HSM . . . 72
6.2.1 Analytic expression . . . 72
6.2.2 Numerical evaluation for the scaling factors . . . 73
6.3 Discriminating the HSM and the Type-I THDM . . . 75
6.4 Summary . . . 79

7 Radiative corrections to the Higgs boson couplings in the HTM 83
7.1 Renormalization in the HTM . . . 83
7.1.1 Renormalization of the electroweak parameters . . . 83
Models without $\rho_{\rm tree} = 1$ . . . 83
7.1.2 Renormalization of the Higgs potential . . . 85
7.2 Higgs couplings at the one-loop level . . . 89
7.2.1 Higgs to the diphoton decay . . . 89
7.2.2 Renormalized hVV coupling . . . 92
7.2.3 Renormalized hhh coupling . . . 93
7.3 Summary . . . 96

8 Summary of this thesis 97

A Decay rate of scalar bosons 99
A.1 Kinematics . . . 99
A.2 Decay rate of the CP-even scalar boson φ . . . 100

B Feynman rule 103
B.1 Feynman rule of the THDM . . . 103
B.2 Feynman rule of the HSM . . . 105
B.3 Feynman rule in the HTM . . . 107

C Loop functions **117**
C.1 A function 118
C.2 B function 118
C.2.1 B_0 function. 118
C.2.2 B_1 function. 119
C.2.3 B_{21} and B_{22} function 120
C.3 C function 120
C.3.1 C_0 function. 120
C.3.2 C_{11} function 121
C.3.3 C_{21} function 121

D 1PI diagrams **123**
D.1 1PI diagrams in the THDMs 123
D.1.1 One-point functions 123
D.1.2 Two-point functions 124
D.1.3 Three-point functions 127
D.2 1PI diagrams in the HSM 137
D.2.1 One point functions 137
D.2.2 Two point functions 137
D.2.3 Three point functions 140
D.2.4 1PI diagrams in the HTM 148
D.2.5 One-point functions 148
D.2.6 Two-point functions 149
D.2.7 Three-point functions 155

Chapter 1

Introduction

1.1 Overview

The standard model (SM) was established as a theory which can describe the world of elementary particles well. The SM is based on two pillars, namely the gauge principle and the spontaneously symmetry breaking. In particular, in the SM, three kinds of fundamental interactions can be expressed by the gauge symmetries $SU(3)_C \times SU(2)_L \times U(1)_Y$, where $SU(3)_C$, $SU(2)_L$ and $U(1)_Y$ represent the symmetry of color, isospin and hypercharge, respectively. The $SU(2)_L \times U(1)_Y$ symmetry spontaneously breaks into $U(1)_{EM}$ which represents the electromagnetic symmetry. The physics had been verified experimentally at several collider experiments such as LEP experiments from the 1980's to the 2000's; i.e. discoveries of weak gauge bosons and precision measurements of their observables and so on [1]. In 2012, the other of the two pillars has been proved by the discovery of the Higgs boson which plays an essential role for spontaneous symmetry breaking [2, 3]. Since the Higgs boson was the only undiscovered particle in the SM for a long time, the discovery led the SM to be completed. Experimental data for observables of the discovered Higgs boson are consistent with the predicted values in the SM [4–6]. In addition, there is no report which tells discoveries of other new particles such as superpartner particles.

Although the discovered Higgs particle is a SM-like one, a lot of things are still unknown for the Higgs sector; e.g. the origin of the negative mass term in the SM Higgs potential, the essence of the Higgs field (elementary scalar or composite?) and the shape of the Higgs sector (how many Higgs particles?). The minimal Higgs sector of the SM is just an assumption. There are possibilities that the Higgs sector is extended, and all extended Higgs sectors have not been excluded at all by the data of the LHC.

On the other hand, there are some phenomena beyond the SM; i.e. neutrino oscillations [7,8], the existence of dark matter (DM) [9] and baryon asymmetry of the Universe [10] and so on. We need a more polished theory which can explain such phenomena too. Many researchers have tried to build up various theories to solve the problems. Of course, there is only one correct theory. In order to clarify the true theory, we must test and narrow down these new physics models by experiments.

The collider experiment is one of most powerful experiments to detect new physics observables. The LHC [11] experiment restarted in May 2015 with increasing the center-of-mass energy ($\sqrt{s}$) from 8 TeV to 13 TeV. Therefore new particles may be discovered in the near future. Not only direct discoveries of new particles but also detecting deviations of some ob-

servables from those on the SM such as the production cross sections and decay branching ratios of the Higgs boson can be expected. Moreover some electron-positron collider experiments are planning such as the International Linear Collider (ILC) [12, 13], the Compact LInear Collider (CLIC) [14] and Future e^+e^- Circular Collider (FCCee) [15,16] in order to detect new particles and to precisely measure various observables. In order to come closer to understanding the theory of beyond the SM by testing several new physics models at the future collider experiments, we should investigate theoretical properties of those models, and calculate theoretical predictions of the observables as accurately as possible.

1.2 Standard Model

In the SM, interactions among particles can be described by gauge symmetries, $SU(3)_C \times SU(2)_L \times U(1)_Y$, where $SU(3)_C$, $SU(2)_L$ and $U(1)_Y$ are symmetries of the color, the isospin and the hypercharge, respectively. Particles obtain their masses via the spontaneously symmetry breaking, in which $SU(2)_L \times U(1)_Y$ symmetry breaks to $U(1)_{EM}$. The symmetry breaking occurs by the Higgs field getting the vacuum expectation value (VEV) v.

In the SM, the Higgs potential is given by

$$V = \mu^2|\Phi|^2 + \lambda|\Phi|^4, \tag{1.1}$$

where Φ is the isospin doublet scalar field. In order to realize the spontaneously symmetry breaking, the sign of μ^2 is required to be negative. In the Higgs potential, there are two independent parameters μ^2 and λ. μ^2 can be replaced by v as we will show in Chapter. 2., and v is determined by the Fermi constant G_F as $v = 1/(\sqrt{2}G_F)^{1/2}$ ($\simeq 246$ GeV). The remaining parameter λ has been determined by the Higgs boson mass m_h as $\lambda = m_h^2/(2v^2) \simeq 0.131$.

1.3 Higgs boson searches and discovery

At the LEP experiment [1], observables of the Z boson were precisely measured by tuning $\sqrt{s}$ to be around 91 GeV the mass of Z. The other purpose of the LEP experiment was to discover the Higgs boson h. Although the Higgs boson did not discovered at LEP, the lower bound on the mass of the Higgs boson m_h ($m_h > 114.4$ GeV [1]) was given by the Higgs boson search via the production process $e^+e^- \to hZ$, where center of mass energy was $\sqrt{s} = 189 - 209$ GeV. In addition, an upper bound on the mass of the SM Higgs boson ($m_h < 144$ GeV [1]) was indirectly given by precision measurements.

In 2012, the discovery of the new particle was announced by the ATLAS and the CMS collaborations at the LHC [2, 3]. The new particle was verified to be the Higgs boson by following detail measurements as the LHC Run-I. The LHC Run I started in 2008 with $\sqrt{s} = 7$ TeV, and it ran with upgrading $\sqrt{s}$ to 8 TeV for the one-year period from 2012.

The Higgs boson was mainly produced through following processes;

1. $gg \to h$, gluon-gluon fusion (ggF)

2. $qq(q') \to qq(q')h$, vector boson fusion (VBF)

3. $qq(q') \to Vh$, association with a vector boson V (Vh, $V = W, Z$)

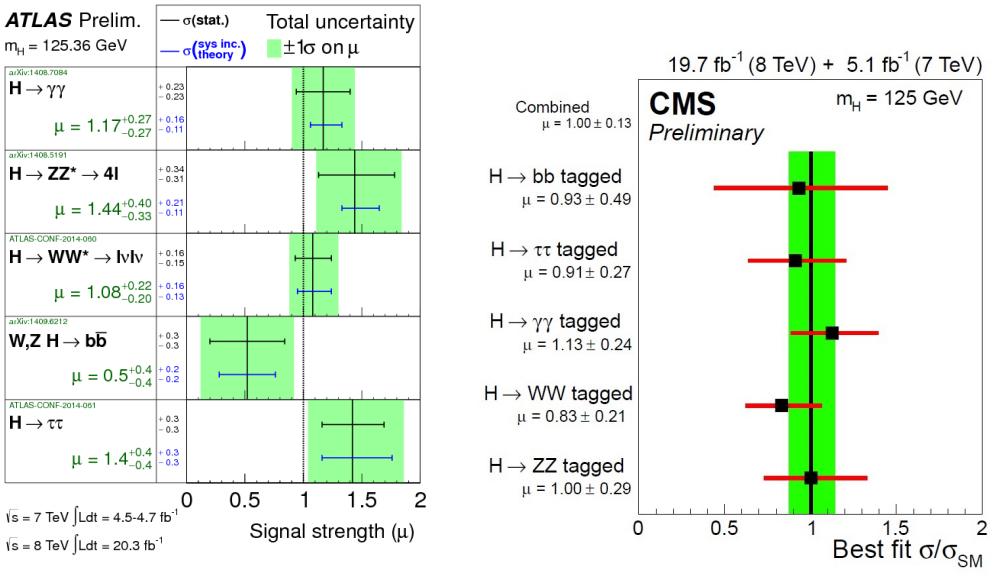

Figure 1.1: Signal strengths of each decay mode evaluated by ATLAS (left panel) [19] and CMS (right panel) [18].

4. $gg \to tth$. association with top quarks (tth)

The ggF process is the most influential process for the production of the Higgs boson with $m_h \simeq 125$ GeV. The sensitive decay channel of the Higgs boson at the LHC are the modes $\gamma\gamma$, 4 leptons (4ℓ), WW, $\tau\tau$ and $b\bar{b}$.

The mass was measured by inputting the data from the $\gamma\gamma$ and 4-lepton decay channels. ATLAS and CMS reported $m_h = 125.36 \pm 0.37(\text{stat}) \pm 0.18(\text{syst})$ [17] and $m_h = 125.03^{+0.37}_{-0.27}(\text{stat})\ ^{+0.13}_{-0.15}(\text{syst})$ [18], respectively. It can be said that the both data are consistent each other.

ATLAS and CMS evaluated the signal strength μ defined as a measured cross section times a branching ratio of the Higgs boson for a given process divided by the SM expectation, because it is important to test the validity of the SM. Fig. 1.1 shows the signal strengths of each decay mode evaluated by ATLAS (left panel) and CMS (right panel). The ATLAS's and the CMS's results for all channels agree with the predictions of the SM within uncertainties of 2σ.

The scaling factor κ_i is also an important quantity, where κ_i is defined as the ratio of the Higgs boson coupling to the particle i from that in the SM. λ_{jk} is the ratio of two values κ_j and κ_k. Namely, the κ_i and λ_{jk} indicate deviations in the Higgs boson coupling from the SM predictions. In Fig. 1.2, the scaling factor values of various couplings evaluated by the both collaborations are shown. In the analyses for κ_i, κ_i of all Yukawa couplings $hf\bar{f}$ are presumed to be universal values, and the κ_Z also presumed to be the same as the κ_W. We can see that all the SM predictions ($\kappa_i = 1$) are included within the 2σ uncertainty of the measured scaling factors, where the current 1σ uncertainties of the scaling factors are typically of $\mathcal{O}(10\%)$.

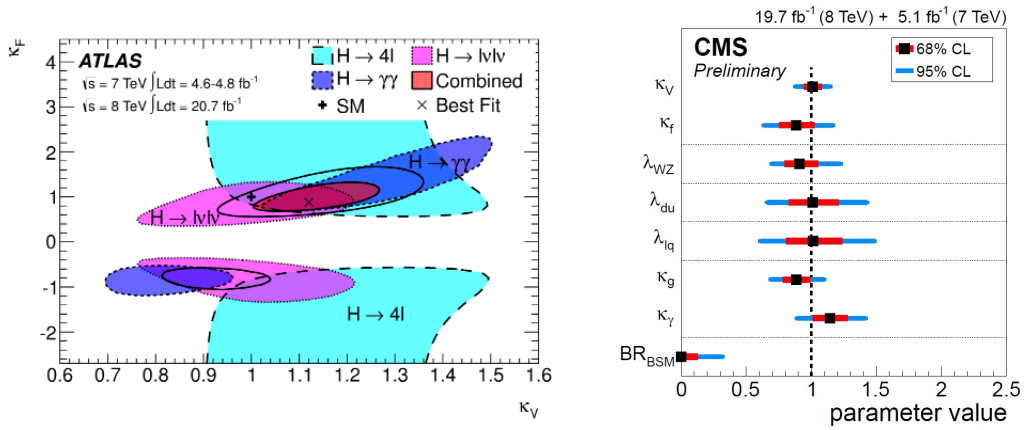

Figure 1.2: Scaling factors of several couplings evaluated by ATLAS (left panel) [20] and CMS (right panel) [18].

1.4 Problems with the Higgs sector of the Standard Model

Although the properties of the discovered Higgs boson are similar to those in the SM [4], it does not mean that the discovered Higgs boson is the Higgs boson of the SM, and there are a lot of questions (or mystery) in the SM Higgs sector.

For example, in the SM, in order to realize the spontaneously symmetry breaking, it is required the sign of the mass term in the Higgs potential to be negative. We do not understand the reason. We also do not have the clear understanding of the essence of the Higgs field. The Higgs field is presumed to be the elementary scalar field in the SM. On the other hand, there has been several studies to investigate possibilities the Higgs field is the composite scalar field [21–26]. In fact, there is no scalar field up to now except the discovered Higgs boson. If the essence of the Higgs field is determined, we may decide the next paradigm of particle physics.

In the SM, the Higgs sector is assumed to be the minimum form, in which there is only one isospin doublet Higgs field. But there is no compelling theoretical reason for such a minimal form. There are possibilities for extended structures of the Higgs sector with some number and representation of additional Higgs fields; e.g., models with the doublet field and additional singlet fields, doublet fields and/or triplet fields. These extended Higgs sectors can also explain the current LHC data for the discovered Higgs boson in some portions of their parameter regions.

There are also some questions from observations, as we discuss before. We should clarify such questions by using information of the discovered Higgs boson.

1.5 Hierarchy problem of the Higgs boson mass

The hierarchy problem of m_h is caused by the Higgs sector of the SM. In the SM, the renormalized Higgs boson mass can be expressed by,

$$m_h^2 = m_{h0}^2 - \frac{y_t^2}{4\pi}\Lambda^2 + \cdots , \tag{1.2}$$

where m_{h0}^2 is the bare mass of the Higgs boson, y_t is the Yukawa coupling of the top quark, Λ is the cut off scale, and the part "$\cdots$" indicates contributions of other loop diagrams. The second

term in the right side of Eq. (2.9) is the top quark loop contributions to the Higgs boson mass. If the limit of the application of the theory is the Planck scale, namely $\Lambda \sim \mathcal{O}(10^{19})$ GeV, the toq quark contribution corresponds to the quadratic divergence with $(\mathcal{O}(19^{19})\ \text{GeV})^2$. Then, the Higgs boson mass with about 125 GeV is derived via the huge fine tuning as $(125\text{GeV})^2 = (\mathcal{O}(10^{19})\text{GeV})^2 - (\mathcal{O}(10^{19})\text{GeV})^2$. This unnatural fine tuning is called "the hierarchy problem of the Higgs boson mass". There are several new physics paradigms motivated by solving the hierarchy problem, such as supersymmetry, dynamical breaking of electroweak symmetry and gauge-Higgs unification.

1.6 Phenomena beyond the standard model

Although the properties of the discovered Higgs boson are very similar to those in the SM, the true theory of particle physics cannot be the SM because there are phenomena which cannot be explained in the SM. In this section, we give brief reports of some of them.

1.6.1 Neutrino masses

The experiments with solar, atmospheric, reactor and accelerator neutrinos have shown that oscillations of neutrinos caused by nonzero neutrino masses and neutrino mixing. According to the neutrino oscillation data [7,8], in the case of 3-neutrino mixing, one of the two independent neutrino mass squared differences Δm^2_{21} is much smaller in absolute value than the second one Δm^2_{31}, i.e. $|\Delta m^2_{21}| \ll |\Delta m^2_{31}|$. Current data show,

$$|\Delta m^2_{21}| \simeq 7.5 \times 10^{-5}\text{eV}^2, \tag{1.3}$$

$$|\Delta m^2_{31}| \simeq 2.5 \times 10^{-3}\text{eV}^2, \tag{1.4}$$

where $|\Delta m^2_{21}|$ and $|\Delta m^2_{31}|$ were observed at experiments for measuring the solar neutrino and the atmosphere neutrino. Although the experimental fact of neutrino oscillation imply neutrinos have non-zero masses, the masses of neutrinos are zero because there is no right handed neutrino in the SM. Therefore, we need new physics to explain neutrino masses.

1.6.2 Dark matter

It is known that the dark matter exists in the Universe via various observation experiments. At first, the existence of dark matter had been known via galactic scales by precision galaxy rotation measurements [27]. Currently, measurements the fluctuation of cosmic microwave background radiation at the WMAP experiment [9] and the Planck experiment [10] reported that the energy density of the baryon accounts for only about 4.5% of that of the Universe and most of the rest is composed of that of dark matter with about 22.7% and that of dark energy with 72.8%. We know the following properties of the dark matter,

- Stable
- Electrically neutral
- Non-relativestic
- It can explain the observation, the dark matter mass density is $\Omega_{\text{DM}} \simeq 0.2$ [10]

The SM does not contain the dark matter candidate.

1.6.3 Baryon asymmetry of the Universe

We know that the ratio of the baryon number density to entropy density is $n_B/s \sim 10^{-10}$ [10]. Namely, the baryon number is asymmetry in the Universe (BAU). To explain numerically this ratio is an important problem between cosmology and particle physics. According to the Sakharov's conditions [28], following three conditions must be satisfy, in order to generate the baryon asymmetry from the baryon symmetry Universe.

- Baryon number violation
- C and CP violation
- Departure from equilibrium

The third condition cannot be satisfied in the SM because the measured m_h is too large. In addition, the CP violating phase in the Kobayashi-Maskawa matrix is too small to generate the baryon asymmetry. There are some of scenarios to solve BAU; Leptogenesis [29,30], Afleck0Dine mechanism and electroweak baryogenesis [31, 32].

1.7 Physics of extended Higgs sectors

We should consider various types of Higgs sectors without limiting the minimal Higgs sector, because there is no theoretical principle to limit the Higgs sector to be the minimal structure. In addition, new physics can be the motive to consider extended Higgs sectors because extended Higgs sectors are often introduced in various new physics models. Although infinite number of extended Higgs sectors can be considered, we focus on second simplest Higgs sectors which have an additional Higgs field. The reason is that models containing the second simplest Higgs sectors are effective theories of the infinite extended Higgs models.

We should take into account some experimental constraints on structures of Higgs sectors. The electroweak rho parameter (ρ) [33] is one of them. The experimental value of ρ is close to unity, which suggests that there is a global $SU(2)$ symmetry, so-called the custodial symmetry [33]. The rho parameter strongly depends on the property of the Higgs sector; i.e., the number of Higgs multiplets and their hypercharges. In the Higgs sector composed from only $SU(2)$ doublets and/or singlets, the rho parameter is unity at the tree level because of the custodial symmetry [34]. Thus, these Higgs sectors can be regarded as the natural extension of the Higgs sector.

We also should consider the constraint on the Higgs sector from several bounds on the existence of flavor changing neutral currents (FCNCs). In the SM, FCNCs are automatically absent at the tree level [35] because the Yukawa coupling matrix (Y_f) and the fermion mass matrix ($M_f = Y_f v$) can be simultaneously diagonalized. However, in general, if additional doublet Higgs fields are introduced into the Higgs sector, FCNCs appear at the tree level [36,37]. For example, if two kinds of doublet Higgs fields (Φ_1 and Φ_2) couple to a kind of fermion field, the fermion mass matrix M_f is expressed by a linear combination of some matrix as $M_f = M_{f1}v_1 + M_{f2}v_2$, where v_1 and v_2 are VEVs of Φ_1 and Φ_2, respectively. On the other hand, the matrix of Yukawa couplings is given by $Y_f = -M_{f1}\sin\theta + M_{f2}\cos\theta$, where θ is the mixing angle between the CP-even component of Φ_1 and that of Φ_2. In such a case, since M_f and Y_f are not simultaneously diagonalized, tree level FCNCs can appear.

1.7.1 Two Higgs doublet models

The two Higgs doublet model (THDM) [38] which has an additional isospin doublet field with the hypercharge $Y = 1/2$ is often motivated in new physics models beyond the SM. For example, the Minimal Supersymmetric SM (MSSM) [33] requires the Higgs sector with two doublet fields. Multi Higgs structures can contain additional CP violating phases [39] and also realization of the strong first order phase transition, both of which are required to realize electroweak baryogenesis.

Also, electroweak precision data indicate that ρ is very close to unity [40], and this fact strongly constrains parameters in extended Higgs models. In the THDM, a relation $\rho = 1$ is well satisfied at the tree level.

In general, if additional doublet Higgs fields are introduced into the Higgs sector, FCNCs appear at the tree level [36,37]. Such a situation is very severe, because FCNCs are constrained by flavour experiments. Therefore, we often consider THDMs in which FCNCs are forbidden at the tree level by imposing a softly-broken discrete Z_2 symmetry [36]. In this case, four types of Yukawa interactions appear depending on the way of the assignment of the Z_2 charge for particles [41]. These four types of THDMs provide variety of phenomenological consequences [42], which are tested at collider experiments.

1.7.2 Supersymmetric standard models

As mentioned in Sec. 1.5, it is known that the SM Higgs sector holds the hierarchy problem of the Higgs boson mass. The supersymmetric theory is one of theories which can explain the hierarchy between the scale of the Higgs boson mass and the Planck scale. In the supersymmetric theory, the quadratic divergence in the Higgs boson mass is naturally cancelled by loop contributions of superpartner particles whose spins are different from the SM counterparts by one half.

At least two iso-spin doublet Higgs (Φ_u and Φ_d) fields are required in models of the supersymmetric theory. Φ_u with $Y = -1/2$ and Φ_d with $Y = 1/2$ give masses to up-type quarks and down-type quarks, respectively. The supersymmetry (SUSY) forbids charge conjugations of the Higgs fields to exist in the Lagragian. Moreover the $Q_L \Phi_u u_R$ term are forbidden by the hypercharge invariance. Then, an additional Higgs doublet field is required to give masses to up-type quarks. Namely, Higgs sectors of supersymmetric models are extended Higgs sectors. The minimal supersymmetric extension of the SM (MSSM) are composed of all the SM particles, an additional iso-spin doublet Higgs field and their superpartner particles. The Higgs sector in the MSSM is the same as that of the THDM (so called Type-II THDM).

1.7.3 Composite Higgs models

What is the origin of the Higgs field? We have not yet obtained the certain answer of this question. There is a possibility which the Higgs boson is a composed state of more fundamental fields with a certain strong dynamics. In the composite scenario, the Higgs boson is the pseude-Nambu-Goldstone boson (pNGB) associated with spontaneous breakdown of a global symmetry [21–25]. The mass of the Higgs boson is generated at the one-loop level by the loop contributions of other particles. The number of pNGB is determined by the number of the broken generators. For example, in the Minimal composite Higgs model (MCHM), the original global symmetry is $SO(5) \times U(1)_X$. The $SO(5)$ is spontaneously broken into $SO(4)$ by some dynamics [26], so that four NGBs appear which correspond to four components of the doublet

Higgs field. Namely, the MCHM can naturally explain the structure of the Higgs sector in the SM.

1.7.4 Higgs singlet model

The Higgs singlet model (HSM) with an additional real scalar field with the hypercharge $Y = 0$ is also one of minimal extended Higgs models [43]. Because the VEV of the singlet field does not contribute to the electroweak symmetry breaking, the rho parameter are not modified from that of the SM at the tree level. In the $U(1)_{B-L}$ gauge model, the Higgs sector is required to spontaneously break the $U(1)_{B-L}$ symmetry by introducing a singlet scalar field for such a purpose [44–46]. The breaking may be related to the mechanism of neutrino mass generation. The HSM also realize the strong first order phase transition [47]. If the model respect an additional global $U(1)$ symmetry [48] and/or a discrete symmetry such as a Z_2 symmetry [49], the singlet field can be a candidate of dark matter.

1.7.5 Higgs triplet model

The minimal Higgs triplet model (HTM) has an additional complex triplet scalar field with the hypercharge $Y = 1$ [50]. In the HTM, there is a mechanism to generate majorana neutrino masses, which is called as the Type-II seesaw mechanism. One of the important features in this model is that ρ deviates from the unity at the tree level due to the nonzero VEV of the triplet field v_Δ, therefore $v_\Delta \ll v$ ($\simeq 246$ GeV). There are seven physical mass eigenstates; i.e., triplet-like Higgs bosons ($H^{\pm\pm}, H^{\pm}, A, H$) and the SM-like Higgs boson h. In particular, collider phenomenology of the doubly charged Higgs bosons $H^{\pm\pm}$ are very interesting and important because particles with electromagnetic charge $Q = 2$ are not contained in the SM, and the dominant decay process of $H^{\pm\pm}$ strongly depends on v_Δ and the mass difference among triplet like Higgs bosons [51].

1.7.6 Exotic Higgs models with $\rho = 1$ at tree level

The ρ deviates from unity at the tree level in the Higgs sector with exotic representation fields such as triplets [33, 34, 52]. In such a model, VEVs of such an exotic field violates the custodial symmetry, so that the VEV is severely constrained by the rho parameter data. There is another extended Higgs sector in which an alignment of the triplet VEVs makes the rho parameter to be unity at the tree level, named as the Georgi-Machacek (GM) model [53]. Furthermore, it is known that the addition of the isospin septet field with the hypercharge Y = 2 does not change the rho parameter from unity at the tree level [33, 34, 52]. As a striking feature of exotic Higgs sectors, there appears the $H^{\pm}W^{\mp}Z$ vertex at the tree level [54], where $H^{\pm}$ are physical singly-charged Higgs boson. In the multi-doublet model, this vertex is induced at the one loop level, so that the magnitude of the $H^{\pm}W^{\mp}Z$ vertex tends to be smaller than that in exotic Higgs sectors [55]. Therefore, precise measurement of the $H^{\pm}W^{\mp}Z$ vertex can be used to constrain exotic Higgs sectors. In addition that, there is an interesting property that the hVV couplings ($V = W, Z$) can be larger than those of the SM [34, 52]. If the hVV couplings are proved to be larger than the SM values in future precision coupling measurements, it will be decisive evidence of the exotic Higgs sector.

1.8 In this thesis

Because we do not know the shape of the Higgs sector, we can consider various possibilities of the Higgs sector. The structure of the Higgs sector is strongly related with the new physics models. Namely, the Higgs sector is an important key to approach the new Lagrangian beyond the SM. In this thesis, we discuss how the structure of the Higgs sector can be determined by testing various extended Higgs sectors at future collider experiments. In particular, we focus on the indirect search of the second Higgs boson. If an extra Higgs boson is directly discovered at the collider experiments, it will be the clear evidence of an extended Higgs sector. But there is also the possibility that no particle is discovered. Even in such a case, precision measurements of the Higgs boson properties will bring important information. In particular, the Higgs boson couplings will be precisely measured at the LHC Run II and future collider experiment such as the high luminosity LHC (HL-LHC) [56] and the ILC [12, 13]. Such future precision measurements may observe deviations in the Higgs boson couplings from those of the SM, which are indirect evidences of new physics. Although there are studies of the Higgs boson couplings at the tree level in such models [57], it is not enough to calculate them at the tree level in order to determine the Higgs sector by comparing with the future precision measurement. Therefore, we calculate the various Higgs boson couplings including one-loop corrections in the THDMs [58, 59] and the HSM [60] and the HTM [61, 62].

First, we define each model, and briefly review the tree level properties to fix notation. After that, we show how the Higgs boson couplings deviate from the SM predictions at the tree level. Then, we calculate various couplings of Higgs boson at the one-loop level by the on-shell renormalization scheme in those models. It is essentially important to calculate various couplings comprehensively because the pattern of deviation in the Higgs boson couplings depends on the model. We study how extended Higgs sectors can be discriminated by the pattern of the deviations, and how we can test the extended Higgs sectors via precision measurements at the HL-LHC and the ILC. We investigate the possibility of determining the Higgs sector without information from direct searches.

1.9 Organization

This thesis is organized as follows. In Chapter 2 and Chapter 3, we give the review of the Higgs physics in the SM and some extended Higgs models, respectively. In Chapter 4, we review the prospects of additional Higgs boson searches at future collider experiments. In Chapter 5, Chapter 6 and Chapter 7, we present our studies for radiative corrections to the Higgs boson couplings in the THDMs, the HSM and the HTM, respectively. We discuss how we can determine the structure of the Higgs sector by using our precise calculations and future precision measurements of the Higgs boson couplings. Finally, we give the summary of this thesis in Chapter 8.

Chapter 2

Review of the Standard Model

2.1 Lagrangian

In the SM, interactions among particles are described under following gauge symmetries,

$$U(1)_Y \times SU(2)_I \times SU(3)_C, \tag{2.1}$$

where $U(1)_Y$, $SU(2)_I$, $SU(3)_C$ indicate symmetries of the hypercharge, the iso-spin and the color, respectively. We summarize quantum numbers of particles under these symmetries in Tab. 2.1. Lagrangian of the SM is composed of the gauge self interaction term ($\mathcal{L}_{\text{gauge}}$), the kinetic term of fermion fields ($\mathcal{L}_{\text{fermi}}$) and the Higgs sector term ($\mathcal{L}_{\text{Higgs}}$),

$$\mathcal{L} = \mathcal{L}_{\text{gauge}} + \mathcal{L}_{\text{fermi}} + \mathcal{L}_{\text{Higgs}} \tag{2.2}$$

The Higgs sector $\mathcal{L}_{\text{Higgs}}$ is,

$$\mathcal{L}_{\text{Higgs}} = |D_\mu \Phi|^2 - V(\Phi) + \mathcal{L}_{\text{Yukawa}}, \tag{2.3}$$

where $V(\Phi)$ and $\mathcal{L}_{\text{Yukawa}}$ indicate the Higgs potential and the Yukawa interaction term, respectively. We define the covariant derivative such as

$$D_\mu = \partial_\mu - i\frac{g}{2}\tau^i W_\mu^i - i\frac{g'}{2}B_\mu, \tag{2.4}$$

where τ^i is Pauli matrix.

The Higgs potential is given by,

$$V(\Phi) = \mu^2|\Phi|^2 + \lambda|\Phi|^4. \tag{2.5}$$

Higgs doublet field is parametrized as,

$$\Phi = \begin{pmatrix} G^+ \\ \frac{1}{\sqrt{2}}(h + v + iG^0) \end{pmatrix}, \tag{2.6}$$

where v is a VEV and G^+ and G^0 are Numbu-Goldstone bosons which are eaten by the longitudinal components of weak gauge field. If μ^2 is negative value ($\mu^2 < 0$), the spontaneous

Table 2.1: Fields and their quantum number of symmetries.

Field	Y	I	C
Φ	$\frac{1}{2}$	2	1
G^C_μ	0	1	8
W^i_μ	0	3	1
B_μ	0	1	1
Q_L	$\frac{1}{6}$	2	3
u_R	$\frac{2}{3}$	1	3
d_R	$-\frac{1}{3}$	1	3
L_L	$-\frac{1}{2}$	2	1
e_R	-1	1	1

electroweak symmetry breaking is realized. In the Higgs potential, the vacuum is determined by imposing a vacuum condition as,

$$\left.\frac{\partial V}{\partial h}\right|_{h=0} = 0, \tag{2.7}$$

and we obtain a relation as,

$$\mu^2 = -\lambda v^2. \tag{2.8}$$

Moreover, the mass of the Higgs boson m_h^2 is given by the definition of the mass;

$$m_h^2 \equiv \left.\frac{\partial^2 V}{\partial h^2}\right|_{h=0} = 2\lambda v^2. \tag{2.9}$$

Masses of weak gauge bosons are given from the kinetic term $\mathcal{L}_{\text{kine}}$ as,

$$\mathcal{L}_{\text{kine}} = -\frac{g^2}{4}\frac{v^2}{2}(W^1_\mu - iW^2_\mu)(W_1^\mu + iW_2^\mu) - \frac{1}{4}\frac{v^2}{2}(gW^3_\mu - g'B_\mu)(gW_3^\mu - g'B^\mu). \tag{2.10}$$

We here define the gauge fields as

$$W_\mu = \frac{1}{\sqrt{2}}(W^1_\mu - iW^2_\mu), \tag{2.11}$$

$$W^\dagger_\mu = \frac{1}{\sqrt{2}}(W^1_\mu + iW^2_\mu),$$

$$Z_\mu = \frac{1}{\sqrt{g^2+g'^2}}(gW^3_\mu - g'B_\mu). \tag{2.12}$$

Mass eigenstates of neutral gauge fields are expressed as

$$\begin{aligned}\begin{pmatrix} A_\mu \\ Z_\mu \end{pmatrix} &= \frac{1}{\sqrt{g^2+g'^2}}\begin{pmatrix} g & g' \\ -g' & g \end{pmatrix}\begin{pmatrix} B_\mu \\ W^3_\mu \end{pmatrix} \\ &\equiv \begin{pmatrix} \cos\theta_W & \sin\theta_W \\ -\sin\theta_W & \cos\theta_W \end{pmatrix}\begin{pmatrix} B_\mu \\ W^3_\mu \end{pmatrix}. \end{aligned} \tag{2.13}$$

Then masses of redefined weak gauge bosons are given as,

$$m_W^2 = \frac{g^2}{4}v^2, \;\; m_Z^2 = \frac{g^2+g'^2}{4}v^2. \tag{2.14}$$

As you can see, the photon field does not obtain own mass, because the electromagnetic $U(1)_{EM}$ symmetry are not broken.

Next, we discuss Yukawa interaction term given by,

$$\mathcal{L}_{\text{Yukawa}} = -Y_u^{ij}\bar{Q}_L^i\tilde{\Phi}q_{uR}^j - Y_u^{ij}\bar{Q}_L^i\Phi q_{dR}^j - Y_e^{ij}\bar{L}_L^i\Phi l_R^j + \text{h.c}, \tag{2.15}$$

where $\tilde{\Phi}$ is charge conjugate expression $\tilde{\Phi} = i\tau_2\Phi^*$, and $Y_{u,d,e}$ are 3×3 Yukawa matrices. We can take basis of fermion fields as

$$Q_L^i = \begin{pmatrix} u_L^i \\ d_L'^i \end{pmatrix} = \begin{pmatrix} u_L^i \\ (U_{CKM}^{ij})^\dagger d_L^i \end{pmatrix}, \tag{2.16}$$

where U_{CKM} is the Cabibbo-Kobayashi-Maskawa matrix [63] which is an unitary matrix, so that the $Y_{u,d}$ are diagonalized as,

$$\mathcal{L}_{Yukawa} \to -\bar{Q}_L(Y_u^{diag})\tilde{\Phi}q_{uR} - \bar{Q}_L(U_{CKM}^\dagger Y_d)\Phi q_{dR} - \bar{L}_L(Y_e^{diag})\Phi l_R + \text{h.c}, \tag{2.17}$$

$$= -\bar{Q}_L Y_u^{diag}\tilde{\Phi}q_{uR} - \bar{Q}_L Y_d^{diag}\Phi q_{dR} - \bar{L}_L Y_e^{diag}\Phi l_R + \text{h.c}. \tag{2.18}$$

Components of these diagonalized matrices $Y_{u,d,e}^{diag}$ are given by,

$$Y_u^{diag} = \begin{pmatrix} y_u & 0 & 0 \\ 0 & y_c & 0 \\ 0 & 0 & y_t \end{pmatrix}, \;\; Y_d^{diag} = \begin{pmatrix} y_d & 0 & 0 \\ 0 & y_s & 0 \\ 0 & 0 & y_b \end{pmatrix}, \;\; Y_e^{diag} = \begin{pmatrix} y_e & 0 & 0 \\ 0 & y_\mu & 0 \\ 0 & 0 & y_\tau \end{pmatrix}, \tag{2.19}$$

where y_f indicates Yukawa couplings of a fermion field f. By the Higgs field obtaining the VEV v, masses of fermion fields are given by,

$$\mathcal{L}_{\text{Yukawa}} = -\frac{m_u}{v}\bar{u}u\left(1+\frac{h}{v}\right) - \frac{m_d}{v}\bar{d}d\left(1+\frac{h}{v}\right) - \frac{m_e}{v}\bar{e}e\left(1+\frac{h}{v}\right) \tag{2.20}$$

$$+ (\text{the same mass terms of other charged fermion particles}),$$

where

$$m_u = \frac{y_u}{\sqrt{2}}v, \quad m_d = \frac{y_d}{\sqrt{2}}v, \quad m_e = \frac{y_e}{\sqrt{2}}v. \tag{2.21}$$

In the SM, all elementary particles couple with the Higgs boson. As shown at Eqs. (2.9), (2.14), (2.21), the all couplings are proportional to their masses at the tree level.

We here describe the mechanism to forbid the FCNC processes at the tree level. As shown in the previous paragraph, left handed down-type quark fields in the doublet fields (d', s' and b') are different from their mass eigenstates (d, s and b). d', s' and b' are related with d, s and b by the Cabibbo-Kobayashi-Maskawa matrix U_{CKM} as defined by Eq. (2.16). In the SM, the tree level FCNC processes do not appear through the U_{CKM}. FCNC processes interacting the Higgs

boson automatically vanish because the Yukawa coupling matrix (Y_f) and the fermion mass matrix ($M_f = Y_f v$) can be simultaneously diagonalized. FCNC processes interacting neutral gauge bosons are absent at the tree level because of unitary feature of U_{CMK},

$$J^\mu_{\rm NC} = -\bar{d^i_L}\gamma^\mu d^i_L + \cdots \tag{2.22}$$
$$= \bar{d^j_L} U^{ji}_{CKM}\gamma^\mu (U^\dagger_{CKM})^{ik} d^k_L \tag{2.23}$$
$$= \bar{d^j_L}\delta^{jk}\gamma^\mu d^k_L, \tag{2.24}$$
$$\tag{2.25}$$

where indices i, j, k identify flavour. This mechanism is so-called GIM mechanism [35].

2.2 Custodial symmetry

We here consider the $SU(2)_L \times SU(2)_R$ symmetry which can be rewritten by $SU(2)_L \times SU(2)_R = SU(2)_V \times SU(2)_A$. Under the symmetry, an arbitrary field matrix M is transformed as,

$$M \to e^{i\theta^i_L \tau_i} M e^{-i\theta^j_R \tau_i j}. \tag{2.26}$$

In the theory respecting the $SU(2)_V \times SU(2)_A$ symmetry, the $SU(2)_A$ is broken by the electroweak symmetry breaking. Then, the $SU(2)_V$ symmetry so-called the "custodial symmetry" remains in the theory. After the $SU(2)_A$ is broken, a relation $\theta_L = \theta_R = \theta_V$ holds. Then, the transformation given at Eq. (2.26) can be regarded as the transformation to rotate from both the right side the rotation and the left side with the same angle.

If we here introduce a field matrix defined as,

$$M \equiv (i\tau_2 \Phi^* \Phi) = \begin{pmatrix} \phi^0 & \phi^+ \\ -\phi^- & \phi^0 \end{pmatrix}, \tag{2.27}$$

the Higgs potential in the SM given at Eq. (2.5) can be expressed by,

$$V = \frac{\mu^2}{2}{\rm Tr}[M^\dagger M] + \frac{\lambda}{4}({\rm Tr}[M^\dagger M])^2. \tag{2.28}$$

Since this Higgs potential obviously is invariant under the transformation $M \to e^{i\theta^i_V \tau_i} M e^{-i\theta^j_V \tau_j}$, we can say that the Higgs sector in the SM respects the custodial symmetry [33].

2.3 Electroweak rho parameter ρ

Electroweak rho parameters ρ indicates the ratio of the strength of the charged current and that of the neutral current in the weak interaction, and it defines by

$$\rho \equiv \frac{m^2_W}{\cos^2\theta_W m^2_Z}. \tag{2.29}$$

Formula of ρ are expressed by the isospin and the hypercharge of Higgs fields in general model. We show the formula of ρ in the general Higgs sector. We consider an extended Higgs sector that contains N Higgs multiplets Φ_i $(i = 1, \cdots, N)$ with the isospin T_i and the

hypercharge Y_i. We assume CP conservation of the Higgs sector. The definition of neural Higgs components is given by,

$$\phi_i^0 = \left(c_c^i \varphi_i + c_v^i v_i + c_z^i z_i\right), \tag{2.30}$$
$$\eta_j^0 = \left(\varphi_j + v_j\right). \tag{2.31}$$

The kinetic term is given by

$$\mathcal{L}_{\rm kin} = \Sigma_i |D^\mu \Phi_i|^2 + \frac{1}{2}\Sigma_j |D^\mu \eta_j|^2, \tag{2.32}$$

where the first term and the second term are the kinetic term of complex scalar fields and real scalar fields, respectively. Masses of weak gauge bosons are obtained from Eq. (2.32) as

$$m_W^2 = g^2 \Sigma_i \left(|c_v^i v_i|^2 [T_i(T_i+1) - Y_i^2]\right) + \frac{g^2}{2}\Sigma_j \left(|v_j|^2 [T_j(T_j+1)]\right), \tag{2.33}$$
$$m_Z^2 = g_Z^2 \Sigma_i \left(2|c_v^i v_i|^2 Y_i^2\right). \tag{2.34}$$

The VEV v ($\equiv (\sqrt{2}G_F)^{1/2} \simeq 246$ GeV) is expresses as

$$v^2 = 4\left\{\Sigma_i \left(|c_v^i v_i|^2 [T_i(T_i+1) - Y_i^2]\right) + \frac{1}{2}\Sigma_j \left(|v_j|^2 [T_j(T_j+1)]\right)\right\}, \tag{2.35}$$

Now we obtain the general formula [34] of ρ from Eqs. (2.29), (2.33), (2.34),

$$\rho = \frac{g^2 \Sigma_i \left(|c_v^i v_i|^2 [T_i(T_i+1) - Y_i^2]\right) + \frac{g^2}{2}\Sigma_j \left(|v_j|^2 [T_j(T_j+1)]\right)}{g^2 \Sigma_i \left(2|c_v^i v_i|^2 Y_i^2\right)}. \tag{2.36}$$

Radiative corrections to the rho parameter ($\delta\rho$) show whether the model respects the custodial symmetry or not. In the SM, $\delta\rho$ is roughly expressed by [33],

$$\delta\rho \sim \frac{g^2 N_C}{64\pi^2 m_W^2}\left(m_t^2 + m_b^2 - \frac{2m_t^2 m_b^2}{m_t^2 - m_b^2}\ln\frac{m_t^2}{m_b^2}\right), \tag{2.37}$$

where N_C is the color number of quarks. Eq. (2.37) shows that the custodial symmetry is broken in the fermion sector. The limit where masses of up-type quarks are the same as those of down-type quarks, is the limit to respect the custodial symmetry.

2.4 Theoretical Constraints on the Higgs boson mass

2.4.1 Perturbative unitarity

We discuss the bound on the Higgs boson mass from the constraint of S wave amplitude for two-body to two-body scattering. The details of this constraint are explained in Ref. [64]. First, we consider the $W_L^+ W_L^- \to W_L^+ W_L^-$ scattering, where W_L is the longitudinally polarized W boson. By performing the partial wave expansion for scattering amplitude for the $W_L^+ W_L^- \to W_L^+ W_L^-$, we obtain

$$T_i(s,t) = T(E, \cos\theta) \tag{2.38}$$
$$= 16\pi \sum_J (2J+1) a_i^J(s) P_J(cos\theta), \tag{2.39}$$

where s and t are Mandelstam variables, θ is the scattering angle and E is the collision energy. In the limit where $s \gg m_h^2$, the S wave amplitude a_0 for the process is given by

$$a_0 = -\frac{G_F m_h^2}{4\sqrt{2}\pi}. \tag{2.40}$$

By substituting Eq. (2.40) in the optical theorem $|a_J|^2 \leq |\mathrm{Im} a_J|$, the following constraint is given,

$$|a_0| \leq \frac{1}{2} \quad \rightarrow \quad m_h < 850\mathrm{GeV}. \tag{2.41}$$

Moreover, by taking into account unitarity of S wave amplitudes for other neutral scattering channels, namely scattering channels between $W_L^+ W_L^-$, $Z_L Z_L$, hh and hZ states, more restrictive bound is derived. In the SM, the strongest bound in the Higgs boson mass from the S wave amplitude unitarity is

$$m_h^2 \leq \frac{4\sqrt{2}\pi}{3G_F} \simeq (700\mathrm{GeV})^2. \tag{2.42}$$

2.4.2 Triviality and vacuum stability

The running coupling of the Higgs coupling λ is also critical for discussing the bound on the Higgs boson [65–67]. The renormalization group equation (RGE) of the λ in the SM is roughly expressed by,

$$Q\frac{d\lambda(Q)}{dQ} = 24\lambda^2 - 7y_t^4 + 12\lambda y_t^2 + \cdots, \tag{2.43}$$

where Q indicates an arbitrary scale and y_t is the Yukawa coupling given at Eq. (2.18). The right side corresponds to the β-function of the quartic coupling of the Higgs field. From Eq. (2.43), we find that if the mass of the Higgs boson ($m_h^2 = 2\lambda v^2$) is too large, $\lambda(Q)$ becomes larger for higher energies and blows up at some high energy point (the Landau pole). In contrast, when m_h^2 is too small and the β-function is negative because of the term of the fourth power of the top-quark Yukawa coupling. The situation which the β-function become negative below the Planck scale is not favored because it means the vacuum stability is broken below the Planck scale.

Now, we know the value of m_h to be around 125 GeV which corresponds to $\lambda \sim 0.26$. The β-function substituting the value of λ means risky results for the vacuum stability. The result strongly depends on the value of m_t and α_s. The measured top quark mass has a error not small, which comes from both QCD calculation uncertainty and measurement error. The experimental value of the m_t including the error is $m_t = 173.1 \pm 0.7$ GeV (3σ) (direct measurement mass) [68]. If we use the center value of the experimental value of m_t, i.e. $m_t = 173.1$ GeV, vacuum stability is broken at around $Q \sim \mathcal{O}(10^{10})$ GeV. Then, the precision measurement of m_t is essentially important for vacuum stability.

We can avoid the situation of vacuum instability by introducing additional scalar fields. The additional scalar boson contributions to the quartic Higgs coupling can put up the β-function because the sign of the scalar loop contributions is positive.

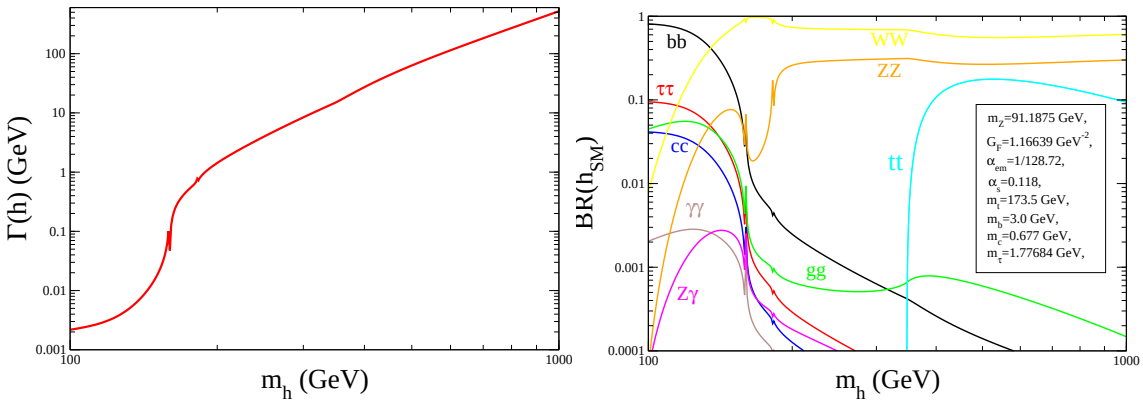

Figure 2.1: The left(right) figure is the total width(the decay branching ratio) of the Higgs boson in the standard model.

2.5 Decay of the Higgs boson

In Fig. 2.1, the left panel shows the decay branching ratios of h as a function of m_h. Decay branching ratios of the h depends on masses of children particles. If m_h is smaller than about 160 GeV, the $h \to b\bar{b}$ decay mode is dominant. The reason is that the bottom quark is the heaviest in light fermions and it has a color factor 3. If m_h is larger than about 160 GeV, the on-shell decay mode of $h \to WW$ opens and the mode can be dominant. In the region with $m_h \gtrsim 350$ GeV, h can decay into $t\bar{t}$.

Although h does not couple with γ and g directly, h can decay into $\gamma\gamma$, $Z\gamma$ and gg through loop processes of charged particles and colored particles. Since the decay modes are loop induce decay modes, the decay branching ratios are relatively small.

As you can see, the $h \to VV$ $(V = W, Z)$ decay modes can appear in the region with $m_h < 2m_V$. It implicates h decays into three bodies $(Vf\bar{f})$ through the decay into virtual weak bosons, i.e., $h \to VV^* \to Vf\bar{f}$.

We have already known the value of m_h which is about 125 GeV. Namely, the value of the x-axis of this panel has been determined. Because branching ratios of various decay modes is larger than $\mathcal{O}(10^{-3})$ in m_h 125 GeV, it means that various decay modes can be detected at the collider experiments. Indeed, at the LHC Run-I, $h \to \gamma\gamma, ZZ, WW, b\bar{b}$ and $\tau\tau$ modes have been detected.

The right panel of Fig. 2.1 shows m_h dependence of the total width Γ_h of h. We note that Γ_h drastically increases in $m_h \simeq 2m_t$ because the decay mode $h \to t\bar{t}$ opens. The total decay width of h with $m_h = 125$ GeV is $\Gamma_h \simeq \mathcal{O}(10^{-3})$ GeV.

2.6 Radiative corrections in the SM

2.6.1 Renormalization in the SM

In this section, we describe the renormalization of the SM in order to calculate the [69, 70]. We describe how to determine each counter term in the gauge sector, the Yukawa sector and the Higgs sector.

Renormalization in gauge and Higgs sector in the SM

The gauge sector is described by three independent parameters as in the SM. When we choose m_W, m_Z and $\alpha_{\rm em}$ as the input parameters, all the other parameters such as v and weak mixing angle $\sin\theta_W$ (s_W) are given in terms of these three input parameters as

$$v^2 = \frac{m_W^2}{\pi\alpha_{\rm em}}\left(1-\frac{m_W^2}{m_Z^2}\right), \quad s_W^2 = 1-\frac{m_W^2}{m_Z^2}. \tag{2.44}$$

These parameters and gauge fields; namely $W_\mu^\pm, Z_\mu$ and A_μ, are shifted into renormalized parameters, renormalized fields and counter terms,

$$m_W^2 \to m_W^2 + \delta m_W^2, \tag{2.45}$$
$$m_Z^2 \to m_Z^2 + \delta m_Z^2, \tag{2.46}$$
$$\alpha_{\rm em} \to \alpha_{\rm em} + \delta\alpha_{\rm em}, \tag{2.47}$$
$$v \to v + \delta v, \tag{2.48}$$
$$s_W^2 \to s_W^2 + \delta s_W^2, \tag{2.49}$$
$$W_\mu^\pm \to (1+\frac{1}{2}\delta Z_W)W_\mu^\pm, \tag{2.50}$$
$$\begin{pmatrix} A_\mu \\ Z_\mu \end{pmatrix} \to \begin{pmatrix} 1+\frac{1}{2}\delta Z_\gamma & \frac{1}{2}\delta Z_{\gamma Z}+\frac{1}{2s_W c_W}\delta s_W^2 \\ \frac{1}{2}\delta Z_{\gamma Z}-\frac{1}{2s_W c_W}\delta s_W^2 & 1+\frac{1}{2}\delta Z_Z \end{pmatrix}\begin{pmatrix} A_\mu \\ Z_\mu \end{pmatrix}. \tag{2.51}$$

Renormalized two point functions of gauge fields, $W^+W^-, ZZ, \gamma\gamma$ and γZ mixing, are given by using above counter terms and 1PI diagrams

$$\hat\Pi_{WW}[p^2] = \Pi_{WW}^{\rm 1PI}[p^2] + (p^2-m_W^2)\delta Z_W - \delta m_W^2, \tag{2.52}$$
$$\hat\Pi_{ZZ}[p^2] = \Pi_{ZZ}^{\rm 1PI}[p^2] + (p^2-m_Z^2)\delta Z_Z - \delta m_Z^2, \tag{2.53}$$
$$\hat\Pi_{\gamma\gamma}[p^2] = \Pi_{\gamma\gamma}^{\rm 1PI}[p^2] + p^2\delta Z_\gamma, \tag{2.54}$$
$$\hat\Pi_{\gamma Z}[p^2] = \Pi_{\gamma Z}^{\rm 1PI}[p^2] - \frac{1}{2}(2p^2-m_Z^2)\delta Z_{\gamma Z} - \frac{m_Z^2}{2s_W c_W}\delta s_W^2, \tag{2.55}$$

where

$$\begin{pmatrix} \delta Z_\gamma \\ \delta Z_Z \end{pmatrix} = \begin{pmatrix} c_W^2 & s_W^2 \\ s_W^2 & c_W^2 \end{pmatrix}\begin{pmatrix} \delta Z_B \\ \delta Z_W \end{pmatrix}, \quad \delta Z_{\gamma Z} = s_W c_W(\delta Z_W - \delta Z_B) = \frac{s_W c_W}{c_W^2-s_W^2}(\delta Z_Z - \delta Z_\gamma), \tag{2.56}$$

and explicit expressions of 1PI diagrams for gauge boson two point functions are given in Appendix.

Imposing following five renormalization conditions as [69]

$$\begin{aligned} &{\rm Re}\hat\Pi_{WW}[m_W^2]=0,\ {\rm Re}\hat\Pi_{ZZ}[m_Z^2]=0,\ \hat\Gamma^\mu_{ee\gamma}[q^2=0,\not{p}_1=\not{p}_2=m_e] = ie\gamma^\mu, \\ &\frac{d}{dp^2}\hat\Pi_{\gamma\gamma}[0]=0,\ \hat\Pi_{\gamma Z}[0]=0, \end{aligned} \tag{2.57}$$

five independent counter terms $\delta m_W^2, \delta m_Z^2, \delta\alpha_{\rm em}, \delta Z_\gamma$ and $\delta Z_{\gamma Z}$ are determined as,

$$\delta m_W^2 = {\rm Re}\Pi_{WW}^{\rm 1PI}[m_W^2], \tag{2.58}$$

$$\delta m_Z^2 = {\rm Re}\Pi_{ZZ}^{\rm 1PI}[m_Z^2], \tag{2.59}$$

$$\frac{\delta e}{e} = \frac{1}{2}\frac{d}{dp^2}\Pi_{\gamma\gamma}^{\rm 1PI}[p^2]\Big|_{p^2=0} - \frac{s_W}{c_W}\frac{\Pi_{\gamma Z}^{\rm 1PI}[0]}{m_Z^2}, \tag{2.60}$$

$$\delta Z_\gamma = -\frac{d}{dp^2}\Pi_{\gamma\gamma}^{\rm 1PI}[p^2]\Big|_{p^2=0}, \tag{2.61}$$

$$\delta Z_{\gamma Z} = -\frac{2}{m_Z^2}\Pi_{\gamma Z}^{\rm 1PI}[0] + \frac{1}{s_W c_W}\delta s_W^2. \tag{2.62}$$

Because of relations as (2.44) and (2.56), other counter terms can be expressed by using above counter terms,

$$\begin{aligned}\frac{\delta s_W^2}{s_W^2} &= \frac{c_W^2}{s_W^2}\left(\frac{\delta m_Z^2}{m_Z^2} - \frac{\delta m_W^2}{m_W^2}\right) \\ &= \frac{c_W^2}{s_W^2}\left(\frac{{\rm Re}\Pi_{ZZ}^{\rm 1PI}[m_Z^2]}{m_Z^2} - \frac{{\rm Re}\Pi_{WW}^{\rm 1PI}[m_W^2]}{m_W^2}\right),\end{aligned} \tag{2.63}$$

$$\begin{aligned}\frac{\delta v}{v} &= \frac{1}{2}\left(\frac{\delta m_W^2}{m_W^2} - \frac{\delta\alpha_{\rm em}}{\alpha_{\rm em}} + \frac{\delta s_W^2}{s_W^2}\right) \\ &= \frac{1}{2}\left(\frac{s_W^2 - c_W^2}{s_W^2}\frac{{\rm Re}\Pi_{WW}^{\rm 1PI}[m_W^2]}{m_W^2} + \frac{c_W^2}{s_W^2}\frac{{\rm Re}\Pi_{ZZ}^{\rm 1PI}[m_Z^2]}{m_Z^2} - \frac{d}{dp^2}\Pi_{\gamma\gamma}^{\rm 1PI}[0]\Big|_{p^2=0} - \frac{2s_W}{c_W}\frac{\Pi_{\gamma Z}^{\rm 1PI}[0]}{m_Z^2}\right),\end{aligned} \tag{2.64}$$

$$\begin{aligned}\delta Z_Z &= \delta Z_\gamma + \frac{c_W^2 - s_W^2}{s_W c_W}\delta Z_{\gamma Z} \\ &= \frac{c_W^2 - s_W^2}{s_W^2}\left(\frac{{\rm Re}\Pi_{ZZ}^{\rm 1PI}[m_Z^2]}{m_Z^2} - \frac{{\rm Re}\Pi_{WW}^{\rm 1PI}[m_W^2]}{m_W^2}\right) - \frac{d}{dp^2}\Pi_{\gamma\gamma}^{\rm 1PI}[0]\Big|_{p^2=0} + \frac{2}{m_Z^2}\frac{c_W^2 - s_W^2}{s_W c_W}\Pi_{\gamma Z}^{\rm 1PI}[0],\end{aligned} \tag{2.65}$$

$$\begin{aligned}\delta Z_W &= \delta Z_\gamma + \frac{c_W}{s_W}\delta Z_{\gamma Z} \\ &= \frac{c_W^2}{s_W^2}\left(\frac{{\rm Re}\Pi_{ZZ}^{\rm 1PI}[m_Z^2]}{m_Z^2} - \frac{{\rm Re}\Pi_{WW}^{\rm 1PI}[m_W^2]}{m_W^2}\right) - \frac{d}{dp^2}\Pi_{\gamma\gamma}^{\rm 1PI}[0]\Big|_{p^2=0} + \frac{2c_W}{s_W}\frac{{\rm Re}\Pi_{\gamma Z}[0]}{m_Z^2}.\end{aligned} \tag{2.66}$$

Renormalization in fermion sector in the SM

We here discuss renormalization in the one-fermion sector, in which there is a kind of fermions, because of simplification. Lagrangian of the fermion sector is

$$\mathcal{L}_f = \bar\Psi_L i\partial\!\!\!/\Psi_L + \bar\Psi_R i\partial\!\!\!/\Psi_R - m_f(\bar\Psi_L\Psi_R + \bar\Psi_R\Psi_L). \tag{2.67}$$

In the fermion sector, there are one parameter m_f and left handed fermions Ψ_L and right handed fermions Ψ_R. They are shifted into renormalized parameter and renormalized fields,

and counter terms,

$$m_f \to m_f + \delta m_f, \tag{2.68}$$

$$\Psi_L \to \Psi_L + \frac{1}{2}\delta Z_L^f, \tag{2.69}$$

$$\Psi_R \to \Psi_L + \frac{1}{2}\delta Z_R^f. \tag{2.70}$$

Two point functions of fermion fields are composed of following two parts,

$$\hat{\Pi}_{ff}[p^2] = \hat{\Pi}_{ff,V}[p^2] + \hat{\Pi}_{ff,A}[p^2]. \tag{2.71}$$

Each part is expressed,

$$\hat{\Pi}_{ff,V}[p^2] = \not{p}\Pi_{ff,V}^{\rm 1PI}[p^2] + \not{p}\delta Z_V^f + m_f\Pi_{ff,S}^{\rm 1PI}[p^2] - m_f\delta Z_V^f - \delta m_f, \tag{2.72}$$

$$\hat{\Pi}_{ff,A}[p^2] = -\not{p}\gamma_5\left(\Pi_{ff,A}^{\rm 1PI}[p^2] + \delta Z_A^f\right), \tag{2.73}$$

where

$$\delta Z_V^f = \frac{1}{2}(\delta Z_L^f + \delta Z_R^f), \quad \delta Z_A^f = \frac{1}{2}(\delta Z_L^f - \delta Z_R^f). \tag{2.74}$$

We determine the counter terms by following conditions,

$$\hat{\Pi}_{ff,V}[m_f]\Big|_{p^2=m^2} = 0, \quad \frac{d}{d\not{p}}\hat{\Pi}_{ff,V}[p^2]\Big|_{p^2=m^2} = 0, \quad \frac{d}{d\not{p}}\hat{\Pi}_{ff,A}[p^2]\Big|_{p^2=m^2} = 0. \tag{2.75}$$

Then we obtain each counter term,

$$\delta m_f = m_f\left(\Pi_{ff,V}^{\rm 1PI}[m_f^2] + \Pi_{ff,S}^{\rm 1PI}[m_f^2]\right), \tag{2.76}$$

$$\delta Z_V^f = -\Pi_{ff,V}^{\rm 1PI}[m_f^2] - 2m_f^2\left(\frac{d}{dp^2}\Pi_{ff,V}^{\rm 1PI}[p^2] + \frac{d}{dp^2}\Pi_{ff,S}^{\rm 1PI}[p^2]\right)\Big|_{p^2=m_f^2}, \tag{2.77}$$

$$\delta Z_A = -\Pi_{ff,A}^{\rm 1PI}[m_f^2] + 2m_f^2\frac{d}{dp^2}\Pi_{ff,A}^{\rm 1PI}[p^2]\Big|_{p^2=m_f^2}. \tag{2.78}$$

2.7 One-loop level corrected electroweak observables

2.7.1 Renormalized electroweak parameters

Because we have obtained explicit forms of counter terms for all independent parameters in the gauge sector, we can calculate the one-loop level predictions for electroweak observables such as electroweak precision parameter Δr and renormalized W boson mass $m_W^{\rm reno}$. We here list the renormalized electroweak parameter Δr and renormalized W boson mass $m_W^{\rm reno}$. They can be expressed as [69]

$$\begin{aligned}\Delta r = {} & \frac{d}{dp^2}\Pi_{\gamma\gamma}^{\rm 1PI}[p^2]\Big|_{p^2=0} - \frac{c_W^2}{s_W^2}\left(\frac{{\rm Re}\Pi_{ZZ}^{\rm 1PI}[m_Z^2]}{m_Z^2} - \frac{{\rm Re}\Pi_{WW}^{\rm 1PI}[m_W^2]}{m_W^2} - \frac{2s_W}{c_W}\frac{\Pi_{\gamma Z}^{\rm 1PI}[0]}{m_Z^2}\right) \\ & + \frac{\Pi_{WW}^{\rm 1PI}[0] - \Pi_{WW}^{\rm 1PI}[m_W^2]}{m_W^2} + \delta_{VB},\end{aligned} \tag{2.79}$$

$$(m_W^{\rm reno})^2 = \frac{m_Z^2}{2}\left(1 + \sqrt{1 - \frac{4\pi\alpha_{\rm em}}{\sqrt{2}G_F m_Z^2(1-\Delta r)}}\right), \tag{2.80}$$

where δ_{VB} is the box and the vertex diagram contributions to the muon decay process, which is given by [69]

$$\delta_{VB} = \frac{\alpha_{\rm em}}{4\pi s_W^2}\left(6 + \frac{7-4s_W^2}{2s_W^2}\ln\frac{m_W^2}{m_Z^2}\right). \tag{2.81}$$

Moreover, we also can calculate electroweak S, T and U parameters as [79]

$$S = \frac{16\pi}{m_Z^2}{\rm Re}\left[\frac{c_{2W}}{eg_Z}\left(\Pi^{\rm 1PI}_{Z\gamma}[m_Z^2] - \Pi^{\rm 1PI}_{Z\gamma}[0]\right) + \frac{s_W^2 c_W^2}{e^2}\left(\Pi^{\rm 1PI}_{\gamma\gamma}[m_Z^2] - \Pi^{\rm 1PI}_{\gamma\gamma}[0]\right) + \frac{1}{g_Z^2}\left(\Pi^{\rm 1PI}_{ZZ}[0] - \Pi^{\rm 1PI}_{ZZ}[m_Z^2]\right)\right], \tag{2.82}$$

$$T = \frac{1}{\alpha_{\rm em}}{\rm Re}\left[-\frac{\Pi^{\rm 1PI}_{WW}[0]}{m_W^2} + \frac{\Pi^{\rm 1PI}_{ZZ}[0]}{m_Z^2} + 2\frac{s_W}{c_W}\frac{\Pi^{\rm 1PI}_{\gamma Z}[0]}{m_Z^2} + \frac{s_W^2}{c_W^2}\frac{\Pi^{\rm 1PI}_{\gamma\gamma}[0]}{m_Z^2}\right], \tag{2.83}$$

$$U = 16\pi{\rm Re}\left[-\frac{1}{m_Z^2}\left\{\frac{1}{g_Z^2}\left(\Pi^{\rm 1PI}_{ZZ}[0] - \Pi^{\rm 1PI}_{ZZ}[m_Z^2]\ \right) + \frac{2s_W^2}{eg_Z}\left(\Pi^{\rm 1PI}_{Z\gamma}[0] - \Pi^{\rm 1PI}_{Z\gamma}[m_Z^2]\right) + \frac{s_W^4}{e^2}\left(\Pi^{\rm 1PI}_{\gamma\gamma}[0] - \Pi^{\rm 1PI}_{\gamma\gamma}[m_Z^2]\right) + \frac{1}{g^2 m_W^2}\left(\Pi^{\rm 1PI}_{WW}[0] - \Pi^{\rm 1PI}_{WW}[m_W^2]\right)\right\}\right], \tag{2.84}$$

where $g_Z = g/c_W$.

2.7.2 Renormalized Higgs couplings

In this subsection, we give formulae of renormalized Higgs couplings composed of three parts; namely the tree level part, the counter term part and 1PI diagram part. hVV couplings and hff couplings are composed of a number of form factors as,

$$\hat\Gamma_{hVV}[p_1^2,p_2^2,q^2] = \hat\Gamma^1_{hVV}[p_1^2,p_2^2,q^2]g^{\mu\nu} + \hat\Gamma^2_{hVV}[p_1^2,p_2^2,q^2]\frac{p_1^\nu p_2^\mu}{m_V^2} + i\hat\Gamma^3_{hVV}[p_1^2,p_2^2,q^2]\epsilon^{\mu\nu\rho\sigma}\frac{p_{1\rho}p_{2\sigma}}{m_V^2}, \tag{2.85}$$

$$\begin{aligned}\hat\Gamma_{hff}[p_1^2,p_2^2,q^2] = {}& \hat\Gamma^S_{hff}[p_1^2,p_2^2,q^2] + \gamma_5\hat\Gamma^P_{hff}[p_1^2,p_2^2,q^2] + \not{p}_1\hat\Gamma^{V1}_{hff}[p_1^2,p_2^2,q^2] + \not{p}_2\hat\Gamma^{V2}_{hff}[p_1^2,p_2^2,q^2]\\ &+ \not{p}_1\gamma_5\hat\Gamma^{A1}_{hff}[p_1^2,p_2^2,q^2] + \not{p}_2\gamma_5\hat\Gamma^{A2}_{hff}[p_1^2,p_2^2,q^2]\\ &+ \not{p}_1\not{p}_2\hat\Gamma^T_{hff}[p_1^2,p_2^2,q^2] + \not{p}_1\not{p}_2\gamma_5\hat\Gamma^{TP}_{hff}[p_1^2,p_2^2,q^2].\end{aligned} \tag{2.86}$$

Each renormalized form factor is given by,

$$\Gamma^i_{hVV}[p_1^2,p_2^2,q^2] = \frac{2m_V^2}{v}\kappa_{V,\rm tree} + \delta\Gamma^i_{hVV} + \Gamma^{\rm 1PI}_{hVV,i}[p_1^2,p_2^2,q^2], \quad (i=1,2,3) \tag{2.87}$$

$$\Gamma^j_{hff}[p_1^2,p_2^2,q^2] = -\frac{m_f}{v}\kappa_{f,\rm tree} + \delta\Gamma^j_{hff} + \Gamma^{\rm 1PI}_{hff,j}[p_1^2,p_2^2,q^2], \quad (j=S,P,V1,V2,A1,A2,T,TP), \tag{2.88}$$

where specific forms of counter terms are

$$\delta\Gamma^1_{hVV} = \frac{2m_V^2}{v}\left(\frac{\delta m_V^2}{m_V^2} - \frac{\delta v}{v} + \delta Z_V + \frac{1}{2}\delta Z_h\right), \tag{2.89}$$

$$\delta\Gamma^2_{hVV} = \delta\Gamma^3_{hVV} = 0, \tag{2.90}$$

$$\delta\Gamma^S_{hff} = -\frac{m_f}{v}\left(\frac{\delta m_f}{m_f} - \frac{\delta v}{v} + \delta Z_f^V + \frac{1}{2}\delta Z_h\right), \tag{2.91}$$

$$\delta\Gamma^P_{hff} = \delta\Gamma^{V1}_{hff} = \delta\Gamma^{V2}_{hff} = \delta\Gamma^{A1}_{hff} = \delta\Gamma^{A2}_{hff} = \delta\Gamma^T_{hff} = \delta\Gamma^{TP}_{hff} = 0, \tag{2.92}$$

where δm_W^2, δZ_V and δv are given in Sec. 2.6.1 and δm_f and δZ_f^V are given in Sec. 2.6.1.

On the other hand, there is only a form factor of the scalar vertex in all orders in the the Higgs self coupling. The renormalized Higgs triple coupling is given by,

$$\Gamma_{hhh}[p_1^2, p_2^2, q^2] = 3!\lambda_{hhh} + 3!\delta\Gamma_{hhh} + \Gamma^{\rm 1PI}_{hhh}[p_1^2, p_2^2, q^2], \tag{2.93}$$

where λ_{XYZ} is the coefficient of the XYZ coupling in the Lagrangian and $\delta\Gamma_{hhh}$ is expressed as

$$\delta\Gamma_{hhh} = -\frac{\delta m_h^2}{2v} + \frac{m_h^2}{2v^2}\delta v + \frac{3}{2}\lambda_{hhh}\delta Z_h. \tag{2.94}$$

If we expand $\Gamma_{hhh}[p_1^2, p_2^2, q^2]$ in the limit $m_t \to \infty$, the quartic power of m_t appears in $\Gamma_{hhh}[p_1^2, p_2^2, q^2]$ as follows,

$$\Gamma_{hhh}[p_1^2, p_2^2, q^2] = \frac{3m_h^2}{v}\left(1 - \frac{N_{C_t}}{3\pi^2}\frac{m_t^4}{v^2 m_h^2}\right), \tag{2.95}$$

where N_{C_t} is the color number of the top quark. This result corresponds with that calculated by the effective potential method [70].

Fig. 2.7.2 shows the one-loop contributions of electroweak sectors to hhh couplings as a functions of $\sqrt{q^2}$ in the SM, where q^μ is the momentum of the off-shell h in $h^* \to hh$. We take the mass of the Higgs boson and that of top quark to be 126 GeV and 173 GeV, respectively. We can see that the one-loop contributions becomes negative value in the limit $q^2 \to 0$. The result is consistent with Eq. (2.95). The threshold effect at $q = 2m_t$ contributes the one-loop corrections to be positive value.

Effective potential method

We describe effective potential method for calculation of the renormalized hhh coupling [70]. We can comparatively easily evaluate the renormalized quantity with zero external momenta at each loop level by using effective potential method. The one-loop level effective potential of the SM is given by,

$$V_{\rm eff}[\varphi] = V_{\rm tree}[\varphi] + \frac{1}{64\pi^2}N_{C_i}N_{S_i}(-1)^{2S_i}M_i^4[\varphi]\left(\ln\left[\frac{M_i^2[\varphi]}{Q^2}\right] - \frac{3}{2}\right), \tag{2.96}$$

where φ, N_{c_i}, N_{S_i}, S_i, $M_i[\varphi]$ and Q indicate the order parameter, the color number of a particle i, the degree of the spin for a particle i, the spin, the mass of i and the renormalization scale,

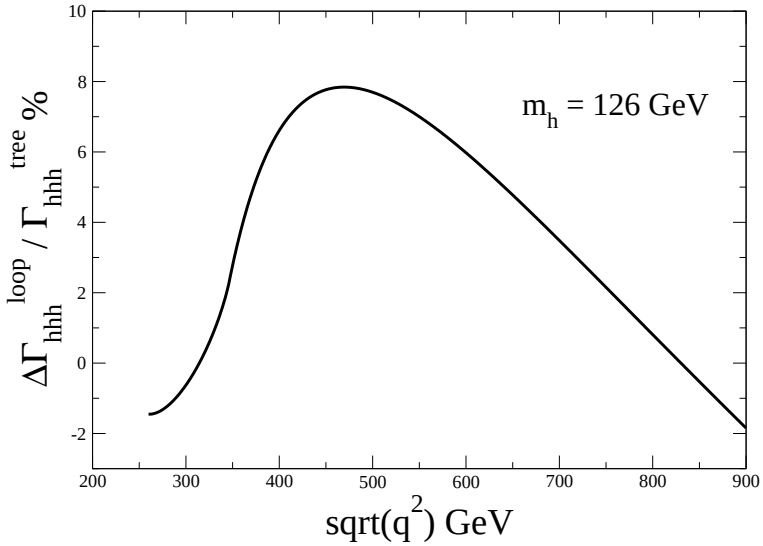

Figure 2.2: The one-loop contributions of electroweak sectors to hhh couplings as a functions of $\sqrt{q^2}$ in the SM, where q^μ is the momentum of the off-shell h in $h^* \to hh$.

respectively. The renormalization scale Q can be absorbed by the following renormalization conditions,

$$\frac{\partial}{\partial\varphi} V_{\rm eff}[\varphi]\Big|_{\varphi=v} = 0, \tag{2.97}$$

$$\frac{\partial^2}{\partial\varphi^2} V_{\rm eff}[\varphi]\Big|_{\varphi=v} = m_h^2. \tag{2.98}$$

The renormalized Higgs self coupling $\Gamma^{\rm SM}_{hhh}$ can be calculated by

$$\frac{\partial^3}{\partial\varphi^3} V_{\rm eff}[\varphi]\Big|_{\varphi=v} \sim \frac{3m_h^2}{v}\left\{1 - \frac{1}{\pi^2}\frac{m_t^4}{v^2 m_h^2}\right\}. \tag{2.99}$$

This result is consistent with that calculated by the diagrammatic method.

Chapter 3

Review of extended Higgs sectors

3.1 Review of four types of the THDMs

3.1.1 Lagrangian of the the THDMs

There are two isospin doublet scalar fields Φ_1 and Φ_2 with $Y = 1/2$. Parts of Lagrangian which are different from that of the SM is given by,

$$\mathcal{L} = \mathcal{L}_{\rm kine} + \mathcal{L}_{\rm Y} - V, \tag{3.1}$$

where $\mathcal{L}_{\rm kine}$, $\mathcal{L}_{\rm Y}$ and V express the kinetic term of the Higgs fields, the Yukawa interaction term and the Higgs potential, respectively.

The kinetic term is

$$\mathcal{L}_{\rm kine} = |D^\mu \Phi_1|^2 + |D^\mu \Phi_2|^2, \tag{3.2}$$

where D^μ is

$$D^\mu = \partial^\mu - i\frac{g}{2}\tau_i W_i^\mu - i\frac{g'}{2}B^\mu. \tag{3.3}$$

The two doublet fields can be parameterized as

$$\Phi_i = \begin{pmatrix} \omega_i^+ \\ \phi_i \end{pmatrix}, \quad \phi_i = \frac{1}{\sqrt{2}}(h_i + v_i + iz_i),\ i = 1, 2, \tag{3.4}$$

where v_i is the VEV of each Higgs field. Masses of weak gauge bosons are derived from $\mathcal{L}_{\rm kine}$ as,

$$m_W^2 = \frac{g^2}{4}\left(v_1^2 + v_2^2\right), \quad m_Z^2 = \frac{g_Z^2}{4}\left(v_1^2 + v_2^2\right), \tag{3.5}$$

where $g_Z = g/\cos\theta_W$. Since existence of v_1 and v_2 occur the electroweak symmetry breaking, the VEVs can be defined by $v^2 \equiv v_1^2 + v_2^2 = \sqrt{2}G_F^{-1} \simeq (246\text{GeV})^2$.

The general Higgs potential [38] is given by,

$$\begin{aligned} V =& m_1^2\Phi_1^\dagger\Phi_1 + m_2^2\Phi_2^\dagger\Phi_2 - m_3^2(\Phi_1^\dagger\Phi_2 + \Phi_2^\dagger\Phi_1) \\ &+ \frac{\lambda_1}{2}(\Phi_1^\dagger\Phi_1)^2 + \frac{\lambda_2}{2}(\Phi_2^\dagger\Phi_2)^2 + \lambda_3(\Phi_1^\dagger\Phi_1)(\Phi_2^\dagger\Phi_2) + \lambda_4(\Phi_1^\dagger\Phi_2)(\Phi_2^\dagger\Phi_1) \\ &+ \frac{\lambda_5}{2}\left[(\Phi_1^\dagger\Phi_2)^2 + (\Phi_2^\dagger\Phi_1)^2 + \lambda_6|\Phi_1|^2\Phi_1^\dagger\Phi_2 + \lambda_7|\Phi_2|^2\Phi_1^\dagger\Phi_2 + h.c.\right], \end{aligned} \tag{3.6}$$

where m_1^2, m_2^2, $\lambda_1 - \lambda_4$ are real parameters, while m_3^2 and λ_5-λ_7 are generally complex.

We here retake the basis of the two Higgs fields so that only one of the pair has a VEV,

$$\begin{pmatrix} \Phi_1 \\ \Phi_2 \end{pmatrix} = R(\beta) \begin{pmatrix} \Phi \\ \Psi \end{pmatrix}, \tag{3.7}$$

where

$$\Phi = \begin{pmatrix} G^+ \\ \frac{1}{\sqrt{2}}(h_1' + v + iG^0) \end{pmatrix}, \quad \Psi = \begin{pmatrix} H^+ \\ \frac{1}{\sqrt{2}}(h_2' + iA) \end{pmatrix}, \tag{3.8}$$

where $v \simeq 246$ GeV, $\tan\beta = v_2/v_1$ and $G^\pm$ and G^0 are Nambu-Gorldstone bosons. This basis is so-called the Georgi basis. Higgs field components of the Georgi basis are related with those of the original basis as,

$$\begin{pmatrix} h_1 \\ h_2 \end{pmatrix} = R(\beta) \begin{pmatrix} h_1' \\ h_2' \end{pmatrix}, \quad \begin{pmatrix} z_1 \\ z_2 \end{pmatrix} = R(\beta) \begin{pmatrix} G^0 \\ A \end{pmatrix}, \quad \begin{pmatrix} \omega_1^+ \\ \omega_2^+ \end{pmatrix} = R(\beta) \begin{pmatrix} G^+ \\ H^+ \end{pmatrix}. \tag{3.9}$$

$H^\pm$ and A are the pair of charged Higgs bosons and a CP-odd Higgs boson and they are mass eigenstates. On the other hand, in general, CP-even scalar components h_1' and h_2' are not diagnarized at this stage.

Using the Georgi basis, the Yukawa interaction term $\mathcal{L}_{\rm Y}$ can be expressed as,

$$-\mathcal{L}_{\rm Y} = \bar{Q}_L \left(\frac{M_d}{v}\Phi + Y_d \Psi \right) d_R + \bar{Q}_L \left(\frac{M_u}{v}\tilde{\Phi} + Y_u \tilde{\Psi} \right) u_R + \bar{L}_L \left(\frac{M_l}{v}\Phi + Y_l \Psi \right) l_R + h.c., \tag{3.10}$$

where M_i and Y_i $(i = u, d, l)$ are the mass matrix and any matrix, respectively. In contrast to M_i which is diagnarized, Y_i is the non-diagonarizec matrix. Because there is no matrix which can perform simultaneous diagonalization of the mass matrices and the Yukawa interaction matrices, FCNCs appear at the tree level [36,37]. Tree level FCNCs can be naturally forbidden by introducing any symmetry. For example, it is known that there is a way to forbid tree level FCNCs by a discrete Z_2 symmetry [36].

In order to discuss the Yukawa interaction of the THDMs with the discrete Z_2 symmetry, we restore the basis of Higgs fields. There can be four different types of Yukawa interactions, depending on the assignment of the Z_2 charge for Φ_1, Φ_2 and fermion fields [41]. We call them, the Type-I, the Type-II, the Type-X and the Type-Y THDM [42]. We define the Z_2 charges for scalar and fermion fields as shown in Tab. 3.1. Then, each fermion couples to only one kind of Higgs field in the Yukawa interaction term as follows,

$$-\mathcal{L}_{\rm Y} = \bar{Q}_L Y_d \Phi_i d_R + \bar{Q}_L Y_u \tilde{\Phi}_j u_R + \bar{L}_L Y_l \Phi_k l_R + h.c., \tag{3.11}$$

where Y_i indicates any non-diagnarized matrix and $\Phi_{i,j,k}$ are Φ_1 or Φ_2. Matrices U_{CKM} as given at Eqs. (2.16) can diagnarize Y_d matrix as,

$$-\mathcal{L}_{\rm Y} = \bar{Q}_L Y_u^{diag} \tilde{\Phi}_i u_R - \bar{Q}_L (U_{CKM} Y_d^{diag}) \Phi_j d_R - \bar{L}_L Y_l^{diag} \Phi_k l_R + \text{h.c} \tag{3.12}$$

$$= -\bar{Q}_L \frac{M_u}{v_i} \tilde{\Phi}_i u_R - \bar{Q'}_L \frac{M_d}{v_j} \Phi_j d_R - \bar{L}_L \frac{M_l}{v_k} \Phi_k l_R + \text{h.c.}, \tag{3.13}$$

where

$$Q' = U_{CKM}^{\dagger} Q = U_{CKM}^{\dagger} \begin{pmatrix} u \\ d' \end{pmatrix} = \begin{pmatrix} U_{CKM}^{\dagger} u \\ d \end{pmatrix} = \begin{pmatrix} u' \\ d \end{pmatrix}. \tag{3.14}$$

We find that FCNC processes do not appear at the tree level in the Yukawa interaction term because the mass matrix and the Yukawa interaction matrix of each fermion field are the same one.

	Z_2 charge							Mixing factor		
	Φ_1	Φ_2	Q_L	L_L	u_R	d_R	e_R	ξ_u	ξ_d	ξ_e
Type-I	+	−	+	+	−	−	−	$\cot\beta$	$\cot\beta$	$\cot\beta$
Type-II	+	−	+	+	−	+	+	$\cot\beta$	$-\tan\beta$	$-\tan\beta$
Type-X	+	−	+	+	−	−	+	$\cot\beta$	$\cot\beta$	$-\tan\beta$
Type-Y	+	−	+	+	−	+	−	$\cot\beta$	$-\tan\beta$	$\cot\beta$

Table 3.1: Charge assignment of the softly-broken Z_2 symmetry and the mixing factors in Yukawa interactions given in Eq. (3.13).

In the THDMs with the softly broken Z_2 symmetry, the Higgs potential [38] is written as

$$\begin{aligned} V =& m_1^2 \Phi_1^{\dagger}\Phi_1 + m_2^2 \Phi_2^{\dagger}\Phi_2 - m_3^2(\Phi_1^{\dagger}\Phi_2 + \Phi_2^{\dagger}\Phi_1) \\ &+ \frac{\lambda_1}{2}(\Phi_1^{\dagger}\Phi_1)^2 + \frac{\lambda_2}{2}(\Phi_2^{\dagger}\Phi_2)^2 + \lambda_3(\Phi_1^{\dagger}\Phi_1)(\Phi_2^{\dagger}\Phi_2) + \lambda_4(\Phi_1^{\dagger}\Phi_2)(\Phi_2^{\dagger}\Phi_1) \\ &+ \frac{\lambda_5}{2}\left[(\Phi_1^{\dagger}\Phi_2)^2 + (\Phi_2^{\dagger}\Phi_1)^2\right], \end{aligned} \tag{3.15}$$

where m_3 means the soft broken scale of the Z_2 symmetry.

Tadpoles for Higgs potential in this model are

$$T_{h_1} = v_1\left(m_1^2 - \frac{M^2 v_2^2}{v^2} + \frac{1}{2}\lambda_1 v_1^2 + \frac{1}{2}(\lambda_3+\lambda_4+\lambda_5)v_2^2\right), \tag{3.16}$$

$$T_{h_2} = v_2\left(m_2^2 - \frac{M^2 v_1^2}{v^2} + \frac{1}{2}\lambda_2 v_2^2 + \frac{1}{2}(\lambda_3+\lambda_4+\lambda_5)v_1^2\right). \tag{3.17}$$

The stationary conditions $T_{h_1} = 0$ and $T_{h_2} = 0$ can make m_1 and m_2 dependent parameters as,

$$m_1^2 = \frac{M^2 v_2^2}{v^2} - \frac{1}{2}\lambda_1 v_1^2 - \frac{1}{2}(\lambda_3+\lambda_4+\lambda_5)v_2^2, \tag{3.18}$$

$$m_2^2 = \frac{M^2 v_1^2}{v^2} - \frac{1}{2}\lambda_2 v_2^2 - \frac{1}{2}(\lambda_3+\lambda_4+\lambda_5)v_1^2. \tag{3.19}$$

The mass term of the Higgs potential $V_{\rm mass}$ can be arranged as follows,

$$
\begin{aligned}
V_{\rm mass} &= (\omega_1^+, \omega_2^+) \begin{pmatrix} \left(M^2 - \frac{v^2}{2}(\lambda_4+\lambda_5)\right) s_\beta^2 & \left(-M^2 + \frac{v^2}{2}(\lambda_4+\lambda_5)\right) s_\beta c_\beta \\ \left(-M^2 + \frac{v^2}{2}(\lambda_4+\lambda_5)\right) s_\beta c_\beta & \left(M^2 - \frac{v^2}{2}(\lambda_4+\lambda_5)\right) c_\beta^2 \end{pmatrix} \begin{pmatrix} \omega_1^- \\ \omega_2^- \end{pmatrix} \\
&+ \frac{1}{2}(z_1, z_2) \begin{pmatrix} (M^2 - \lambda_5 v^2) s_\beta^2 & (-M^2 + \lambda_5 v^2) s_\beta c_\beta \\ (-M^2 + \lambda_5 v^2) s_\beta c_\beta & (M^2 - \lambda_5 v^2) c_\beta^2 \end{pmatrix} \begin{pmatrix} z_1^- \\ z_2^- \end{pmatrix} \\
&+ \frac{1}{2}(h_1, h_2) \begin{pmatrix} \frac{1}{2}\left(M^2 + \lambda_1 v^2 + (-M^2 + \lambda_1 v^2) c_{2\beta}\right) & \left(-M^2 + v^2(\lambda_4+\lambda_5)\right) s_\beta c_\beta \\ \left(-M^2 + v^2(\lambda_4+\lambda_5)\right) s_\beta c_\beta & \frac{1}{2}\left(M^2 + \lambda_2 v^2 + (M^2 - \lambda_2 v^2) c_{2\beta}\right) \end{pmatrix} \begin{pmatrix} h_1 \\ h_2 \end{pmatrix} \\
&= (\omega_1^+, \omega_2^+) R(\beta) \begin{pmatrix} 0 & 0 \\ 0 & m_{H^+}^2 \end{pmatrix} R^{-1}(\beta) \begin{pmatrix} \omega_1^- \\ \omega_2^- \end{pmatrix} \\
&+ \frac{1}{2}(z_1, z_2) R(\beta) \begin{pmatrix} 0 & 0 \\ 0 & m_A^2 \end{pmatrix} R^{-}(\beta) \begin{pmatrix} z_1 \\ z_2 \end{pmatrix} \\
&+ \frac{1}{2}(h_1, h_2) R(\beta) \begin{pmatrix} m_H^2 & 0 \\ 0 & m_h^2 \end{pmatrix} R^{-1}(\beta) \begin{pmatrix} h_1 \\ h_2 \end{pmatrix}, \qquad (3.20)
\end{aligned}
$$

where s_θ and c_θ express $\sin\theta$ and $\cos\theta$, respectively. Then, the mass eigenstates can be expressed by

$$
\begin{pmatrix} G^+ \\ H^+ \end{pmatrix} = R^{-1}(\beta) \begin{pmatrix} \omega_1^+ \\ \omega_2^+ \end{pmatrix}, \quad \begin{pmatrix} G^0 \\ A \end{pmatrix} = R^{-1}(\beta) \begin{pmatrix} z_1 \\ z_2 \end{pmatrix}, \quad \begin{pmatrix} H \\ h \end{pmatrix} = R^{-1}(\alpha) \begin{pmatrix} h_1 \\ h_2 \end{pmatrix}, \qquad (3.21)
$$

and mass formulae of Higgs fields are derived as,

$$
\begin{aligned}
m_{H^+}^2 &= M^2 - \frac{v^2}{2}(\lambda_4 + \lambda_5), && (3.22)\\
m_A^2 &= M^2 - \lambda_5 v^2, && (3.23)\\
m_H^2 &= c_\alpha^2 M_{\rm even11}^2 + s_{2\alpha} M_{\rm even12}^2 + s_\alpha^2 M_{\rm even22}^2, && (3.24)\\
m_h^2 &= s_\alpha^2 M_{\rm even11}^2 - s_{2\alpha} M_{\rm even12}^2 + c_\alpha^2 M_{\rm even22}^2. && (3.25)
\end{aligned}
$$

Original parameters in the Higgs potential can be written using physical parameters by,

$$
\begin{aligned}
\lambda_1 &= \frac{1}{v^2 c_\beta^2}\left(s_\alpha^2 m_h^2 + c_\alpha^2 m_H^2 - M^2 s_\beta^2\right), && (3.26)\\
\lambda_2 &= \frac{1}{v^2 s_\beta^2}\left(c_\alpha^2 m_h^2 + s_\alpha^2 m_H^2 - M^2 c_\beta^2\right), && (3.27)\\
\lambda_3 &= \frac{s_{2\alpha}}{v^2 s_{2\beta}}\left(m_h^2 - m_H^2\right) - \frac{1}{v^2}\left(M^2 - 2m_{H^+}^2\right), && (3.28)\\
\lambda_4 &= \frac{1}{v^2}(m_A^2 - 2m_{H^+}^2 + M^2), && (3.29)\\
\lambda_5 &= \frac{1}{v^2}(M^2 - m_A^2). && (3.30)
\end{aligned}
$$

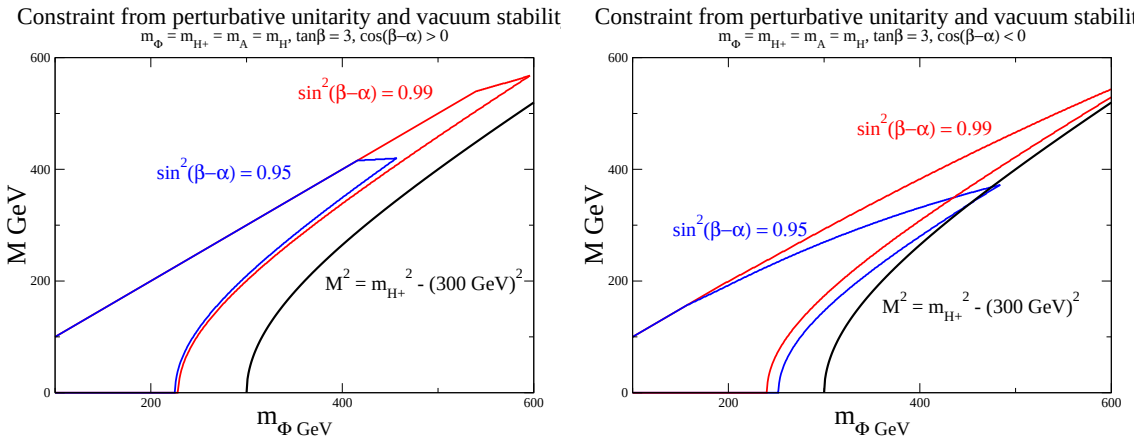

Figure 3.1: The left and the right panel show bounds on the mass of extra Higgs bosons m_Φ and M from perturbative unitarity and vacuum stability for $\cos(\beta-\alpha) > 0$ and $\cos(\beta-\alpha) < 0$, respectively. Inner regions of the red (blue) line are allowed parameter regions for $\sin(\beta-\alpha) = 0.99$ (0.95). All extra Higgs bosons are degenerated in this analysis and $\tan\beta$ is fixed to be 3.

Perturbative unitarity and vacuum stability

Constraints from perturbative unitarity and vacuum stability in the THDMs have been studied in Refs. [71–74] and Refs [75–77], respectively.

There are 14 two-body neutral scattering scattering channels and 8 charged two-body scattering channels. Diagnarizing the 14×14 matrix of $S-$wave amplitudes of the neutral scattering channels and the 8×8 matrix of $S-$wave amplitudes of the charged scattering channels, 7 and 1 eigenstates appear, respectively, as shown below,

$$a_1^\pm = \frac{1}{16\pi}\left\{\frac{3}{2}(\lambda_1+\lambda_2) \pm \sqrt{\frac{9}{4}(\lambda_1-\lambda_2)^2+(2\lambda_3+\lambda_4)^2}\right\} \tag{3.31}$$

$$a_2^\pm = \frac{1}{16\pi}\left\{\frac{1}{2}(\lambda_1+\lambda_2) \pm \sqrt{\frac{1}{4}(\lambda_1-\lambda_2)^2+\lambda_4^2}\right\} \tag{3.32}$$

$$a_3^\pm = d_\pm = \frac{1}{16\pi}\left\{\frac{1}{2}(\lambda_1+\lambda_2) \pm \sqrt{\frac{1}{4}(\lambda_1-\lambda_2)^2+\lambda_5^2}\right\} \tag{3.33}$$

$$a_4^\pm = \frac{1}{16\pi}(\lambda_3+2\lambda_4\pm3\lambda_5) \tag{3.34}$$

$$a_5^\pm = \frac{1}{16\pi}(\lambda_3\pm\lambda_4) \tag{3.35}$$

$$a_6^\pm = \frac{1}{16\pi}(\lambda_3\pm\lambda_5). \tag{3.36}$$

The perturbative unitarity bound from scalar fields 2-body scattering $S-$wave amplitudes are given by

$$|a_i^\pm| < \frac{1}{2}. \quad (i=1-6) \tag{3.37}$$

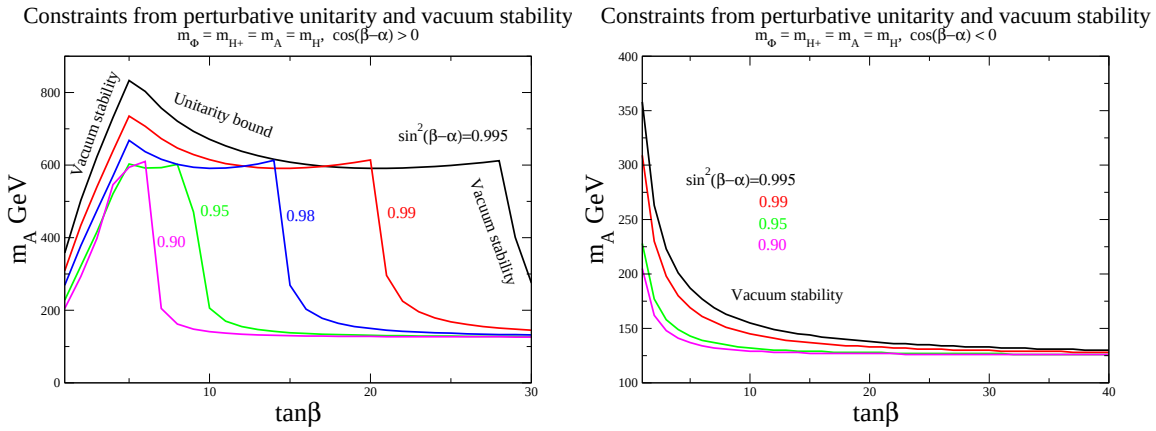

Figure 3.2: Constraints for $\tan\beta$-m_A plane from perturbative unitarity and vacuum stability. Lower regions from the black, the red, the blue, the green and the magenta line are allowed parameter regions for $\sin^2(\beta-\alpha) = 0.995$, 0.99, 0.98, 0.95 and 0.90, respectively. All extra Higgs bosons are degenerated in this analysis and M^2 is scanned with the range $0 \leq M^2 \leq m_\Phi^2$. The left and the right plane are the case for $\cos(\beta-\alpha) > 0$ and $\cos(\beta-\alpha) < 0$, respectively.

On the other hand, the conditions of vacuum stability are expressed by

$$\lambda_1 > 0,\ \lambda_2 > 0,\ \sqrt{\lambda_1\lambda_2} + \lambda_3 + \mathrm{MIN}(0, \lambda_4+\lambda_5, \lambda_4-\lambda_5) > 0. \tag{3.38}$$

These theoretical constraints give bounds on masses od Higgs bosons and mixing parameters. Fig. 3.1.1 shows bounds on the mass of extra Higgs bosons m_Φ and M from perturbative unitarity and vacuum stability. Inner regions of the red (blue) line are allowed parameter regions for $\sin(\beta-\alpha) = 0.99$ (0.95). All extra Higgs bosons are degenerated in this analysis and $\tan\beta$ is fixed to be 3. The left and the right plane indicate the case for $\cos(\beta-\alpha) > 0$ and $\cos(\beta-\alpha) < 0$, respectively. We can find that only parameter regions for $m_\Phi^2 \simeq M^2$ are allowed in the large extra Higgs boson mass regions. If the value of $\tan\beta$ is larger, the bounds on the parameters become more strict.

In Fig. 3.1.1, we shows constraints for $\tan\beta$-m_A plane from perturbative unitarity and vacuum stability. Lower regions from the black, the red, the blue, the green and the magenta line are allowed parameter regions for $\sin^2(\beta-\alpha) = 0.995$, 0.99, 0.98, 0.95 and 0.90, respectively. All extra Higgs bosons are degenerated in this analysis and M^2 is scanned with the range $0 \leq M^2 \leq m_\Phi^2$. The left and the right plane are the case for $\cos(\beta-\alpha) > 0$ and $\cos(\beta-\alpha) < 0$, respectively. If the value of $\tan\beta$ becomes large, the bound on m_Φ becomes more strict. In particular, the bound on m_Φ in the case with $\cos(\beta-\alpha) < 0$ is stronger than that in the case with $\cos(\beta-\alpha) < 0$.

Decay branching rations of Higgs bosons

In order to try to directly detect extra Higgs bosons, it is important to know how the extra Higgs bosons decay into light particles. In this subsection, we show total widths and decay branching rations of extra Higgs bosons H, A and $H^\pm$ [42, 57, 78]. A full set formulae of decay rates for extra Higgs bosons are given in Appendix.

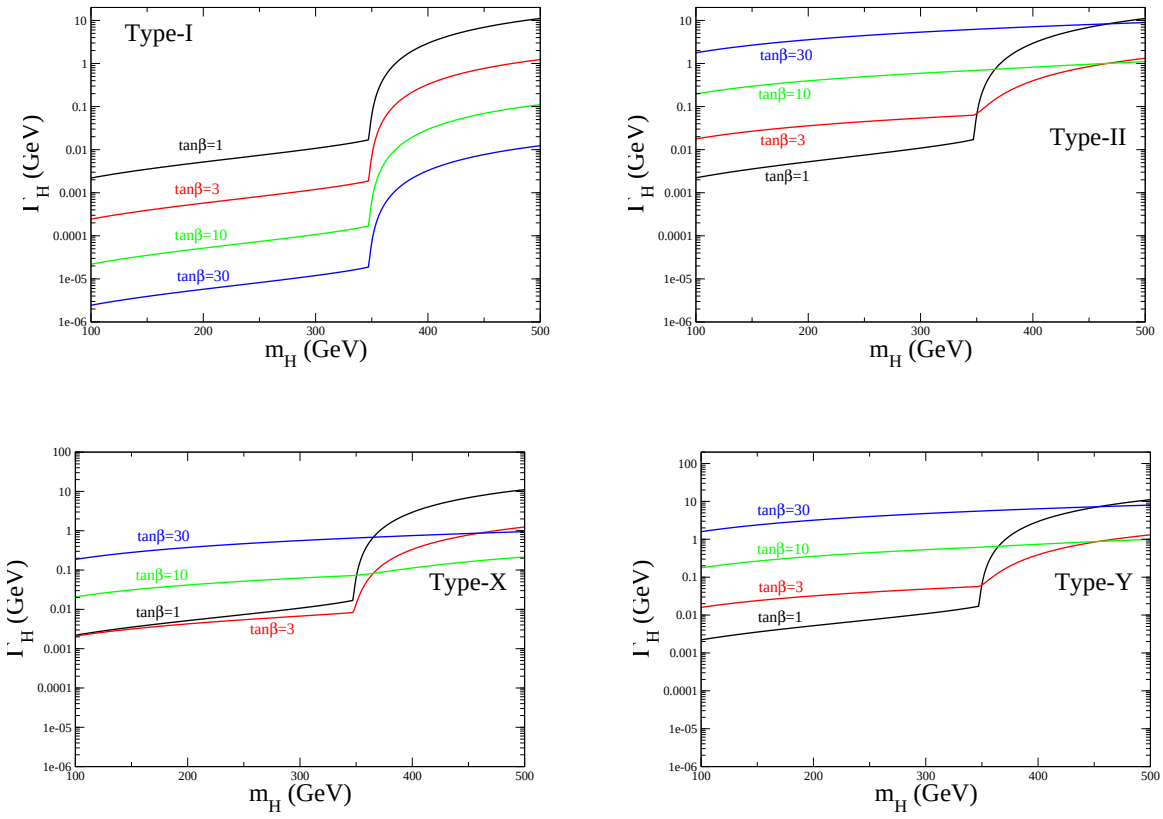

Figure 3.3: These panels are the total width (the decay branching ratio) of the Higgs boson(H) in the THDM. Here, masses of additional Higgs bosons are fixed, $m_H = m_A = m_{H^+}$.The mass of the soft breaking parameter M is $M = m_H - 1$GeV. Mixing angle among scalar fields are set $\sin(\beta - \alpha) = 1$.

In Fig. 3.1.1, the black, the red, the green and the blue lines show the total decay width (Γ_H) of H as a function of m_H in four types of THDMs for $\tan\beta = 1$, 2, 3 and 4, respectively. We also take $m_{H^\pm} = m_A = m_H = M$ and $\sin(\beta - \alpha) - 1$. Γ_H is drastically enhanced around $m_H = m_t$ because the decay channel $H \to t\bar{t}$ is opened. In the Type-II, X and Y, Γ_H is increased as the value of $\tan\beta$ becomes larger because of the factor $\tan\beta$ in the $h\bar{b}b$ and/or $h\tau\tau$ vertices. In Fig. 3.1.1, each colored line is the decay branching ratio of the extra Higgs bosons for each channel ($\Phi \to XX$) as a function of $\tan\beta$ in four types of the THDMs. We also take all the extra Higgs bosons degenerated with $m_\Phi = 150$ GeV and fix $\sin(\beta - \alpha)$ to be 1. There in no processes where Φ decays into weak gauge bosons W/Z because of $\sin(\beta - \alpha) = 1$, so that lighter H and A dominantly decay into $b\bar{b}$ and $H^\pm$ dominantly decay into $\tau\nu$. In the Type-II and X, the $H(A) \to \tau\tau$ decay mode is also important in the case where the value of $\tan\beta$ is large.

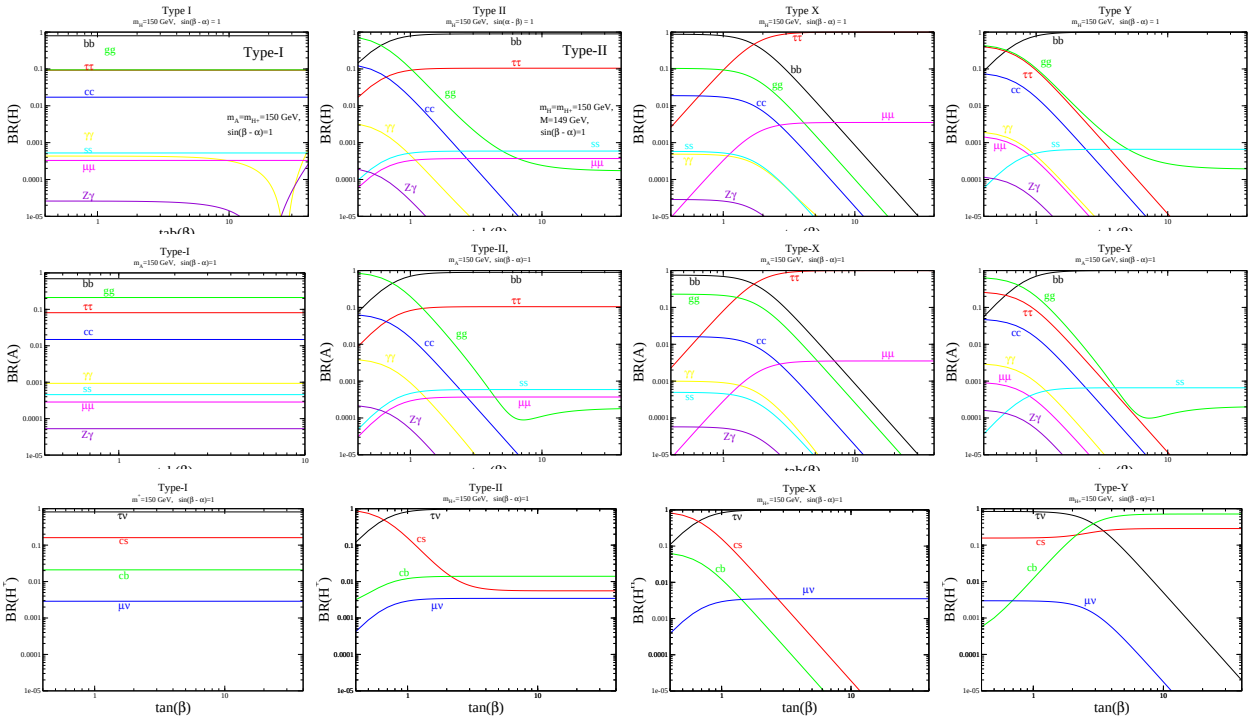

Figure 3.4: These figure are the decay branching ratio of the Higgs boson(H) in the THDM. Here, masses of additional Higgs bosons are fixed, $m_H = m_A = m_{H^+} = 150$GeV.The mass of the soft breaking parameter M is $M = m_H - 1$GeV.Mixing angle among scalar fields are set $\sin(\beta - \alpha) = 1$.

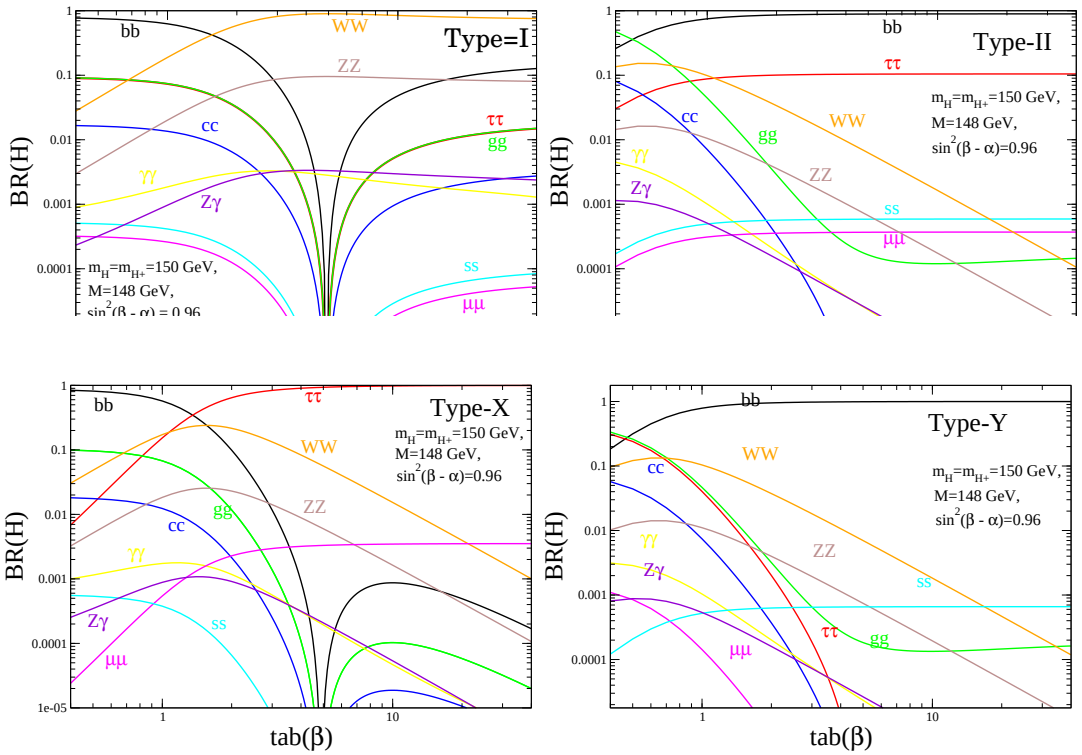

Figure 3.5: These figure are the decay branching ratio of the Higgs boson(H) in the THDM. Here, masses of additional Higgs bosons are fixed, $m_H = m_A = m_{H^+} = 150$GeV. The mass of the soft breaking parameter M is $M = m_H - 2$GeV.Mixing angle among scalar fields are set $\sin^2(\beta - \alpha) = 0.96$.

3.1.2 Electroweak S, T and U parameters

The S, T and U parameters [79] proposed are modified in the THDM [80] from those predicted in the SM due to the additional Higgs boson loop contributions and the different value of coupling constants among the SM-like Higgs boson h and gauge bosons. We define the differences of S, T and U parameters as $\Delta S = S_{\rm THDM} - S_{\rm SM}$, $\Delta T = T_{\rm THDM} - T_{\rm SM}$ and $\Delta U = U_{\rm THDM} - U_{\rm SM}$. These are calculated in terms of x defined as $x \equiv \pi/2 - (\beta - \alpha)$,

$$
\begin{aligned}
\Delta S = \frac{1}{4\pi}\Bigg\{ & F_5'(m_Z^2; m_H, m_A) - \frac{1}{3}\ln m_{H^\pm}^2 \\
& + x^2\Big[F_\Delta'\Big(\frac{m_A}{m_h}, \frac{m_Z}{m_h}\Big) - F_\Delta'\Big(\frac{m_A}{m_H}, \frac{m_Z}{m_H}\Big) + G_\Delta'\Big(\frac{m_H}{m_Z}, \frac{m_h}{m_Z}\Big)\Big]\Bigg\} + \mathcal{O}(x^3), \\
\Delta T = \frac{1}{4\pi e^2 v^2}\Bigg\{ & F_5(0; m_A, m_{H^\pm}) + m_H^2 F_\Delta\left(\frac{m_{H^\pm}}{m_H}, \frac{m_A}{m_H}\right) \\
& + x^2\Big[m_H^2 F_\Delta\left(\frac{m_A}{m_H}, \frac{m_{H^\pm}}{m_H}\right) + m_h^2 F_\Delta\left(\frac{m_{H^\pm}}{m_h}, \frac{m_A}{m_h}\right) \\
& + m_W^2 F_\Delta\left(\frac{m_H}{m_W}, \frac{m_h}{m_W}\right) + m_Z^2 F_\Delta\left(\frac{m_h}{m_Z}, \frac{m_H}{m_Z}\right) \\
& + 4m_W^2 G_\Delta\Big(\frac{m_H}{m_W}, \frac{m_h}{m_W}\Big) - 4m_Z^2 G_\Delta\Big(\frac{m_H}{m_Z}, \frac{m_h}{m_Z}\Big)\Big]\Bigg\} + \mathcal{O}(x^3), \\
\Delta U = \frac{1}{4\pi}\Bigg\{ & F_\Delta'\Big(\frac{m_A}{m_{H^\pm}}, \frac{m_H}{m_{H^\pm}}\Big) - \frac{1}{3}\ln m_{H^\pm}^2 - F_5'(m_Z^2; m_A, m_H) \\
& + x^2\Big[F_\Delta'\Big(\frac{m_A}{m_H}, \frac{m_Z}{m_H}\Big) - F_\Delta'\Big(\frac{m_A}{m_h}, \frac{m_Z}{m_h}\Big) + F_\Delta'\Big(\frac{m_{H^\pm}}{m_h}, \frac{m_W}{m_h}\Big) - F_\Delta'\Big(\frac{m_{H^\pm}}{m_H}, \frac{m_W}{m_H}\Big) \\
& + G_\Delta'\Big(\frac{m_H}{m_Z}, \frac{m_h}{m_Z}\Big) - G_\Delta'\Big(\frac{m_H}{m_W}, \frac{m_h}{m_W}\Big)\Bigg\} + \mathcal{O}(x^3),
\end{aligned}
\tag{3.39}
$$

where

$$
F_5(p^2, m_1, m_2) = \int_0^1 dx\,\left[(2x-1)(m_1^2 - m_2^2) + p^2(2x-1)^2\right]\ln[xm_1^2 + (1-x)m_2^2 - x(1-x)p^2], \tag{3.40}
$$

$$
F_\Delta'(x_1, x_2) = \frac{1}{3}\left[\frac{2(x_1^2 - x_2^2)(1 - x_1^2 x_2^2)}{(1-x_1^2)^2(1-x_2^2)^2} - \frac{x_1^4(x_1^2-3)}{(1-x_1^2)^3}\ln x_1^2 + \frac{x_2^4(x_2^2-3)}{(1-x_2^2)^3}\ln x_2^2\right], \tag{3.41}
$$

$$
G_\Delta'(x_1, x_2) = 2\left[-\frac{1 - x_1^4 + 2x_1^2\ln x_1^2}{(1-x_1^2)^3} + \frac{1 - x_2^4 + 2x_2^2\ln x_1^2}{(1-x_2^2)^3}\right]. \tag{3.42}
$$

where

$$
\Delta_B = -x(1-x)p^2 + xm_1^2 + (1-x)m_2^2. \tag{3.43}
$$

In the case of $p^2 = 0$, the F_5 function is expressed by

$$F_5(0; m_1, m_2) = \frac{1}{2}(m_1^2 + m_2^2) + \frac{2m_1^2 m_2^2}{m_1^2 - m_2^2} \ln \frac{m_2}{m_1}, \tag{3.44}$$

which gives zero in the case of $m_1 = m_2$. Therefore, it is seen that ΔT becomes zero when $x = 0$ and $m_A = m_{H^\pm}$ or $x = 0$ and $m_H = m_{H^\pm}$ is taken [81].

3.1.3 Constraints from current experiments

In this section, we list bounds on model parameters from collider experiments and flavour experiments.

The lower limit on $m_{H^\pm}$ as $m_{H^\pm} \gtrsim 80$ GeV had been given by data of the LEP experiment [82]. A process $e^+e^- \to H^+H^-$ was assumed in the analysis. Currently, in the MSSM, $m_{H^\pm}$ has been more strongly constrained by data of the LHC Run-I [83, 84]. and the bound is $m_{H^\pm} \gtrsim 140$ GeV. The production process is $gg \to t\bar{t} \to b\bar{b}H^+W$ and the decay process is $H^+ \to \tau^+\nu$. In the MSSM, the mass of A also has been constrained by the search of the process $gg \to b\bar{b}A \to b\bar{b}\tau^+\tau^-$ at the LHC Run-I [85]. The lower bound depends on the value of $\tan\beta$; e.g., $m_A \gtrsim 350$ GeV for $\tan\beta = 10$ an $m_A \gtrsim 800$ GeV for $\tan\beta = 50$. In the Type-I and II THDMs, the mass of H have been given the lower bound depending on the value of $\sin(\beta - \alpha)$ by the LHC Run-I data, where the decay process is assumed to be $H \to WW \to l\nu l\nu$ [86]. The strongest constraint is $m_H \gtrsim 220$ GeV for $\tan\beta \gtrsim 1$.

Constraints on $m_{H^\pm}$ are summarized in Ref. [87]. The constraint from the measurement of the $b \to s$ process is the most important. $m_{H^\pm} \lesssim 500$ GeV for all $\tan\beta$ region have been excluded in the Type-II and Y THDMs by the data. In also the Type-I and X, $m_{H^\pm}$ have been strongly constrained depending on the value of $\tan\beta$; e.g., $m_{H^\pm} \lesssim 800$ GeV for $\tan\beta = 1$ and $m_{H^\pm}$ GeV for $\tan\beta = 2$. In the Type-II THDM, the $D_s \to \tau\nu$ process also gave the strong bound on $m_{H^\pm}$ in the large $\tan\beta$ region; e.g., $m_{H^\pm} \gtrsim 400$ GeV for $\tan\beta = 40$. In all types of THDMs, $m_{H^\pm} \lesssim 500$ GeV are excluded in the regions with $\tan\beta < 1$ by the $B_0 - \bar{B}_0$ mixing.

3.2 Review of the HSM

3.2.1 Lagrangian of the HSM

Lagrangian

The scalar sector of the HSM is composed of a complex isospin doublet field Φ with hypercharge $Y = 1/2$ and a real singlet field S with $Y = 0$. The most general Higgs potential is given by

$$V(\Phi, S) = m_\Phi^2|\Phi|^2 + \lambda|\Phi|^4 + \mu_{\Phi S}|\Phi|^2 S + \lambda_{\Phi S}|\Phi|^2 S^2 + t_S S + m_S^2 S^2 + \mu_S S^3 + \lambda_S S^4, \quad (3.45)$$

where all parameters are real. The Higgs fields Φ and S can be parametrised,

$$\Phi = \begin{pmatrix} G^+ \\ \frac{1}{\sqrt{2}}(\phi + v + iG^0) \end{pmatrix}, \; S = s + v_S, \quad (3.46)$$

where v and v_S are vacuum expectation values (VEVs) of Φ and S, respectively. The fields G^+ and G^0 are Nambu-Goldstone bosons to be absorbed in longitudinaly polarized weak gauge bosons. Notice that v is determined by the Fermi constant G_F by $v = 1/(\sqrt{2}G_F)^{1/2}$ ($\simeq 246$ GeV) while v_S does not affect electroweak symmetry breaking. As it has been pointed it out in Refs. [88, 89], the potential in Eq. (3.45) is invariant under the transformation of $v_S \to v_S'$ by redefining all the potential parameters associated with S.

At the tree level, tadpoles are given by

$$T_\phi = v\{m_\Phi^2 + \lambda v^2 + v_S(\lambda_{\Phi S} v_S + \mu_{\Phi S})\}, \quad (3.47)$$

$$T_s = t_S + 2m_S^2 v_S + 4\lambda_S v_S^3 + \lambda_{\Phi S} v^2 v_S + 3\mu_S v_S^2 + \frac{\mu_{\Phi S} v^2}{2}. \quad (3.48)$$

By imposing the stationary condition $T_\Phi = 0$ and $T_S = 0$, m_Φ^2 and t_S are related to the other parameters as

$$m_\Phi^2 = -\lambda v^2 - \lambda_{\Phi S} v_S^2 - \mu_{\Phi S} v_S, \quad (3.49)$$

$$t_S = -2m_S^2 v_S - 4\lambda_S v_S^3 - \lambda_{\Phi S} v_S v^2 - 3v_S^2 \mu_S - \frac{1}{2} v^2 \mu_{\Phi S}. \quad (3.50)$$

After the electroweak symmetry breaking, mass terms of the scalar fields can be expressed as

$$\mathcal{L}_{\rm mass} = -\frac{1}{2}(s, \phi) \begin{pmatrix} M_{11}^2 & M_{12}^2 \\ M_{12}^2 & M_{22}^2 \end{pmatrix} \begin{pmatrix} s \\ \phi \end{pmatrix}, \quad (3.51)$$

where

$$M_{11}^2 = \mathcal{M}^2 + \lambda_{\Phi S} v^2, \quad (3.52)$$

$$M_{12}^2 = (2\lambda_{\Phi S} v_S + \mu_{\Phi S}) v, \quad (3.53)$$

$$M_{22}^2 = 2\lambda v^2, \quad (3.54)$$

with

$$\mathcal{M}^2 = 2m_S^2 + 12\lambda_S v_S^2 + 6\mu_S v_S. \quad (3.55)$$

We diagonalize the mass matrix by introducing the mixing angle α, and express the scalar fields by mass eigenstates H and h,

$$\mathcal{L}_{\rm mass} = -\frac{1}{2}(H,h)\begin{pmatrix} m_H^2 & 0 \\ 0 & m_h^2 \end{pmatrix}\begin{pmatrix} H \\ h \end{pmatrix}, \tag{3.56}$$

where mass eigenstate H and h are related to the original fields s and ϕ by

$$\begin{pmatrix} s \\ \phi \end{pmatrix} = \begin{pmatrix} \cos\alpha & -\sin\alpha \\ \sin\alpha & \cos\alpha \end{pmatrix}\begin{pmatrix} H \\ h \end{pmatrix}. \tag{3.57}$$

The masses of H and h are given by

$$m_H^2 = (\sin\alpha)^2 M_{11}^2 + (\cos\alpha)^2 M_{22}^2 + \sin(2\alpha) M_{12}^2, \tag{3.58}$$
$$m_h^2 = (\cos\alpha)^2 M_{11}^2 + (\sin\alpha)^2 M_{22}^2 - \sin(2\alpha) M_{12}^2, \tag{3.59}$$

where h identified to be the discovered Higgs boson with $m_h \simeq 125$ GeV. The mixing angle α can be written in terms of the parameters in the potential as

$$\tan(2\alpha) = \frac{2v(2\lambda_{\Phi S} v_S + \mu_{\Phi S})}{\mathcal{M}^2 - v^2(2\lambda - \lambda_{\Phi S})}. \tag{3.60}$$

We note that the SM limit is realized by taking $\mathcal{M}^2$ to be infinity. In the following discussion, we use s_α and c_α to express $\sin\alpha$ and $\cos\alpha$, respectively.

By using physical parameters m_h^2, m_H^2 and α, the three parameters in the potential, λ, m_S^2, and μ_S, can be expressed as

$$\lambda = \frac{1}{2v^2}(c_\alpha^2 m_h^2 + s_\alpha^2 m_H^2), \tag{3.61}$$
$$m_S^2 = \frac{c_\alpha^2 m_H^2}{2} + \frac{s_\alpha^2 m_h^2}{2} - 6\lambda_S v_S^2 - \lambda_{\Phi S} v^2 - 12 v_S \mu_S, \tag{3.62}$$
$$\mu_{\Phi S} = \frac{m_H^2}{v^2} c_\alpha(-2v_S c_\alpha + v s_\alpha) - \frac{m_h^2}{v^2} s_\alpha(v c_\alpha + 2 v_S s_\alpha). \tag{3.63}$$

There are eight parameters in the Higgs potential m_Φ^2, λ, $\mu_{\Phi S}$, $\lambda_{\Phi S}$, t_S, m_S^2, μ_S and λ_S, which are replaced by v, m_h^2, m_H^2, α, v_S, $\lambda_{\Phi S}$, λ_S and μ_S.

The kinetic terms for the scalar fields are given by

$$\mathcal{L}_{\rm kine} = |D^\mu \Phi|^2 + \frac{1}{2}(\partial^\mu S)^2, \tag{3.64}$$

where $D^\mu = \partial^\mu - i\frac{g}{2}\tau_a W_a^\mu - i\frac{g'}{2}B^\mu$. We obtain interaction terms between weak gauge fields and scalar fields as

$$\mathcal{L}_{\rm kine} = (s_\alpha H + c_\alpha h)\frac{2m_W^2}{v} g^{\mu\nu} W_\mu^+ W_\nu^- + (s_\alpha H + c_\alpha h)\frac{m_Z^2}{v} g^{\mu\nu} Z_\mu Z_\nu + \cdots, \tag{3.65}$$

where m_W and m_Z are the masses of W and Z bosons, respectively. Although the Yukawa interaction is the same form as that in the SM, Yukawa couplings of H and h are modified by the field mixing,

$$\mathcal{L}_Y = -\frac{m_f}{v}(s_\alpha \bar{f} f H + c_\alpha \bar{f} f h). \tag{3.66}$$

We define the scaling factors as ratios of the Higgs boson couplings in the HSM from those in the SM,

$$\kappa_V \equiv \frac{g_{hVV}^{\rm HSM}}{g_{hVV}^{\rm SM}}, \ \text{ for } V = W, Z, \ \ \kappa_f \equiv \frac{y_{hff}^{\rm HSM}}{y_{hff}^{\rm SM}}, \ \ \kappa_h \equiv \frac{\lambda_{hhh}^{\rm HSM}}{\lambda_{hhh}^{\rm SM}}, \tag{3.67}$$

where $g_{hVV}^{\rm HSM(SM)}, y_{hff}^{\rm HSM(SM)}$ and $\lambda_{hhh}^{\rm HSM(SM)}$ are coefficients of hVV, hff and hhh vertices in the HSM (SM), respectively. Tree level values of κ_V, κ_f and κ_h are derived from Eqs.(3.65), (3.66) and (3.45) as

$$\kappa_V = \kappa_f = c_\alpha, \tag{3.68}$$

$$\kappa_h = c_\alpha^3 + \frac{2v}{m_h^2} s_\alpha^2 (\lambda_{\Phi S} v c_\alpha - \mu_S s_\alpha - 4 s_\alpha \lambda_S v_S). \tag{3.69}$$

Perturbative unitarity, vacuum stability and wrong vacuum condition

In this section, we discuss three theoretical constraints; i.e., perturbative unitarity, vacuum stability and the condition to avoid wrong vacuum.

The constraints from the perturbative unitarity in the HSM had discussed in Ref. [90]. Under the perturbative unitarity bound, the matrix of the S-wave amplitude for the two-body to two-body scattering of scalar fields has to be satisfied in following condition,

$$|\langle \varphi_3 \varphi_4 | a_0 | \varphi_1 \varphi_2 \rangle| < \xi, \ \ \text{where } \xi = 1 \text{ or } \frac{1}{2}. \tag{3.70}$$

In the HSM, there are seven neutral scattering processes.[1] Digonalizing the matrix of the neutral scattering processes, we obtain following independent eigenvalues,

$$a_\pm = \frac{1}{16\pi} \left(3\lambda + 6\lambda_S \pm \sqrt{(3\lambda - 6\lambda_S)^2 + 4\lambda_{\Phi S}^2} \right), \tag{3.71}$$

$$b_0 = \frac{1}{8\pi}\lambda, \tag{3.72}$$

$$c_0 = \frac{1}{8\pi}\lambda_{\Phi S}. \tag{3.73}$$

Because we take the constraint with $\xi = \frac{1}{2}$, specific bounds of eq. (3.107) are

$$\left(3\lambda + 6\lambda_S \pm \sqrt{(3\lambda - 6\lambda_S)^2 + 4\lambda_{\Phi S}^2} \right) < 8\pi, \quad \lambda < 4\pi, \quad \lambda_{\Phi S} < 4\pi. \tag{3.74}$$

As conditions of vacuum stability [47], we require the value of the potential to be positive at large Φ and S. Because terms of the quartic interactions are dominant in the potential with large values of the fields,

$$\lambda |\Phi|^4 + \lambda_{\Phi S} |\Phi|^2 S^2 + \lambda_S S^4 > 0 \tag{3.75}$$

[1] Although there are one doubly charged cannel and three singly charged cannels in addition to seven neutral channels, independent eigenvalues is exhausted in eigenvalues of neutral scattering amplitudes. Because of that, it is sufficient to consider only neutral cannels.

must be satisfied. In order to satisfy 3.75, following bounds for λ parameters are imposed,

$$\lambda > 0, \;\; \lambda_S > 0, \;\; 4\lambda\lambda_S > \lambda_{\Phi S}^2, \tag{3.76}$$

where the third bound is applied when $\lambda_{\Phi S}$ is negative.

We are free to choose the value of v_S. We take to be $(v, v_S) = (v_{EW}, 0)$, because the singlet field does not contribute to electroweak symmetry breaking. However, even $(v_{EW}, 0)$ is the extrema, there is a possibility that there are lower extremes at other points. According to Refs. [88, 89], five kinds of other extrema. If one or more than one extrema given in Eq. (24) and (B1) Ref. [89] become deeper than $V(v_{EW}, 0)$, then such a vacuum should be regarded as a wrong vacuum. In the analyses of this paper, we use the condition to avoid the wrong vacuum given in Ref. [89].

3.2.2 Constraints from an extra Higgs boson searches

Null results from the Higgs boson searches at LEP and the LHC Run-I can constrain the signal rate of the second Higgs boson which is defined as $S[H] \equiv \sigma[H] \times BR[H \to XY]^2$ where σ_H and $BR[H \to XY]$ are the production cross section of H and the branching fraction of the $H \to XY$ decay process in the HSM, respectively. If we assume $BR[H \to hh] = 0$, $S[H]$ is given by s_α^2 times the signal rate of the SM Higgs boson. In that case, constraints from LEP and LHC simply depend on m_H and α. In Ref. [92], the excluded parameter region on m_H and α has been presented using the LEP and the LHC results under the assumption of $BR[H \to hh] = 0$. In the region with $m_H < 80$ GeV, most of the parameter regions of α have been excluded with 95 % CL. In the region between 130 GeV and 500 GeV, $|s_\alpha| \gtrsim 0.4$ is excluded with 95 % CL. There are no constraints on $|s_\alpha|$ for $m_H \gtrsim 800$ GeV.

3.2.3 Electroweak S, T and U parameters

In Refs. [91,92], the one-loop corrections to m_W has been calculated in the HSM with a discrete Z_2 symmetry. The limits on s_α and m_H have been derived by comparing the prediction of m_W and its measured value at the LEP experiment, namely, $|s_\alpha| \gtrsim 0.3$ (0.2) with $m_H = 300$ (800) GeV is excluded at the 2σ level. Although the electroweak S, T and U parameters have also been calculated in Ref. [92], constraints from those parameters are weaker than those from m_W.

[2] Although we can obtain constraints on the signal rate of the additional Higgs boson by using the data at Tevetron, these constraints are entirely superseded by the one of the LHC Run-I [92].

3.3 Review of the HTM

3.3.1 Lagrangian of the HTM

The scalar sector of the HTM is composed of the isospin doublet field Φ with hypercharge $Y = 1/2$ and the triplet field Δ with $Y = 1$. The relevant terms in the Lagrangian are given by

$$\mathcal{L}_{\rm HTM} = \mathcal{L}_{\rm kin} + \mathcal{L}_Y - V(\Phi, \Delta), \tag{3.77}$$

where $\mathcal{L}_{\rm kin}$, $\mathcal{L}_Y$ and $V(\Phi, \Delta)$ are the kinetic term, the Yukawa interaction and the Higgs potential, respectively.

The kinetic term of the Higgs fields is given by

$$\mathcal{L}_{\rm kin} = (D_\mu \Phi)^\dagger (D^\mu \Phi) + {\rm Tr}[(D_\mu \Delta)^\dagger (D^\mu \Delta)], \tag{3.78}$$

where the covariant derivatives are defined as

$$D_\mu \Phi = \left(\partial_\mu + i\frac{g}{2}\tau^a W^a_\mu + i\frac{g'}{2} B_\mu \right) \Phi, \quad D_\mu \Delta = \partial_\mu \Delta + i\frac{g}{2}[\tau^a W^a_\mu, \Delta] + ig' B_\mu \Delta. \tag{3.79}$$

The Higgs fields can be parameterized by

$$\Phi = \begin{bmatrix} \phi^+ \\ \frac{1}{\sqrt{2}}(\phi + v_\phi + i\chi) \end{bmatrix}, \quad \Delta = \begin{bmatrix} \frac{\Delta^+}{\sqrt{2}} & \Delta^{++} \\ \Delta^0 & -\frac{\Delta^+}{\sqrt{2}} \end{bmatrix} \text{ with } \Delta^0 = \frac{1}{\sqrt{2}}(\delta + v_\Delta + i\eta), \tag{3.80}$$

where v_ϕ and v_Δ are the VEVs of the doublet Higgs field and the triplet Higgs field, respectively which satisfy $v^2 \equiv v_\phi^2 + 2v_\Delta^2 \simeq (246\ {\rm GeV})^2$. The masses of the W boson and the Z boson are obtained at the tree level as

$$m_W^2 = \frac{g^2}{4}(v_\phi^2 + 2v_\Delta^2), \quad m_Z^2 = \frac{g^2}{4\cos^2\theta_W}(v_\phi^2 + 4v_\Delta^2). \tag{3.81}$$

The electroweak rho parameter can deviate from unity at the tree level;

$$\rho \equiv \frac{m_W^2}{m_Z^2 \cos^2\theta_W} = \frac{1 + \frac{2v_\Delta^2}{v_\phi^2}}{1 + \frac{4v_\Delta^2}{v_\phi^2}}. \tag{3.82}$$

The experimental value of the rho parameter is quite close to unity; i.e., $\rho^{\rm exp} = 1.0008^{+0.0017}_{-0.0007}$ [99], so that v_Δ has to be less than about 8 GeV from the tree level formula given in Eq. (3.82).

The Yukawa interaction for neutrinos [50] is given by

$$\mathcal{L}_Y = h_{ij} \overline{L_L^{ic}} i\tau_2 \Delta L_L^j + {\rm h.c.}, \tag{3.83}$$

where h_{ij} is the 3×3 complex symmetric Yukawa matrix. Notice that the triplet field Δ carries the lepton number of -2. The mass matrix for the left-handed neutrinos is obtained as

$$(\mathcal{M}_\nu)_{ij} = \sqrt{2} h_{ij} v_\Delta. \tag{3.84}$$

The most general form of the Higgs potential under the gauge symmetry is given by

$$V(\Phi,\Delta) = m^2\Phi^\dagger\Phi + M^2\mathrm{Tr}(\Delta^\dagger\Delta) + \left[\mu\Phi^T i\tau_2\Delta^\dagger\Phi + \mathrm{h.c.}\right] + \lambda_1(\Phi^\dagger\Phi)^2 + \lambda_2\left[\mathrm{Tr}(\Delta^\dagger\Delta)\right]^2 + \lambda_3\mathrm{Tr}[(\Delta^\dagger\Delta)^2] + \lambda_4(\Phi^\dagger\Phi)\mathrm{Tr}(\Delta^\dagger\Delta) + \lambda_5\Phi^\dagger\Delta\Delta^\dagger\Phi, \tag{3.85}$$

where m and M are the dimension full real parameters, μ is the dimension full complex parameter which violates the lepton number, and λ_1-λ_5 are the coupling constants which are real. We here take μ to be real.

The potential respects additional global symmetries in some limits. First, when the μ term is absent, there is the global $U(1)$ symmetry in the potential, which conserves the lepton number. As long as we assume that the lepton number is not spontaneously broken, the triplet field does not carry the VEV; i.e., $v_\Delta = 0$. Next, when both the μ term and the λ_5 term are zero, an additional global $SU(2)$ symmetry appears. Under this $SU(2)$ symmetry, Φ and Δ can be transformed with the different $SU(2)$ phases. In this case, all the physical triplet-like Higgs bosons are degenerate in mass.

The tadpoles for the ϕ and δ fields are obtained as

$$T_\Phi = -v_\phi\left[m^2 + v_\phi^2\lambda_1 + \frac{v_\Delta^2}{2}(\lambda_4+\lambda_5) - \sqrt{2}\mu v_\Delta\right], \tag{3.86}$$

$$T_\Delta = -v_\Delta\left[M^2 + v_\Delta^2(\lambda_2+\lambda_3) + \frac{v_\phi^2}{2}(\lambda_4+\lambda_5) - M_\Delta^2\right], \text{ with } M_\Delta^2 \equiv \frac{v_\phi^2\mu}{\sqrt{2}v_\Delta}. \tag{3.87}$$

Because the tadpoles must be vanished at the tree level ($T_\Phi = T_\Delta = 0$), we can eliminate m^2 and M^2 in the potential. The mass matrices for the scalar bosons can be diagonalized by rotating the scalar fields as

$$\begin{pmatrix}\phi^\pm\\ \Delta^\pm\end{pmatrix} = \begin{pmatrix}\cos\beta & -\sin\beta\\ \sin\beta & \cos\beta\end{pmatrix}\begin{pmatrix}G^\pm\\ H^\pm\end{pmatrix}, \quad \begin{pmatrix}\chi\\ \eta\end{pmatrix} = \begin{pmatrix}\cos\beta' & -\sin\beta'\\ \sin\beta' & \cos\beta'\end{pmatrix}\begin{pmatrix}G^0\\ A\end{pmatrix},$$
$$\begin{pmatrix}\phi\\ \delta\end{pmatrix} = \begin{pmatrix}\cos\alpha & -\sin\alpha\\ \sin\alpha & \cos\alpha\end{pmatrix}\begin{pmatrix}h\\ H\end{pmatrix}, \tag{3.88}$$

with the mixing angles

$$\tan\beta = \frac{\sqrt{2}v_\Delta}{v_\phi}, \quad \tan\beta' = \frac{2v_\Delta}{v_\phi}, \quad \tan 2\alpha = \frac{v_\Delta}{v_\phi}\frac{2v_\phi^2(\lambda_4+\lambda_5) - 4M_\Delta^2}{2v_\phi^2\lambda_1 - M_\Delta^2 - 2v_\Delta^2(\lambda_2+\lambda_3)}. \tag{3.89}$$

We note that the mixing angle of the charged scalar states (β) and that of the CP-odd scalar states (β') are different in the triplet model. In the two Higgs doublet model, corresponding two mixing angles are the same at the tree level. This is because the kinetic term of the two doublet fields can be rewritten in terms of so-called the Georgi basis, where only one of the doublets has a non-zero VEV in which the NG bosons are included. Original basis and the Georgi basis are related to a single angle. In the HTM, because Φ and Δ are the different representation of SU(2), the kinetic term given in Eq. (3.78) cannot be rewritten in terms of the Georgi basis. Thus, the diagonalization of the mass matrices has to be done by each component scalar field, and mixing angles for the charged scalar states and the CP-odd scalar states are different in general.

In addition to the three NG bosons $G^{\pm}$ and G^0 which are absorbed by the longitudinal components of the W boson and the Z boson, there are seven physical mass eigenstates $H^{\pm\pm}$, $H^{\pm}$, A, H and h. The masses of these physical states are expressed as

$$m^2_{H^{++}} = M^2_\Delta - v^2_\Delta \lambda_3 - \frac{\lambda_5}{2} v^2_\phi, \tag{3.90}$$

$$m^2_{H^{+}} = \left(M^2_\Delta - \frac{\lambda_5}{4} v^2_\phi \right) \left(1 + \frac{2v^2_\Delta}{v^2_\phi} \right), \tag{3.91}$$

$$m^2_{A} = M^2_\Delta \left(1 + \frac{4v^2_\Delta}{v^2_\phi} \right), \tag{3.92}$$

$$m^2_{H} = \mathcal{M}^2_{11} \sin^2\alpha + \mathcal{M}^2_{22} \cos^2\alpha - \mathcal{M}^2_{12} \sin 2\alpha, \tag{3.93}$$

$$m^2_{h} = \mathcal{M}^2_{11} \cos^2\alpha + \mathcal{M}^2_{22} \sin^2\alpha + \mathcal{M}^2_{12} \sin 2\alpha, \tag{3.94}$$

where $\mathcal{M}^2_{11}$, $\mathcal{M}^2_{22}$ and $\mathcal{M}^2_{12}$ are the elements of the mass matrix $\mathcal{M}^2_{ij}$ for the CP-even scalar states in the (ϕ, δ) basis which are given by

$$\mathcal{M}^2_{11} = 2v^2_\phi \lambda_1, \tag{3.95}$$

$$\mathcal{M}^2_{22} = M^2_\Delta + 2v^2_\Delta (\lambda_2 + \lambda_3), \tag{3.96}$$

$$\mathcal{M}^2_{12} = -\frac{2v_\Delta}{v_\phi} M^2_\Delta + v_\phi v_\Delta (\lambda_4 + \lambda_5). \tag{3.97}$$

The six parameters μ and λ_1-λ_5 in the Higgs potential in Eq. (3.85) can be written in terms of the physical scalar masses, the mixing angle α and VEVs v_ϕ and v_Δ as

$$\mu = \frac{\sqrt{2} v_\Delta}{v^2_\phi} M^2_\Delta = \frac{\sqrt{2} v_\Delta}{v^2_\phi + 4v^2_\Delta} m^2_A, \tag{3.98}$$

$$\lambda_1 = \frac{1}{2v^2_\phi} (m^2_h \cos^2\alpha + m^2_H \sin^2\alpha), \tag{3.99}$$

$$\lambda_2 = \frac{1}{2v^2_\Delta} \left[2m^2_{H^{++}} + v^2_\phi \left(\frac{m^2_A}{v^2_\phi + 4v^2_\Delta} - \frac{4m^2_{H^+}}{v^2_\phi + 2v^2_\Delta} \right) + m^2_H \cos^2\alpha + m^2_h \sin^2\alpha \right], \tag{3.100}$$

$$\lambda_3 = \frac{v^2_\phi}{v^2_\Delta} \left(\frac{2m^2_{H^+}}{v^2_\phi + 2v^2_\Delta} - \frac{m^2_{H^{++}}}{v^2_\phi} - \frac{m^2_A}{v^2_\phi + 4v^2_\Delta} \right), \tag{3.101}$$

$$\lambda_4 = \frac{4m^2_{H^+}}{v^2_\phi + 2v^2_\Delta} - \frac{2m^2_A}{v^2_\phi + 4v^2_\Delta} + \frac{m^2_h - m^2_H}{2v_\phi v_\Delta} \sin 2\alpha, \tag{3.102}$$

$$\lambda_5 = 4 \left(\frac{m^2_A}{v^2_\phi + 4v^2_\Delta} - \frac{m^2_{H^+}}{v^2_\phi + 2v^2_\Delta} \right). \tag{3.103}$$

When the triplet VEV v_Δ is much less than the doublet VEV v_ϕ, which is required by the rho parameter data, there appear relationships among the masses of the triplet-like Higgs

bosons by neglecting $\mathcal{O}(v_\Delta^2/v_\phi^2)$ terms as

$$m_{H^{++}}^2 - m_{H^+}^2 = m_{H^+}^2 - m_A^2 \quad \left(= -\frac{\lambda_5}{4}v^2\right), \tag{3.104}$$

$$m_A^2 = m_H^2 \quad (= M_\Delta^2). \tag{3.105}$$

In the limit of $v_\Delta/v_\phi \to 0$, the four mass parameters of the triplet-like Higgs bosons are determined by two parameters. Eqs. (3.104) and (3.105) can be regarded as the consequence of the global symmetries which are mentioned in just below Eq. (3.85).

3.3.2 Perturbative unitarity and vacuum stability

From now on, we show the constraints from the unitarity and the vacuum stability. The condition for the vacuum stability bound has been derived in Ref. [93]. The unitarity bound has been discussed in Ref. [94] in the GM model [53] which contains the HTM. The unitarity bound in the HTM has also been discussed in Ref. [93].

The necessary and sufficient condition for the requirement of the vacuum stability is given by [93]

$$\begin{aligned}
&\lambda_1 > 0, \quad \lambda_2 + \mathrm{MIN}\left[\lambda_3,\ \frac{1}{2}\lambda_3\right] > 0, \\
&\lambda_4 + \mathrm{MIN}[0,\ \lambda_5] + 2\mathrm{MIN}[\sqrt{\lambda_1(\lambda_2+\lambda_3)}, \sqrt{\lambda_1(\lambda_2+\lambda_3/2)}] > 0.
\end{aligned} \tag{3.106}$$

In the unitarity bound, we require that the matrix of the S-wave amplitude for the elastic scatterings of two scalar boson states $\langle\varphi_3\varphi_4|a_0|\varphi_1\varphi_2\rangle$ are satisfied the following condition;

$$|\langle\varphi_3\varphi_4|a_0|\varphi_1\varphi_2\rangle| < 1 \quad \text{or} \quad |\mathrm{Re}\langle\varphi_3\varphi_4|a_0|\varphi_1\varphi_2\rangle| < \frac{1}{2}, \tag{3.107}$$

where φ_i denote the NG bosons and the physical Higgs bosons. In the HTM, there are 35 possible scattering processes, i.e., 15 neutral channels, 10 singly-charged channels, 7 doubly-charged channels, 2 triply-charged channels and one quadruply-charged channel. Thus, there are 35 corresponding eigenvalues, but some of them have the same expressions. In fact, 12 eigenvalues can be regarded as independent eigenvalues, these are

$$\begin{aligned}
&y_1 = 2\lambda_1, \quad y_2 = 2(\lambda_2+\lambda_3), \quad y_3 = 2\lambda_2, \\
&y_4^\pm = \lambda_1+\lambda_2+2\lambda_3 \pm \sqrt{\lambda_1^2 - 2\lambda_1(\lambda_2+2\lambda_3) + \lambda_2^2 + 4\lambda_2\lambda_3 + 4\lambda_3^2 + \lambda_5^2}, \\
&y_5^\pm = 3\lambda_1+4\lambda_2+3\lambda_3 \pm \sqrt{9\lambda_1^2 - 6\lambda_1(4\lambda_2+3\lambda_3) + 16\lambda_2^2 + 24\lambda_2\lambda_3 + 9\lambda_3^2 + 6\lambda_4^2 + 2\lambda_5^2}, \\
&y_6 = \lambda_4, \quad y_7 = \lambda_4+\lambda_5, \quad y_8 = \frac{1}{2}(2\lambda_4+3\lambda_5), \quad y_9 = \frac{1}{2}(2\lambda_4-\lambda_5), \quad y_{10} = 2\lambda_2-\lambda_3.
\end{aligned} \tag{3.108}$$

The unitarity constrains by the following condition:

$$|y_i| < \zeta, \quad i = 1, \ldots, 10, \tag{3.109}$$

where ζ is the upper limit for these eigenvalues. In Eq. (3.107), when we impose the former (latter) condition to the S-wave amplitude, this corresponds to $\zeta = 16\pi$ (8π). In our numerical

analysis for the constraint from the unitarity bound, we take both the cases with $\zeta = 8\pi$ and $\zeta = 16\pi$. These eigenvalues can be rewritten as a simple form by using $\lambda_\Delta (> 0)$ by

$$x_1 = 3\lambda_1 + 7\lambda_\Delta + \sqrt{(3\lambda_1 - 7\lambda_\Delta)^2 + \frac{3}{2}(2\lambda_4 + \lambda_5)^2}, \tag{3.110}$$

$$x_2 = \frac{1}{2}(2\lambda_4 + 3\lambda_5), \tag{3.111}$$

$$x_3 = \frac{1}{2}(2\lambda_4 - \lambda_5). \tag{3.112}$$

3.3.3 Constraints from collider experiments

A direct search for doubly charged Higgs bosons $H^{\pm\pm}$ is one of the most important probes in the HTM. The main decay mode of $H^{\pm\pm}$ depends on the value of v_Δ. Accordingly, bounds on $m_{H^{\pm\pm}}$ drastically change depending on the decay mode [51].

We here consider the case with no mass difference among triplet like Higgs bosons. In such a case, if v_Δ is smaller than about 1 MeV, $H^{\pm\pm}$ mainly decay into the same sign dilepton, namely $H^{\pm\pm} \to l^\pm l^\pm$. By asuuming the case where $H^{\pm\pm}$ decays into the same sign dilepton, the most stringent lower limit on $m_{H^{\pm\pm}}$ has been obtained to be about 550 GeV [95] at the LHC. On the other hand, if v_Δ is larger than about 1 MeV, the decay process $H^{\pm\pm} \to W^\pm W^\pm$ is dominant. The lower limit on $m_{H^{\pm\pm}}$ have been evaluated in the case where the dominant decay mode is $H^{\pm\pm} \to W^\pm W^{\pm(*)}$, by using the same-sign dilepton search performed by ATLAS Collaboration with 20.3 fb^{-1} data at the collision energy of 8 TeV [96]. By the study, the bound on the lower bound to be $m_{H^{\pm\pm}}$ was updated to be $m_{H^{\pm\pm}} \gtrsim 84$ GeV [97].

In the case with non-zero mass difference among triplet like Higgs bosons, the cascade decay of $H^{\pm\pm}$ dominates depending on the value of v_Δ and the magnitude of the mass difference among triplet like Higgs bosons [51]. If H^{++} is the heaviest particle in triplet like Higgs bosons, the cascade dacay $H^{++} \to H^+ W^{+(*)} \to \phi^0 W^{+(*)} W^{+(*)}$ can be dominant as long as v_Δ is neither too small nor too large. However, no bound on $m_{H^{\pm\pm}}$ has been given in the case where the cascade decay is the main decay mode.

Chapter 4

Future experiments

We here describe how it can be tested extended Higgs sectors by the direct searches and the indirect searches at the LHC Run-II and future e^+e^- collider experiment ILC.

4.1 Second Higgs boson searches at collider experiments

In this section, we describe the direct searches of extra Higgs boson focusing on the THDMs as a bench mark model. There are a lot of studies about the direct searches of additional Higgs bosons at the LHC Run-II [13, 57, 78] and the ILC [78, 98].

4.1.1 Direct search at the LHC

First, we discuss the direct search in the case for $\sin(\beta-\alpha)=1$ for simplification. Basically, the production cross section of gluon fusion process $gg \to H/A$ is the biggest for the production without the enhanced factor discussion. In the four types of THDMs, some of vertices of Yukawa couplings have enhanced factors as shown in Tab. 3.1. In the Type-II THDM, it can be expected that the bottom quark associate production process $gg \to H/Ab\bar{b}$ is useful for the production of H/A because there is the enhanced factor $\tan^2\beta$ in the $H\bar{b}b$ ($A\bar{b}b$) vertex. The $gb \to H^{\pm}t$ process is useful as the production of $H^{\pm}$ for the same season. In the Type-X THDM, in addition to the gluon fusion production process, the $q\bar{q} \to H/A$ process is also important. In the Type-I and the Type-Y, the gluon fusion process and the bottom quark associate process can be the main production process of H/A, respectively. For the decay mode, the $H/A \to b\bar{b}$ and/or the $H/A \to \tau^+\tau^-$ can be the main decay mode in all types of THDMs as shown in Fig. 3.1.1.

Fig. 4.1 [57] shows expected excluded regions on the $\tan\beta - m_A$ plane at the 95% CL by expected significance of the $gg \to H/A \to \tau^+\tau^-$ and $gg \to b\bar{b}H/A \to b\bar{b}\tau^+\tau^-$ in the case of $m_A = m_H$ and $\sin(\beta-\alpha)=1$ in the Type-II. The blue (red) shaded regions are excluded regions assuming the integrated luminosity to be 300 fb^{-1} (3000 fb^{-1}). Exclusion reach of m_A increases in region with the large value of $\tan\beta$, because the cross sections of the bottom quark associated processes are enhanced due to the enhanced factor $\tan\beta$ at the $A\bar{b}b$ vertex and the branching ratio of $H/A \to \tau^+\tau^-$ is approaching to be 10% in high $\tan\beta$ regions as shown in Figs. 3.1.1.

4.1.2 Direct search at the ILC

In this subsection, we describe the direct search in the SM-like limit case, i.e. $\sin(\beta-\alpha)=1$.

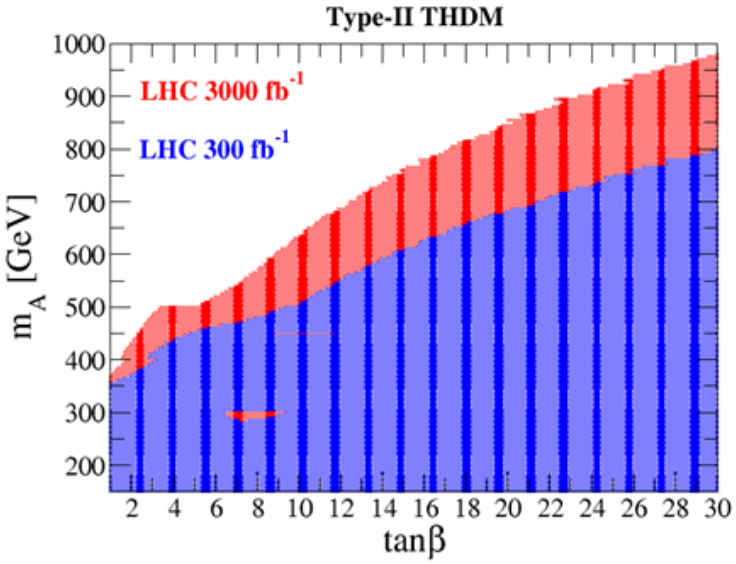

Figure 4.1: Expected excluded regions on the $\tan\beta - m_A$ plane at the 95% CL in the case of $m_A = m_H$ and $\sin(\beta - \alpha) = 1$ in the Type-II. The blue (red) shaded regions are excluded regions assuming the integrated luminosity to be 300 fb^{-1} (3000 fb^{-1}). This figure is taken from Ref. [57].

In the case with $\sqrt{s} > m_H + m_A(2m_{H^\pm})$, pair production processes of extra Higgs boson can open, so that the main production processes of extra Higgs bosons are expected to be $e^+e^- \to HA$ and $e^+e^- \to H^+H^-$. Cross sections of these pair production processes depend of the Yukawa interaction type, because a pair of additional Higgs bosons is produced via gauge interactions. For energies below the threshold $\sqrt{s} = m_H + m_A(2m^2_{H^\pm})$, the single production processes, $e^+e^- \to H(A)f\bar{f}$ and $e^+e^- \to H^\pm f\bar{f}'$, can be the leading contributions. The production processes are increased as the relevant Yukawa coupling constants of the $\Phi f\bar{f}^{(\prime)}$ vertices become large.

It is planned that the ILC runs with $\sqrt{s} = 250$, 500 and 1 TeV. As long as the collision energy is enough to product extra Higgs bosons, we expect various signatures depending on the types of Yukawa interaction and $\tan\beta$.

4.2 Fingerprints of the Higgs boson couplings

4.2.1 Pattern of deviations in the Higgs boson couplings

In the case where the Higgs sector is extended, coupling of the Higgs boson with 125 GeV mass can deviate from predicted values of the SM by new physics effects such as mixing effects and loop contributions of new particles. The pattern of deviations in the Higgs boson couplings depends on the structure of the Higgs sector; i.e., kinds of symmetries in the theory, Higgs field representations under the symmetries, the number of Higgs fields and so on. Therefore, the pattern is useful to discriminate extended Higgs models [13, 57]. In order to demonstrate discriminating models by the pattern of deviations in the Higgs boson couplings, we define the

Model	κ_V	κ_t	κ_b	κ_τ
HSM	c_α	c_α	c_α	c_α
Type-I	c_α	$s_{\beta-\alpha}+\cot\beta c_{\beta-\alpha}$	$s_{\beta-\alpha}+\cot\beta c_{\beta-\alpha}$	$s_{\beta-\alpha}+\cot\beta c_{\beta-\alpha}$
Type-II	$s_{\beta-\alpha}$	$s_{\beta-\alpha}+\cot\beta c_{\beta-\alpha}$	$s_{\beta-\alpha}-c_\beta c_{\beta-\alpha}$	$s_{\beta-\alpha}-c_\beta c_{\beta-\alpha}$
Type-X	$s_{\beta-\alpha}$	$s_{\beta-\alpha}+\cot\beta c_{\beta-\alpha}$	$s_{\beta-\alpha}+\cot\beta c_{\beta-\alpha}$	$s_{\beta-\alpha}-c_\beta c_{\beta-\alpha}$
Type-Y	$s_{\beta-\alpha}$	$s_{\beta-\alpha}+\cot\beta c_{\beta-\alpha}$	$s_{\beta-\alpha}-c_\beta c_{\beta-\alpha}$	$s_{\beta-\alpha}+\cot\beta c_{\beta-\alpha}$
HTM	$c_\beta c_\alpha+\sqrt{2}s_\beta s_\alpha$	c_α	c_α	c_α

Table 4.1: Tree level scaling factors of the gauge coupling and Yukawa couplings in the HSM, four Types of THDMs and the HTM.

scaling factors by normalizing the Higgs boson couplings which will be precisely determined by future collier experiments;

$$\mathcal{L}=\kappa_V h\left(\frac{2m_W^2}{v}W_\mu^+W_\nu^-+\frac{m_Z^2}{v}Z_\mu Z_\nu\right)g^{\mu\nu}-\sum_i\kappa_f\frac{m_f}{v}h\bar{f}f. \tag{4.1}$$

In Tab. 4.1, we summarized tree level scaling factors of the gauge coupling and Yukawa couplings in the HSM, four types of THDMs and the HTM. Moreover, Tabs. 4.2 show directions of modifications for the hVV coupling and the $h\bar{f}f$ couplings in the HSM, four types of THDMs and the HTM [13, 16, 57]. The difference between the left table and the right table is the sign of $\cos(\beta-\alpha)$. The up (down) arrow denotes that the Higgs boson coupling is larger than the value of the SM.

As you can see, a characteristic pattern of deviations in various Higgs boson couplings appears in each extended Higgs model. In the HSM, if the field mixing between CP-even Higgs contents is non-zero, hVV and $h\bar{f}f$ couplings are reduced than values of the SM with the same ratio. On the other hand, in four types of THDMs, magnitudes of the deviations are different for each the Higgs boson coupling. The $h\bar{f}f$ couplings tend to more largely deviate from the SM values than the hVV couplings. Because formulae of scaling factors of the Yukawa couplings depend on the Higgs field interacting with the fermion field, deviation patterns in $h\bar{f}f$ couplings are different among four types. As I mentioned in the Introduction, there is an interesting property that the hVV couplings can be greater than those of the SM.

In Fig. 4.2, we discuss numerically deviation patterns of various couplings of the 125 GeV Higgs boson in the four types of THDMs and the HSM and the HTM. The left panel shows the pattern of κ_b and the κ_τ couplings in four types of THDMs. Red and blue curves indicate tree level predictions of κ_b and κ_τ in the case with $\sin(\beta-\alpha)=0.99$ and 0.95, respectively, in each value of $\tan\beta$. We take the sign of $\cos(\beta-\alpha)$ to be negative. At the tree level, in the case with $\sin(\beta-\alpha)=1$, predictions of all the types get close to those of the SM. If $\sin(\beta-\alpha)$ slightly deviate from unity, κ_f for each type lead to deviate in different directions. However it is difficult to discriminate the types of THDMs by evaluating only κ_b and κ_τ because behaviors of κ_b and κ_τ depend on the sign of $\cos(\beta-\alpha)$. If $\cos(\beta-\alpha)$ is negative (positive), predictions of $\kappa_{t(c)}$ in all the types are less (larger) than 1. Therefore we can determine the sign of $\cos(\beta-\alpha)$ by using measurements of $\kappa_{t(c)}$. Then we can discriminate all types of Yukawa interactions by

Model	hVV	$h\bar{t}t$	$h\bar{b}b$	$h\tau\tau$
HSM	↓	↓	↓	↓
Type-I	↓	↓	↓	↓
Type-II	↓	↓	↑	↑
Type-X	↓	↓	↓	↑
Type-Y	↓	↓	↑	↓
HTM	↑↓	↓	↓	↓

Model	hVV	$h\bar{t}t$	$h\bar{b}b$	$h\tau\tau$
HSM	↓	↑	↑	↑
Type-I	↓	↑	↑	↑
Type-II	↓	↑	↓	↓
Type-X	↓	↑	↑	↓
Type-Y	↓	↑	↓	↑
HTM	↑↓	↑	↑	↑

Table 4.2: Direction of modifications for each the Higgs boson coupling in the HSM, four types of THDMs and the THDM. The left and right tables show the case with $\cos(\beta-\alpha) < 0$ and $\cos(\beta-\alpha) > 0$, respectively. The up (down) arrow denotes that the Higgs boson coupling is larger than the value of the SM.

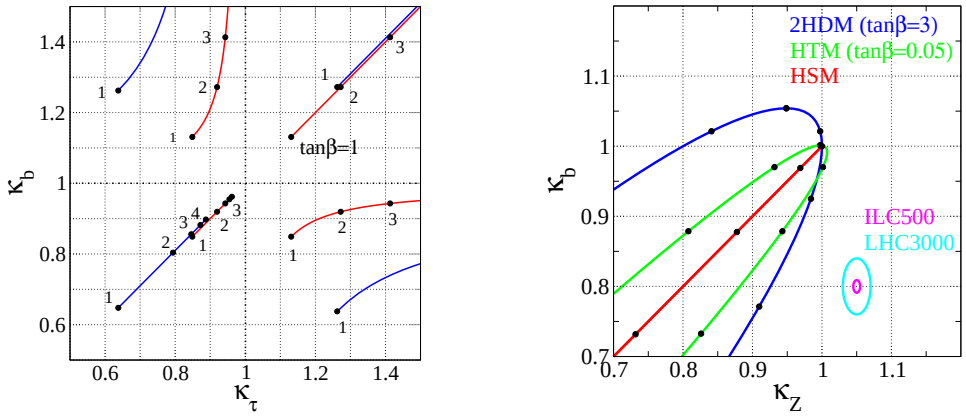

Figure 4.2: The left panel shows the pattern of κ_b and the κ_τ couplings in four types of THDMs. Red and blue curves indicate tree level predictions of κ_b and κ_τ in the case with $\sin(\beta-\alpha) = 0.99$ and 0.95, respectively, in each value of $\tan\beta$. We take the sign of $\cos(\beta-\alpha)$ to be negative. The right panel shows the pattern of κ_Z and κ_f in the Type-I THDM with $\tan\beta = 3$ (blue curve), the HSM (red line) and the HTM with $\tan\beta = 0.05$ (green curve). Black dots show values of α.

the pattern of deviations in these $h\bar{f}f$ couplings. These analyses of Yukawa couplings at the tree level have already been discussed in Refs..

The right panel shows the pattern of κ_Z and κ_f in the Type-I THDM with $\tan\beta = 3$ (blue curve), the HSM (red line) and the HTM with $\tan\beta = 0.05$ (green curve). Black dots show values of α. In the three models, the Yukawa couplings of the Higgs boson are universal formulae, i.e., $\kappa_f \equiv \kappa_t = \kappa_b = \kappa_\tau$. As it was previously mentioned, in the HSM, because κ_V and κ_f take a common form at the tree level, the hVV and the $h\bar{f}f$ couplings deviate to the directions with the rate $1:1$ by the mixing effect. In the Type-I THDM with $\cos(\beta-\alpha) < 0$, the magnitude of κ_f is smaller than that in the HSM for the same value of κ_Z. On the other hand, in the case of $\cos(\beta-\alpha) > 0$, κ_f is larger than that of the HSM for the same value of κ_Z. If the value of $\tan\beta$ becomes large, the κ_Z and κ_f plane prediction in the Type I THDM approximate the line of $1:1$. As you can see, in the HTM, although it is seen that there are regions in which κ_Z is larger than unity, the maximum value of κ_Z can not much be larger, e.g., it can not become greater from 1 to more than 1%. The reason is that the value of $\tan\beta$ is too small. $\tan\beta$ is determined by the value of the VEV of the triplet field v_Δ by $\tan\beta = 2v_\Delta/\sqrt{v^2 - 2v_\Delta^2}$ as shown at Eq. (3.89). The magnitude of v_Δ is constrained to be less than about 8 GeV from the experimental value of the rho parameter $\rho_{\rm exp} = 1.0008^{+0.00017}_{-0.00007}$ [99].

As we numerically showed in Fig. 4.2, a pattern of deviations in these observables strongly depends on the structure of the Higgs sector, so that we may be able to fingerprint extended Higgs sectors and new physics models if we can detect a special pattern of the deviations at future experiments.

4.2.2 Future precision measurements of the Higgs boson couplings

After the Higgs boson discovery, coupling constants of the discovered Higgs boson with SM particles became new observables to be measured as precisely as possible at current and future colliders. Both the ATLAS and CMS Collaborations have provided scaling factors for the Higgs boson couplings extracted from combined data of Higgs boson searches with $\sqrt{s} = 7$ and 8 TeV and 25fb^{-1} of the integrated luminosity. Under assumptions of the universal scaling factors for fermions and vector bosons; i.e., $\kappa_f = \kappa_t = \kappa_b = \kappa_\tau$ and $\kappa_V = \kappa_W = \kappa_Z$, current data gives

$$\kappa_V = 1.15 \pm 0.08, \kappa_f = 0.99^{+0.08}_{-0.15}, \quad \text{ATLAS [5]}, \tag{4.2}$$

$$\kappa_V = 1.01 \pm 0.07, \kappa_f = 0.87^{+0.14}_{-0.13}, \quad \text{CMS [6]}, \tag{4.3}$$

from the two parameters (κ_V and κ_V) fit analysis based on Ref.. The scaling factors for the loop induced Higgs boson couplings κ_g and κ_γ have also been measured under the assumptions of $\kappa_V = \kappa_f = 1$,

$$\kappa_g = 1.08^{+0.15}_{-0.13}, \kappa_\gamma = 1.19^{+0.15}_{-0.12}, \quad \text{ATLAS [5]}, \tag{4.4}$$

$$\kappa_g = 0.89^{+0.11}_{-0.10}, \kappa_\gamma = 1.14^{+0.12}_{-0.13}, \quad \text{CMS [6]}, \tag{4.5}$$

from the two parameters (κ_g and κ_γ) fit analysis based on Ref.. We can see that all the SM predictions ($\kappa_X = 1$) are included within the 2-σ uncertainty of the measured scaling factors, where the current 1-σ uncertainties of the scaling factors are typically of $\mathcal{O}(10\%)$.

The Higgs boson couplings are expected to be measured with more precision at future experiments such as the LHC Run-II, the high luminosity (HL)-LHC [16,100] with the integrated

Facility	LHC300	LH-LHC	ILC500	ILC500-up	ILC1000	ILC1000-up
κ_γ	$5-7\%$	$2-5\%$	8.3%	4.4%	3.8%	2.3%
κ_g	$6-8\%$	$3-5\%$	2.0%	1.1%	1.1%	0.67%
κ_W	$4-6\%$	$2-5\%$	0.39%	0.21%	0.21%	0.2%
κ_Z	$4-6\%$	$2-4\%$	0.49%	0.24%	0.50%	0.3%
κ_ℓ	$6-8\%$	$2-5\%$	1.9%	0.98%	1.3%	0.72%
$\kappa_d = \kappa_b$	$10-13\%$	$4-7\%$	0.93%	0.60%	0.51%	0.4%
$\kappa_u = \kappa_t$	$14-15\%$	$7-10\%$	2.5%	1.3%	1.3%	0.9%

Table 4.3: Expected precisions on the Higgs boson couplings and total width from a constrained 7-parameter fit quoted from Table 1-20 in Ref. [100].

luminosity of 3000 fb^{-1} and future lepton colliders like the ILC [12, 13, 16, 100]. In particular, measurement uncertainties of the Higgs boson couplings will be improved drastically to the order of 1 % or even better at future lepton colliders, such as the ILC [12, 13, 16, 100], the CLIC [14, 16, 100] and Future e^+e^- Circular Collider (FCCee) [15, 100] as shown in Tab. 4.3. Therefore, these future electron-positron colliders are idealistic tools for fingerprinting Higgs sector and new physics models via precise measurements of the Higgs boson couplings. In order to compare theory predictions with such precision measurements, calculations with higher order corrections are clearly necessary.

Chapter 5

Radiative corrections to the Higgs boson couplings in the THDMs

5.1 Renormalization in the THDMs

We perform renormalization calculations based on the on-shell scheme which has been applied in Ref. [70][1]. However, it has been pointed out that there remains gauge dependence in the determination of the counter term of β in Ref. [101]. We thus construct the new renormalization scheme for β to get rid of the gauge dependence.

First, we prepare the set of counter terms by shifting all the relevant bare parameters in the Lagrangian. We then give the renormalized one- and two-point functions which are written in terms of the contributions from 1PI diagrams and counter terms. After that, we set the same number of renormalization condition as the number of counter terms to determine them. For the renormalization scheme of the gauge and the fermion sector, we employ the same renormalization scheme as that of the SM. in the following of this section, we focus on the renormalization of the Higgs sector.

In the Higgs potential, there are eight paramaters,

$$m_1^2, m_2^2, m_3^2, \lambda_1, \lambda_2, \lambda_3, \lambda_4, \lambda_5. \tag{5.1}$$

As described in Sec. 3.1.1, they can be written in terms of the physical parameters m_h^2, m_H^2, $m_{H^\pm}^2$, m_A^2, α, β, v and M^2.

First, we shift the physical parameters form bare parameters to renormalized parameters following as,

$$m_h^2 \to m_h^2 + \delta m_h^2, \tag{5.2}$$
$$m_H^2 \to m_H^2 + \delta m_H^2, \tag{5.3}$$
$$m_{H^+}^2 \to m_{H^+}^2 + \delta m_{H^+}^2, \tag{5.4}$$
$$m_A^2 \to m_A^2 + \delta m_A^2, \tag{5.5}$$
$$v \to v + \delta v, \tag{5.6}$$
$$\alpha \to \alpha + \delta\alpha, \tag{5.7}$$
$$\beta \to \beta + \delta\beta, \tag{5.8}$$
$$M^2 \to M^2 + \delta M^2. \tag{5.9}$$

[1]For the determination of the counter term for M^2, the minimal subtraction scheme has been applied.

We also shift tadpoles of H and h,

$$T_H \to T_H + \delta T_H, \tag{5.10}$$
$$T_h \to T_h + \delta T_h, \tag{5.11}$$

where T_H and T_h are related with T_1 and T_2,

$$\delta T_1 = c_\alpha \delta T_H - s_\alpha \delta T_h, \tag{5.12}$$
$$\delta T_2 = s_\alpha \delta T_H + c_\alpha \delta T_h. \tag{5.13}$$

Each scalar field is shifted to the renormalized field and the wave function renormalization,

$$\begin{pmatrix} H \\ h \end{pmatrix} \to \begin{pmatrix} 1+\frac{1}{2}\delta Z_H & \delta C_{Hh}+\delta\alpha \\ -\delta\alpha+\delta C_{hH} & 1+\frac{1}{2}\delta Z_h \end{pmatrix} \begin{pmatrix} H \\ h \end{pmatrix}, \tag{5.14}$$
$$\begin{pmatrix} G^0 \\ A \end{pmatrix} \to \begin{pmatrix} 1+\frac{1}{2}\delta Z_{G^0} & \delta C_{GA}+\delta\beta \\ -\delta\beta+\delta C_{AG} & 1+\frac{1}{2}\delta Z_A \end{pmatrix} \begin{pmatrix} G^0 \\ A \end{pmatrix}, \tag{5.15}$$
$$\begin{pmatrix} G^+ \\ H^+ \end{pmatrix} \to \begin{pmatrix} 1+\frac{1}{2}\delta Z_{G^+} & \delta C_{G^+H^-}+\delta\beta \\ -\delta\beta+\delta C_{H^+G^-} & 1+\frac{1}{2}\delta Z_{H^+} \end{pmatrix} \begin{pmatrix} G^+ \\ H^+ \end{pmatrix}. \tag{5.16}$$

Renormalized one and two point functions at one-loop level are expressed as

$$\hat{\Gamma}_H = 0 + \delta T_H + \Gamma_H^{\rm 1PI}, \tag{5.17}$$
$$\hat{\Gamma}_h = 0 + \delta T_h + \Gamma_h^{\rm 1PI}, \tag{5.18}$$
$$\hat{\Pi}_{H^+H^-}[p^2] = (p^2 - m_{H^+}^2)\delta Z_{H^+} - \delta m_{H^+}^2 + \frac{s_\beta^2}{c_\beta}\frac{\delta T_1}{v} + \frac{c_\beta^2}{s_\beta}\frac{\delta T_2}{v} + \Pi_{H^+H^-}^{\rm 1PI}[p^2], \tag{5.19}$$
$$\begin{aligned}\hat{\Pi}_{H^+G^-}[p^2] &= \left(p^2 - m_{H^+}^2\right)\left(-\delta\beta + \delta C_{H^+G^-}\right) + p^2\left(\delta C_{G^+H^-} + \delta\beta\right) \\ &\quad + 2\left(c_\beta\frac{\delta T_2}{v} - s_\beta\frac{\delta T_1}{v}\right) + \Pi_{H^+G^-}^{\rm 1PI}[p^2],\end{aligned} \tag{5.20}$$
$$\hat{\Pi}_{G^+G^-}[p^2] = p^2\delta Z_{G^+} + c_\beta\frac{\delta T_1}{v} - s_\beta\frac{\delta T_2}{v} + \Pi_{G^+G^-}^{\rm 1PI}[p^2], \tag{5.21}$$
$$\hat{\Pi}_{AA}[p^2] = (p^2 - m_A^2)\delta Z_A - \delta m_A^2 + \frac{s_\beta^2}{c_\beta}\frac{\delta T_1}{v} + \frac{c_\beta^2}{s_\beta}\frac{\delta T_2}{v} + \Pi_{AA}^{\rm 1PI}[p^2], \tag{5.22}$$
$$\hat{\Pi}_{GA}[p^2] = \left(p^2 - m_A^2\right)\left(\delta Z_{AG} - \delta\beta\right) + p^2(\delta Z_{GA} + \delta\beta) - s_\beta\frac{\delta T_1}{v} + c_\beta\frac{\delta T_2}{v} + \Pi_{GA}^{\rm 1PI}[p^2], \tag{5.23}$$
$$\hat{\Pi}_{GG}[p^2] = p^2\delta Z_{G^0} - \delta m_A^2 + \frac{s_\beta^2}{c_\beta}\frac{\delta T_1}{v} + \frac{c_\beta^2}{s_\beta} + \Pi_{AA}^{1PI}[p^2], \tag{5.24}$$
$$\hat{\Pi}_{HH}[p^2] = (p^2 - m_H^2)\delta Z_H - \delta m_H^2 + \frac{c_\alpha^2}{c_\beta}\frac{\delta T_1}{v} + \frac{s_\alpha^2}{s_\beta}\frac{\delta T_2}{v} + \Pi_{HH}^{\rm 1PI}[p^2], \tag{5.25}$$
$$\begin{aligned}\hat{\Pi}_{Hh}[p^2] &= (p^2 - m_H^2)(\delta C_{Hh} + \delta\alpha) + (p^2 - m_h^2)(\delta C_{hH} - \delta\alpha) \\ &\quad + c_\alpha s_\alpha\left(-\frac{1}{c_\beta}\frac{\delta T_1}{v} + \frac{1}{s_\beta}\frac{\delta T_2}{v}\right) + \Pi_{hH}^{\rm 1PI}[p^2],\end{aligned} \tag{5.26}$$
$$\hat{\Pi}_{hh}[p^2] = (p^2 - m_h^2)\delta Z_h - \delta m_h^2 + \frac{s_\alpha^2}{c_\beta}\frac{\delta T_1}{v} + \frac{c_\alpha^2}{s_\beta}\frac{\delta T_2}{v} + \Pi_{hh}^{\rm 1PI}[p^2], \tag{5.27}$$

where analytic formulae of 1PI diagram parts are given in Appendix.

In order to determine counter terms, we impose renormalization conditions. We start from renormalizations of the tadpole. We impose them on-shell conditions as renormalization conditions.

$$\Gamma_H[p^2] = 0, \;\; \Gamma_h[p^2] = 0. \tag{5.28}$$

Then we obtain

$$\delta T_H = -T_H^{1PI}[0], \;\; \delta T_h = -T_h^{1PI}[0]. \tag{5.29}$$

The seven counter terms related to the CP-even Higgs sectors (δm_h^2, δm_H^2, $\delta\alpha$, δC_{Hh}, δC_{hH}, δZ_H and δZ_H) are determined by following seven renormalized conditions,

$$\hat{\Pi}_{HH}[m_H^2] = 0, \;\; \frac{d}{dp^2}\hat{\Pi}_{HH}[p^2]\Big|_{p^2=m_H^2} = 0, \tag{5.30}$$

$$\hat{\Pi}_{hh}[m_h^2] = 0, \;\; \frac{d}{dp^2}\hat{\Pi}_{hh}[p^2]\Big|_{p^2=m_h^2} = 0, \tag{5.31}$$

$$\hat{\Pi}_{hH}[m_h^2] = 0, \;\; \hat{\Pi}_{hH}[m_H^2] = 0, \;\; \delta C_{hH} = \delta C_{Hh} (\equiv \delta C_h), \tag{5.32}$$

by which we obtain

$$\delta m_h^2 = \Pi_{hh}^{\rm 1PI}[m_h^2] + \frac{s_\alpha^2}{c_\beta}\frac{\delta T_1}{v} + \frac{c_\alpha^2}{s_\beta}\frac{\delta T_2}{v}, \tag{5.33}$$

$$\delta m_H^2 = \Pi_{HH}^{\rm 1PI}[m_H^2] + \frac{c_\alpha^2}{c_\beta}\frac{\delta T_1}{v} + \frac{s_\alpha^2}{s_\beta}\frac{\delta T_2}{v}, \tag{5.34}$$

$$\delta Z_h = -\frac{d}{dp^2}\Pi_{hh}^{\rm 1PI}[p^2]\Big|_{p^2=m_h^2}, \tag{5.35}$$

$$\delta Z_H = -\frac{d}{dp^2}\Pi_{HH}^{\rm 1PI}[p^2]\Big|_{p^2=m_H^2}, \tag{5.36}$$

$$\delta\alpha = \frac{1}{2(m_H^2 - m_h^2)}\left\{2c_\alpha s_\alpha\left(-\frac{1}{c_\beta}\frac{\delta T_1}{v} + \frac{1}{s_\beta}\frac{\delta T_2}{v}\right) + \Pi_{Hh}^{\rm 1PI}[m_H^2] + \Pi_{Hh}^{\rm 1PI}[m_h^2]\right\}, \tag{5.37}$$

$$\delta C_h = \frac{1}{2(m_H^2 - m_h^2)}\left(\Pi_{Hh^{\rm 1PI}}[m_h^2] - \Pi_{Hh}^{\rm 1PI}[m_H^2]\right). \tag{5.38}$$

There are seven counter terms related to the CP-odd Higgs sectors (δm_A^2, $\delta\beta$, δC_{AG}, δC_{GA}, δZ_A and δZ_{G^0}). First, we determine δm_A^2, δZ_A, δZ_{G^0} following conditions

$$\hat{\Pi}_{AA}[m_H^2] = 0, \;\; \frac{d}{dp^2}\hat{\Pi}_{AA}[p^2]\Big|_{p^2=m_A^2} = 0, \tag{5.39}$$

$$\frac{d}{dp^2}\hat{\Pi}_{GG}[p^2]\Big|_{p^2=0} = 0, \tag{5.40}$$

by which we obtain

$$\delta m_A^2 = \Pi_{AA}^{1PI}[m_A^2] + \frac{s_\beta^2}{c_\beta}\frac{\delta T_1}{v} + \frac{c_\beta^2}{s_\beta}\frac{\delta T_2}{v}, \tag{5.41}$$

$$\delta Z_A = -\frac{d}{dp^2}\Pi_{AA}^{1PI}[p^2]|_{p^2=m_A^2}, \tag{5.42}$$

$$\delta Z_{G^0} = -\frac{d}{dp^2}\Pi_{GG}^{1PI}[p^2]|_{p^2=0}. \tag{5.43}$$

According to Ref. [101], gauge dependence remains in $\delta\beta$ depending on kinds of renormalizaton conditions. For example, if we employ following the set of renormalization conditions, gauge dependence remain in $\delta\beta$,

$$\Pi_{GA}[0] = 0, \tag{5.44}$$

$$\Pi_{GA}[m_A^2] = 0, \tag{5.45}$$

$$\delta C_{AG} = \delta C_{GA}\cdot, \tag{5.46}$$

by which we obtain

$$\delta\beta = -\frac{1}{2m_A^2}\tilde{\Pi}_{GA}[m_A^2], \tag{5.47}$$

$$\delta C_{AG} = \delta\beta. \tag{5.48}$$

When we derive a form $\delta C_{AG^0} = \delta\beta$, We use NG theorem $\tilde{\Pi}_{G^0A}[0] = 0$.

In order to remove gauge dependence from $\delta\beta$, we determine three counter terms by following method. In order to determine three counter terms, we need to impose one more renormalization condition in addition to that given in Eqs. (5.39), (5.40). This third condition can be used to remove the gauge dependence in $\delta\beta$ which was already mentioned in the beginning of this section. To define such a condition, we separate $\tilde{\Pi}_{AG}^{1\mathrm{PI}}(p^2)$ into the gauge dependent (G.D.) part and the gauge independent (G.I.) part as

$$\tilde{\Pi}_{AG}^{1\mathrm{PI}}(p^2) = \tilde{\Pi}_{AG}^{1\mathrm{PI}}(p^2)\big|_{\mathrm{G.D.}} + \tilde{\Pi}_{AG}^{1\mathrm{PI}}(p^2)\big|_{\mathrm{G.I.}}. \tag{5.49}$$

Then, we imposed the third condition as

$$\delta\beta = -\frac{1}{2m_A^2}\tilde{\Pi}_{AG}^{1\mathrm{PI}}(m_A^2)\big|_{\mathrm{G.I.}}. \tag{5.50}$$

The remaining two counter terms are also determined:

$$\delta C_{AG} = -\frac{1}{2m_A^2}\left[\tilde{\Pi}_{AG}^{1\mathrm{PI}}(m_A^2)\big|_{\mathrm{G.I.}} - 2\tilde{\Pi}_{AG}^{1\mathrm{PI}}(0)\big|_{\mathrm{G.D.}}\right], \tag{5.51}$$

$$\delta C_{GA} = -\frac{1}{2m_A^2}\left[\tilde{\Pi}_{AG}^{1\mathrm{PI}}(m_A^2)\big|_{\mathrm{G.I.}} + 2\tilde{\Pi}_{AG}^{1\mathrm{PI}}(m_A^2)\big|_{\mathrm{G.D.}}\right]. \tag{5.52}$$

We note that in $\tilde{\Pi}_{AG}^{1\mathrm{PI}}(0)$ only the G.D. part is survived; i.e., $\tilde{\Pi}_{AG}^{1\mathrm{PI}}(0) = \tilde{\Pi}_{AG}^{1\mathrm{PI}}(0)\big|_{\mathrm{G.D.}}$. As it can be seen in Eqs. (5.51) and (5.52), there still remains the gauge dependence in δC_{AG} and δC_{GA}.

However, they do not appear in the following calculations for the renormalization of the Higgs boson couplings. Instead of applying the above renormalization scheme for $\delta\beta$, we can apply the $\overline{\rm MS}$ scheme in which the gauge dependence can also be removed at the one-loop level as discueed in Ref. [101]. In the following discussion, we apply the renormalized $\tan\beta$ determined by Eq. (5.50).

There are seven counter terms related to the singly charged Higgs sectors ($\delta m^2_{H^\pm}$, $\delta\beta$, δC_{HG}, δC_{GH}, δZ_H and $\delta Z_{G^\pm}$). One of them $\delta\beta$ already has been determined in the renormalization of CP-odd Higgs states Eq. (5.50). We determine them following conditions

$$\hat{\Pi}_{H^+H^-}[m^2_{H^\pm}] = 0, \quad \frac{d}{dp^2}\hat{\Pi}_{H^+H^-}[p^2]\Big|_{p^2=m^2_{H^\pm}} = 0, \tag{5.53}$$

$$\frac{d}{dp^2}\hat{\Pi}_{G^+G^-}[p^2]\Big|_{p^2=0} = 0, \tag{5.54}$$

$$\hat{\Pi}_{H^+G^-}[m^2_{H^\pm}] = \hat{\Pi}_{H^+G^-}[0] = 0 \tag{5.55}$$

by which we obtain

$$\delta m^2_{H^+} = \frac{s^2_\beta}{c_\beta}\frac{\delta T_1}{v} + \frac{c^2_\beta}{s_\beta}\frac{\delta T_2}{v} + \Pi^{1PI}_{H^+H^-}[0], \tag{5.56}$$

$$\delta Z_{H^\pm} = -\frac{d}{dp^2}\Pi^{1PI}_{H^+H^-}[p^2]\Big|_{p^2=m^2_{H^+}}, \tag{5.57}$$

$$\delta Z_{G^\pm} = -\frac{d}{dp^2}\Pi^{1PI}_{G^+G^-}[p^2]\Big|_{p^2=0}. \tag{5.58}$$

Until here, we did not discuss the determination of δM^2. As adopted in Ref. [70], we apply the minimal subtraction scheme for δM^2, where it is determined so as to absorb only the divergent part in the hhh vertex at the one-loop level, that is

$$\frac{\delta M^2}{M^2} = \frac{1}{16\pi^2 v^2}\Big[2\sum_f N^f_c m^2_f \xi^2_f + 4M^2 - 2m^2_{H^\pm} - m^2_A + \frac{\sin 2\alpha}{\sin 2\beta}(m^2_H - m^2_h) - 3(2m^2_W - m^2_Z)\Big]\Delta, \tag{5.59}$$

where Δ is the divergence part given by $\Delta \equiv \frac{1}{\epsilon} - \gamma_E + \ln 4\pi + \ln\mu^2$.

5.2 Renormalized Higgs boson couplings in the THDMs

5.2.1 Analytic expressions

In the previous section, all the counter terms are deternimed by the set of renormalization conditions. Now, we can evaluate the renormalized Higgs boson couplings hWW [59], hZZ [59, 70], $hf\bar{f}$ [58,59,102] and hhh [59,70]. In addition to the above couplings, we also give formulae for the loop induced decay rates; $h \to \gamma\gamma$ [102–104], $h \to Z\gamma$ [104] and $h \to gg$ [105].

The renormalized hVV, $hf\bar{f}$ and hhh vertices are expressed as

$$\hat{\Gamma}^i_{hVV}(p^2_1, p^2_2, q^2) = \Gamma^{i,\rm tree}_{hVV} + \delta\Gamma^i_{hVV} + \Gamma^{i,\rm 1PI}_{hVV}(p^2_1, p^2_2, q^2), \quad (i = \text{1-3}), \tag{5.60}$$

$$\hat{\Gamma}_{hff}(p^2_1, p^2_2, q^2) = \Gamma^{\rm tree}_{hff} + \delta\Gamma_{hff} + \Gamma^{\rm 1PI}_{hff}(p^2_1, p^2_2, q^2), \tag{5.61}$$

$$\hat{\Gamma}_{hhh}(p^2_1, p^2_2, q^2) = \Gamma^{\rm tree}_{hhh} + \delta\Gamma_{hhh} + \Gamma^{\rm 1PI}_{hhh}(p^2_1, p^2_2, q^2), \tag{5.62}$$

	$\delta\xi_h^u$	$\delta\xi_h^d$	$\delta\xi_h^e$
Type-I	$-\frac{c_\alpha}{s_\beta}(\cot\beta\delta\beta+\tan\alpha\delta\alpha)$	$-\frac{c_\alpha}{s_\beta}(\cot\beta\delta\beta+\tan\alpha\delta\alpha)$	$-\frac{c_\alpha}{s_\beta}(\cot\beta\delta\beta+\tan\alpha\delta\alpha)$
Type-II	$-\frac{c_\alpha}{s_\beta}(\cot\beta\delta\beta+\tan\alpha\delta\alpha)$	$-\frac{s_\alpha}{c_\beta}(\tan\beta\delta\beta+\cot\alpha\delta\alpha)$	$-\frac{s_\alpha}{c_\beta}(\tan\beta\delta\beta+\cot\alpha\delta\alpha)$
Type-X	$-\frac{c_\alpha}{s_\beta}(\cot\beta\delta\beta+\tan\alpha\delta\alpha)$	$-\frac{c_\alpha}{s_\beta}(\cot\beta\delta\beta+\tan\alpha\delta\alpha)$	$-\frac{s_\alpha}{c_\beta}(\tan\beta\delta\beta+\cot\alpha\delta\alpha)$
Type-Y	$-\frac{c_\alpha}{s_\beta}(\cot\beta\delta\beta+\tan\alpha\delta\alpha)$	$-\frac{s_\alpha}{c_\beta}(\tan\beta\delta\beta+\cot\alpha\delta\alpha)$	$-\frac{c_\alpha}{s_\beta}(\cot\beta\delta\beta+\tan\alpha\delta\alpha)$

Table 5.1: The counter term for the mixing factors in Yukawa interactions.

where $\Gamma^{\rm tree}_{hXX}$, $\delta\Gamma_{hXX}$ and $\Gamma^{\rm 1PI}_{hXX}$ are the contributions from the tree level, the counter terms and the 1PI diagrams for the hXX vertices, respectively. In the above expressions, p_1 and p_2 ($q=p_1+p_2$) are the incoming momenta of particle X (outgoing momentum for h). For the hVV vertex, the index i labels the following three form factors;

$$\hat{\Gamma}^{\mu\nu}_{hVV}=\hat{\Gamma}^1_{hVV}g^{\mu\nu}+\hat{\Gamma}^2_{hVV}\frac{p_1^\mu p_2^\nu}{m_V^2}+i\hat{\Gamma}^3_{hVV}\epsilon^{\mu\nu\rho\sigma}\frac{p_{1\rho}p_{2\sigma}}{m_V^2}. \tag{5.63}$$

The tree-level contributions are given as

$$\Gamma^{1,\rm tree}_{hVV}=\frac{2m_V^2}{v}\sin(\beta-\alpha),\quad \Gamma^{2,\rm tree}_{hVV}=\Gamma^{3,\rm tree}_{hVV}=0,\quad \Gamma^{\rm tree}_{hff}=-\frac{m_f}{v}\xi_h^f,\quad \Gamma^{\rm tree}_{hhh}=-6\lambda_{hhh}. \tag{5.64}$$

The counter-term contributions are

$$\delta\Gamma^1_{hVV}=\frac{2m_V^2}{v}\left[\sin(\beta-\alpha)\left(\frac{\delta m_V^2}{m_V^2}+\delta Z_V+\frac{1}{2}\delta Z_h-\frac{\delta v}{v}\right)+\cos(\beta-\alpha)(\delta\beta+\delta C_h)\right],$$
$$\delta\Gamma^2_{hVV}=\delta\Gamma^3_{hVV}=0, \tag{5.65}$$
$$\delta\Gamma_{hff}=-\frac{m_f}{v}\xi_h^f\left[\frac{\delta m_f}{m_f}-\frac{\delta v}{v}+\delta Z_V^f+\frac{1}{2}\delta Z_h+\frac{\delta\xi_h^f}{\xi_h^f}+\frac{\xi_H^f}{\xi_h^f}(\delta C_h+\delta\alpha)\right], \tag{5.66}$$
$$\delta\Gamma_{hhh}=6\left[\delta\lambda_{hhh}+\frac{3}{2}\delta Z_h+\lambda_{Hhh}(\delta\alpha+\delta C_h)\right]. \tag{5.67}$$

The counter terms in the Yukawa couplings $\delta\xi_h^f$ are expressed in terms of $\delta\beta$ and $\delta\alpha$ as listed in Table 5.1. We define the renormalized scaling factors by the following way;

$$\hat{\kappa}_V=\frac{\hat{\Gamma}^1_{hVV}(m_V^2,m_h^2,q^2)_{\rm THDM}}{\hat{\Gamma}^1_{hVV}(m_V^2,m_h^2,q^2)_{\rm SM}}, \tag{5.68a}$$
$$\hat{\kappa}_f=\frac{\hat{\Gamma}_{hff}(m_f^2,m_f^2,q^2)_{\rm THDM}}{\hat{\Gamma}_{hff}(m_f^2,m_f^2,q^2)_{\rm SM}}, \tag{5.68b}$$
$$\hat{\kappa}_h=\frac{\hat{\Gamma}_{hhh}(m_h^2,m_h^2,q^2)_{\rm THDM}}{\hat{\Gamma}_{hhh}(m_h^2,m_h^2,q^2)_{\rm SM}}. \tag{5.68c}$$

The deviation in these scaling factors from the SM prediction can be described by

$$\Delta\kappa_i = \hat{\kappa}_i - 1. \tag{5.69}$$

We also give the loop induced decay rates for $h \to \gamma\gamma$, $h \to Z\gamma$ and $h \to gg$ in the Appendix. We then define the ratio of these decay rates;

$$R_{XY} = \frac{\Gamma(h \to XY)_{\rm THDM}}{\Gamma(h \to XY)_{\rm SM}}, \quad \text{for} \quad XY = \gamma\gamma,\ Z\gamma,\ \text{and}\ gg. \tag{5.70}$$

The deviations in renormalized Higgs boson couplings are approximately expressed by keeping the non-decoupling effects of extra Higgs bosons and top and bottom masses dependence ($m_A \simeq m_H$ is assumed) as

$$\Delta\hat{\kappa}_V \simeq -\frac{1}{2}\,x^2 - \frac{1}{16\pi^2}\frac{1}{6}\sum_{\Phi=A,H,H^\pm} c_\Phi \frac{m_\Phi^2}{v^2}\left(1-\frac{M^2}{m_\Phi^2}\right)^2, \tag{5.71}$$

$$\Delta\hat{\kappa}_\tau \simeq \Delta\hat{\kappa}_V + \xi_e\, x, \tag{5.72}$$

$$\Delta\hat{\kappa}_c \simeq \Delta\hat{\kappa}_V + \xi_u\, x, \tag{5.73}$$

$$\Delta\hat{\kappa}_b \simeq \Delta\hat{\kappa}_V + \xi_d\, x - \frac{1}{16\pi^2}\xi_u\xi_d\frac{2m_t^2}{v^2}\left(1-\frac{m_t^2}{m_{H^\pm}^2}-\frac{M^2}{m_{H^\pm}^2}\right) - \frac{1}{16\pi^2}\frac{1}{6}\xi_d^2\sum_{\Phi=A,H,H^\pm}\frac{m_b^4}{v^2 m_\Phi^2}, \tag{5.74}$$

$$\Delta\hat{\kappa}_t \simeq \Delta\hat{\kappa}_V + \xi_u\, x - \frac{1}{16\pi^2}\frac{1}{6}\left[\xi_u^2\sum_{\Phi=A,H,H^\pm}\frac{m_t^4}{v^2 m_\Phi^2} + \xi_d^2\frac{m_b^2 m_t^2}{v^2 m_{H^\pm}^2}\right], \tag{5.75}$$

$$\Delta\hat{\kappa}_h \simeq \left(\frac{3}{2}-\frac{2M^2}{m_h^2}\right)x^2 + \frac{1}{16\pi^2}\sum_{\Phi=A,H,H^\pm} c_\Phi\frac{4}{3}\frac{m_\Phi^4}{m_h^2 v^2}\left(1-\frac{M^2}{m_\Phi^2}\right)^3. \tag{5.76}$$

We can see that there appears the term $m_\Phi^2/v^2\,(1-M^2/m_\Phi^2)^2$ in $\Delta\hat{\kappa}_V$ which comes from the counter term δZ_h; i.e., the derivative of the h two point function given in Eq. (5.35). When we consider the case with $M^2 \lesssim v^2$, this term gives the quadratic power like dependence of the mass of additional Higgs bosons. This corresponds to the case where the mass of additional Higgs bosons, which is expressed schematically as $m_\Phi^2 = \lambda_i v^2 + M^2$, mostly comes from the Higgs VEV v. In such a situation, it is known that the decoupling theorem does not work. On the other hand, if we consider the case of $M^2 \gg v^2$, the amount of $\Delta\hat{\kappa}_f$ is reduced as $1/m_\Phi^2$ according to the decoupling theorem. The same contribution from δZ_h is also seen in $\Delta\hat{\kappa}_f$ ($f = \tau, c, b, t$) through the term $\Delta\hat{\kappa}_V$. Notice here that there are additional terms proportional to the top or bottom quark masses in $\Delta\hat{\kappa}_b$ and $\Delta\hat{\kappa}_t$. They come from the additional Higgs boson loop contributions to the 1PI $hb\bar{b}$ or $ht\bar{t}$ diagrams. Apart from $\Delta\hat{\kappa}_V$ and $\Delta\hat{\kappa}_f$, let us discuss the expression of $\Delta\hat{\kappa}_h$. There appears the term $m_\Phi^4/(m_h^2 v^2)\,(1-M^2/m_\Phi^2)^3$ which comes from the additional Higgs boson loop contributions to the 1PI hhh diagrams. When we consider the non-decoupling case; i.e., $M^2 \lesssim v^2$, it gives the quartic power like dependence of m_Φ. Similar to the case in $\Delta\kappa_V$, this effect is decoupled by $1/m_\Phi^2$ when $M^2 \gg v^2$ is taken.

Similarly, the decay rates of $h \to \gamma\gamma$ and $h \to gg$ are expressed in terms of x ($x \ll 1$) as

$$\Gamma(h \to \gamma\gamma) \simeq \frac{G_F \alpha_{\rm em}^2 m_h^3}{128\sqrt{2}\pi^3} \left| -\frac{1}{3}\left(1 - \frac{M^2}{m_{H^\pm}^2}\right) + Q_f N_c^f (1 + \xi_f\, x - \frac{x^2}{2}) I_f + (1 - \frac{x^2}{2}) I_W \right|^2 , \quad (5.77)$$

$$\Gamma(h \to gg) \simeq \frac{G_F \alpha_s^2 m_h^3}{64\sqrt{2}\pi^3} \left| (1 + \xi_q\, x - \frac{x^2}{2}) I_q \right|^2 . \quad (5.78)$$

The first term in $\Gamma(h \to \gamma\gamma)$ expressed by $(1 - M^2/m_{H^\pm}^2)$ is the charged Higgs boson loop contribution. When we take the limit of $M^2 \to 0$, this term approaches to the constant $-1/3$. This can also be understood as the consequence of the non-decoupling effect of the charged Higgs boson loop contribution, but it is not like the quartic (quadratic) power like dependence seen in the $\Delta\hat{\kappa}_h$ ($\Delta\hat{\kappa}_V$ and $\Delta\hat{\kappa}_f$).

5.2.2 Deviations in the Higgs boson couplings at the one-loop level in the THDMs

In the following, we show numerical results for the Higgs boson couplings at the one-loop level. We use the following inputs [99];

$$m_Z = 91.1875 \text{ GeV},\ G_F = 1.16639 \times 10^{-5} \text{ GeV}^{-2},\ \alpha_{\rm em}^{-1} = 137.035989,\ \Delta\alpha_{\rm em} = 0.06635,$$
$$m_t = 173.07 \text{ GeV},\ m_b = 4.66 \text{ GeV},\ m_c = 1.275 \text{ GeV},\ m_\tau = 1.77684 \text{ GeV}. \quad (5.79)$$

We first show the case of $\sin(\beta - \alpha) = 1$. In this case, the deviations in the Higgs boson couplings purely comes from the additional Higgs boson loop effects. We note that the $\tan\beta$ dependence in the renormalized scaling factors appears only in κ_f. We take all the masses of additional Higgs bosons to be the same; $m_{H^\pm} = m_A = m_H$ ($\equiv m_\Phi$) for simplicity, and we fix the squared momentum to be $q^2 = (m_h + m_V)^2$, m_h^2, and $(2m_h)^2$ for $\hat{\kappa}_V$, $\hat{\kappa}_f$ and $\hat{\kappa}_h$, respectively.

In Fig. 5.1, we show the decoupling behavior of additional Higgs boson loop contributions to the Higgs boson couplings. The upper-left, upper-right, lower-left and lower-right panels respectively show $\Delta\kappa_h$, $\Delta\kappa_V$, $\Delta\kappa_b$ and ΔR as a function of m_Φ for several fixed values of λv^2 ($= m_\Phi^2 - M^2$). We take $\tan\beta = 1$ in this figure. We can see that all the deviations approach to zero in the large mass region due to the decoupling theorem.

In Fig. 5.2, we show the deviation in the Higgs boson couplings $\Delta\kappa_h$ (upper-left), $\Delta\kappa_V$ (upper-right), $\Delta\kappa_f$ (lower-left) and ΔR (lower-right) as a function of m_Φ. We take $M^2 = 0$ and $\tan\beta = 1$ for all panels. In this case, the magnitude of deviations increase when m_Φ becomes larger except for ΔR.

5.3 Discriminating four types of the THDMs

A pattern of deviations in the Higgs boson couplings from their SM predictions depends on the structure of the Higgs sector and the Yukawa interaction. The pattern of deviations depend on the number of the Higgs field, their representations and the mass of Higgs bosons in the loop. It is possible to discriminate extended Higgs sectors by using future precision data and comprehensively evaluating all coupling constants of h in each model. In this section, we evaluate the deviations in these coupling constants from predictions of the SM at the one-loop level, and study how to discriminate extended Higgs sectors by comparing the precise

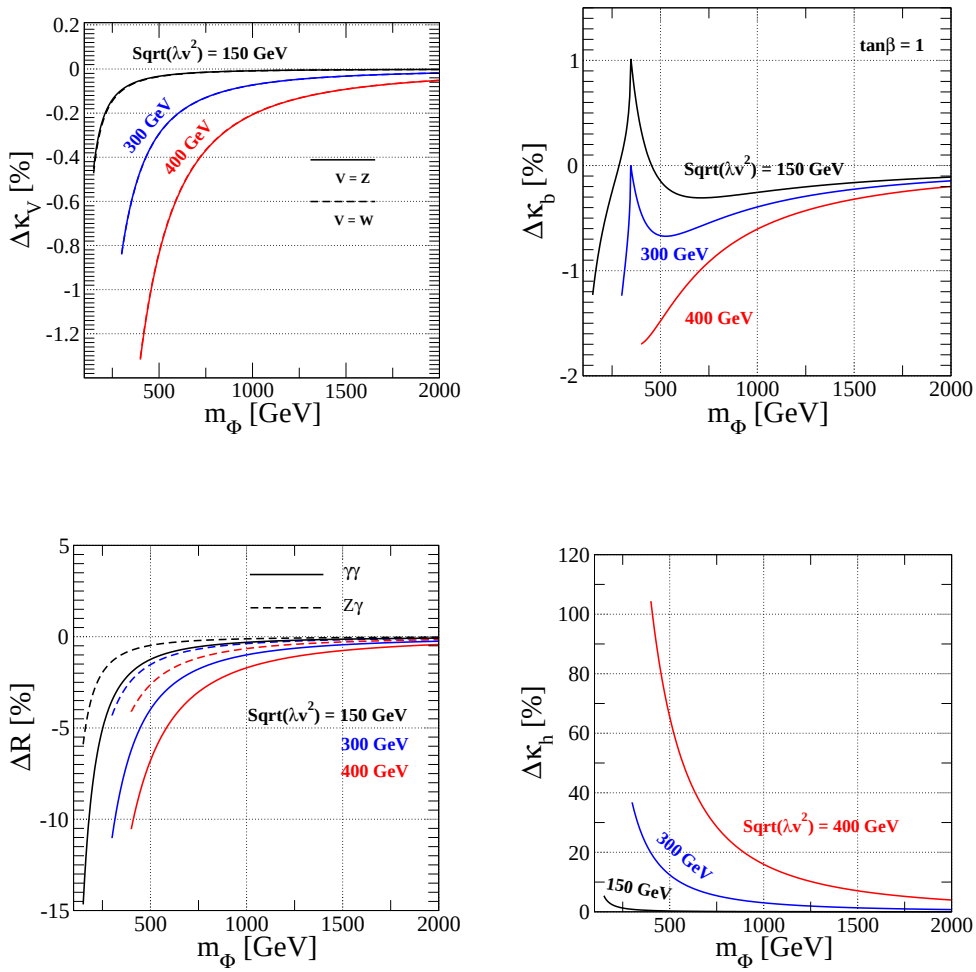

Figure 5.1: Deviations in the renormalized scaling factors for hhh (upper left), hVV (upper right) and $hb\bar{b}$ (bottom left), and those in the decay rates $\Delta R_{\gamma\gamma/Z\gamma}$ (bottom right) as a function of m_Φ in the case of $\sin(\beta-\alpha)=1$ and $\tan\beta=1$. Each curve denotes the results in the cases of λv^2 =150, 300 and 400 GeV.

predictions of characteristic pattern of deviations with future precision measurements of the coupling constants of h at future collider experiments, in particular at the ILC.

In this subsection, we investigate Yukawa interaction type of THDMs by correlations among Yukawa couplings at the one-loop level. In THDMs, different characteristic patterns of deviation in Yukawa coupling constants ($hf\bar{f}$) can be allowed depending on four types of Yukawa interactions.

In the SM like limit, renormalized scale factor of Yukawa couplings can be approximately expressed as

$$\hat{\kappa}_f = 1 - \frac{1}{16\pi^2}\frac{1}{6}\sum_{\Phi=A,H,H^\pm} c_\Phi \frac{m_\Phi^2}{v^2}\left(1-\frac{M^2}{m_\Phi^2}\right)^2, \tag{5.80}$$

where $c_\Phi = 2$ (1) in $\Phi = H^\pm$ (A, H). The second term in right-hand side of Eq. (6.2) is a deviation from the SM predictions due to loop effects of extra Higgs bosons. We can see

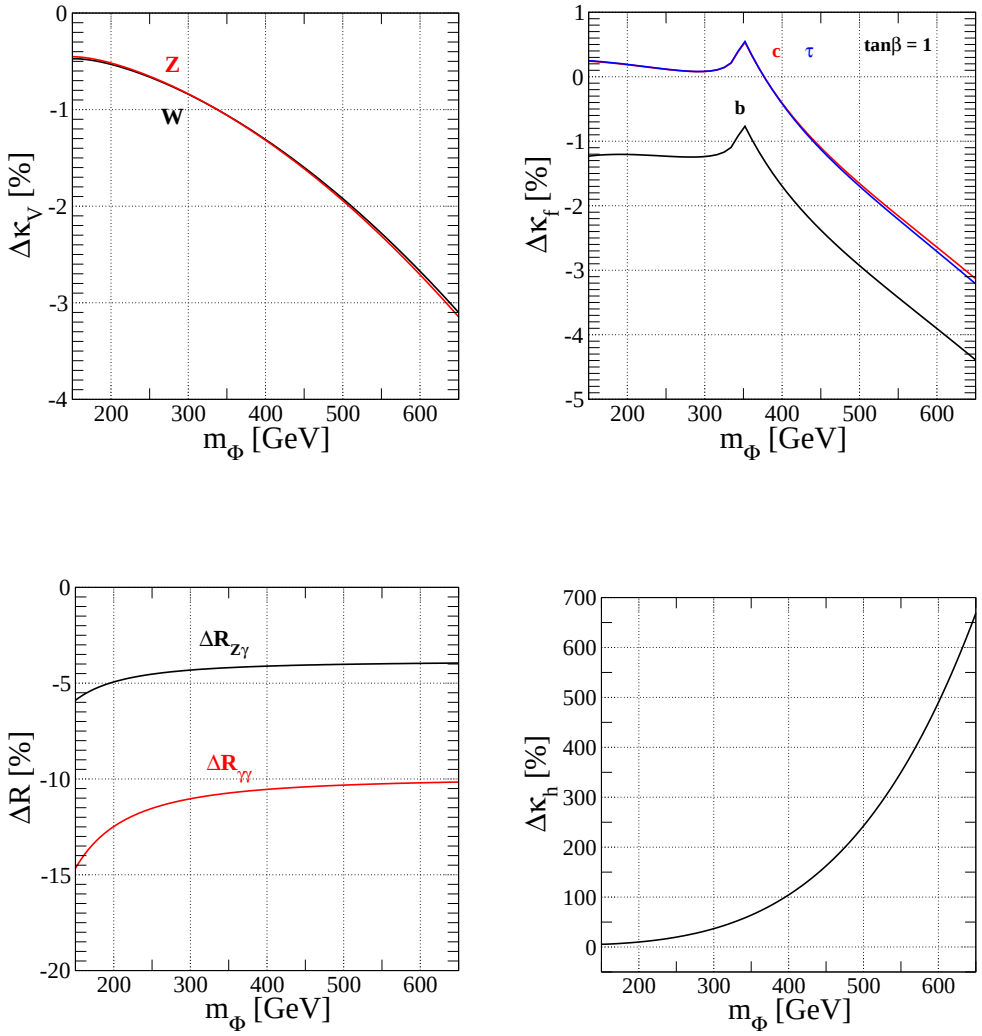

Figure 5.2: Deviations in the renormalized scaling factors for hhh (upper left), hVV (upper right) and $hb\bar{b}$ (bottom left), and those in the decay rates $\Delta R_{\gamma\gamma/Z\gamma}$ (bottom right) as a function of m_Φ in the case of $M^2 = 0$, $\sin(\beta-\alpha) = 1$ and $\tan\beta = 1$.

that the effect can be both decoupling and non-decoupling, depending on the balance between m_Φ^2 and M^2. If M^2 is as large as m_Φ^2, the effect becomes decoupling in the large mass limit. Otherwise, quadratic dependences of m_Φ appear.

In Fig. 5.3, we show the decoupling behavior of the one-loop corrections to each Yukawa coupling . We plot the deviations in the renormalized Yukawa couplings; i.e., $\hat{\kappa}_f - 1$ for $f = b, \tau$ and c as a function of m_Φ in the Type-I (the top), Type-II (the second panel from the top), Type-X (the third one from the top) and Type-Y(the lowest) THDMs with $\sin^2(\beta-\alpha) = 1$, $\tan\beta = 1$ (the solid curves) and $\tan\beta = 3$ (the dashed curves). We here fix $m_\Phi^2 - M^2$ to be $(300\text{GeV})^2$ as just an example. You notice that the value of the deviations approaches to 0 in the large mass region. Because M^2/m_Φ^2 gets close to 1 as m_Φ become larger, the extra Higgs loop contributions written in Eq. (6.2) are reduced. Thus, we can verify that the renormalized $hf\bar{f}$ couplings approach to the SM prediction in the large mass limit. The peak at around $m_\Phi = 2m_t$ is the resonance of the top quark loop contributions to the two point function

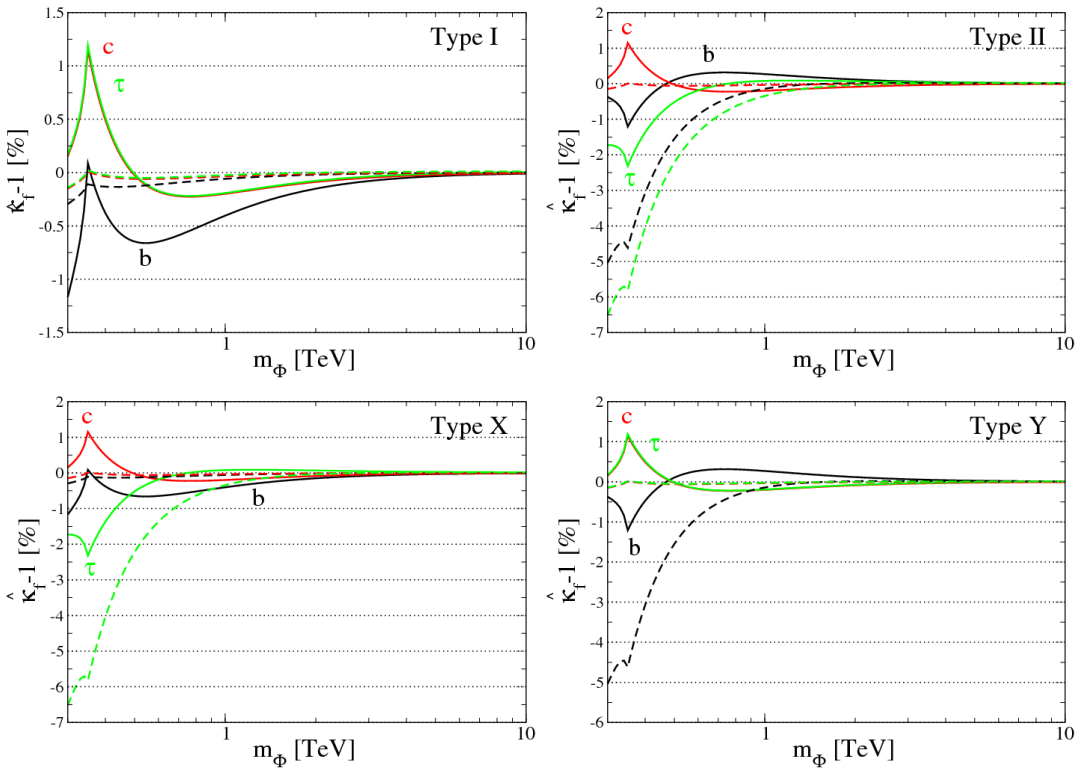

Figure 5.3: Deviations in $hf\bar{f}$ ($f = b, \tau, c$) couplings in four types of THDMs as a function of m_Φ ($\Phi = H^\pm, A, H$) when $\sin^2(\beta-\alpha) = 1$, $M^2 = m_\Phi^2 - (300\text{GeV})^2$ [58]. Solid lines and dashed lines show the case of $\tan\beta = 1$ and $\tan\beta = 3$, respectively. Those panels show results in Type-I, Type-II, Type-X and Type-Y of THDMs from the top.

among A and G^0.

In Fig. 5.4, we discuss non-decoupling effects for deviations in coupling constants of hcc, hbb and $h\tau\tau$ in Type-I (the top), Type-II (the second panel from the top), Type-X (the third one from the top) and Type-Y (the lowest). They are deviations including one-loop radiative corrections as functions of masses of extra Higgs bosons. We take the mixing angles to be $\sin^2(\beta-\alpha) = 1$ with $\tan\beta = 1$ (solid line) and $\tan\beta = 3$ (dashed line). We here fix the value of M^2 to be zero. We can find that deviations from the SM predictions can be several percent at the large mass region due to non-decoupling loop effects in the all types of Yukawa interactions even in the case with $\sin^2(\beta-\alpha) = 0$. However, the unitarity bound excludes parameter regions where masses of extra Higgs bosons are larger than about 600 GeV (230 GeV) in $\tan\beta = 1(3)$.

In Fig. 5.5, we show the behavior of the scale factors at the tree level $\kappa_\tau^{\text{tree}}$, κ_b^{tree} and one-loop corrected scale factors $\hat{\kappa}_\tau$, $\hat{\kappa}_b$ in the four types of THDMs [58]. The left panel and the right panel correspond to results in the case with $\cos(\beta-\alpha) > 0$ and $\cos(\beta-\alpha) < 0$, respectively. Doted lines indicate predictions at the tree level in $\sin^2(\beta-\alpha) = 0.99$ and 0.95, and black dots being on these lines are the tree level results with $\tan\beta = 1, 2, 3$ and 4. At the tree level, in the case with $\sin^2(\beta-\alpha) = 1$, predictions of all the types get close to those of the SM. If $\sin(\beta-\alpha)$ slightly deviate from unity, κ_f^{tree} for each type lead to deviate in different directions. However it

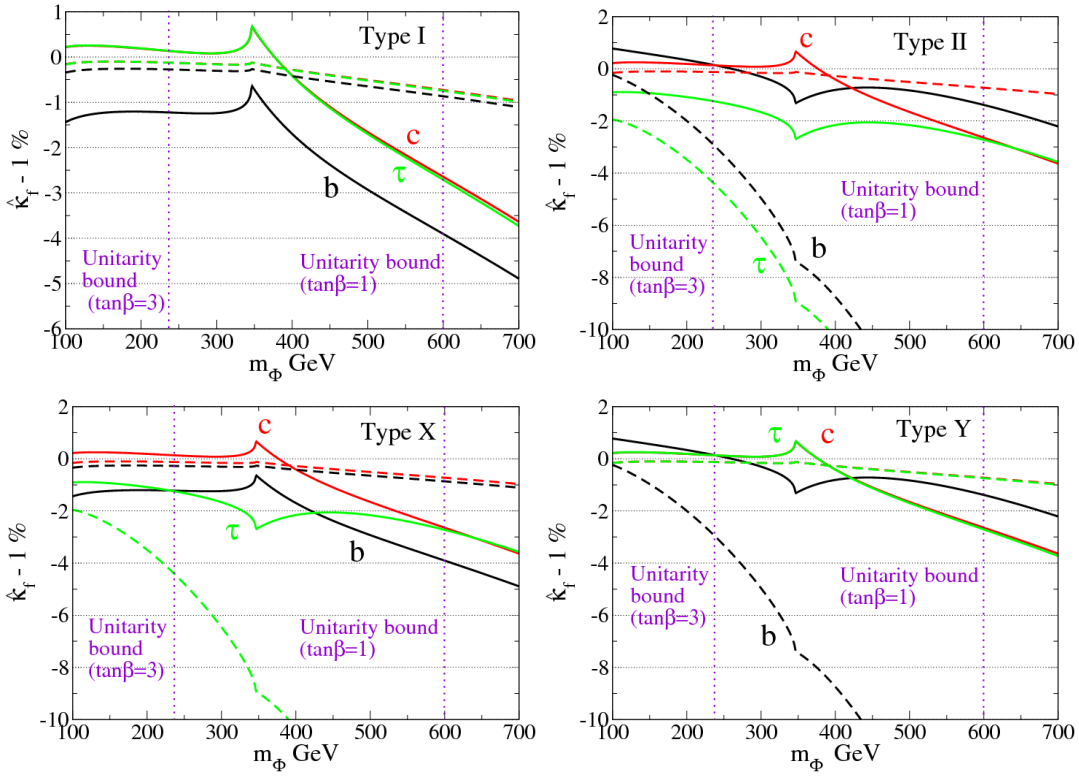

Figure 5.4: Deviations in Yukawa coupling constants for b, τ and c as a function of m_Φ when $\sin^2(\beta-\alpha)=1$, $M=0$ [58]. Solid lines and dashed lines show the case of $\tan\beta=1$ and $\tan\beta=3$, respectively. They are results in Type-I, Type-II, Type-X and Type-Y of THDMs from the top.

is diffecult to discriminate the types of THDMs by evaluating only κ_b and κ_τ because behaviors of κ_b and κ_τ depend on the sign of $\cos(\beta-\alpha)$. If $\cos(\beta-\alpha)$ is negative (positive), predictions of $\kappa_{t(c)}$ in all the types are less (larger) than 1. Therefore we can determine the sign of $\cos(\beta-\alpha)$ by using measurements of $\kappa_{t(c)}$. Then we can discriminate all types of Yukawa interactions by the pattern of deviations in these $hf\bar{f}$ couplings. These analysis of Yukawa couplings at the tree level have already been discussed in Refs. [13, 57, 106].

In Fig. 5.5, we also plot those including full electroweak and scalar bosons loop corrections which are shown by colored regions around black dots. Red regions (blue regions) are modified regions by extra Higgs loop contributions for the case with $\sin^2(\beta-\alpha)=0.99$ (0.95). We scan $m_\Phi(=m_{H^\pm}=m_A=m_H)$ and M over from 100 GeV to 1 TeV and from 0 to m_Φ, respectively. We find that results can be modified from the tree level values in several percent by extra Higgs loop effects. Even if radiative corrections become maximal values, predictions of $\hat{\kappa}_f$ $(f=c,b,\tau)$ in the types of Yukawa interaction don't overlap each other. Therefore we can discriminate all the types when $\sin^2(\beta-\alpha)$ deviates from the SM prediction by about 1%.

At the HL-LHC, $h\tau\tau$ and hbb couplings are expected to be measured with about 8% and 11%, respectively [56, 100]. When $\sin^2(\beta-\alpha)$ is different about 1% from unity, hbb and $h\tau\tau$ coupling constants can differ about 10% from the predictions of the SM depending on the value of $\tan\beta$. In that case, we can discriminate the types of Yukawa interactions by using those HL-

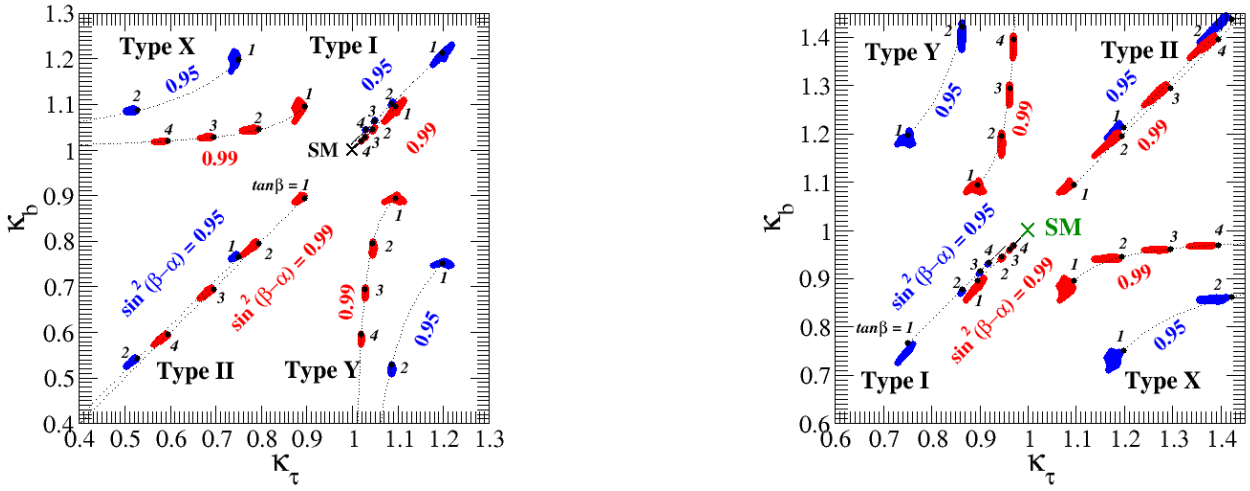

Figure 5.5: Plots of scale factors of τ and b in four types of Yukawa interactions [58]. The left panel and the right panel are predictions with $\cos(\beta-\alpha) > 0$ and $\cos(\beta-\alpha) < 0$, respectively. Each black dot indicates a result at the tree level with $\tan\beta = 1, 2, 3$ and 4. Red region (blue region) show one-loop results with $\sin^2(\beta-\alpha) = 0.99$ ($\sin^2(\beta-\alpha) = 0.95$) where m_Φ and M are scanned over from 100 GeV to 1 TeV and 0 to m_Φ, respectively, under the constraints of perturbative unitarity and vacuum stability.

LHC data. At the ILC500, however, the Higgs coupling measurements have typically $\mathcal{O}(1)\%$ level resolution: e.g., h coupling constants to τ and b can be determine with 2.3% and 1.6% uncertainty, respectively [13]. In order to compare with such precision coupling measurements at the ILC, we must not neglect the effects of radiative corrections.

5.4 Determination of inner parameters from the Higgs boson coupling measurements

In this section, we investigate how we can fingerprint the THDMs using the one-loop corrected Higgs boson couplings and also future precision measurements of these couplings at the HL-LHC and the ILC. We carefully see how the tree level analysis for the model discrimination discussed in Sec. II or in Ref. [57] can be improved by the analysis with radiative corrections. Furthermore, we demonstrate how the inner parameters such as x, $\tan\beta$ and masses of additional Higgs bosons can be extracted from the measurement of the couplings for the Higgs boson h. In our analysis below, we assume that the deviations in scale factors of the Higgs boson couplings are measured as expected in Table 5.2. We also assume that the SM values of these coupling constants are well predicted without large uncertainties which mainly come from QCD corrections[2].

[2]According to Refs. [107, 108], the current uncertainty of the bottom Yukawa coupling $hb\bar{b}$ due to the QCD corrections is 0.77% in the SM. This uncertainty could be reduced in future studies using the lattice calculation up to 0.10% [108] which is better than the expected accuracy of the measurement of the $hb\bar{b}$ coupling at the ILC1000-up as listed in Ref. [100] (0.4%).

	Set A	Set B	Set C	Set D	Set E
$\Delta\kappa_V$	-2%	-2%	-2%	-1%	-0.4%
$\Delta\kappa_\tau$	$+18\%$	$+10\%$	$+5\%$	$+18\%$	$+18\%$
$\Delta\kappa_b$	$+18\%$	$+10\%$	$+5\%$	$+18\%$	$+18\%$

Table 5.2: Benchmark sets for the central values of measured scaling factors for the hVV, $hb\bar{b}$ and $h\tau\tau$ couplings. The expected 1-σ uncertainties for each scaling factor at the HL-LHC and the ILC 500 are shown in Eq. (5.81).

Let us suppose that $\Delta\kappa_V$, $\Delta\kappa_\tau$ and $\Delta\kappa_b$ are measured at the HL-LHC and the ILC500. We consider five benchmark sets for the central values of $(\Delta\kappa_V, \Delta\kappa_\tau, \Delta\kappa_b)$ as listed in Table 5.2. Set A is the typical case where Yukawa couplings deviate from the SM values rather significantly (18%) with a relatively large deviation in the hVV couplings (-2%). Set B and Set C correspond to the cases with smaller deviations in Yukawa couplings with the same deviation in gauge couplings as Set A. Set D and Set E do to the cases with smaller deviations in gauge couplings with fixing the same deviation in Yukawa couplings as Set A. According to Ref. [100], the 1-σ uncertainty for these scaling factors are given as

$$\begin{aligned} &[\sigma(\kappa_V), \sigma(\kappa_b), \sigma(\kappa_\tau)] = [2\%,\ 4\%,\ 2\%], && \text{for HL-LHC,} \\ &[\sigma(\kappa_V), \sigma(\kappa_b), \sigma(\kappa_\tau)] = [0.4\%,\ 0.9\%,\ 1.9\%], && \text{for ILC500.} \end{aligned} \tag{5.81}$$

From Fig. 5.5, these benchmark sets indicate that the Higgs sector is the THDM with the Type-II (Type-I) Yukawa interaction assuming $x \simeq \cos(\beta-\alpha) < 0$ ($x > 0$). In order to further discriminate Type-I or Type-II, we need additional information to determine the sign of x such as the measurement of $\Delta\kappa_c$, namely, if $\Delta\kappa_c$ is given to be a negative (positive) value, then we can completely determine the Yukawa interaction to be Type-II (Type-I). In the following, we consider the case of $\Delta\kappa_c < 0$, so that we assume the case of the Type-II THDM.

For all Set A to Set E, we survey parameter regions in which values of κ's are predicted around the central values within the 1-σ uncertainty expressed in Eq. (5.81) by scanning the inner parameters x, $\tan\beta$, m_Φ ($= m_{H^\pm} = m_A = m_H$) and M^2 in the Type-II THDM. We also take into account the constraints from vacuum stability and perturbative unitarity in order to constrain the parameter space. The scanned regions for $\tan\beta$ and m_Φ are taken as $\tan\beta \geq 1$ and $m_\Phi \geq 300$ GeV, respectively. Values of the other parameters M^2 and x are scanned over ranges which are enough wide to obtain the maximally allowed parameter spaces.

In Fig. 5.6, we show the allowed parameter regions on the x-$\tan\beta$, x-$\bar{m}_\Phi$, m_Φ-ζ and m_Φ-$\tan\beta$ planes from the left to right panels, where we define

$$\zeta \equiv 1 - M^2/m_\Phi^2, \quad \bar{m}_\Phi \equiv m_\Phi \zeta. \tag{5.82}$$

The parameters x and $\bar{m}_\Phi$ give deviations of the Higgs boson couplings by the mixing effect and the loop effect, respectively. Notice that the scale of $\bar{m}_\Phi$ corresponds to the mass of the extra Higgs boson when $M^2 = 0$. The physics meaning of ζ is to measure the magnitude of non-decouplingness of the loop effects of extra Higgs bosons. If ζ is unity, we have $M^2 = 0$, while if

$\zeta < 1$ with nonzero value of M^2 (> 0), the mass of the extra Higgs bosons partially comes from M^2 so that the non-decouplingness is smaller. The central values of $\Delta\kappa$'s are chosen from Set A, B, C, D and E from the upper to bottom panels. The blue and red points correspond to the region within the 1-σ uncertainty at the HL-LHC and ILC500, respectively, from the central value in Table 5.2.

For Set A in Fig. 5.6, let us first explain the behavior of the red points on the x-tan β plane. In this case, $-2.4\% < \Delta\kappa_V < -1.6\%$ is allowed at the ILC500, which can be explained by taking $-0.22 \lesssim x \lesssim -0.18$ at the tree level from the expression of $\Delta\kappa_V \simeq -x^2/2$. At the same time, both $\Delta\kappa_\tau$ and $\Delta\kappa_b$ are approximately given by $-x\tan\beta$ in the Type-II THDM at the tree level, so that $\tan\beta$ is determined by a fixed value of x from $\tan\beta \simeq -\Delta\kappa_{\tau/b}/x$, which is around unity if we take the central value of $\Delta\kappa_V$ and $\Delta\kappa_{\tau/b}$. In fact, by looking at the top-left panel in Fig. 5.6, the above mentioned values of x and $\tan\beta$ are allowed. However, the actual allowed region of x inclucing radiative corrections is about from -0.22 to -0.12 which is wider than the allowed region estimated at the tree level. This can be understood by taking into account the additional Higgs boson loop contributions to κ_V at the one-loop level. The approximate formula for $\Delta\hat{\kappa}_V$ is given in Eq. (5.71), where the second term in the right hand side corresponds to the one-loop contribution. The point here is that the sign of one-loop effect is negative, and it is proportional to the factor ζ^2. Therefore, the allowed region above $x \simeq -0.18$ is explained from the one-loop contribution with a non-zero value of ζ. On the other hand, the one-loop correction to κ_τ is given by the same form as for κ_V as given in Eq. (5.72), so that the difference $\Delta\hat{\kappa}_\tau - \Delta\hat{\kappa}_V$ is approximately given by the same form $-x\tan\beta$ as that given at the tree level. Now from the measurement, since the difference is determined with the uncertainty, $-x\tan\beta$ is also fixed at the one-loop level. We thus can understand the shape of the allowed region of this plot. Although for $\Delta\hat{\kappa}_b$ the top quark, the bottom quark and $H^\pm$ loop diagrams give an additional contribution as shown in Eq. (5.74), this is not so significant in the scanned regions. As a consequence for Set A, when the measurement at the ILC500 is assumed, the allowed value of x and $\tan\beta$ can be determined to be about from -0.22 to -0.12 and from 1 to 2, respectively. On the other hand at the HL-LHC, $\Delta\kappa_V = 0$ is included within the 1-σ uncertainty. Thus, $x \simeq 0$ is still allowed, so that the value of $\tan\beta$ is not determined at all because of the relation $\tan\beta \simeq -\Delta\kappa_{\tau/b}/x$. In addition, we can only extract the lower limit of x to be about -0.22.

Next, we discuss the behavior of the second panel for Set A in Fig. 5.6. As we mentioned in the above, the vertical axis $\bar{m}_\Phi$ measures the size of one-loop contribution to the deviation in the Higgs boson couplings. At the ILC500, in the region with $x \simeq -0.20$, the value of $\bar{m}_\Phi$ is determined to be a smaller value, but $\bar{m}_\Phi \simeq 0$ is not included because of the constraint from vacuum stability. This can be understood that the deviation from the tree level mixing is dominant in this case. On the other hand, when the value of x approaches to zero, a sizable value of $\bar{m}_\Phi$ is extracted, in which the deviation driven by the one-loop contribution becomes more important to compensate the reduced contribution from the tree level mixing. In addition, the upper limit of $\bar{m}_\Phi$ to be about 450 GeV is determined by the constraint from perturbative unitarity. At the HL-LHC, although the blue plots are spread over the region with $x \simeq 0$ as we observed in the x-tan β plot, the upper and lower limit of $\bar{m}_\Phi$ is given by the constraint from unitarity and vacuum stability, respectively.

The third panel for Set A in Fig. 5.6 shows the allowed region on the m_Φ-ζ plane, where ζ is the parameter indicating the non-decouplingness of the extra Higgs bosons. For Set A,

the allowed regions for ILC500 are shown by the red points while those for HL-LHC by the blue points. There are upper and lower bounds for ζ for each value of m_Φ. They are crossed at around $m_\Phi = 850$ GeV which corresponds to the upper bound of the mass of extra Higgs boson. The region of ζ is from 0.2 to 1.4 at $m_\Phi = 300$ GeV. The region of $\zeta > 1$ corresponds to $M^2 < 0$, where non-decoupling effects are effectively large. The exclusion of $\zeta < 0.2$ means that there must be some non-decoupling loop effects of extra Higgs bosons in order to explain this benchmark point. At the HL-LHC, the similar behavior can be observed. However, $\zeta = 0$ is still allowed, so that we cannot say something about the non-decoupling effect.

The last panel for Set A in Fig. 5.6 shows the allowed regions on the m_Φ-$\tan\beta$ plane. At the ILC500, $\tan\beta$ can be determined to be less than 2, and the upper bound of the mass of the extra Higgs bosons are obtained to be less 850 GeV, while at the HL-LHC, $\tan\beta$ is undetermined and only the upper bound of the mass of the extra Higgs bosons is obtained.

The panels shown in the second and third rows in Fig. 5.6 display the allowed parameter regions for Set B and Set C, respectively, where the central value of $\Delta\kappa_\tau (= \Delta\kappa_b)$ is taken to be smaller than that of Set A, while $\Delta\kappa_V$ is taken to be the same. By looking at the panels for the x-$\tan\beta$ plane, we can see that a smaller value of $|x|$ is preferred as compared to the case for Set A. Furthermore, a smaller value of $\tan\beta$ is favored in addition to a smaller value of $|x|$ as seen in the result at the ILC500. These tendencies can be understood in such a way that the deviations in Yuakwa couplings are proportional to $-x\tan\beta$ at the tree level. Because of the smaller value of $|x|$, the deviation in κ_V cannot be explained only from the tree level contribution, so that the one-loop effect is necessary to compensate the tree level contribution. That is the reason why the red points in the second and the third panels for Set B and Set C are given in the upper region which does not include $\bar{m}_\Phi \simeq 0$ and $\zeta \simeq 0$. Therefore, the non-decoupling effect can be extracted at the ILC500 for these two benchmark sets. From the results of ILC500, the upper limit on m_Φ is extracted to be about 950 GeV and 800 GeV for Set B and Set C, respectively.

The panels shown in the fourth and fifth rows in Fig. 5.6 display the allowed parameter regions for Set D and Set E, respectively, where the central value of $\Delta\kappa_V$ is taken to be smaller than that of Set A, while $\Delta\kappa_\tau$ $(= \Delta\kappa_b)$ is taken to be the same. From the red points in the left panels, it is seen that the values of smaller $|x|$ and larger $\tan\beta$ are allowed, which can be explained by the tree level formulae of $\Delta\kappa_V = -x^2/2$ and $\Delta\kappa_{\tau/b} = -x\tan\beta$. For Set E unlike the other benchmark sets, values of x and $\tan\beta$ are not well determined even at the ILC500, because $\Delta\kappa_V \simeq 0$ is included within the 1-σ uncertainty of ILC500. The extraction for $\bar{m}_\Phi$, ζ and m_Φ is done from the ILC500 as $50 \lesssim \bar{m}_\Phi \lesssim 300$ GeV, $0.1 \lesssim \zeta \lesssim 1.1$ GeV and $m_\Phi < 850$ GeV for Set D and $0 \lesssim \bar{m}_\Phi \lesssim 200$ GeV, $0 \lesssim \zeta \lesssim 0.7$ GeV and $m_\Phi < 800$ GeV for Set E.

Up to now, we have discussed the extraction of the inner parameters from the three experimental inputs; i.e., $\Delta\kappa_V$, $\Delta\kappa_\tau$ and $\Delta\kappa_b$. In Fig. 5.7, we show how the extraction can be improved by adding information of κ_γ in addition to the above three inputs. The panels shown in the first row are the same as those shown in the first row in Fig. 5.6, which are displayed in order to compare the results with κ_γ. The panels displayed in the second, third and fourth rows respectively show the allowed region for Set A with the central value of κ_γ of 0.98, 1.00 and 1.02 within the 1-σ uncertainty of $\pm 2\%$ as expected at the HL-LHC. Because the accuracy of the measurement of κ_γ at the ILC500 is not better than that of the best value at the HL-LHC, 2%, we also use 2% for the analysis at the ILC500. As we see Eq. (5.77), the $H^\pm$ loop contribution to the decay rate of the $h \to \gamma\gamma$ mode gives a different dependence of the

non-decouplingness from that in $\Delta\hat{\kappa}_V$ and $\Delta\hat{\kappa}_f$, which is not proportional to $\bar{m}_\Phi$, but proportional to ζ, so that the non-decouplingness ζ can be expected to be extracted more precisely depending on the measured value of κ_γ. In fact, we can observe that ζ is determined more precisely to be $0.5 \lesssim \zeta \lesssim 1.0$, $0.25 \lesssim \zeta \lesssim 1.1$ and $0.2 \lesssim \zeta \lesssim 0.5$ at the ILC500 for the cases with the central value of $\kappa_\gamma = 0.98$, $\kappa_\gamma = 1.00$ and $\kappa_\gamma = 1.02$, respectively, as compared to the case without κ_γ ($0.2 \lesssim \zeta \lesssim 1.2$). The determination of $\bar{m}_\Phi$ is also improved, because $\bar{m}_\Phi$ is given as a function of ζ. We note that smaller values of ζ and $\bar{m}_\Phi$ are favored in the case of the larger central value of κ_γ, because the $H^\pm$ loop effect gives a destructive contribution to the W boson loop contribution.

In Fig. 5.8, we also show the allowed parameter region with additional information of κ_γ for Set D. Similar to the results in the previous figure, ζ and $\bar{m}_\Phi$ are well extracted as compared to the case without κ_γ displayed in the first row in Fig. 5.8. For example, ζ is determined to be $0.3 \lesssim \zeta \lesssim 0.8$, $0.1 \lesssim \zeta \lesssim 0.6$ and $0.1 \lesssim \zeta \lesssim 0.6$ for the cases with the central value of $\kappa_\gamma = 0.98$, $\kappa_\gamma = 1.00$ and $\kappa_\gamma = 1.02$, respectively.

5.5 Summary

We can obtain the results that the hVV and $h\bar{f}f$ can be modified by about 2% from the tree level predictions by one-loop contributions. Taking into account the coupling measurement accuracies as shown in Tab. 4.3, we cannot ignore the radiative corrections. Moreover, it can be realized that the one-loop corrections to the Higgs triple coupling are $\mathcal{O}(100)\%$ via the non-decoupling effects of m_Φ^4. In the tree level discussion, the four types of THDMs can be classified by using deviation pattern between $h\bar{b}b$ and $h\tau\tau$ couplings if the gauge couplings deviate from the predictions of the SM by about 1%. Even in the case including radiative corrections, the separation of four types can be done, without prediction regions overlapping each other, if $\sin(\beta - \alpha)$ is sifted from 1 by about 1%.

We have discussed how the inner parameters of the THDMs can be determined by the future precision measurements of these couplings at the HL-LHC and the ILC. We have found that the inner parameters of the THDM, e.g. upper bounds on the masses of extra Higgs bosons, mixing parameters and the magnitude of loop contributions and so on, can be determined to a considerable extent as long as κ_V will be measured with the deviation about 1%. The extraction of the inner parameters using the ILC500 is much better than that using the HL-LHC. That is mainly due to the good accuracy of the hVV coupling measurement at the ILC500 whose uncertainty is expected to be less than 1%. Although we have discussed fingerprinting by using only κ_V, κ_b, κ_τ, and κ_γ, the information of κ_g, κ_c, κ_t and κ_h is also important to determine the structure of the Higgs sector more precisely. The combination of the future data for all kinds of the couplings for the Higgs boson hand their predictions with radiative corrections in various extended Higgs sectors is an useful approach to determine the structure of the Higgs sector and further to explore new physics beyond the SM, even if a new particle is not directly discovered in the future experiments.

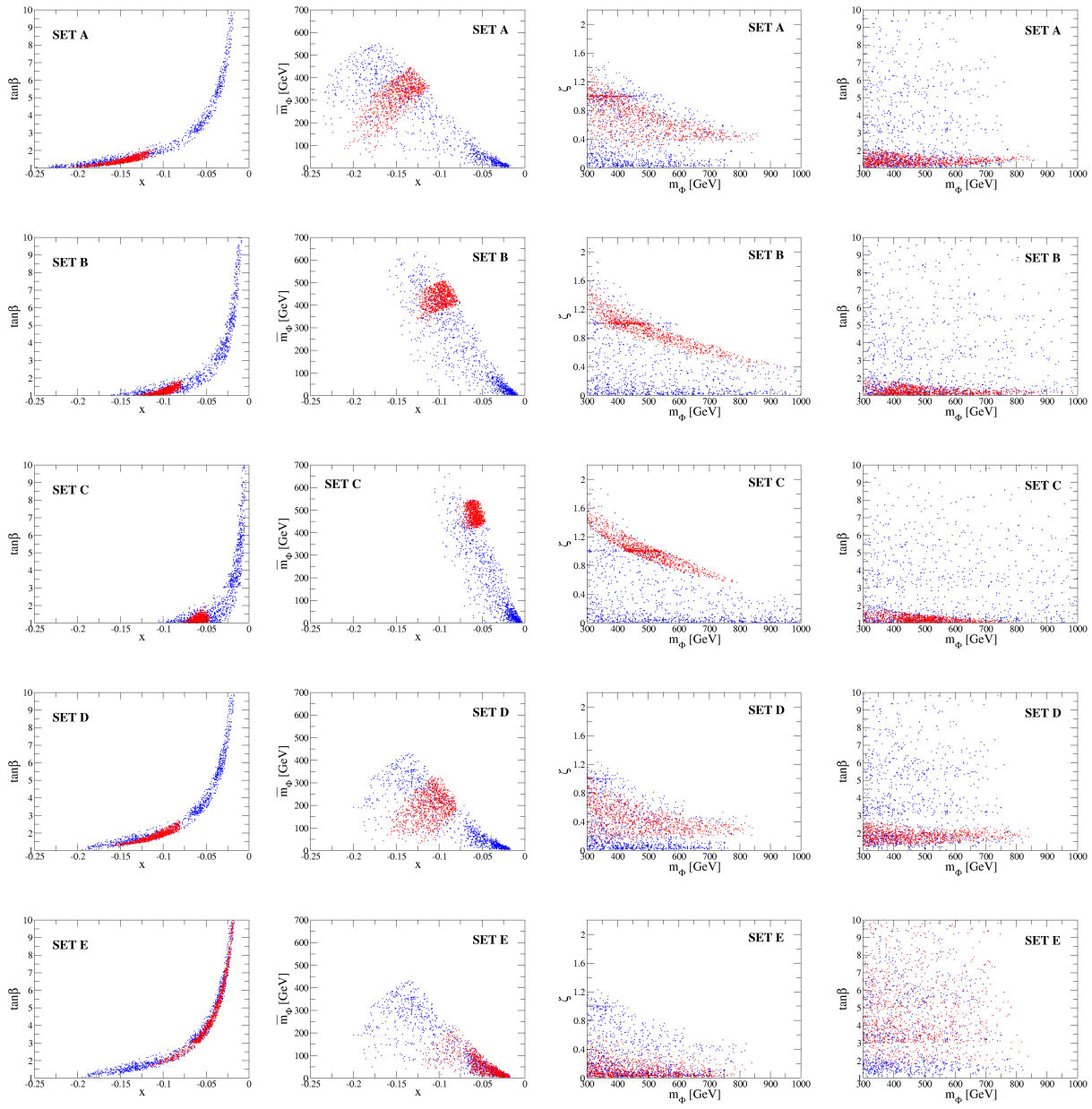

Figure 5.6: Scatter plots for Set A, B, C, D and E from upper to bottom panels. The cyan and red points satisfy the benchmark sets within the 1-σ uncertainty at the HL-LHC and ILC500 given in Eq. (5.81), respectively. For the panels shown in the second and the third columns, the vertical axis $\bar{m}_\Phi$ and ζ are respectively defined by $\bar{m}_\Phi \equiv m_\Phi(1 - M^2/m_\Phi^2)$ and $\zeta \equiv 1 - M^2/m_\Phi^2$.

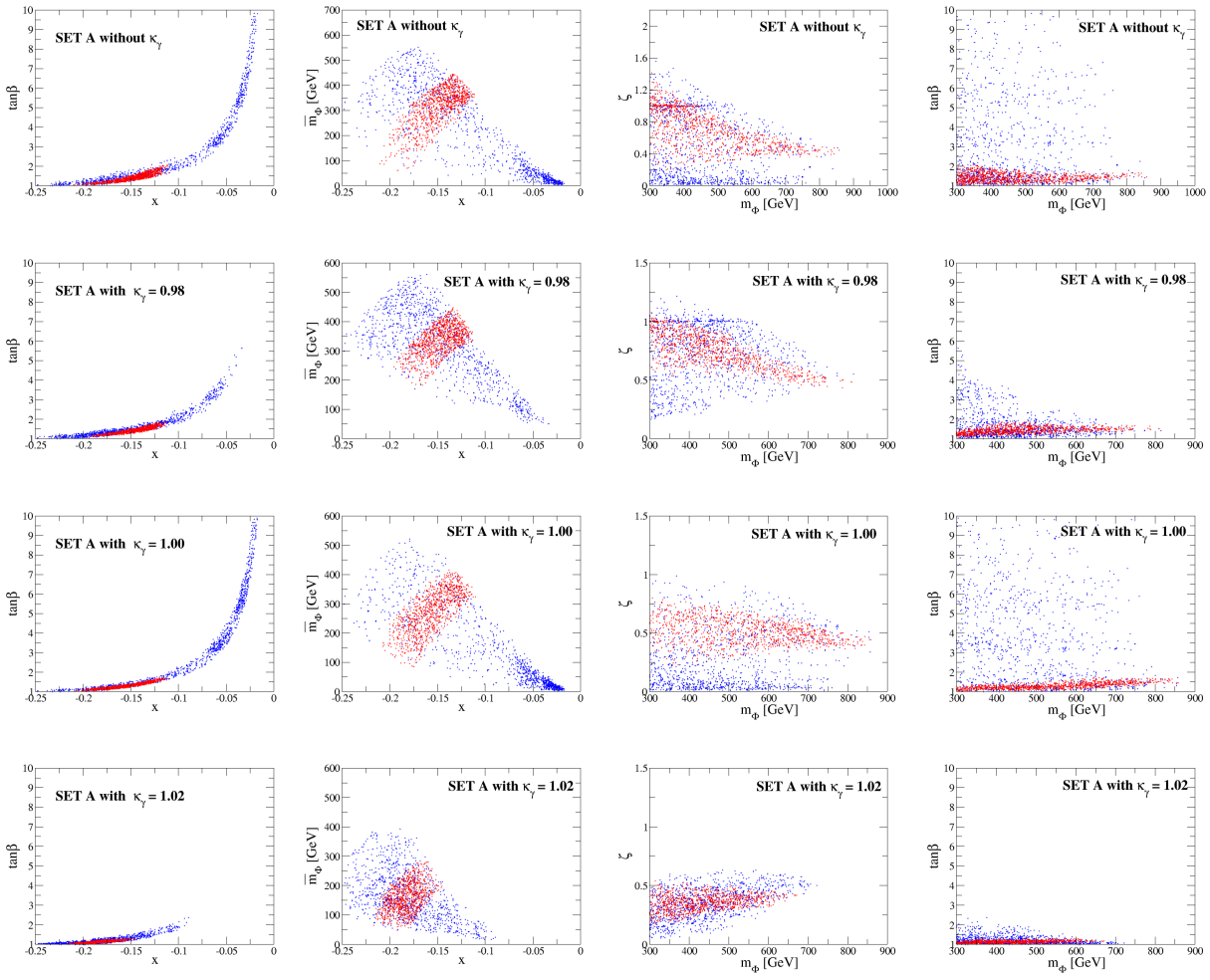

Figure 5.7: Scatter plots for Set A with the additional constraint from $\kappa_\gamma = 0.98,\ 1.00$ and 1.02 for upper, center and bottom panels. The 1-σ uncertainty of κ_γ is assumed to be 2% as expected at the HL-LHC. The cyan and red points satisfy the benchmark sets within the 1-sigma uncertainty at the HL-LHC and ILC500 given in Eq. (5.81), respectively. For the panels shown in the second and the third columns, the vertical axis $\bar{m}_\Phi$ and ζ are respectively defined by $\bar{m}_\Phi \equiv m_\Phi(1 - M^2/m_\Phi^2)$ and $\zeta \equiv 1 - M^2/m_\Phi^2$.

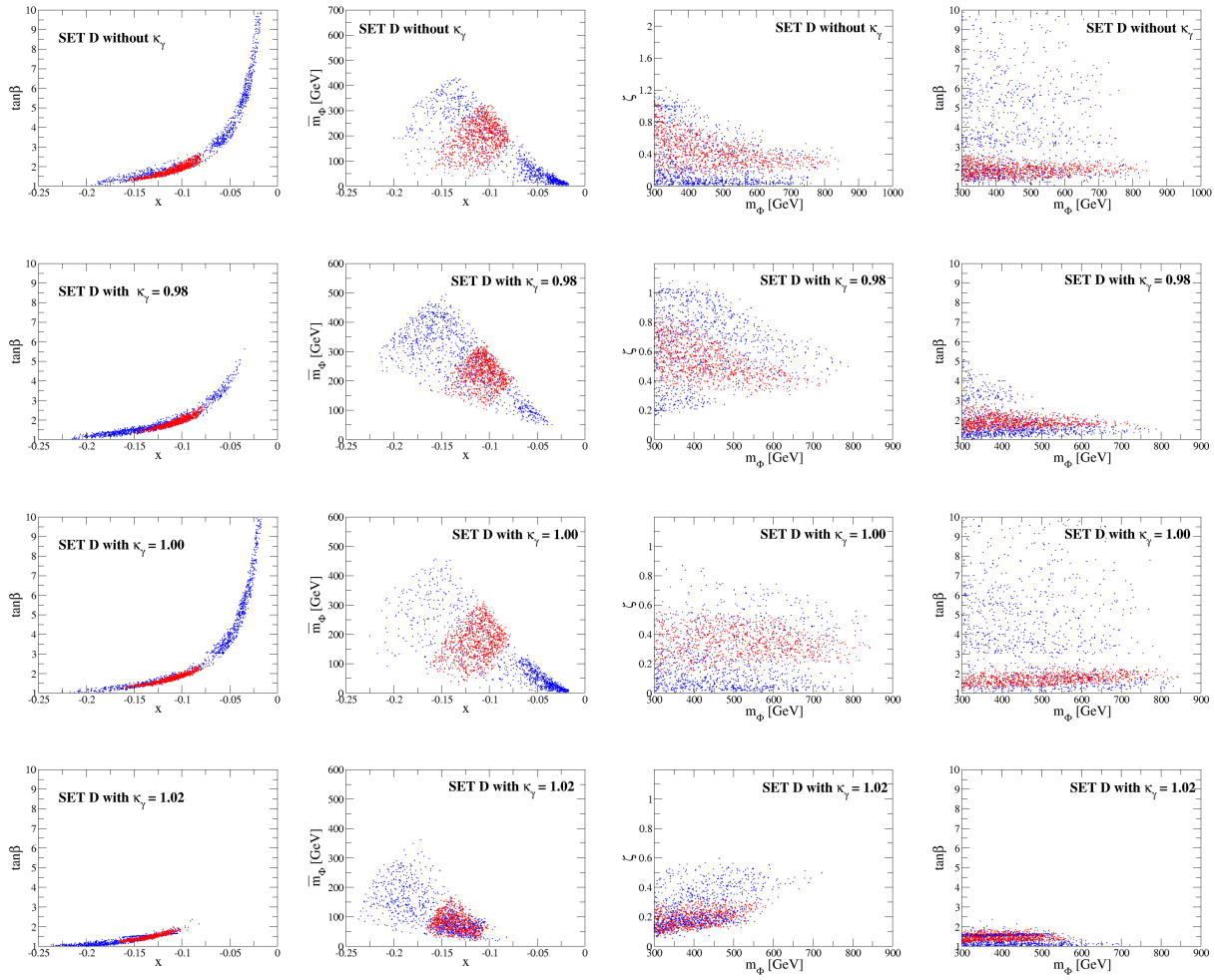

Figure 5.8: Scatter plots for Set D with the additional constraint from $\kappa_\gamma = 0.98,\ 1.00$ and 1.02 for upper, center and bottom panels. The 1-σ uncertainty of κ_γ is assumed to be 2% as expected at the HL-LHC. The cyan and red points satisfy the benchmark sets within the 1-sigma uncertainty at the HL-LHC and ILC500 given in Eq. (5.81), respectively. For the panels shown in the second and the third columns, the vertical axis $\bar{m}_\Phi$ and ζ are respectively defined by $\bar{m}_\Phi \equiv m_\Phi(1 - M^2/m_\Phi^2)$ and $\zeta \equiv 1 - M^2/m_\Phi^2$.

Chapter 6

Radiative corrections to the Higgs boson couplings in the HSM

6.1 Renormalization in the HSM

There are eight following parameters in the Higgs potential,

$$m_\Phi^2, \lambda, \mu_{\Phi S}, \lambda_{\Phi S}, t_S, m_S^2, \mu_S, \lambda_S. \tag{6.1}$$

As described in Sec. 3.2.1, four of them can be rewritten in terms of the physical parameters m_h^2, m_H^2, α and v by using Eqs. (3.49), (3.61), (3.62), (3.63). Remained parameters are $\lambda_{\Phi S}, v_S, \mu_S, \lambda_S$, where t_S is replaces by v_S as described in Eq. (3.48).

First, we shift the bare parameters into renormalized parameters,

$$m_h^2 \to m_h^2 + \delta m_h^2, \tag{6.2}$$
$$m_H^2 \to m_H^2 + \delta m_H^2, \tag{6.3}$$
$$\alpha \to \alpha + \delta\alpha, \tag{6.4}$$
$$v \to v + \delta v, \tag{6.5}$$
$$\lambda_{\Phi S} \to \lambda_{\Phi S} + \delta\lambda_{\Phi S}, \tag{6.6}$$
$$v_S \to v_S + \delta v_S, \tag{6.7}$$
$$\lambda_S \to \lambda_S + \delta\lambda_S, \tag{6.8}$$
$$\mu_S \to \mu_S + \delta\mu_S. \tag{6.9}$$

Two physical scalar fields are shifted to the reonrmalized fields and the wave function renormalizations,

$$\begin{pmatrix} H \\ h \end{pmatrix} \to \begin{pmatrix} 1 + \frac{1}{2}\delta Z_h & \delta C_{hH} + \delta\alpha \\ \delta C_{Hh} - \delta\alpha & 1 + \frac{1}{2}\delta Z_H \end{pmatrix} \begin{pmatrix} H \\ h \end{pmatrix}. \tag{6.10}$$

We also have to shift the tadpoles as

$$T_h \to T_h + \delta T_h, \;\; T_H \to T_H + \delta T_H, \tag{6.11}$$

where T_H and T_h are related with T_ϕ and T_S as

$$\begin{pmatrix} T_S \\ T_\phi \end{pmatrix} = \begin{pmatrix} c_\alpha & -s_\alpha \\ s_\alpha & c_\alpha \end{pmatrix} \begin{pmatrix} T_H \\ T_h \end{pmatrix}. \tag{6.12}$$

Renormalized one and two point functions at the one-loop level are given by

$$\hat{\Gamma}_h = 0 + \delta T_h + \Gamma_h^{\rm 1PI}, \tag{6.13}$$

$$\hat{\Gamma}_H = 0 + \delta T_H + \Gamma_H^{\rm 1PI}, \tag{6.14}$$

$$\hat{\Pi}_{hh}[p^2] = (p^2 - m_h^2)(1+\delta Z_h) - \delta m_h^2 + \frac{c_\alpha^2}{v}\delta T_\Phi + \Pi_{hh}^{\rm 1PI}[p^2], \tag{6.15}$$

$$\hat{\Pi}_{hH}[p^2] = (p^2 - m_h^2)\delta C_{Hh} + (p^2 - m_H^2)\delta C_{hH} + (m_h^2 - m_H^2)\delta\alpha + \frac{c_\alpha s_\alpha}{v}\delta T_\phi + \Pi_{hH}^{\rm 1PI}[p^2], \tag{6.16}$$

$$\hat{\Pi}_{HH}[p^2] = (p^2 - m_H^2)(1+\delta Z_H) - \delta m_H^2 + \frac{s_\alpha^2}{v}\delta T_\phi + \Pi_{HH}^{\rm 1PI}[p^2], \tag{6.17}$$

where analytic expressions of 1PI diagram parts are given in the Appendix.

We note that there are 14 independent counter terms in the Higgs sector. By imposing following nine renormalized on-shell conditions,

$$\hat{\Gamma}_h = 0, \quad \hat{\Gamma}_H = 0, \tag{6.18}$$

$$\hat{\Pi}_{hh}[m_h^2] = 0, \quad \hat{\Pi}_{HH}[m_h^2] = 0, \tag{6.19}$$

$$\hat{\Pi}_{hH}[m_h^2] = 0, \quad \hat{\Pi}_{hH}[m_H^2] = 0, \quad \delta C_{hH} = \delta C_{Hh} \equiv \delta C_h \tag{6.20}$$

$$\frac{d}{dp^2}\hat{\Pi}_{hh}[p^2]\Big|_{p^2=m_h^2} = 1, \quad \frac{d}{dp^2}\hat{\Pi}_{HH}[p^2]\Big|_{p^2=m_H^2} = 1. \tag{6.21}$$

we determine following nine counter terms,

$$\delta T_h = -\Gamma_h^{\rm 1PI}, \quad \delta T_H = -\Gamma_H^{\rm 1PI}, \tag{6.22}$$

$$\delta m_h^2 = \frac{c_\alpha^2}{v}\delta T_\phi + \Pi_{hh}^{\rm 1PI}[m_h^2], \quad \delta m_H^2 = \frac{s_\alpha^2}{v}\delta T_\phi + \Pi_{HH}^{\rm 1PI}[m_H^2], \tag{6.23}$$

$$\delta C_{hH} = \delta C_{Hh} (\equiv \delta C_h) = \frac{1}{2(m_H^2 - m_h^2)}\left[\Pi_{hH}^{\rm 1PI}[m_h^2] - \Pi_{hH}^{\rm 1PI}[m_H^2]\right], \tag{6.24}$$

$$\delta\alpha = \frac{1}{2(m_H^2 - m_h^2)}\left[\frac{2 s_\alpha c_\alpha}{v}\delta T_\phi + \Pi_{hH}^{\rm 1PI}[m_h^2] + \Pi_{hH}^{\rm 1PI}[m_H^2]\right], \tag{6.25}$$

$$\delta Z_h = -\frac{d}{dp^2}\Pi_{hh}^{\rm 1PI}[p^2]\Big|_{p^2=m_h^2}, \quad \delta Z_H = -\frac{d}{dp^2}\Pi_{HH}^{\rm 1PI}[p^2]\Big|_{p^2=m_H^2}. \tag{6.26}$$

As shown in Sec. 2.6.1, δv can be determined by the renormalization in the Gauge sector. We note that forms of $\delta\lambda_{\Phi S}, \delta v_S, \delta\lambda_S$ and $\delta\mu_S$ cannot be determine above conditions. These do not appear in the one-loop calculation of the hVV and hff vertices. When one-loop corrections to the triple scalar couplings such as the hhh coupling, these counter terms have to be determined by additional renormalization conditions as discussed in Ref. [59, 70] in the context of the THDM. The study of one-loop corrections to the triple Higgs boson coupling in the HSM is discussed elsewhere [109].

6.2 Renormalized Higgs couplings in the HSM

6.2.1 Analytic expression

In this subsection, we give formulae of renormalized Higgs couplings composed of three parts; namely the tree level part, the counter term part and 1PI diagram part. hVV couplings and

hff couplings are composed of a number of form factors as,

$$\hat{\Gamma}_{hVV}[p_1^2,p_2^2,q^2] = \hat{\Gamma}^1_{hVV}[p_1^2,p_2^2,q^2]g^{\mu\nu} + \hat{\Gamma}^2_{hVV}[p_1^2,p_2^2,q^2]\frac{p_1^\nu p_2^\mu}{m_V^2} + i\hat{\Gamma}^3_{hVV}[p_1^2,p_2^2,q^2]\epsilon^{\mu\nu\rho\sigma}\frac{p_{1\rho}p_{2\sigma}}{m_V^2}, \tag{6.27}$$

$$\begin{aligned}\hat{\Gamma}_{hff}[p_1^2,p_2^2,q^2] &= \hat{\Gamma}^S_{hff}[p_1^2,p_2^2,q^2] + \gamma_5\hat{\Gamma}^P_{hff}[p_1^2,p_2^2,q^2] + \not{p}_1\hat{\Gamma}^{V1}_{hff}[p_1^2,p_2^2,q^2] + \not{p}_2\hat{\Gamma}^{V2}_{hff}[p_1^2,p_2^2,q^2] \\ &+ \not{p}_1\gamma_5\hat{\Gamma}^{A1}_{hff}[p_1^2,p_2^2,q^2] + \not{p}_2\gamma_5\hat{\Gamma}^{A2}_{hff}[p_1^2,p_2^2,q^2] + \not{p}_1\not{p}_2\hat{\Gamma}^{T}_{hff}[p_1^2,p_2^2,q^2] + \not{p}_1\not{p}_2\gamma_5\hat{\Gamma}^{TP}_{hff}[p_1^2,p_2^2,q^2].\end{aligned} \tag{6.28}$$

Each renormalized form factor is given by,

$$\Gamma^i_{hVV}[p_1^2,p_2^2,q^2] = \frac{2m_V^2}{v}\kappa_{V,\text{tree}} + \delta\Gamma^i_{hVV} + \Gamma^{\text{1PI}}_{hVV,i}[p_1^2,p_2^2,q^2], \quad (i=1,2,3) \tag{6.29}$$

$$\Gamma^j_{hff}[p_1^2,p_2^2,q^2] = -\frac{m_f}{v}\kappa_{f,\text{tree}} + \delta\Gamma^j_{hff} + \Gamma^{\text{1PI}}_{hff,j}[p_1^2,p_2^2,q^2], \quad (j=S,P,V1,V2,A1,A2,T,TP), \tag{6.30}$$

where specific forms of counter terms are

$$\delta\Gamma^1_{hVV} = \frac{2m_V^2}{v}\cos\alpha\left(\frac{\delta m_V^2}{m_V^2} - \frac{\delta v}{v} + \frac{s_\alpha}{c_\alpha}\delta C_h + \delta Z_V + \frac{1}{2}\delta Z_h\right), \tag{6.31}$$

$$\delta\Gamma^2_{hVV} = \delta\Gamma^3_{hVV} = 0, \tag{6.32}$$

$$\delta\Gamma^S_{hff} = -\frac{m_f}{v}\cos\alpha\left(\frac{\delta m_f}{m_f} - \frac{\delta v}{v} + \frac{s_\alpha}{c_\alpha}\delta C_h + \delta Z_f^V + \frac{1}{2}\delta Z_h\right), \tag{6.33}$$

$$\delta\Gamma^P_{hff} = \delta\Gamma^{V1}_{hff} = \delta\Gamma^{V2}_{hff} = \delta\Gamma^{A1}_{hff} = \delta\Gamma^{A2}_{hff} = \delta\Gamma^{T}_{hff} = \delta\Gamma^{TP}_{hff} = 0, \tag{6.34}$$

where δm_W^2, δZ_V and δv are given in Sec. 2.6.1 and δm_f and δZ_f^V are given in Sec. 2.6.1.

6.2.2 Numerical evaluation for the scaling factors

We here present some of the numerical results of our numerical program for the one-loop corrected Higgs boson couplings of hVV and hff. The leading order prediction of the $h\gamma\gamma$ vertex is also calculated. Our numerical program is written as a FORTRAN program, and the package; LoopTools [110] is used for the one-loop integrations.

Our numerical results are shown in terms of the scaling factors. Deviations in the one-loop corrected scaling factors for hVV and hff couplings are defined as

$$\Delta\hat{\kappa}_V \equiv \frac{\hat{\Gamma}^1_{hVV}[p_1^2,p_2^2,q^2]}{\hat{\Gamma}^1_{hVV,\text{SM}}[p_1^2,p_2^2,q^2]} - 1, \tag{6.35}$$

$$\Delta\hat{\kappa}_f \equiv \frac{\hat{\Gamma}^S_{hff}[p_1^2,p_2^2,q^2]}{\hat{\Gamma}^S_{hff,\text{SM}}[p_1^2,p_2^2,q^2]} - 1, \tag{6.36}$$

where $\hat{\Gamma}^1_{hVV,\text{SM}}$ and $\hat{\Gamma}^S_{hff,\text{SM}}$ are the one-loop corrected hVV and hff couplings in the SM. The formulae for the one-loop decay rates $h\to\gamma\gamma$, $h\to Z\gamma$ and $h\to gg$ are given in Appendix A.2.

We numerically evaluate deviations in the scaling factor of the $h\gamma\gamma$ effective coupling defined as

$$\Delta\kappa_\gamma \equiv \frac{\sqrt{\Gamma[h\to\gamma\gamma]}}{\sqrt{\Gamma[h\to\gamma\gamma]_{\rm SM}}} - 1, \tag{6.37}$$

$$\Delta\kappa_{\gamma Z} \equiv \frac{\sqrt{\Gamma[h\to\gamma Z]}}{\sqrt{\Gamma[h\to\gamma Z]_{\rm SM}}} - 1, \tag{6.38}$$

$$\Delta\kappa_g \equiv \frac{\sqrt{\Gamma[h\to gg]}}{\sqrt{\Gamma[h\to gg]_{\rm SM}}} - 1, \tag{6.39}$$

where $\Gamma[h\to XY]$ ($\Gamma[h\to XY]_{\rm SM}$) is the prediction of the decay rate for $h\to XY$ mode in the HSM (in the SM). Because the additional Higgs boson does not have electromagnetic charge and color charge, decay rates ($\Gamma[h\to XY]$) of these modes are modified only by field mixing effects at the one-loop level. The scaling factor of the $h\gamma\gamma$, $h\gamma Z$ and hgg vertex, $\Delta\kappa_\gamma$, $\Delta\kappa_{\gamma Z}$ and $\Delta\kappa_g$ are given by

$$\Delta\kappa_\gamma = \Delta\kappa_{\gamma Z} = \Delta\kappa_g = c_\alpha - 1. \tag{6.40}$$

In our numerical evaluation, we use the following values for the input parameters [99]:

$$\begin{aligned} &G_F = 1.1663787^{-5}\,{\rm GeV}^{-2},\ \ m_Z = 91.1876\,{\rm GeV},\ \ \alpha_{\rm em} = 1/137.035999074,\ \ \Delta\alpha_{\rm em} = 0.06637,\\ &m_t = 173.21\,{\rm GeV},\ \ m_b = 4.66\,{\rm GeV},\ \ m_c = 1.275\,{\rm GeV},\ \ m_\tau = 1.77682\,{\rm GeV},\\ &m_h = 125{\rm GeV}, \end{aligned} \tag{6.41}$$

where $\Delta\alpha_{\rm em}$ is defined as defined as $1-\frac{\alpha_{\rm em}}{\hat\alpha_{\rm em}(m_Z)}$ with $\hat\alpha_{\rm em}(m_Z)$ being the fine structure constant at the scale of m_Z. Furthermore, we set the momenta (p_1^2, p_2^2, q^2) to be $(m_h^2, m_h^2, 4m_h^2)$, $(m_V^2, m_h^2, (m_h+m_V)^2)$ and (m_f^2, m_f^2, m_h^2) for $\Delta\hat\kappa_h$, $\Delta\hat\kappa_V$ and $\Delta\hat\kappa_f$, respectively. As we mentioned in Sec. 3.2.1, we can take the value of v_S freely without changing physics. We fix v_S to be 0 in the following numerical analyses.

First, we discuss approximate formulae in the case for $\alpha = 0$ which can be expressed following simple forms

$$\Delta\hat\kappa_Z = \Delta\kappa_f \simeq -\frac{1}{16\pi^2}\frac{1}{6}\frac{m_H^2}{v^2}\left(1-\frac{\mathcal{M}^2}{m_H^2}\right)^2. \tag{6.42}$$

The most right hand side of Eq. (6.42) comes from the H loop contributions of δZ_h. The structures of these one-loop contributions are the same as those in the THDMs as described in Ref. [59]. Since the form of the hHH coupling becomes $\lambda_{hHH} \simeq -(m_H^2 - \mathcal{M}^2)/v$ in the case for $s_\alpha \ll 1$. When m_S^2 is much larger than v^2, these loop contributions to $\Delta\hat\kappa_V$ and $\Delta\hat\kappa_f$ are reduced as $1/m_H^2$. If $\mathcal{M}^2$ is comparable to v^2, the non-decoupling effects significantly modify the hVV and hff couplings due to the quantum corrections which are proportional to m_H^2.

In Fig. 6.1, we show the decoupling behavior of H loop contributions to the Higgs couplings under the constraints from perturbative unitarity, vacuum stability and the conditions to avoid wrong vacuum in the case for $\alpha = 0$. The left and right panels are $\Delta\hat\kappa_Z$ and $\Delta\hat\kappa_b$ as a function of m_H, respectively. We fix $\lambda_S = 1$ and $\mu_S = 50$ GeV. Green, blue and orange curves indicate

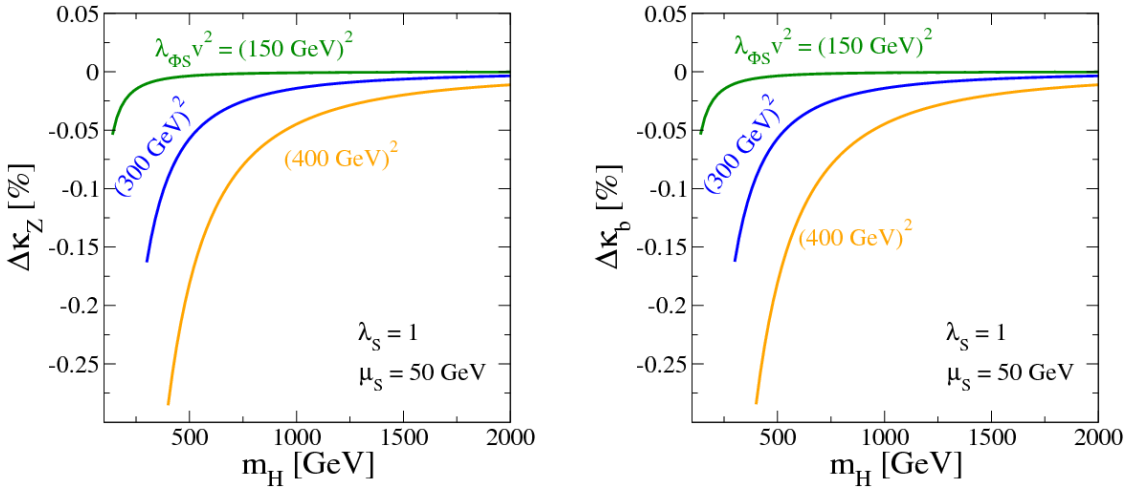

Figure 6.1: $\Delta\hat{\kappa}_Z$ (left panel) and $\Delta\hat{\kappa}_b$ (right panel) as a function of m_H, respectively under the constraints from perturbative unitarity, vacuum stability and the conditions to avoid wrong vacuum in the case for $\alpha = 0$. We take $m_S^2 = m_H^2/2$, $\lambda_S = 1$ and $\mu_S = 50$ GeV. Green, blue and orange curves are the results for $\lambda_{\Phi S}v^2 = (150\mathrm{GeV})^2$, $(300\mathrm{GeV})^2$ and $(400\mathrm{GeV})^2$, respectively.

predictions for $\lambda_{\Phi S}v^2 = (150\mathrm{GeV})^2$, $(300\mathrm{GeV})^2$ and $(400\mathrm{GeV})^2$, respectively. Since the value of M^2 grows as m_H^2 becomes large, we can see that deviations by loop effects are reduced in the large mass regions.

In Fig. 6.2, we show $\Delta\hat{\kappa}_Z$ (the left panel) and $\Delta\hat{\kappa}_b$ (the right panel) as a function of m_H^2 in the case for $\alpha = 0$. We fix $\lambda_S = 1$ and $\mu_S = 50$ GeV. We investigate the behavior of $\Delta\hat{\kappa}_X$ for various values of $\mathcal{M}^2$ such as $\mathcal{M}^2 = 0$, $(200\mathrm{GeV})^2$ and $(400\mathrm{GeV})^2$. In this case, the magnitude of the deviations increase when m_H becomes large in each the Higgs coupling, because the non-decoupling effect of m_H.

In Figs. 6.3, we show scatter plots of allowed regions under the constraints of perturbative unitarity, vacuum stability and the conditions of a wrong vacuum on the m_H-$\Delta\kappa_Z$ plane (left panel) and the $|\sin\alpha|$-$\Delta\kappa_Z$ plane (right panel). Brown points are the results of the tree level calculation, while blue points are those of the one-loop calculation. We scan parameters as 100 GeV $< m_H <$ 10 TeV, $0.91 \leq \cos\alpha \leq 1.00$ and $-m_H^2 < \mathcal{M}^2 < m_H^2$ with fixing $\lambda_S = 0.1$ and $\mu_S = 0$. In Fig. 6.3 (left), we learn that $\Delta\hat{\kappa}_Z$ is zero in the large mass limit for H. For a nonzero negative value of $\Delta\kappa_Z$ there is an upper bound on m_H. The upper bound evaluated at the one-loop level is almost the same as that at the tree level for each value of negative $\Delta\kappa_Z$. If by future precision measurements $\Delta\kappa_Z$ is determined as $\Delta\kappa_Z = -2 \pm 0.5\%$, the upper bound on m_H is obtained to be about 4 TeV. In Fig. 6.3 (right), the tree level results are on the curve described by $\sim -1/2\sin^2\alpha$ for small $|\sin\alpha|$. At the one-loop level the magnitude of the deviation from the tree level prediction is typically about 1%. For smaller values of $|\sin\alpha|$ $\Delta\hat{\kappa}_Z$ is smaller than the tree level prediction, while for larger $|\sin\alpha|$ the one-loop corrected value $\Delta\hat{\kappa}_Z$ can be larger than the tree level prediction but the sign of $\Delta\hat{\kappa}_Z$ is always negative.

6.3 Discriminating the HSM and the Type-I THDM

In this section, we discuss examples of how we can distinguish the simplest extended Higgs sectors by using one-loop corrected Higgs couplings and future precision measurements of the

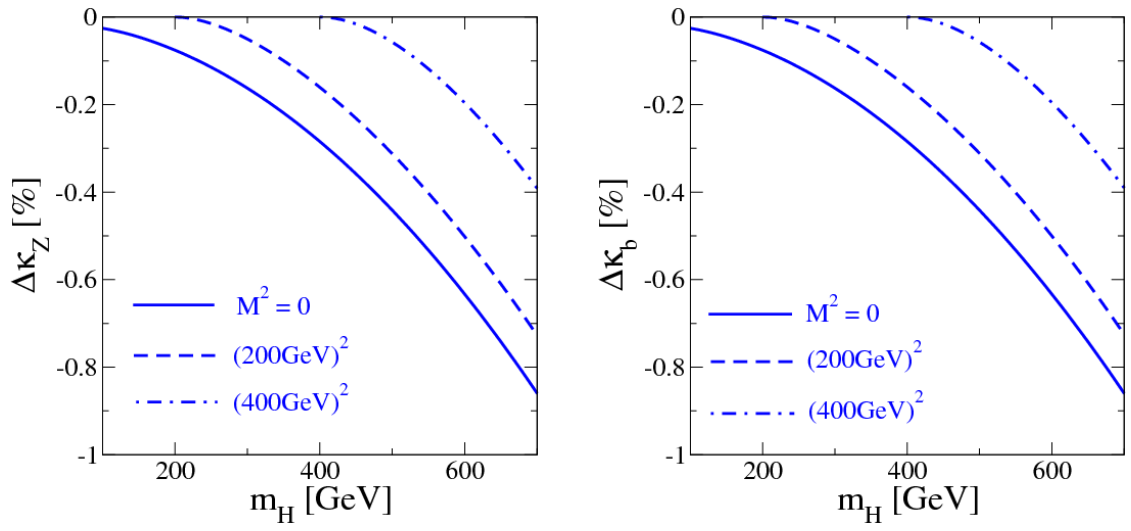

Figure 6.2: $\Delta\hat{\kappa}_Z$ (left panel) and $\Delta\hat{\kappa}_b$ (right panel) as a function of m_H, respectively under the constraints from perturbative unitarity, vacuum stability and the conditions to avoid wrong vacuum in the case for $\alpha = 0$ We take $\lambda_S = 1$ and $\mu_S = 50$ GeV. Solid, dashed and dot-dash curves are the results for $\mathcal{M}^2 = 0$, $(200\text{GeV})^2$ and $(400\text{GeV})^2$, respectively.

Higgs boson couplings. In Ref. [57], the patterns of deviations in these couplings have been discussed at the tree level in the extended Higgs sectors which predict $\rho = 1$ at the tree level; i.e., four types of THDMs, the HSM, the GM model and the septet model. It has been shown that four types of THDMs can be basically separated by measuring Yukawa coupling constants of $h\tau\tau$, $h\bar{b}b$, $h\bar{c}c$ and/or $h\bar{t}t$ except for the decoupling regions [13, 57, 58]. On the other hand, the Type-I THDM, in which only one of the Higgs doublets couples to all the fermions, and all the other extended Higgs sectors (the HSM, the GM model and the septet model) can be distinguished by the precision measurement of the hVV coupling and the universal coupling of $h\bar{f}f$ as long as the deviations in κ_V is detected. One of the notable features of the predictions in the *exotic* extended Higgs sectors such as the GM model and the model with the septet field is the prediction that the scaling factor κ_V can be grater than unity [34, 50, 52, 53], while both THDMs and the HSM always predict $\kappa_V \leq 1$.

In order to compare the theory calculations with precision measurements at future lepton colliders such as the ILC, where most of the Higgs couplings are expected to be measured with high accuracies at the typically $\mathcal{O}(1)$ % level or even better [100], the above tree level analyses in Ref. [57] must be improved by using the predictions with radiative corrections. In Refs. [58,59], the one-loop corrected scaling factors in the four types of THDMs have been calculated in the on-shell scheme, and the above tree level discussions in Ref. [57] have been repeated but at the one-loop level. Even in the case including one-loop corrections, it is useful to discriminate types of Yukawa interactions by using the pattern of deviations among the hff couplings. It is also demonstrated in Ref. [59] that information of inner parameters can be considerably extracted by combination of the precision measurements on the Higgs boson couplings when a deviation in κ_V is large enough to be detected.

We here show the one-loop corrected scaling factors of hZZ, hbb and hhh coupling in the HSM in comparison with those in the Type I THDM. The expected 1σ uncertainties for these

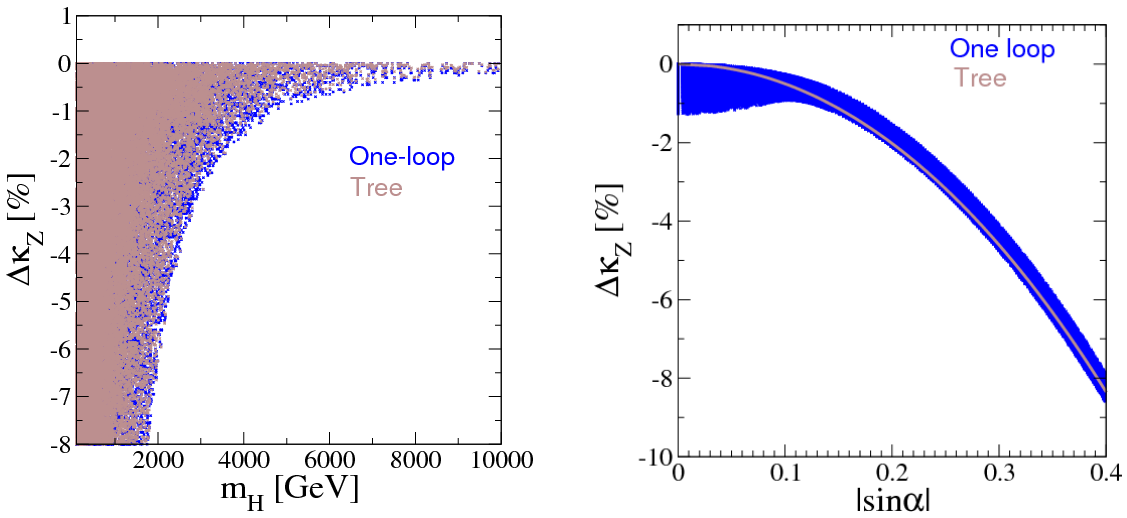

Figure 6.3: Scatter plots of allowed regions under the constraints of perturbative unitarity, vacuum stability and the conditions of a wrong vacuum on the m_H-$\Delta\kappa_Z$ plane (left panel) and the $|\sin\alpha|$-$\Delta\kappa_Z$ plane (right panel). Brown points are the results of the tree level calculation, while blue points are those of the one-loop calculation. Parameters are scanned as 100 GeV $< m_H <$ 10 TeV, $0.91 \leq \cos\alpha \leq 1.00$ and $-m_H^2 < \mathcal{M}^2 < m_H^2$ with fixing $\lambda_S = 0.1$ and $\mu_S = 0$.

scaling factors at the LHC with the center-of-mass energy ($\sqrt{s}$) to be 14 TeV and the integrated luminosity (L) to be 3000 fb^{-1} (HL-LHC) and also the ILC with the combination of the run with $\sqrt{s} = 250$ GeV with $L = 250$ fb^{-1} and that with $\sqrt{s} = 500$ GeV with $L = 500$ fb^{-1} (ILC500) are given by [100]

$$\begin{aligned}
&[\sigma(\kappa_Z), \sigma(\kappa_b), \sigma(\kappa_\gamma)] = [2\%, 4\%, 2\%], \qquad \text{HL-LHC}, \\
&[\sigma(\kappa_Z), \sigma(\kappa_b), \sigma(\kappa_\gamma)] = [0.49\%, 0.93\%, 8.3\%], \qquad \text{ILC500},
\end{aligned} \tag{6.43}$$

For the predictions at the one-loop level in the THDM, we fully use the formulae and the numerical program developed in Ref. [59].

In Fig. 6.4, we show the one-loop corrected predictions of the allowed regions of the HSM and the Type I THDM on the plane of $\Delta\hat{\kappa}_Z$ and $\Delta\hat{\kappa}_b$. The inner parameters are scanned under the constraints of perturbative unitarity, vacuum stability and the condition to avoid wrong vacuum, which are shown given in Sec. 3.2.1. The list of scanned parameters and scanned ranges of these parameters are shown in Tab. 6.1. Red regions indicate the predictions of the HSM. Brown, blue, cyan, green and orange regions are the allowed regions in the Type I THDM for $\tan\beta = 1.5$, 2, 3, 5 and 10, respectively, with varied $m_\Phi (m_H = m_A = m_{H^\pm})$ and M, where definitions of the parameters are given in Ref. [59]. The blue and red ellipses show the measurement uncertainties ($\pm 1\sigma$) for $\Delta\kappa_Z$ and $\Delta\kappa_b$ at the HL-LHC and the ILC500 [100], respectively.

First, we discuss the behavior for predictions of the HSM in Fig. 6.4. We find that magnitude of the deviations in the one-loop corrected κ_Z and κ_b are almost similar in the HSM. The reason is that tree level predictions of $\Delta\kappa_Z$ and $\Delta\kappa_b$ take a common form $(\cos\alpha - 1)$. Namely, $\Delta\hat{\kappa}_Z$ and $\Delta\hat{\kappa}_b$ dominantly deviate from the SM predictions to the directions with the rate 1 : 1 by the mixing effect, and the small width of the line of 1 : 1 is made by the one-loop contributions.

Table 6.1: Parameter regions in the HSM and the Type I THDM for scan analyses in Figure. 6.4, Fig. 6.5 and Fig. 6.6, where definitions of the parameters in the Type I THDM are given in Ref. [59]

HSM	THDM
$300\text{GeV} < m_H < 1\text{TeV}$	$300\text{GeV} < m_H (= m_A = m_{H^\pm}) < 1\text{TeV}$
$\cos\alpha < 1$	$\sin(\beta-\alpha) < 1$
$-15 < \lambda_{\Phi S} < 15$	$0 < M^2 < (1\text{TeV})^2$
$-15 < \lambda_S < 15$	
$-2\text{TeV} < \mu_S < 2\text{TeV}$	

Next, we explain the behavior for predictions of the Type I THDM. The scaling factors for the hVV couplings at the tree level are different from those of hff couplings [57]. In the case for $\cos(\beta-\alpha) < 0$, $\Delta\hat{\kappa}_b$ in the THDM ($\Delta\hat{\kappa}_b^{\text{THDM}}$) is negative and its magnitude is grater than $\Delta\hat{\kappa}_b$ in the HSM ($\Delta\hat{\kappa}_b^{\text{HSM}}$) for the same deviation in $\Delta\hat{\kappa}_Z$. On the other hand, in the case of $\cos(\beta-\alpha) > 0$, $\Delta\hat{\kappa}_b^{\text{THDM}}$ is larger than $\Delta\hat{\kappa}_b^{\text{HSM}}$ for the same value of $\Delta\hat{\kappa}_Z$. $\Delta\hat{\kappa}_Z$ and $\Delta\hat{\kappa}_b$ deviate from the SM predictions according to the tree level predictions due to the tree level mixing effect, and the one-loop contributions make the deviations from the tree level prediction by typically a few %. We find that $\Delta\hat{\kappa}_Z$ and $\Delta\hat{\kappa}_b$ are substantially modified by radiative corrections in the case for low $\tan\beta$ values than the case for large $\tan\beta$ values. As the value of $\tan\beta$ become large, the $\Delta\hat{\kappa}_Z$ and $\Delta\hat{\kappa}_b$ plane prediction in the Type I THDM approximate the line of $1:1$. Larger deviations in $\Delta\hat{\kappa}_Z$ and $\Delta\hat{\kappa}_b$ in the case with $\tan\beta \geq 10$, $\cos(\beta-\alpha) < 0$ and $m_\Phi > 300$ GeV are excluded by the constraints from perturbative unitarity and vacuum stability.

In Fig. 6.5, we show the one-loop corrected predictions of the allowed regions of the HSM and the Type I THDM on the plane of $\Delta\hat{\kappa}_Z$ and $\Delta\kappa_\gamma$. We scan inner parameters in each model within the ranges listed in Tab. 6.1 under the constraints of perturbative unitarity, vacuum stability and the condition to avoid wrong vacuum and the conditions to avoid wrong vacuum. Definitions of color for allowed regions are the same as those in Fig. 6.4. Blue and red ellipses are shown measurement uncertainties ($\pm1\sigma$) for $\Delta\hat{\kappa}_Z$ and $\Delta\kappa_\gamma$ at the HL-LHC and the ILC500 [100]. Since uncertainty of $\Delta\kappa_\gamma$ measurement at the HL-LHC is smaller than that at the ILC500, we here use expected uncertainty for $\Delta\kappa_\gamma$ at the HL-LHC in both case the HL-LHC and the ILC500.

In the HSM, the correlation between $\Delta\hat{\kappa}_Z$ and $\Delta\kappa_\gamma$ follows the line of $1:1$ with the small width, which comes from radiative corrections. Because there is no charged new particle in the HSM, deviations in $\Delta\kappa_\gamma$ are made by mixing effects. In the THDM, in addition to mixing effects, singly charged Higgs bosons loop contributions modify the value of $\Delta\kappa_\gamma$. The magnitude of $\Delta\kappa_\gamma$ depends on the sign of $\cos(\beta-\alpha)$ as the behavior of $\Delta\hat{\kappa}_b$. Predictions distributing in region of smaller $|\Delta\kappa_\gamma|$ values is the case for $\cos(\beta-\alpha) > 0$. The other regions show the predictions with $\cos(\beta-\alpha) < 0$. In the limit for $\tan\beta \to \infty$, the predictions of the Type I THDM are close the line of $1:1$. There are allowed regions with $\Delta\kappa_\gamma > 0$, which are caused by inversing the sign of the hH^+H^- coupling. If it is difficult to identify the results of each

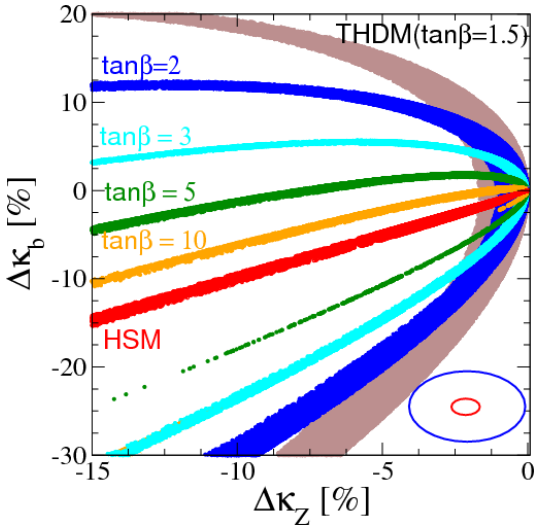

Figure 6.4: Predictions of the allowed regions of the HSM and the Type I THDM at the one-loop level on the plane of $\Delta\kappa_Z$ and $\Delta\kappa_b$. The inner parameters are scanned under the constraints of perturbative unitarity, vacuum stability and the condition to avoid wrong vacuum, given in Sec. 3.2.1. The list of scanned parameters and scanned range of these parameters are shown in Tab. 6.1. Red regions indicate the predictions of the HSM. Brown, blue, cyan, green and orange regions is allowed regions in the Type I THDM for $\tan\beta = 1.5$, 2, 3, 5 and 10, respectively. Blue and red ellipses are shown measurement uncertainties ($\pm 1\sigma$) for $\Delta\kappa_Z$ and $\Delta\kappa_b$ at the HL-LHC and the ILC500 [100].

value of $\tan\beta$ in the plane of $\Delta\kappa_Z$ and $\Delta\kappa_\gamma$, you can see their behavior more clearly by using Fig. 6.6. In each panel of Fig. 6.6, we show allowed regions of $\Delta\hat{\kappa}_Z$ and $\Delta\kappa_\gamma$ in the HSM and the Type I THDM for each value of $\tan\beta$. The definition of colors and ellipses, and the way of analysis are same as those in Fig. 6.4 and Fig. 6.5.

Finally, we discuss how we can discriminate the HSM and the Type I THDM by using theoretical predictions of $\Delta\kappa_Z$, $\Delta\kappa_b$ and $\Delta\kappa_\gamma$ with radiative corrections and Higgs boson coupling measurements at the HL-LHC and the ILC500. We find that if κ_V will be measured to be deviated by 2 % from the SM predictions, we can discriminate the HSM and the Type I THDM in most of parameter regions by using precision measurements of $\Delta\kappa_Z$ and $\Delta\kappa_b$ at the ILC. In addition, in the plane of $\Delta\kappa_Z$ and $\Delta\kappa_\gamma$, the predictions of the HSM separate from those of the Type I THDM for $\cos(\beta-\alpha) > 0$. However, when the value of $\tan\beta$ is extremely large; i.e., $\tan\beta > 10$, $\Delta\kappa_Z^{\rm THDM}$, $\Delta\kappa_b^{\rm THDM}$ and $\Delta\kappa_\gamma^{\rm THDM}$ approach to the predictions in the HSM. In such a situation, it is difficult to discriminate the models by only using these coupling constants.

6.4 Summary

We have calculated a full set of renormalized Higgs boson couplings at the one-loop level in the on-shell scheme in the HSM. These coupling constants can deviate from the SM predictions due to the mixing effect and the one-loop contributions of the extra scalar boson. We numerically have investigated how they can be significant under the theoretical constraints from perturbative unitarity and vacuum stability and also the condition of avoiding the wrong vacuum. Finally,

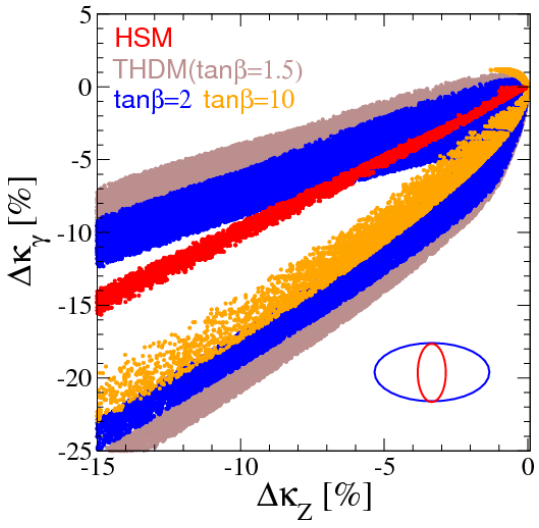

Figure 6.5: Predictions of the allowed regions of the HSM and the Type I THDM on the plane of one-loop corrected $\Delta\kappa_Z$ and $\Delta\kappa_\gamma$. Blue ellipse is shown measurement uncertainties ($\pm 1\sigma$) for $\Delta\kappa_Z$ and $\Delta\kappa_\gamma$ at the HL-LHC [100]. Red one is shown measurement uncertainties ($\pm 1\sigma$) for $\Delta\kappa_Z$ at the ILC500 [100] and $\Delta\kappa_\gamma$ at the HL-LHC. The others are same as in Fig. 6.4.

comparing with the predictions at the one-loop level in the four types of THDMs, we have studied how the HSM can be distinguished from those models and identified by using precision measurements of the Higgs boson couplings at future collider experiments. We found that if hVV couplings deviate 2 % from the SM predictions, we can discriminate the HSM and the Type I THDM in most of parameter regions by using precision measurements of $\Delta\kappa_Z$ and $\Delta\kappa_b$ at the ILC. In addition that, in the plane of $\Delta\kappa_Z$ and $\Delta\kappa_\gamma$, the predictions of the HSM separate from those of the Type I THDM for $\cos(\beta-\alpha) > 0$. Therefore, by comparing the predicted values of the hZZ, $hb\bar{b}$ and $h\gamma\gamma$ couplings and corresponding measured values, we may be able to distinguish the HSM from the Type I THDM in the most of the parameter space. However, when the value of $\tan\beta$ is extremely large as $\tan\beta > 10$, deviations in $\Delta\kappa_Z^{\rm THDM}$, $\Delta\kappa_b^{\rm THDM}$ and $\Delta\kappa_\gamma^{\rm THDM}$ approach to the predictions in the HSM. In such a situation, it is difficult to discriminate the models by fingerprinting.

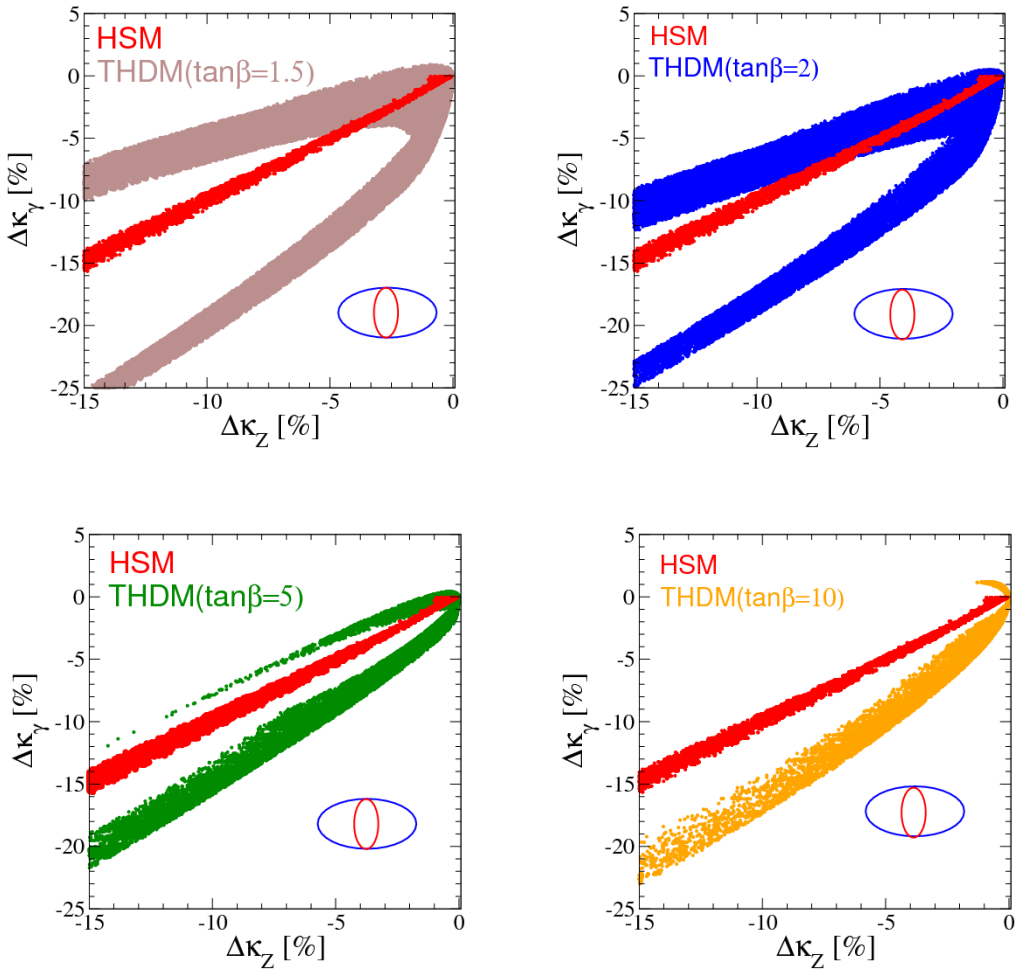

Figure 6.6: Each panel shows predictions of the allowed regions of the HSM and the Type I THDM for each value of $\tan\beta$, i.e. $\tan\beta = 1.5$, 2, 5 and 10, on the plane of one-loop corrected $\Delta\kappa_Z$ and $\Delta\kappa_\gamma$. The others are the same as in Fig. 6.5.

Chapter 7

Radiative corrections to the Higgs boson couplings in the HTM

7.1 Renormalization in the HTM

In this section, we define the on-shell renormalization scheme in order to calculate the one-loop corrected electroweak precision parameters and also the SM-like Higgs boson couplings: hZZ, hWW and hhh. First, we discuss the renormalization of the electroweak sector to calculate the renormalized W boson mass, which can be used to constrain parameters such as the triplet-like Higgs boson masses in the HTM. Second, we consider the renormalization of parameters in the Higgs potential.

7.1.1 Renormalization of the electroweak parameters

The renormalization prescription in models where the tree level rho parameter: $\rho_{\rm tree}$ is predicted to be unity such as the SM is different from that in models without $\rho_{\rm tree} = 1$ such as the HTM. Therefore, we separately discuss the renormalization prescriptions in models with $\rho_{\rm tree} = 1$ and those with $\rho_{\rm tree} \neq 1$ in order to clarify the difference between two prescriptions.

Models without $\rho_{\rm tree} = 1$

We describe the renormalization of the electroweak precision parameters in models without $\rho_{\rm tree} = 1$. In this class of models, the electroweak parameters are described by four independent input parameters. For instance, when we choose m_W, m_Z, $\alpha_{\rm em}$ and $\sin\theta$ as input parameters, all the other parameters are written in these parameters;

$$G_F = \frac{\pi \alpha_{\rm em}}{\sqrt{2} m_W^2 s_W^2}. \tag{7.1}$$

In the renormalization calculation, we shift all the input parameters into the renormalized parameters and the counter-terms. Once we specify the input parameters, all the counter-terms are also described by the three counter-terms which are associated with the four input parameters. We shift all the parameters in the kinetic Lagrangian as follows

$$\begin{aligned} &m_W^2 \to m_W^2 + \delta m_W^2, \quad m_Z^2 \to m_Z^2 + \delta m_Z^2, \quad \alpha_{\rm em} \to \alpha_{\rm em} + \delta\alpha_{\rm em}, \\ &\sin^2\theta_W \to \sin^2\theta_W + \delta s_W^2, \quad B_\mu \to B_\mu + \frac{1}{2}\delta Z_B, \quad W_\mu^a \to W_\mu^a + \frac{1}{2}\delta Z_W. \end{aligned} \tag{7.2}$$

The wave function renormalization for the photon and the Z boson can be obtained by the shift

$$\begin{pmatrix} Z_\mu \\ A_\mu \end{pmatrix} \to \left[1 + \frac{1}{2}\begin{pmatrix} \delta Z_Z & \delta Z_{Z\gamma} \\ \delta Z_{Z\gamma} & \delta Z_\gamma \end{pmatrix} + \frac{1}{2s_W c_W}\begin{pmatrix} 0 & -\delta s_W^2 \\ \delta s_W^2 & 0 \end{pmatrix}\right]\begin{pmatrix} Z_\mu \\ A_\mu \end{pmatrix}, \tag{7.3}$$

where the counter-terms δZ_Z, δZ_γ, $\delta Z_{Z\gamma}$ and δs_W^2 are expressed in terms of the counter-terms defined in Eq. (7.2) as

$$\begin{pmatrix} \delta Z_Z \\ \delta Z_\gamma \end{pmatrix} = \begin{pmatrix} c_W^2 & s_W^2 \\ s_W^2 & c_W^2 \end{pmatrix}\begin{pmatrix} \delta Z_W \\ \delta Z_B \end{pmatrix}, \tag{7.4}$$

$$\delta Z_{Z\gamma} = c_W s_W(\delta Z_W - \delta Z_B) = \frac{c_W s_W}{c_W^2 - s_W^2}(\delta Z_Z - \delta Z_\gamma), \tag{7.5}$$

$$\frac{\delta s_W^2}{s_W^2} = \frac{c_W^2}{s_W^2}\left(\frac{\delta m_Z^2}{m_Z^2} - \frac{\delta m_W^2}{m_W^2}\right). \tag{7.6}$$

The renormalized two point functions for the gauge bosons can be expressed as

$$\hat{\Pi}_{WW}[p^2] = \Pi_{WW}^{\rm 1PI}(p^2) - \delta m_W^2 + \delta Z_W(p^2 - m_W^2), \tag{7.7}$$

$$\hat{\Pi}_{ZZ}[p^2] = \Pi_{ZZ}^{\rm 1PI}(p^2) - \delta m_Z^2 + \delta Z_Z(p^2 - m_Z^2), \tag{7.8}$$

$$\hat{\Pi}_{\gamma\gamma}[p^2] = \Pi_{\gamma\gamma}^{\rm 1PI}(p^2) + p^2\delta Z_\gamma, \tag{7.9}$$

$$\hat{\Pi}_{Z\gamma}[p^2] = \Pi_{Z\gamma}^{\rm 1PI}(p^2) - \delta Z_{Z\gamma}(p^2 - \frac{1}{2}m_Z^2) - m_Z^2\frac{\delta s_W^2}{2s_W c_W}, \tag{7.10}$$

where $\Pi_{XY}^{\rm 1PI}$ ($XY = WW, ZZ, \gamma\gamma$ or $Z\gamma$) are the 1PI diagram contributions to the gauge boson two point functions. We here define derivatives of the renormalized two point functions and 1PI diagram contributions as $\hat{\Pi}'_{XY}[m^2] \equiv \frac{d}{dp^2}\hat{\Pi}_{XY}[p^2]\big|_{p^2=m^2}$ and $\Pi_{XY}^{\rm 1PI\prime}(m^2) \equiv \frac{d}{dp^2}\Pi_{XY}^{\rm 1PI}(p^2)\big|_{p^2=m^2}$.

In order to determine the counter-terms, we impose the following five renormalization conditions:

$$\mathrm{Re}\hat{\Pi}_{WW}[m_W^2] = 0, \quad \mathrm{Re}\hat{\Pi}_{ZZ}[m_Z^2] = 0, \tag{7.11}$$

$$\hat{\Pi}'_{\gamma\gamma}[0] = 0, \quad \hat{\Pi}_{Z\gamma}[0] = 0, \quad \hat{\Gamma}_\mu^{\gamma ee}[q^2 = 0,\ \not{p}_1 = \not{p}_2 = m_e] = ie\gamma_\mu, \tag{7.12}$$

where $\hat{\Gamma}_\mu^{\gamma ee}$ is the renormalized γee vertex. By using these conditions, all the counter-terms in the electroweak sector can be determined as

$$\delta m_W^2 = \mathrm{Re}\Pi_{WW}^{\rm 1PI}(m_W^2), \quad \delta m_Z^2 = \mathrm{Re}\Pi_{ZZ}^{\rm 1PI}(m_Z^2), \quad \frac{\delta\alpha_{\rm em}}{\alpha_{\rm em}} = \Pi_{\gamma\gamma}^{\rm 1PI\prime}(0) - \frac{2s_W}{c_W}\frac{\Pi_{Z\gamma}^{\rm 1PI}(0)}{m_Z^2}, \tag{7.13}$$

$$\delta Z_\gamma = -\Pi_{\gamma\gamma}^{\rm 1PI\prime}(0), \quad \delta Z_{Z\gamma} = -2\frac{\Pi_{Z\gamma}^{\rm 1PI}(0)}{m_Z^2} + \frac{\delta s_W^2}{s_W c_W}, \tag{7.14}$$

$$\delta Z_Z = -\Pi_{\gamma\gamma}^{\rm 1PI\prime}(0) - \frac{2(c_W^2 - s_W^2)}{c_W s_W}\frac{\Pi_{Z\gamma}^{\rm 1PI}(0)}{m_Z^2} + \frac{c_W^2 - s_W^2}{c_W^2}\frac{\delta s_W^2}{s_W^2}, \tag{7.15}$$

$$\delta Z_W = -\Pi_{\gamma\gamma}^{\rm 1PI\prime}(0) - \frac{2c_W}{s_W}\frac{\Pi_{Z\gamma}^{\rm 1PI}(0)}{m_Z^2} + \frac{\delta s_W^2}{s_W^2}, \tag{7.16}$$

Next, we discuss how δs_W^2 is determined. Here, three of four input parameters are chosen from the electroweak precision observables, i.e., m_W, m_Z and $\alpha_{\rm em}$ such as the SM. The other one

is chosen from the mixing angle β' between the CP-odd Higgs boson A and the NG boson G^0 defined in Eqs. (3.88) and (3.89). The counter-term of the mixing angle $\delta\beta'$ can be determined by the conditions:

$$\hat{\Pi}_{AG}[0] = \hat{\Pi}_{AG}[m_A^2] = 0, \tag{7.17}$$

where $\hat{\Pi}_{AG}$ is the renormalized two point function of the G^0-A mixing given in Eq. (7.41). The other counter-terms are determined by the same renormalization conditions given in Eqs. (7.11) and (7.12) as in the SM. In this scheme, the weak mixing angle is not the independent parameter, but it is determined by

$$\cos^2\bar{\theta}_W \equiv \bar{c}_W^2 = \frac{2m_W^2}{m_Z^2(1+c_{\beta'}^2)}. \tag{7.18}$$

In order to distinguish the definition of the weak mixing angle in this scheme from the other definition, we introduced $\bar{c}_W^2$ ($\bar{s}_W^2 = 1-\bar{c}_W^2$). The counter-term for the weak mixing angle is obtained by imposing Eq. (7.13):

$$\delta\bar{s}_W^2 = -\delta\bar{c}_W^2 = \frac{2m_W^2}{m_Z^2(1+c_{\beta'}^2)}\left[\frac{\mathrm{Re}\Pi_{ZZ}^{\mathrm{1PI}}(m_Z^2)}{m_Z^2} - \frac{\mathrm{Re}\Pi_{WW}^{\mathrm{1PI}}(m_W^2)}{m_W^2} - \frac{2c_{\beta'}s_{\beta'}}{1+c_{\beta'}^2}\delta\beta'\right]. \tag{7.19}$$

The expression for Δr can be obtained in the same way as in models with $\rho_{\mathrm{tree}} = 1$:

$$\Delta r = \Delta\alpha - \frac{\bar{c}_W^2}{\bar{s}_W^2}\Delta\rho + \Delta r_{\mathrm{rem}}, \tag{7.20}$$

where $\Delta\alpha$ and Δr_{rem} are given by the same formulae of the SM, but s_W and c_W should be replaced by $\bar{s}_W$ and $\bar{c}_W$. $\Delta\rho$ can be expressed as

$$\Delta\rho = \frac{\Pi_{ZZ}^{\mathrm{1PI}}(0)}{m_Z^2} - \frac{\Pi_{WW}^{\mathrm{1PI}}(0)}{m_W^2} - \frac{2\bar{s}_W}{\bar{c}_W}\frac{\Pi_{Z\gamma}^{\mathrm{1PI}}(0)}{m_Z^2} - \frac{2c_{\beta'}s_{\beta'}}{1+c_{\beta'}^2}\delta\beta'. \tag{7.21}$$

The quadratic mass dependences due to the custodial symmetry breaking such as m_t^2 appear in $\Delta r^{\text{Scheme II}}$ through $\Delta\rho$. The one loop corrected W boson mass can be calculated as

$$(m_W^{\mathrm{ren}})^2_{\text{Scheme II}} = \frac{m_Z^2(1+c_{\beta'}^2)}{4}\left[1+\sqrt{1-\frac{8}{1+c_{\beta'}^2}\frac{\pi\alpha_{\mathrm{em}}}{\sqrt{2}G_F m_Z^2(1-\Delta r^{\text{Scheme II}})}}\right]. \tag{7.22}$$

7.1.2 Renormalization of the Higgs potential

Next we discuss the renormalization of the parameters in the Higgs potential. We here choose the set of input parameters in the Higgs potential as

$$v,\ \alpha,\ \beta,\ \beta',\ m_h^2,\ m_H^2,\ m_A^2,\ m_{H^+}^2,\ m_{H^{++}}^2. \tag{7.23}$$

We work on the mass eigenbasis for the Higgs fields. Now we define the shift of the parameters as

$$T_\Phi \to 0 + \delta T_\Phi,\ T_\Delta \to 0 + \delta T_\Delta, \tag{7.24}$$

$$v \to v + \delta v,\ \alpha \to \alpha + \delta\alpha,\ \beta \to \beta + \delta\beta,\ \beta' \to \beta' + \delta\beta' \tag{7.25}$$

$$m_\varphi^2 \to m_\varphi^2 + \delta m_\varphi^2, \tag{7.26}$$

where $\varphi = h, H, A, H^+$ and H^{++}. In fact, β and β' are not independent from each other, so that the counter-terms $\delta\beta$ and $\delta\beta'$ are also not independent[1]. We start from the mass eigenstates for the Higgs fields at the tree level. The wave function renormalization factors are defined as

$$\begin{aligned}
H^{\pm\pm} &\to \left(1 + \frac{1}{2}\delta Z_{H^{++}}\right) H^{\pm\pm}, \\
\begin{pmatrix} G^\pm \\ H^\pm \end{pmatrix} &\to \begin{pmatrix} 1 + \frac{1}{2}\delta Z_{G^+} & \delta\beta + \delta C_{GH} \\ -\delta\beta + \delta C_{HG} & 1 + \frac{1}{2}\delta Z_{H^+} \end{pmatrix} \begin{pmatrix} G^\pm \\ H^\pm \end{pmatrix}, \\
\begin{pmatrix} G^0 \\ A \end{pmatrix} &\to \begin{pmatrix} 1 + \frac{1}{2}\delta Z_{G^0} & \delta\beta' + \delta C_{GA} \\ -\delta\beta' + \delta C_{AG} & 1 + \frac{1}{2}\delta Z_A \end{pmatrix} \begin{pmatrix} G^0 \\ A \end{pmatrix}, \\
\begin{pmatrix} h \\ H \end{pmatrix} &\to \begin{pmatrix} 1 + \frac{1}{2}\delta Z_h & \delta\alpha + \delta C_{hH} \\ -\delta\alpha + \delta C_{Hh} & 1 + \frac{1}{2}\delta Z_H \end{pmatrix} \begin{pmatrix} h \\ H \end{pmatrix}.
\end{aligned} \tag{7.27}$$

Hereafter, we set $\delta C_{hH} = \delta C_{Hh}$, $\delta C_{GH} = \delta C_{HG}$ and $\delta C_{GA} = \delta C_{AG}$ without loss of generality. The counter-term of δv can be determined by the renormalization of the electroweak parameters as

$$\frac{\delta v}{v} = \frac{1}{2}\left(\frac{\delta m_W^2}{m_W^2} - \frac{\delta\alpha_{\rm em}}{\alpha_{\rm em}} + \frac{\delta\bar{s}_W^2}{\bar{s}_W^2}\right), \tag{7.28}$$

where counter-terms of δm_W^2 and $\delta\alpha_{\rm em}$ are given in Eq. (7.13) and that of $\delta\bar{s}_W^2$ is given in Eq. (7.19). At the one-loop level, one point functions of h and H are given by

$$\hat{T}_h = \delta T_\Phi \cos\alpha + \delta T_\Delta \sin\alpha + T_h^{\rm 1PI}, \tag{7.29}$$

$$\hat{T}_H = -\delta T_\Phi \sin\alpha + \delta T_\Delta \cos\alpha + T_H^{\rm 1PI}, \tag{7.30}$$

where $T_h^{\rm 1PI}$ and $T_H^{\rm 1PI}$ are contributions of one-particle-irreducible diagrams. The condition of vanishing the tadpoles at the one-loop level provides

$$\delta T_\Phi = -T_h^{\rm 1PI}\cos\alpha + T_H^{\rm 1PI}\sin\alpha, \tag{7.31}$$

$$\delta T_\Delta = -T_h^{\rm 1PI}\sin\alpha - T_H^{\rm 1PI}\cos\alpha. \tag{7.32}$$

Similar to the gauge boson two point functions, renormalized two point functions for scalar bosons can be expressed as $\hat{\Pi}_{\phi\phi}[p^2]$ and 1PI diagram contributions can also be denoted by $\Pi_{\phi\phi}^{\rm 1PI}(p^2)$. Derivatives for those functions can be defined as $\hat{\Pi}'_{\phi\phi}[m^2] = \frac{d}{dp^2}\hat{\Pi}_{\phi\phi}(p^2)\big|_{p^2=m^2}$ and $\Pi_{\phi\phi}^{\rm 1PI\prime}[m^2] = \frac{d}{dp^2}\Pi_{\phi\phi}^{\rm 1PI}(p^2)\big|_{p^2=m^2}$.

[1]The counter-terms $\delta\beta$ and $\delta\beta'$ can be written in terms of δv and δv_Δ as $\delta\beta = \frac{v_\Delta}{v}\sqrt{\frac{2}{1-2v_\Delta^2/v^2}}\left(\frac{\delta v_\Delta}{v_\Delta} - \frac{\delta v}{v}\right)$ and $\delta\beta' = \frac{v_\Delta}{v}\frac{2}{(1+2v_\Delta^2/v^2)\sqrt{1-2v_\Delta^2/v^2}}\left(\frac{\delta v_\Delta}{v_\Delta} - \frac{\delta v}{v}\right)$.

The renormalized scalar boson two point functions are given at the one-loop level by

$$\hat{\Pi}_{H^{++}H^{--}}[p^2] = (p^2 - m^2_{H^{++}})\delta Z_{H^{++}} - \delta m^2_{H^{++}} + \frac{\sqrt{2}}{s_\beta}\frac{\delta T_\Delta}{v} + \Pi^{\rm 1PI}_{H^{++}H^{--}}(p^2), \tag{7.33}$$

$$\hat{\Pi}_{H^{+}H^{-}}[p^2] = (p^2 - m^2_{H^{+}})\delta Z_{H^{+}} - \delta m^2_{H^{+}} + \frac{s^2_\beta}{c_\beta}\frac{\delta T_\Phi}{v} + \frac{\sqrt{2}c^2_\beta}{s_\beta}\frac{\delta T_\Delta}{v} + \Pi^{\rm 1PI}_{H^{+}H^{-}}(p^2), \tag{7.34}$$

$$\hat{\Pi}_{G^{+}G^{-}}[p^2] = p^2\delta Z_{G^{+}} + \frac{c_\beta\delta T_\Phi + \sqrt{2}s_\beta\delta T_\Delta}{v} + \Pi^{\rm 1PI}_{G^{+}G^{-}}(p^2), \tag{7.35}$$

$$\hat{\Pi}_{AA}[p^2] = (p^2 - m^2_{A})\delta Z_{A} - \delta m^2_{A} + \frac{s^2_{\beta'}}{c_\beta}\frac{\delta T_\Phi}{v} + \frac{\sqrt{2}c^2_{\beta'}}{s_\beta}\frac{\delta T_\Delta}{v} + \Pi^{\rm 1PI}_{AA}(p^2), \tag{7.36}$$

$$\hat{\Pi}_{GG}[p^2] = p^2\delta Z_{G^0} + \frac{c^2_{\beta'}}{c_\beta}\frac{\delta T_\Phi}{v} + \frac{s^2_{\beta'}}{s_\beta}\frac{\delta T_\Delta}{v} + \Pi^{\rm 1PI}_{GG}(p^2), \tag{7.37}$$

$$\hat{\Pi}_{HH}[p^2] = (p^2 - m^2_{H})\delta Z_{H} - \delta m^2_{H} + \frac{s^2_{\alpha}}{c_\beta}\frac{\delta T_\Phi}{v} + \frac{\sqrt{2}c^2_{\alpha}}{s_\beta}\frac{\delta T_\Delta}{v} + \Pi^{\rm 1PI}_{HH}(p^2), \tag{7.38}$$

$$\hat{\Pi}_{hh}[p^2] = (p^2 - m^2_{h})\delta Z_{h} - \delta m^2_{h} + \frac{c^2_{\alpha}}{c_\beta}\frac{\delta T_\Phi}{v} + \frac{\sqrt{2}s^2_{\alpha}}{s_\beta}\frac{\delta T_\Delta}{v} + \Pi^{\rm 1PI}_{hh}(p^2). \tag{7.39}$$

The renormalized two point functions for the scalar boson mixing are given by

$$\hat{\Pi}_{H^{+}G^{-}}[p^2] = \delta C_{HG}(2p^2 - m^2_{H^{+}}) - \frac{s_\beta\delta T_\Phi - \sqrt{2}c_\beta\delta T_\Delta}{v} + m^2_{H^{+}}\delta\beta + \Pi^{\rm 1PI}_{G^{+}H^{-}}(p^2), \tag{7.40}$$

$$\hat{\Pi}_{AG}[p^2] = \delta C_{AG}(2p^2 - m^2_{A}) - \frac{s^2_{\beta'}}{\sqrt{2}s_\beta}\frac{\delta T_\Phi}{v} + \frac{2c^2_{\beta'}}{c_\beta}\frac{\delta T_\Delta}{v} + m^2_{A}\delta\beta' + \Pi^{\rm 1PI}_{AG}(p^2), \tag{7.41}$$

$$\begin{aligned}\hat{\Pi}_{Hh}[p^2] = {} & \frac{c_\alpha s_\alpha}{c_\beta s_\beta}\frac{\sqrt{2}c_\beta\delta T_\Delta - s_\beta\delta T_\Phi}{v} - \delta\alpha(m^2_h - m^2_H) \\ & + \delta C_{Hh}(2p^2 - m^2_h - m^2_H) + \Pi^{\rm 1PI}_{Hh}(p^2),\end{aligned} \tag{7.42}$$

The counter-terms of the doubly-charged Higgs boson mass $\delta m^2_{H^{++}}$ and its wave function renormalization factor $\delta Z_{H^{++}}$ are determined by the following renormalization conditions:

$$\hat{\Pi}_{H^{++}H^{--}}[m^2_{H^{++}}] = 0, \quad \hat{\Pi}'_{H^{++}H^{--}}[m^2_{H^{++}}] = 0, \tag{7.43}$$

which yield

$$\delta m^2_{H^{++}} = \frac{\sqrt{2}\delta T_\Delta}{v s_\beta} + \Pi^{\rm 1PI}_{H^{++}H^{--}}(m^2_{H^{++}}), \quad \delta Z_{H^{++}} = -\Pi^{\rm 1PI'}_{H^{++}H^{--}}(m^2_{H^{++}}). \tag{7.44}$$

The five parameters related to the CP-odd scalar states (δm^2_A, δZ_{G^0}, δZ_A, δC_{GA} and $\delta\beta'$) are determined by imposing the following five renormalization conditions

$$\hat{\Pi}_{AA}[m^2_A] = 0, \quad \hat{\Pi}'_{AA}[m^2_A] = 0, \tag{7.45}$$

$$\hat{\Pi}'_{GG}[0] = 0, \quad \hat{\Pi}_{AG}[0] = 0, \quad \hat{\Pi}_{AG}[m^2_A] = 0. \tag{7.46}$$

by which we obtain

$$\delta m_A^2 = \frac{s_{\beta'}^2}{c_\beta}\frac{\delta T_\Phi}{v} + \frac{\sqrt{2}c_{\beta'}^2}{s_\beta}\frac{\delta T_\Delta}{v} + \Pi_{AA}^{\rm 1PI}(m_A^2), \tag{7.47}$$

$$\delta Z_{G^0} = -\Pi_{GG}^{\rm 1PI'}(0), \quad \delta Z_A = -\Pi_{AA}^{\rm 1PI'}(m_A^2), \tag{7.48}$$

$$\delta C_{AG} = \frac{1}{2m_A^2}\left[\Pi_{AG}^{\rm 1PI}(0) - \Pi_{AG}^{\rm 1PI}(m_A^2)\right], \tag{7.49}$$

$$\delta\beta' = -\frac{1}{2m_A^2}\left[\Pi_{AG}^{\rm 1PI}(0) + \Pi_{AG}^{\rm 1PI}(m_A^2) - \frac{\sqrt{2}s_{\beta'}^2}{s_\beta}\frac{\delta T_\Phi}{v} - \frac{4c_{\beta'}^2}{c_\beta}\frac{\delta T_\Delta}{v}\right]. \tag{7.50}$$

The four counter-terms related to the singly-charged Higgs boson ($\delta m_{H^+}^2$, δZ_{G^+}, δZ_{H^+} and δC_{GH}) are determined by imposing the following four renormalization conditions

$$\hat{\Pi}_{H^+H^-}[m_{H^+}^2] = 0, \quad \hat{\Pi}'_{G^+G^-}[0] = 0, \tag{7.51}$$

$$\hat{\Pi}'_{H^+H^-}[m_{H^+}^2] = 0, \quad \hat{\Pi}_{HG}[0] = 0, \tag{7.52}$$

by which we obtain

$$\delta m_{H^+}^2 = \frac{s_\beta^2}{c_\beta}\frac{\delta T_\Phi}{v} + \frac{\sqrt{2}c_\beta^2}{s_\beta}\frac{\delta T_\Delta}{v} + \Pi_{H^+H^-}^{\rm 1PI}(m_{H^+}^2), \tag{7.53}$$

$$\delta Z_{G^+} = -\Pi_{G^+G^-}^{\rm 1PI'}(0), \quad \delta Z_{H^+} = -\Pi_{H^+H^-}^{\rm 1PI'}(m_{H^+}^2), \tag{7.54}$$

$$\delta C_{HG} = \delta\beta + \frac{1}{m_{H^+}^2}\left[\Pi_{H^+G^-}^{\rm 1PI}(0) + \frac{-s_\beta\delta T_\Phi + \sqrt{2}c_\beta\delta T_\Delta}{v}\right], \tag{7.55}$$

where $\delta\beta$ is determined through $\delta\beta'$ as

$$\delta\beta = \frac{1+s_\beta^2}{\sqrt{2}}\delta\beta'. \tag{7.56}$$

Finally, the six parameters related to the CP-even Higgs states ($\delta\alpha$, δm_h^2, δm_H^2, δZ_h, δZ_H and δC_{Hh}) are determined by imposing the following six renormalization conditions

$$\hat{\Pi}_{hh}[m_h^2] = 0, \quad \hat{\Pi}'_{hh}[m_h^2] = 0, \tag{7.57}$$

$$\hat{\Pi}_{HH}[m_H^2] = 0, \quad \hat{\Pi}'_{HH}[m_H^2] = 0, \tag{7.58}$$

$$\hat{\Pi}_{Hh}[m_h^2] = 0, \quad \hat{\Pi}_{Hh}[m_H^2] = 0, \tag{7.59}$$

by which we obtain

$$\delta m_h^2 = \frac{\delta T_\Phi}{v}\frac{c_\alpha^2}{c_\beta} + \frac{\sqrt{2}\delta T_\Delta}{v}\frac{s_\alpha^2}{s_\beta} + \Pi_{hh}^{\rm 1PI}(m_h^2), \quad \delta m_H^2 = \frac{\delta T_\Phi}{v}\frac{s_\alpha^2}{c_\beta} + \frac{\sqrt{2}\delta T_\Delta}{v}\frac{c_\alpha^2}{s_\beta} + \Pi_{HH}^{\rm 1PI}(m_H^2), \tag{7.60}$$

$$\delta Z_h = -\Pi_{hh}^{\rm 1PI'}(m_h^2), \quad \delta Z_H = -\Pi_{HH}^{\rm 1PI'}(m_H^2), \tag{7.61}$$

$$\delta\alpha = \frac{1}{2(m_h^2 - m_H^2)}\left[\Pi_{Hh}^{\rm 1PI}(m_h^2) + \Pi_{Hh}^{\rm 1PI}(m_H^2) - \frac{2s_\alpha c_\alpha}{s_\beta c_\beta}\left(\frac{\delta T_\Phi}{v}s_\beta - \frac{\sqrt{2}\delta T_\Delta}{v}c_\beta\right)\right], \tag{7.62}$$

$$\delta C_{Hh} = \frac{1}{2(m_h^2 - m_H^2)}\left[\Pi_{Hh}^{\rm 1PI}(m_H^2) - \Pi_{Hh}^{\rm 1PI}(m_h^2)\right]. \tag{7.63}$$

In the limit of $v_\Delta/v \to 0$, the mass of A is no more independent parameter, which is determined by the masses of $H^{\pm\pm}$ and $H^\pm$. In this limit, the CP-odd Higgs boson mass is expressed at the tree level as

$$(m_A^2)_{\rm tree} \equiv \lim_{v_\Delta/v\to 0} m_A^2 = 2m_{H^+}^2 - m_{H^{++}}^2. \tag{7.64}$$

The renormalized pole mass of A, which has been discussed in Ref. [**?**], can be defined by the following equations

$$\lim_{v_\Delta/v\to 0} \hat{\Pi}_{AA}[p^2 = (m_A^2)_{\rm pole}] = 0. \tag{7.65}$$

From Eq. (7.65), we obtain

$$(m_A^2)_{\rm pole} \simeq (m_A^2)_{\rm tree} + \frac{1}{1+\delta Z_A}\left[\delta m_A^2 - \frac{\delta T_\Delta}{v_\Delta} - \Pi_{AA}^{\rm 1PI}[(m_A^2)_{\rm tree}]\right], \tag{7.66}$$

where we use $\Pi_{AA}[(m_A^2)_{\rm pole}] \simeq \Pi_{AA}[(m_A^2)_{\rm tree}]$. The counter-term δm_A^2 is not independent parameter in the limit of $v_\Delta/v \to 0$, but they can be given by $\delta m_A^2 = 2\delta m_{H^+}^2 - \delta m_{H^{++}}^2$. By using Eqs. (7.44) and (7.53), we obtain

$$(m_A^2)_{\rm pole} \simeq (m_A^2)_{\rm tree} + \left[2\Pi_{H^+H^-}^{\rm 1PI}(m_{H^+}^2) - \Pi_{H^{++}H^{--}}^{\rm 1PI}(m_{H^{++}}^2) - \Pi_{AA}^{\rm 1PI}[(m_A^2)_{\rm tree}]\right]. \tag{7.67}$$

Above the equation indicates that the tree level mass relations among the triplet-like Higgs bosons which are written in Eqs. (3.104) and (3.105) can be deviated by the effects of the radiative correction. The magnitude of this deviation can be parameterized as

$$\Delta R = \frac{m_{H^{++}}^2 - m_{H^+}^2}{m_{H^+}^2 - (m_A^2)_{\rm pole}} - 1. \tag{7.68}$$

In Ref. [61], ΔR has been evaluated numerically in the case of $\alpha = 0$ and $v_\Delta/v \to 0$ as shown in Fig. 7.1.

7.2 Higgs couplings at the one-loop level

In this section, we discuss the SM-like Higgs boson h couplings with the gauge bosons ($\gamma\gamma$, W^+W^- and ZZ) and the Higgs self-coupling hhh at the one-loop level in the favored parameter regions by the unitarity bound, the vacuum stability bound and by the measured W boson mass discussed in previous sections.

7.2.1 Higgs to the diphoton decay

$h \to \gamma\gamma$ process is induced at the one-loop level, because the Higgs boson does not couple to the photon at the tree level. Thus, the decay of $h \to \gamma\gamma$ is sensitive to effects of new charged particle which can couple to the Higgs boson. In the HTM, the doubly-charged Higgs boson $H^{\pm\pm}$ and the singly-charged Higgs boson $H^\pm$ can contribute to the Higgs to diphoton decay. In particular, the contribution from the $H^{\pm\pm}$ loop to the $h \to \gamma\gamma$ is quite important compared to that from $H^\pm$, because $H^{\pm\pm}$ contribution is roughly 4 times larger than that from $H^\pm$ contribution at the amplitude level.

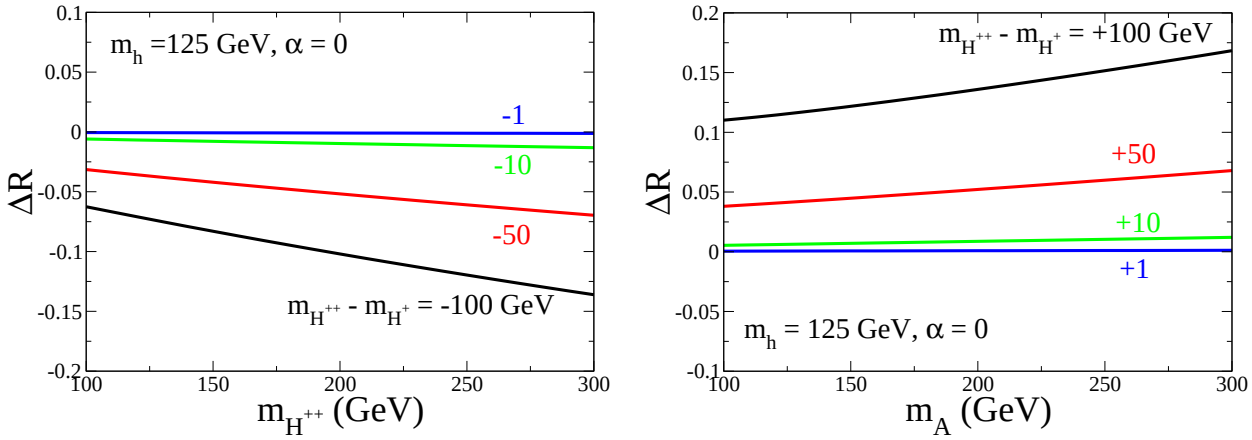

Figure 7.1: ΔR is shown as a function of the lightest triplet-like Higgs boson mass in the case of $\alpha = 0$ and $m_h = 125$ GeV for each fixed value of $m_{H^{++}} - m_{H^+}$ [?]. The left (right) panel shows the results in Case I (Case II).

The decay rate of $h \to \gamma\gamma$ is calculated at the one-loop level by

$$\Gamma(h \to \gamma\gamma) = \frac{G_F \alpha_{\rm em}^2 m_h^3}{128\sqrt{2}\pi^3} \Big| - 2\frac{c_\alpha}{c_\beta} \sum_f N_f^c Q_f^2 \tau_f [1 + (1-\tau_f) f(\tau_f)] + (c_\beta c_\alpha + \sqrt{2} s_\alpha s_\beta)[2 + 3\tau_W + 3\tau_W(2-\tau_W) f(\tau_W)] - Q_{H^{++}}^2 \frac{2v\lambda_{H^{++}H^{--}h}}{m_h^2}[1 - \tau_{H^{++}} f(\tau_{H^{++}})] - Q_{H^+}^2 \frac{2v\lambda_{H^+H^-h}}{m_h^2}[1 - \tau_{H^+} f(\tau_{H^+})] \Big|^2 , \tag{7.69}$$

where the function $f(x)$ is given by

$$f(x) = \begin{cases} [\arcsin(1/\sqrt{x})]^2, & \text{if } x \geq 1, \\ -\frac{1}{4}[\ln \frac{1+\sqrt{1-x}}{1-\sqrt{1-x}} - i\pi]^2, & \text{if } x < 1 \end{cases} . \tag{7.70}$$

In Eq. (7.69), Q_F is the electric charge of the field F, N_f^c is the color factor and $\tau_F = 4m_F^2/m_h^2$. These couplings can be expressed quite a simple form by neglecting the terms proportional to v_Δ:

$$\lambda_{H^{++}H^{--}h} \simeq -v\lambda_4, \quad \lambda_{H^+H^-h} \simeq -\frac{v}{2}(2\lambda_4 + \lambda_5). \tag{7.71}$$

It is well known that the W boson loop contribution to the $h \to \gamma\gamma$ decay rate is dominant compared to the top quark loop contribution in the SM, so that when a new physics effect to the amplitude of the $h \to \gamma\gamma$ process has the same sign of the W-loop contribution, then the decay rate is enhanced compared with the SM prediction. In the HTM, when the sign of the coupling $\lambda_{H^{++}H^{--}h}$ is positive (negative), then the $H^{\pm\pm}$ loop contribution has the same (opposite) sign of the W loop contribution, which can be achieved by taking λ_4 to be a negative (positive)

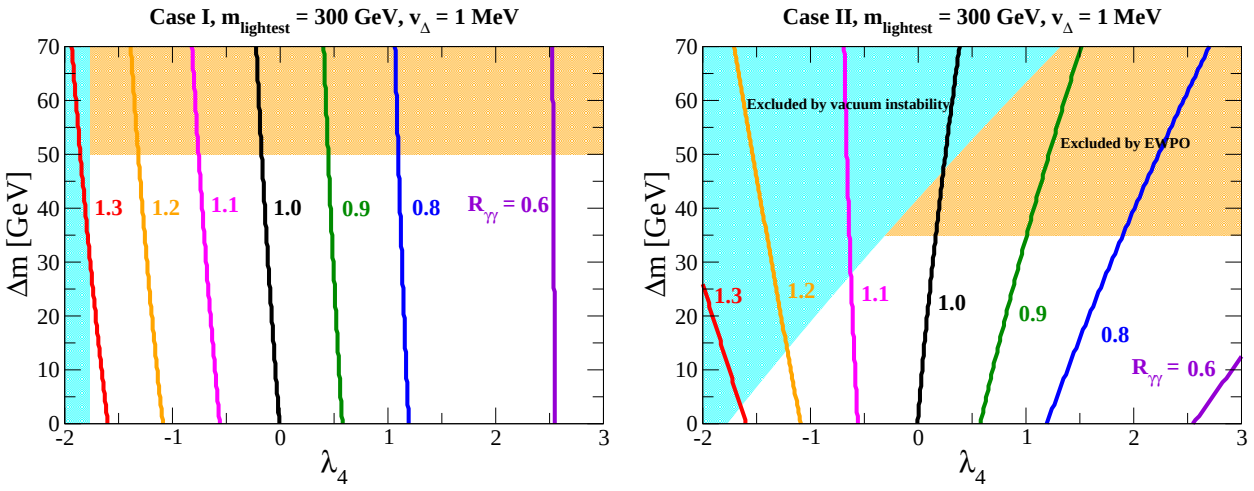

Figure 7.2: Contour plots of $R_{\gamma\gamma}$ for $v_\Delta = 1$ MeV and $m_{\rm lightest} = 300$ GeV in the λ_4-Δm plane. The left panel (right panel) shows the result in Case I (Case II). The blue and orange shaded regions are excluded by the vacuum stability bound and the measured m_W data, respectively.

value. From Eq. (7.71), it can be seen that the λ_5 coupling only affects to the singly-charged Higgs boson coupling with h: $\lambda_{H^+H^-h}$, so that the $h \to \gamma\gamma$ decay rate is not sensitive to the magnitude of λ_5. In other words, the mass difference among the triplet-like Higgs boson is not so important in the $h \to \gamma\gamma$ decay process as long as we keep a fixed value of $m_{H^{++}}$.

In this subsection, we study the deviation of the $h \to \gamma\gamma$ event rate in the HTM from that in the SM taking into account the constraint from the perturbative unitarity, the vacuum stability and the electroweak precision data. We also investigate the correlation between the $h \to \gamma\gamma$ decay rate and the hhh, hWW and hZZ couplings at the one-loop level. To compare the Higgs to diphoton event rate from the SM prediction, we define

$$R_{\gamma\gamma} \equiv \frac{\sigma(gg \to h)_{\rm HTM} \times {\rm BR}(h \to \gamma\gamma)_{\rm HTM}}{\sigma(gg \to h)_{\rm SM} \times {\rm BR}(h \to \gamma\gamma)_{\rm SM}}, \tag{7.72}$$

where $\sigma(gg \to h)_{\rm model}$ is the cross section of the gluon fusion process, and ${\rm BR}(h \to \gamma\gamma)_{\rm model}$ is the branching fraction of the $h \to \gamma\gamma$ mode in a model. In fact, the ratio of the cross section $\sigma(gg \to h)_{\rm HTM}/\sigma(gg \to h)_{\rm SM}$ can be replaced by the factor c_α^2/c_β^2.

In Fig. 7.2, we show the contour plots of $R_{\gamma\gamma}$ for $v_\Delta = 1$ MeV and $m_{\rm lightest} = 300$ GeV in the λ_4-Δm plane. The left panel (right panel) shows the result in Case I (Case II). The blue and orange shaded regions are those excluded by the vacuum stability bound (assuming $\lambda_\Delta = 3$) and the measured m_W data, respectively. In both cases, $R_{\gamma\gamma}$ can be greater (smaller) than 1 for negative (positive) values of λ_4. In Case I, no large Δm dependence appears, while in Case II $R_{\gamma\gamma}$ slightly depends on Δm due to the larger values of $m_{H^{++}}$ which affect $R_{\gamma\gamma}$ via Δm. Under the constraint of the vacuum stability and the electroweak precision observable m_W, larger Δm can be allowed in Case I than in Case II. We find that predicted values of $R_{\gamma\gamma}$ are about 1.3 (about 0.6) in this case when λ_4 is about -1.7 (about 3) in both Case I and Case II.

7.2.2 Renormalized hVV coupling

The most general form factors of the hVV coupling ($V = W^\pm$ or Z) can be written as

$$M^{\mu\nu}_{hVV} = M_1^{hVV} g^{\mu\nu} + M_2^{hVV} \frac{p_1^\mu p_2^\nu}{m_V^2} + i M_3^{hVV} \epsilon^{\mu\nu\rho\sigma} \frac{p_{1\rho} p_{2\sigma}}{m_V^2}, \tag{7.73}$$

where m_V is the mass of the gauge boson V, p_1 and p_2 are the incoming momenta of V. The renormalized form factors are given by

$$M_i^{hVV} = M_{i,\mathrm{tree}}^{hVV} + \delta M_i^{hVV} + M_{i,\mathrm{1PI}}^{hVV}, \quad (i = 1 - 3). \tag{7.74}$$

The tree-level contributions for these form factors are

$$\begin{aligned} M_{1,\mathrm{tree}}^{hZZ} &= \frac{2m_Z^2}{v^2 + 2v_\Delta^2}(v_\phi c_\alpha + 4 v_\Delta s_\alpha), \quad M_{1,\mathrm{tree}}^{hWW} = \frac{2m_W^2}{v^2}(v_\phi c_\alpha + 2 v_\Delta s_\alpha), \\ M_{2,\mathrm{tree}}^{hVV(\mathrm{tree})} &= M_{3,\mathrm{tree}}^{hVV} = 0. \end{aligned} \tag{7.75}$$

The counter-term contributions are

$$\begin{aligned} \delta M_1^{hZZ} &= \frac{2m_Z^2 c_\alpha}{v^2 + 2v_\Delta^2} \left\{ \frac{v_\phi \delta m_Z^2}{m_Z^2} + \frac{v_\phi}{2}(\delta Z_h + 2\delta Z_Z) + 4 v_\Delta \delta C_{Hh} \right. \\ &\qquad \left. + \frac{1}{v_\phi (v^2 + 2v_\Delta^2)} [2 v_\Delta (2v_\Delta^2 - 3v^2)\delta v_\Delta - v(v^2 - 6v_\Delta^2)\delta v] \right\} \\ &\quad + \frac{2m_Z^2 s_\alpha}{v^2 + 2v_\Delta^2} \left[\frac{4 v_\Delta \delta m_Z^2}{m_Z^2} + 2 v_\Delta (\delta Z_h + 2\delta Z_Z) - v_\phi \delta C_{Hh} + \frac{4(v_\phi^2 \delta v_\Delta - 2 v v_\Delta \delta v)}{v^2 + 2v_\Delta^2} \right] \\ \delta M_1^{hWW} &= \frac{v_\phi m_W^2 c_\alpha}{v^2} \left\{ \frac{2\delta m_W^2}{m_W^2} + 2\delta Z_W + \delta Z_h + \frac{4 v_\Delta}{v_\phi} \delta C_{Hh} - \frac{2(v^2 - 4v_\Delta^2)}{v_\phi^2} \frac{\delta v}{v} - \frac{4 v_\Delta^2}{v_\phi^2} \frac{\delta v_\Delta}{v_\Delta} \right\} \\ &\quad + \frac{2 m_W^2 v_\Delta s_\alpha}{v^2} \left(\frac{2\delta m_W^2}{m_W^2} + 2\delta Z_W + \delta Z_h - \frac{v_\phi}{v_\Delta} \delta C_{Hh} - \frac{4\delta v}{v} + \frac{2\delta v_\Delta}{v_\Delta} \right), \\ \delta M_2^{hVV} &= \delta M_3^{hVV} = 0. \end{aligned} \tag{7.76}$$

We define the following quantity to study the deviation of the hVV coupling from the SM prediction:

$$\Delta g_{hVV} \equiv \frac{\mathrm{Re} M_1^{hVV} - \mathrm{Re} M_1^{hVV}(\mathrm{SM})}{\mathrm{Re} M_1^{hVV}(\mathrm{SM})}, \tag{7.77}$$

where $M_1^{hVV} = M_1^{hVV}(m_V^2, (m_h - m_V)^2, m_h^2)$ and $M_1^{hVV}(\mathrm{SM})$ is the corresponding SM prediction.

In Fig. 7.3, we show the contour plots for Δg_{hZZ} for $m_{\mathrm{lightest}} = 300$ GeV and $v_\Delta = 1$ MeV in the λ_4-Δm plane. The left (right) plot shows the result in Case I (Case II). The blue and orange shaded regions are excluded by the vacuum stability bound and the measured m_W data, respectively. The magnitude of the negative corrections is larger for positive larger values of λ_4 for smaller values of Δm. For the cases with large Δm such as about 30 GeV, the region

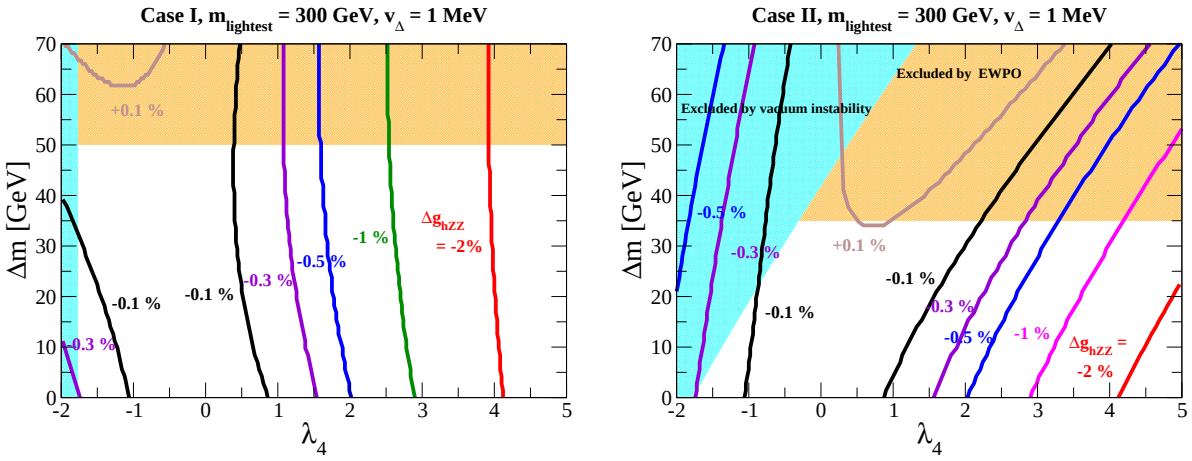

Figure 7.3: Contour plots of Δg_{hZZ} in Eq. (7.77) for $m_{\rm lightest} = 300$ GeV and v_Δ=1 MeV in the λ_4-Δm plane. The left panel (right panel) shows the result in Case I (Case II). The blue and orange shaded regions are excluded by the vacuum stability bound and the measured m_W data, respectively.

with positive corrections appears. This is the striking feature of the HTM. On the contrary, in multi Higgs doublet models the correction is always negative [70]. Under the constraint of the vacuum stability bound and the electroweak precision observable m_W, larger Δm can be allowed in Case I than in Case II. We find that Δg_{hZZ} is predicted to be at most a few %. We can expect that such a deviation will be testable at the ILC [12, 13, 16, 100].

In Fig. 7.4, the similar contour plots are shown for Δg_{hWW} with the same parameter sets in the same plane. The behavior of Δg_{hWW} in this plane is similar to that of Δg_{hZZ}. However, the correction can be positive for smaller values of Δm. We also show the same constraints from the vacuum stability bound and from the electroweak precision observable m_W. Magnitudes of maximum value of the correction are almost the same those of Δg_{hZZ}, especially for $\lambda_4 > 0$.

7.2.3 Renormalized hhh coupling

Finally, we show the numerical results for the deviation of the Higgs trilinear coupling hhh from the SM prediction. The renormalized hhh coupling can be expressed as a function of the external incoming momenta p_1 and p_2 and the outgoing momentum $q = p_1 + p_2$ as

$$\Gamma_{hhh}(p_1^2, p_2^2, q^2) = \Gamma_{hhh}^{\rm tree} + \delta\Gamma_{hhh} + \Gamma_{hhh}^{\rm 1PI}(p_1^2, p_2^2, q^2), \tag{7.78}$$

where the first, second and last terms are corresponding to the tree level, the counter-term, and the 1PI diagram contributions, respectively. The tree level contribution $\Gamma_{hhh}^{\rm tree}$ is calculated as

$$\Gamma_{hhh}^{\rm tree} = -6\left[\left(\frac{c_\alpha^3}{v_\phi} + \frac{s_\alpha^3}{v_\Delta}\right)\frac{m_h^2}{2} + \frac{s_\alpha^2}{v^2 + 2v_\Delta^2}\left(v_\phi c_\alpha - \frac{v_\phi^2}{2v_\Delta}s_\alpha\right)m_A^2\right]. \tag{7.79}$$

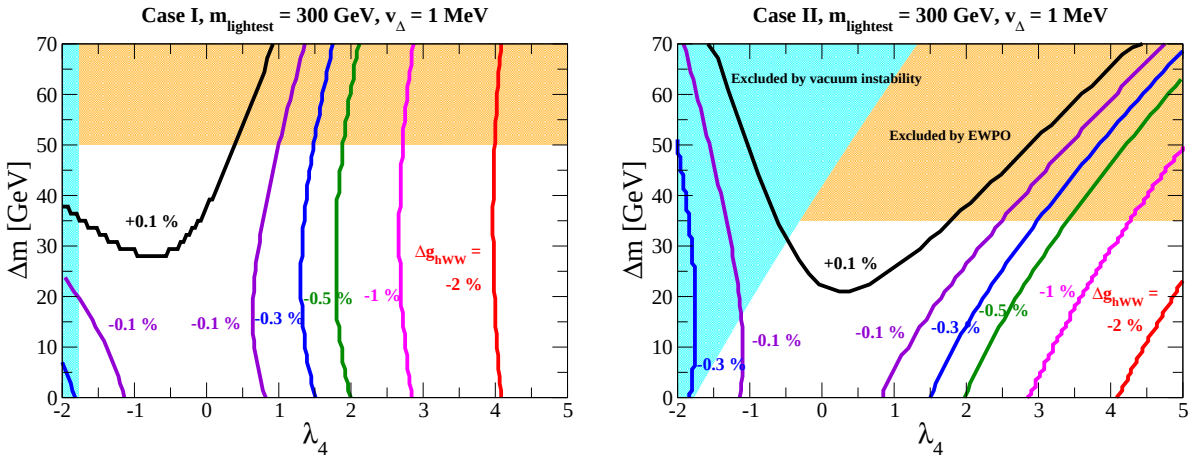

Figure 7.4: Contour plots of Δg_{hWW} defined in Eq. (7.77) for $m_{\rm lightest} = 300$ GeV and v_Δ=1 MeV in the λ_4-Δm plane. The left panel (right panel) shows the result in Case I (Case II). The blue and orange shaded regions are excluded by the vacuum stability bound and the measured m_W data, respectively.

The counter-term contribution $\delta\Gamma_{hhh}$ is evaluated by

$$\begin{aligned}
\delta\Gamma_{hhh} =& -3\left(\frac{c_\alpha^3}{v_\phi}+\frac{s_\alpha^3}{v_\Delta}\right)\delta m_h^2 - \frac{6s_\alpha^2}{v^2+2v_\Delta^2}\left(v_\phi c_\alpha - \frac{v_\phi^2 s_\alpha}{2v_\Delta}\right)\delta m_A^2 - 3(m_h^2-m_H^2)\left(\frac{s_\alpha^2 c_\alpha}{v_\Delta}-\frac{c_\alpha^2 s_\alpha}{v_\phi}\right)\delta\alpha \\
&- \frac{9}{2}\left[m_h^2\left(\frac{c_\alpha^3}{v_\phi}+\frac{s_\alpha^3}{v_\Delta}\right)+\frac{m_A^2 v_\phi s_\alpha^2}{v_\Delta(v^2+2v_\Delta^2)}(2v_\Delta c_\alpha - v_\phi s_\alpha)\right]\delta Z_h \\
&- 3s_\alpha\left\{(2m_h^2+m_H^2)\left(\frac{s_\alpha c_\alpha}{v_\Delta}-\frac{c_\alpha^2}{v_\phi}\right)+\frac{m_A^2 v_\phi}{v_\Delta(v^2+2v_\Delta^2)}\left[2v_\Delta(2c_\alpha^2-s_\alpha^2)-3s_\alpha c_\alpha v_\phi\right]\right\}\delta C_{Hh} \\
&- \frac{3}{v_\phi}\left\{\frac{m_h^2}{v_\phi^2}\left[\frac{v_\Delta}{2}(3c_\alpha+c_{3\alpha})-\frac{v_\phi^3 s_\alpha^3}{v_\Delta^2}\right]+\frac{4m_A^2 s_\alpha^2}{(v^2+2v_\Delta^2)^2}\left[c_\alpha v_\Delta(2v_\Delta^2-3v^2)+v_\phi s_\alpha\left(\frac{v^4}{4v_\Delta^2}+2v^2-v_\Delta^2\right)\right]\right\}\delta v_\Delta \\
&+ \frac{3}{v_\phi}\left\{\frac{m_h^2 v}{v_\phi^2}c_\alpha^3+\frac{2m_A^2 v s_\alpha^2}{(v^2+2v_\Delta^2)^2}\left[(v^2-6v_\Delta^2)c_\alpha+4v_\Delta v_\phi s_\alpha\right]\right\}\delta v. \qquad (7.80)
\end{aligned}$$

Contributions of the 1PI diagram to the hhh coupling is listed in Appendix B.

In the limit of $v_\Delta/v \to 0$, these expressions are reduced to the same expressions in the SM as[2]

$$\Gamma_{hhh}^{\rm tree} \to \frac{-3m_h^2}{v}, \qquad (7.81)$$

$$\delta\Gamma_{hhh} \to -\frac{3\delta m_h^2}{v} - \frac{9}{2}\frac{m_h^2}{v}\delta Z_h + \frac{3m_h^2}{v^2}\delta v. \qquad (7.82)$$

In this limit, the top quark loop and the gauge boson loop contributions to the 1PI diagram is the same as the SM. However, the scalar boson loop contributions can be different from the

[2]As long as we take λ_4 to be $\mathcal{O}(1)$ or less and the triplet-like Higgs boson masses to be $\mathcal{O}(100)$ GeV or more, the magnitude of the mixing angle α is as large as that of v_Δ.

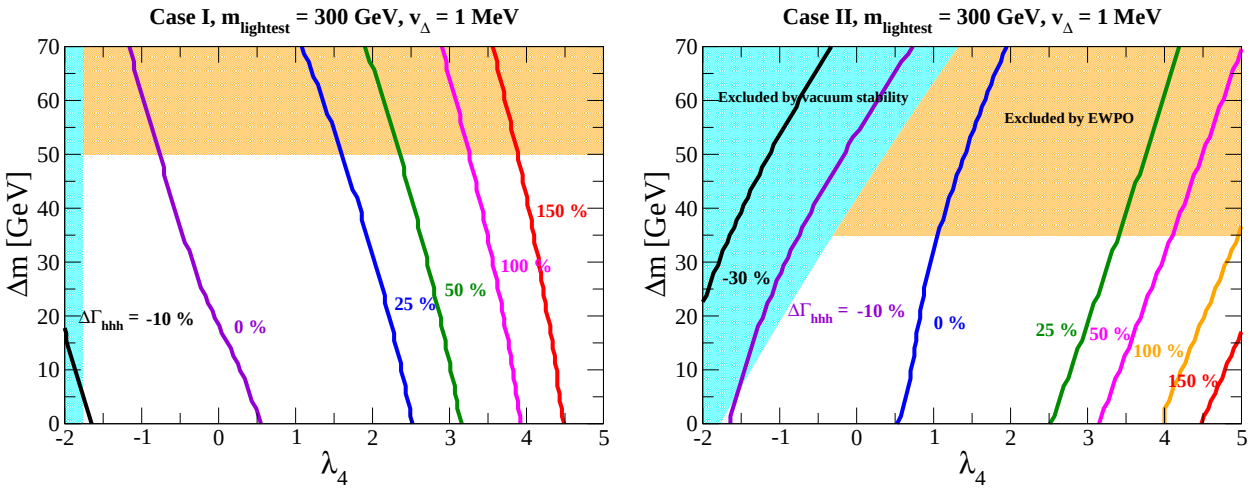

Figure 7.5: Contour plots of $\Delta\Gamma_{hhh}$ defined in Eq. (7.84) for $m_{\rm lightest} = 300$ GeV and $v_\Delta = 1$ MeV. The left panel (right panel) shows the result in Case I (Case II). The blue and orange shaded regions are excluded by the vacuum stability bound and the measured m_W data, respectively.

SM case, because the triplet-like Higgs boson loop contributions can be remained even in this limit. Approximately, the triplet-like Higgs boson loop contributions can be expressed as

$$\begin{aligned}\Gamma_{hhh} &\simeq -\frac{3m_h^2}{v}\left[1-\frac{v}{48\pi^2 m_h^2}\left(\frac{\lambda^3_{H^{++}H^{--}h}}{m^2_{H^{++}}}+\frac{\lambda^3_{H^+H^-h}}{m^2_{H^+}}+\frac{4\lambda^3_{AAh}}{m^2_A}+\frac{4\lambda^3_{HHh}}{m^2_H}\right)+\cdots\right]\\ &\simeq -\frac{3m_h^2}{v}\left\{1+\frac{v^4}{48\pi^2 m_h^2}\left[\frac{\lambda_4^3}{m^2_{H^{++}}}+\frac{(\lambda_4+\frac{\lambda_5}{2})^3}{m^2_{H^+}}+\frac{(\lambda_4+\lambda_5)^3}{2m^2_A}+\frac{(\lambda_4+\lambda_5)^3}{2m^2_H}\right]+\cdots\right\},\end{aligned} \tag{7.83}$$

where dotted terms mean the same correction given in the SM. Therefore, we find that the triplet-like Higgs boson loop contribution to the hhh vertex gives a positive (negative) correction compared to the SM prediction when λ_4 is taken to be a positive (negative) value and $\lambda_5 \simeq 0$.

To illustrate the deviation of the hhh coupling from the SM prediction, we define the following quantity:

$$\Delta\Gamma_{hhh} \equiv \frac{{\rm Re}\Gamma_{hhh} - {\rm Re}\Gamma^{\rm SM}_{hhh}}{{\rm Re}\Gamma^{\rm SM}_{hhh}}, \tag{7.84}$$

where $\Gamma_{hhh} = \Gamma_{hhh}(m_h^2, m_h^2, 4m_h^2)$ and $\Gamma^{\rm SM}_{hhh}$ is the corresponding prediction in the SM.

In Fig. 7.5, contour plot for the deviation of the one-loop corrected hhh coupling from the SM prediction $\Delta\Gamma_{hhh}$ defined in Eq. (7.84) is shown for $m_{\rm lightest} = 300$ GeV and $v_\Delta = 1$ MeV in the λ_4-Δm plane. The left (right) plot shows the result in Case I (Case II). The blue and orange shaded regions are excluded by the vacuum stability bound and the measured m_W data, respectively. In both cases, positive (negative) values of $\Delta\Gamma_{hhh}$ are predicted in the case with a positive (negative) λ_4 whose magnitudes can be greater than about $+150\%$ (-10%). Such a deviation in $\Delta\Gamma_{hhh}$ is expected to be measured at the ILC with a center of mass energy

to be 1 TeV [12, 13, 16, 100]. We note that there is a relations among the one-loop corrected Higgs boson couplings $h\gamma\gamma$, hVV and hhh. In particular, a strong correlation can be found in deviations in $R_{\gamma\gamma}$ and Γ_{hhh}. If $R_{\gamma\gamma} < 1$ ($R_{\gamma\gamma} > 1$) which is predicted for $\lambda_4 > 0$ ($\lambda_4 < 0$), $\Delta\Gamma_{hhh}$ takes sufficiently large positive (negative) values. In conclusion, by measuring these coupling constants accurately, we can discriminate the HTM of the other models, even when additional particles are not directly discovered.

7.3 Summary

We have calculated a full set of one-loop corrected hWW, hZZ and hhh couplings in addition to the electroweak parameters such as the renormalized W boson mass and the electroweak renormalized parameter Δr by on-shell renormalization scheme. We also have computed the decay rate of h into diphoton at the one-loop level. Magnitudes of the deviations in these quantities from the SM predictions have been evaluated in the parameter regions where the unitarity and vacuum stability bounds are satisfied and the predicted W boson mass is consistent with the data. There are strong correlations among deviations in the Higgs boson couplings $h\gamma\gamma$, hVV and hhh. By measuring these deviations in Higgs boson couplings accurately at the HL-LHC and the ILC, the HTM may be distinguished from the other models.

Chapter 8

Summary of this thesis

The coupling measurements of the discovered Higgs boson with high accuracies at future collider experiments provide hope to get a hint for new physics beyond the SM. In this thesis, we have discussed indirect tests of extended Higgs sectors by future precision measurements of the Higgs boson. Since it is not enough to calculate the deviations at the tree level taking into account future precision measurements by typically 1 % accuracies, we have calculated one-loop corrections to various couplings of the Higgs boson in several extended Higgs models such as the HSM, four types of THDMs with the softly broken Z_2 symmetry and the HTM. We investigated possibilities that these models can be discriminated by detecting the characteristic pattern of the deviations in the Higgs boson couplings at future collider experiments.

In the study of the THDMs, we have performed renormalization calculations in the modified on shell scheme, in which the gauge dependence in the mixing parameter β is consistently vanished. We have showed a complete set of the analytic formulae of the renormalized couplings in four types of THDMs. We have investigated how the pattern of deviations in the Yukawa couplings can be modified from the prediction at the tree level by including one-loop contributions under constraints from perturbative unitarity and vacuum stability, and current experimental data. We found that scale factors in different types of THDMs do not overlap each other even in the case with maximum radiative corrections if $\sin(\beta-\alpha)$ are different from the SM predictions large enough to be measured at the ILC. We then numerically evaluated how we can extract inner parameters by future precision measurements of these couplings at the HL-LHC and the ILC500. In this analysis, we considered theoretical constraints such as perturbative unitarity and vacuum stability as well as current experimental data. We have found that mixing parameters such as x and $\tan\beta$ can be determined more precisely, if measurement uncertainties at the ILC are employed. Furthermore, there are possibilities to obtain the upper bound for the mass of extra Higgs bosons without their direct discoveries and also to get information of the decoupling property and the magnitude of loop corrections. In order to determine the structure of the Higgs sector by fingerprinting the Higgs boson couplings, the comprehensive study of radiative corrections to the Higgs boson couplings is an important task.

In the study of the HSM, we have calculated renormalized hVV and $h\bar{f}f$ couplings at the one-loop level in the on-shell scheme. We numerically have investigated how they can be significant under the theoretical constraints from perturbative unitarity and vacuum stability and also the condition of avoiding the wrong vacuum. We have found that the maximal value of the one-loop corrections to the hVV and $h\bar{f}f$ couplings is at most -1% or maximally less than -2% which is obtained in the case where we take the maximally allowed value of m_H from the

unitarity bound with taking $\tilde{M}^2 = 0$ and $\alpha = 0$. We have also discussed how the HSM can be distinguished from four types of THDMs and identified by using precision measurements of the Higgs boson couplings at future collider experiments, The HSM can be distinguished from the Type-II, X and Y THDMs except the decoupling limit, because the Yukawa couplings of the HSM are universal in contrast those of the four types of THDMs are not universal couplings. Moreover, if hVV couplings deviate about 2 % from the SM predictions, we can discriminate the HSM and the Type-I THDM in most of parameter regions by using precision measurements of $\Delta\kappa_Z$ and $\Delta\kappa_b$ at the ILC. In addition that, the pattern between $\Delta\kappa_Z$ and $\Delta\kappa_\gamma$ is also useful for discriminating the HSM and the Type-I THDM for $\cos(\beta-\alpha) > 0$. However, when the value of $\tan\beta$ is extremely larger than about $\tan\beta \simeq 10$, $\Delta\kappa_Z$, $\Delta\kappa_b$ and $\Delta\kappa_\gamma$ of the Type-I THDM approach to the predictions in the HSM. In such a situation, it is challenging to discriminate the models by fingerprinting.

In the study of the HTM, we have calculated the decay rate for $h \to \gamma\gamma$ and the renormalized coupling constants of the hVV and the hhh at the one-loop level. Magnitudes of deviations in these quantities from the predictions in the SM have been evaluated in the parameter regions where unitarity and vacuum stability bounds are satisfied and the predicted W boson mass is consistent with the data. Deviations in the one-loop corrected hVV and hhh vertices can be about -1% and $+50\%$, respectively.

Although we have constructed renormalized various Higgs boson couplings at the one-loop level in several extended Higgs models, we should calculate various observables comparable directly with experimental data such as the production cross section and the decay branching ratio and so on. Then, a set of this study can be regarded as the first step of the fingerprinting project. Indeed it cannot say it is enough to calculate just the Higgs boson couplings in order to determine the inner parameters, but it is meaningful to investigate the feature of extra Higgs loop corrections and mixing effects as discussed in this thesis because the production cross section and the decay branching ratio deviate from the SM predictions through the deviations in the couplings.

Appendix A

Decay rate of scalar bosons

A.1 Kinematics

I show some formulae for kinetic systems which is useful to calculate decay rates.

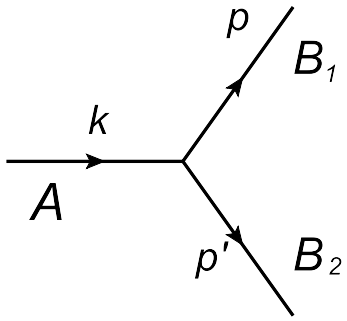

Figure A.1: Kinematic system of 3-point vertex.

We consider 2-body decay of any particle as shown in Fig. A.1, i.e. $A \to B_1 B_2$. Element of four-momentum of A, B_1 and B_2 can be expressed by

$$k = (m_A,\, 0),\;\; p = (E,\, \mathbf{p}),\;\; p' = (E',\, -\mathbf{p}). \tag{A.1}$$

Because the three-momuntum of B_1 is the same as that of B_2, the following relation holds,

$$E'^2 = E^2 - m_1^2 + m_2^2, \tag{A.2}$$

where $m_{1(2)}$ is the mass of B_1. Because of the energy conservation law, there is the following relation,

$$E' = m_A - E, \tag{A.3}$$

By using Eqs. (A.2) and (A.3), E and E' can be expressed as

$$E = \frac{1}{2m_A}\left(m_A^2 + m_1^2 - m_2^2\right), \tag{A.4}$$

$$E' = \frac{1}{2m_A}\left(m_A^2 - m_1^2 + m_2^2\right), \tag{A.5}$$

and

$$EE' = \frac{1}{4m_A^2}\left(m_A^4 - m_1^4 - m_2^4 + 2m_1^2 m_2^2\right). \tag{A.6}$$

The magnitude of the three-momentum $|\mathbf{p}|$ can be expressed using masses as,

$$\begin{aligned} |\mathbf{p}|^2 &= E'^2 - m_2^2 \\ &= \frac{m_A^2}{4}\left(1 + \frac{m_1^4}{m_A^4} + \frac{m_2^4}{m_A^4} - 2\frac{m_1^2}{m_A^2} - 2\frac{m_2^2}{m_A^2} - 2\frac{m_1^2 m_2^2}{m_A^4}\right), \\ |\mathbf{p}| &= \frac{m_A}{2}\left(1 + \frac{m_1^4}{m_A^4} + \frac{m_2^4}{m_A^4} - 2\frac{m_1^2}{m_A^2} - 2\frac{m_2^2}{m_A^2} - 2\frac{m_1^2 m_2^2}{m_A^4}\right)^{1/2}. \end{aligned} \tag{A.7}$$

A.2 Decay rate of the CP-even scalar boson φ

We here list formulae of decay rates for various decay modes of any CP-even Higgs boson φ as,

$$\Gamma[\varphi \to f\bar{f}] = \frac{N_f C_f^2}{4\pi}\frac{m_f^2}{v^2} m_\varphi \lambda^{\frac{3}{2}}\left[\frac{m_f^2}{m_\varphi^2}, \frac{m_f^2}{m_\varphi^2}\right], \tag{A.8}$$

$$\Gamma[\varphi \to WW] = \frac{m_\varphi^3}{64\pi m_W^4}\left(\frac{2m_W^2}{v} C_W\right)^2 \left(1 - 4\frac{m_W^2}{m_\varphi^2} + 12\frac{m_W^4}{m_\varphi^4}\right)\lambda^{\frac{1}{2}}\left[\frac{m_W^2}{m_\varphi^2}, \frac{m_W^2}{m_\varphi^2}\right], \tag{A.9}$$

$$\Gamma[\varphi \to ZZ] = \frac{m_\varphi^3}{32\pi m_W^4}\left(\frac{m_Z^2}{v} C_Z\right)^2 \left(1 - 4\frac{m_Z^2}{m_\varphi^2} + 12\frac{m_Z^4}{m_\varphi^4}\right)\lambda^{\frac{1}{2}}\left[\frac{m_Z^2}{m_\varphi^2}, \frac{m_Z^2}{m_\varphi^2}\right]. \tag{A.10}$$

$$\tag{A.11}$$

where N_f is the color number of f and

$$\lambda[x, y] = 1 - 2x - 2y - 2xy + x^2 + y^2. \tag{A.12}$$

We define coefficient of vertices as,

$$\text{vertices}[\varphi \bar{f} f] \quad : \frac{\sqrt{2} C_f m_f}{v}, \tag{A.13}$$

$$\text{vertices}[\varphi WW] \quad : \frac{2 C_W m_W}{v}, \tag{A.14}$$

$$\text{vertices}[\varphi ZZ] \quad : \frac{C_Z m_Z}{v}. \tag{A.15}$$

Formulae of decay rates for three-body decay modes are given by,

$$\Gamma[h \to WW^* \to Wf\bar{f}'] = \frac{C_W^2 m_W^4 m_\varphi}{32\pi^3 v^4}\left[\frac{(1-8\epsilon^2+20\epsilon^4)\arccos\left(\frac{3\epsilon^2-1}{2\epsilon^3}\right)}{2\sqrt{4\epsilon^2-1}}\right.$$
$$\left. + \frac{1}{12\epsilon^2}\left(-2+15\epsilon^2-60\epsilon^4+47\epsilon^6-6(\epsilon^2-6\epsilon^4+4\epsilon^6)\log\epsilon\right)\right], \quad \text{(A.16)}$$

$$\Gamma[h \to ZZ^* \to Zf\bar{f}'] = \frac{C_Z^2 m_Z^4 m_\varphi}{16\pi^3 v^4}\left[\frac{(1-8\epsilon^2+20\epsilon^4)\arccos\left(\frac{3\epsilon^2-1}{2\epsilon^3}\right)}{2\sqrt{4\epsilon^2-1}}\right.$$
$$\left. + \frac{1}{12\epsilon^2}\left(-2+15\epsilon^2-60\epsilon^4+47\epsilon^6-6(\epsilon^2-6\epsilon^4+4\epsilon^6)\log\epsilon\right)\right] \quad \text{(A.17)}$$
$$(I_f^2 + 2\sin^4\theta_W Q_f^2 - 2I_f \sin^2\theta_W Q_f), \quad \text{(A.18)}$$

where $\epsilon = m_V/m_\varphi$, and I_f and Q_f are the third component of the isospin and the electromagnetic charge of the ferimon f.

The decay rates for the loop induced processes are given by

$$\Gamma(\varphi \to \gamma\gamma) = \frac{\sqrt{2}G_F\alpha_{\rm em}^2 m_\varphi^3}{256\pi^3}\left|C_W I_V + \sum_f Q_f^2 N_c^f C_f I_F - \frac{\lambda_{\varphi H^+H^-}}{v} I_S\right|^2, \quad \text{(A.19)}$$

$$\Gamma(h \to Z\gamma) = \frac{\sqrt{2}G_F\alpha_{\rm em}^2 m_\varphi^3}{128\pi^3}\left(1-\frac{m_Z^2}{m_\varphi^2}\right)^3$$
$$\times \left|C_W J_V + \sum_f C_f Q_f N_c^f v_f J_F - \frac{\lambda_{\varphi H^+H^-}}{v}\frac{g_Z}{2}(c_W^2 - s_W^2) J_S\right|^2, \quad \text{(A.20)}$$

$$\Gamma(h \to gg) = \frac{\sqrt{2}G_F\alpha_s^2 m_\varphi^3}{128\pi^3}\left|\sum_q C_q I_F\right|^2, \quad \text{(A.21)}$$

where $g_Z = g/c_W$ and $v_f = I_f/2 - \sin\theta_W Q_f$. The definition of $\lambda_{\varphi H^+H^-}$ is given by

$$\mathcal{L} = +\lambda_{\varphi H^+H^-}\varphi H^+H^- + \cdots . \quad \text{(A.22)}$$

The loop functions are defined as

$$I_S = \frac{2v^2}{m_\varphi^2}[1 + 2m_{H^\pm}^2 C_0(0,0,m_\varphi^2, m_{H^\pm}, m_{H^\pm}, m_{H^\pm})], \quad \text{(A.23)}$$

$$I_F = -\frac{8m_f^2}{m_\varphi^2}\left[1 + \left(2m_f^2 - \frac{m_\varphi^2}{2}\right)C_0(0,0,m_\varphi^2, m_f, m_f, m_f)\right], \quad \text{(A.24)}$$

$$I_V = \frac{2m_W^2}{m_\varphi^2}\left[6 + \frac{m_\varphi^2}{m_W^2} + (12m_W^2 - 6m_\varphi^2)C_0(0,0,m_\varphi^2, m_W, m_W, m_W)\right], \quad \text{(A.25)}$$

and

$$J_V = \frac{2m_W^2}{s_W c_W (m_\varphi^2 - m_Z^2)} \Big\{ \left[c_W^2 \left(5 + \frac{m_\varphi^2}{2m_W^2} \right) - s_W^2 \left(1 + \frac{m_\varphi^2}{2m_W^2} \right) \right] \left[1 + 2m_W^2 C_0 + \frac{m_Z^2}{m_\varphi^2 - m_W^2} (B_0(m_\varphi^2, m_W, m_W) - B_0(m_Z^2, m_W, m_W)) \right] - 6c_W^2 (m_\varphi^2 - m_Z^2) C_0 + 2s_W^2 (m_\varphi^2 - m_Z^2) C_0 \Big\}, \tag{A.26}$$

$$J_F = -\frac{8m_f^2}{s_W c_W (m_\varphi^2 - m_Z^2)} \Big[1 + \frac{1}{2} (4m_f^2 - m_\varphi^2 + m_Z^2) C_0(0, m_Z^2, m_\varphi^2, m_f, m_f, m_f) + \frac{m_Z^2}{m_\varphi^2 - m_Z^2} (B_0(m_\varphi^2, m_f, m_f) - B_0(m_Z^2, m_f, m_f)) \Big], \tag{A.27}$$

$$J_S = \frac{2v^2}{e(m_\varphi^2 - m_Z^2)} \Big\{ 1 + 2m_{H^\pm}^2 C_0(0, m_Z^2, m_\varphi^2, m_{H^\pm}, m_{H^\pm}, m_{H^\pm}) + \frac{m_Z^2}{m_\varphi^2 - m_Z^2} \left[B_0(m_\varphi^2, m_{H^\pm}, m_{H^\pm}) - B_0(m_Z^2, m_{H^\pm}, m_{H^\pm}) \right] \Big\}, \tag{A.28}$$

where the C_0 function is one of Passarino-Veltoman functions [111] defined in Chap. C.

Appendix B

Feynman rule

In this chapter, we summarize the feynman rule of the Higgs sector in the THDM, the HSM and the HTM.

First, we give feynman rules of trilinear vertices and quartic vertices obtained from the Higgs kinetic term. There are two kinds of trilinear vertices and one kind of quartic vertices; i.e., Scalar-Gauge-Gauge, Scalar-Scalar-Gauge and Scalar-Scalar-Gauge-Gauge type. Their couplings are expressed as

$$\mathcal{L} = g_{\phi V_1 V_2} g^{\mu\nu} \phi V_{1\mu} V_{2\nu} + g_{\phi_1\phi_2 V}(\partial^\mu \phi_1 \phi_2 - \phi_1 \partial^\mu \phi_2) V_\mu + g_{\phi_1\phi_2 V_1 V_2} g^{\mu\nu} \phi_1 \phi_2 V_{1\mu} V_{2\nu} + \cdots . \quad \text{(B.1)}$$

From the Higgs potential, we obtain the scalar trilinear and the scalar quartic couplings. When we use the following notation for these couplings

$$\mathcal{L} = +\lambda_{\phi_i\phi_j\phi_k} \phi_i \phi_j \phi_k + \lambda_{\phi_i\phi_j\phi_k\phi_l} \phi_i \phi_j \phi_k \phi_l + \cdots . \quad \text{(B.2)}$$

B.1 Feynman rule of the THDM

The coefficients of trilinear vertices $g_{\phi V_1 V_2}$ and $g^\mu_{\phi_1\phi_2 V}$, and those of quartic vertices $g_{\phi_1\phi_2 V_1 V_2}$ of the THDMs are listed in Tab. B.1-B.3.

Table B.1: Feynman rules of scalar-scalar-gauge vertex

vertex	coupling	vertex	coupling
$hH^\pm W^\mp_\mu$	$\mp i\frac{m_W}{v} c_{(\beta-\alpha)}$	$HH^\pm W^\mp_\mu$	$\pm i\frac{m_W}{v} s_{(\beta-\alpha)}$
$AH^+ W^-_\mu$	$-\frac{m_W}{v}$	$HG^\pm W^\mp_\mu$	$\mp i\frac{m_W}{v} c_{(\alpha-\beta)}$
$hG^\pm W^\mp_\mu$	$\mp i\frac{m_W}{v} s_{(\beta-\alpha)}$	$G^0 G^+ W^-_\mu$	$-\frac{m_W}{v}$
HAZ	$\frac{m_W}{v c_W} s_{(\beta-\alpha)}$	hAZ	$-\frac{m_W}{v c_W} c_{(\alpha-\beta)}$
$H^+H^-Z_\mu$	$i\frac{m_Z c_{2W}}{v}$	$H^+H^-\gamma_\mu$	$i\frac{2m_W s_W}{v}$
$HG^0 Z_\mu$	$-\frac{m_W}{v c_W} c_{(\alpha-\beta)}$	$hG^0 Z_\mu$	$\frac{m_W}{v c_W} s_{(\alpha-\beta)}$
$G^+G^-Z_\mu$	$i\frac{m_Z c_{2W}}{v}$	$G^+G^-\gamma_\mu$	ie

Table B.2: Feynman rules of scalar-gauge-gauge vertex

vertex	coupling	vertex	coupling
$HW^+_\mu W^-_\nu$	$\frac{2m_W^2 c_{\alpha-\beta}}{v}$	$hW^+_\mu W^-_\nu$	$\frac{2m_W^2 s_{\beta-\alpha}}{v}$
$HZ_\mu Z_\nu$	$\frac{m_Z^2 c_{\alpha-\beta}}{v}$	$hZ_\mu Z_\nu$	$\frac{m_Z^2 s_{\beta-\alpha}}{v}$
$G^+W^-_\mu \gamma_\nu$	$\frac{2m_W^2 s_W}{v}$	$G^+W^-_\mu Z_\nu$	$-\frac{2m_W m_Z s_W^2}{v}$

Table B.3: Feynman rules of scalar-scalar-gauge-gauge vertex

vertex	coupling	vertex	coupling
$\phi\phi W^+_\mu W^-_\nu$	$\frac{m_W^2}{v^2}$	$H^+H^-W^+_\mu W^-_\nu$	$\frac{2m_W^2}{v^2}$
$\phi\phi Z_\mu Z_\nu$	$\frac{m_Z^2}{2v^2}$	$H^+H^-Z_\mu Z_\nu$	$\frac{m_Z^2 c_{2W}^2}{v^2}$
$H^\pm HW^\mp_\mu Z_\nu$	$\frac{2m_W m_Z s_W^2 s_{\beta-\alpha}}{v^2}$	$H^\pm hW^\mp_\mu Z_\nu$	$-\frac{2m_W m_Z s_W^2 c_{\beta-\alpha}}{v^2}$
$H^\pm AW^\mp_\mu Z_\nu$	$\frac{2im_W m_Z s_W^2}{v^2}$	$H^\pm AW^\mp_\mu \gamma_\nu$	$\mp\frac{2im_W^2 s_W}{v^2}$
$H^+H^-\gamma_\mu\gamma_\nu$	$\frac{4m_W^2 s_W^2}{v^2}$	$H^+H^-Z_\mu\gamma_\nu$	$\frac{4m_Z m_W s_W c_{2W}}{v^2}$
$H^\pm HW^\mp_\mu\gamma_\nu$	$-\frac{2m_W^2 s_W s_{\beta-\alpha}}{v^2}$	$H^\pm hW^\mp_\mu\gamma_\nu$	$\frac{2m_W^2 s_W c_{\alpha-\beta}}{v^2}$
$G^+G^-W^+_\mu W^-_\nu$	$\frac{2m_W^2}{v^2}$	$G^0G^0W^+_\mu W^-_\nu$	$\frac{m_W^2}{v^2}$
$G^+G^-Z_\mu Z_\nu$	$\frac{m_Z^2 c_{2W}^2}{v^2}$	$G^0G^0Z\mu Z_\nu$	$\frac{m_Z^2}{2v^2}$
$G^\pm hW^\mp_\mu Z_\nu$	$-\frac{2m_W m_Z s_{\beta-\alpha} s_W^2}{v^2}$	$G^\pm HW^\mp_\mu Z_\nu$	$-\frac{2m_W m_Z c_{\beta-\alpha} s_W^2}{v^2}$
$G^+G^-\gamma_\mu\gamma_\nu$	$\frac{4m_W^2 s_W^2}{v^2}$	$G^+zW^-_\mu Z_\nu$	$\pm\frac{2im_W m_Z s_W^2}{v^2}$
$G^\pm HW^\mp_\mu\gamma_\nu$	$\frac{2m_W^2 s_W c_{\beta-\alpha}}{v^2}$	$G^+G^-Z_\mu\gamma_\nu$	$\frac{4m_W m_Z s_W c_{2W})}{v^2}$
$G^\pm G^0W^\mp_\mu\gamma_\nu$	$-\frac{2im_W^2 s_W}{v^2}$	$G^\pm hW^\mp_\mu\gamma_\nu$	$\frac{2m_W^2 s_W s_{\beta-\alpha}}{v^2}$

These coefficients of scalar self vertices are given by

$$\lambda_{H^+H^-h} = \frac{1}{v}\left[(2M^2 - 2m_{H^\pm}^2 - m_h^2)s_{\beta-\alpha} + 2(M^2 - m_h^2)\cot 2\beta c_{\beta-\alpha}\right], \tag{B.3}$$

$$\lambda_{AAh} = \frac{1}{2v}\left[(2M^2 - 2m_A^2 - m_h^2)s_{\beta-\alpha} + 2(M^2 - m_h^2)\cot 2\beta c_{\beta-\alpha}\right], \tag{B.4}$$

$$\lambda_{HHh} = \frac{s_{\beta-\alpha}}{2v}\Big[(2M^2 - 2m_H^2 - m_h^2)s_{\beta-\alpha}^2 + 2(3M^2 - 2m_H^2 - m_h^2)\cot 2\beta s_{\beta-\alpha}c_{\beta-\alpha} - (4M^2 - 2m_H^2 - m_h^2)c_{\beta-\alpha}^2\Big], \tag{B.5}$$

$$\lambda_{hhh} = -\frac{m_h^2}{2v}s_{\beta-\alpha} + \frac{M^2-m_h^2}{v}s_{\beta-\alpha}c_{\beta-\alpha}^2 + \frac{M^2-m_h^2}{2v}c_{\beta-\alpha}^3(\cot\beta - \tan\beta), \tag{B.6}$$

$$\lambda_{GGh} = -\frac{m_h^2}{2v}s_{\beta-\alpha}, \tag{B.7}$$

$$\lambda_{H^\pm G^\mp h} = -\frac{1}{v}(m_h^2 - m_{H^\pm}^2)c_{\beta-\alpha}, \tag{B.8}$$

$$\lambda_{AGh} = -\frac{1}{v}(m_h^2 - m_A^2)c_{\beta-\alpha}, \tag{B.9}$$

$$\lambda_{H^+H^-H} = -\frac{1}{v}\Big[2(M^2-m_H^2)\cot 2\beta s_{\beta-\alpha} + (2m_{H^\pm}^2 + m_H^2 - 2M^2)c_{\beta-\alpha}\Big], \tag{B.10}$$

$$\lambda_{AAH} = -\frac{1}{2v}\Big[2(M^2-m_H^2)\cot 2\beta s_{\beta-\alpha} + (2m_A^2 + m_H^2 - 2M^2)c_{\beta-\alpha}\Big], \tag{B.11}$$

$$\lambda_{HHH} = -\frac{1}{2v}\Big[2(M^2-m_H^2)\cot 2\beta s_{\beta-\alpha}^3 - 2(M^2-m_H^2)c_{\beta-\alpha}s_{\beta-\alpha}^2 + m_H^2 c_{\beta-\alpha}\Big], \tag{B.12}$$

$$\lambda_{GGH} = -\frac{m_H^2}{2v}c_{\beta-\alpha}, \tag{B.13}$$

$$\lambda_{H^\pm G^\mp H} = \frac{1}{v}(m_H^2 - m_{H^\pm}^2)s_{\beta-\alpha}, \tag{B.14}$$

$$\lambda_{AGH} = \frac{1}{v}(m_H^2 - m_A^2)s_{\beta-\alpha}, \tag{B.15}$$

$$\lambda_{Hhh} = -\frac{c_{\beta-\alpha}}{2v\sin 2\beta}\left[(2m_h^2 + m_H^2 - 3M^2)\sin 2\alpha + M^2\sin 2\beta\right], \tag{B.16}$$

$$\lambda_{H^\pm G^\mp A} = \pm\frac{i}{v}(m_A^2 - m_{H^\pm}^2). \tag{B.17}$$

The four point couplings are given by

$$\lambda_{H^+H^-AG} = -\frac{1}{v}(\lambda_{H^+H^-H}s_{\beta-\alpha} - \lambda_{H^+H^-h}c_{\beta-\alpha}), \tag{B.18}$$

$$\lambda_{G^+G^-AG} = -\frac{1}{v}(\lambda_{G^+G^-H}s_{\beta-\alpha} - \lambda_{G^+G^-h}c_{\beta-\alpha}), \tag{B.19}$$

$$\lambda_{AAAG} = -\frac{1}{v}(\lambda_{AAH}s_{\beta-\alpha} - \lambda_{AAh}c_{\beta-\alpha}), \tag{B.20}$$

$$\lambda_{AGGG} = -\frac{1}{v}(\lambda_{GGH}s_{\beta-\alpha} - \lambda_{GGh}c_{\beta-\alpha}). \tag{B.21}$$

B.2 Feynman rule of the HSM

The coefficients of trilinear vertices $g_{\phi V_1 V_2}$ and $g^\mu_{\phi_1\phi_2 V}$, and those of quartic vertices $g_{\phi_1\phi_2 V_1 V_2}$ of the HSM are listed in Tab. B.4 and Tab. B.5.

Table B.4: The Scalar-Vector-Vector vertices and the Scalar-Scalar-Vector vertices and those coefficients.

$\phi V_{1\mu} V_{2\nu}$ vertices	coefficient	$\phi_1 \phi_2 V_\mu$ vertices	coefficient
$hW_\mu^+ W_\nu^-$	$\frac{2m_W^2}{v} c_\alpha$	$hG^\pm W_\mu^\mp$	$\mp i \frac{m_W}{v} c_\alpha$
$HW_\mu^+ W_\nu^-$	$\frac{2m_W^2}{v} s_\alpha$	$HG^\pm W_\mu^\mp$	$\mp i \frac{m_W}{v} s_\alpha$
$G^\pm Z_\mu W_\nu^\mp$	$-\frac{2m_W m_Z}{v} s_W^2$	$G^0 G^\pm W_\mu^\mp$	$-\frac{m_W}{v}$
$G^\pm \gamma_\mu W_\nu^\mp$	$e m_W$	$G^+ G^- Z_\mu$	$i \frac{m_Z}{v} c_{2W}$
$hZ_\mu Z_\nu$	$\frac{m_Z^2}{v} c_\alpha$	$hG^0 Z_\mu$	$-\frac{m_Z}{v} c_\alpha$
$HZ_\mu Z_\nu$	$\frac{m_Z^2}{v} s_\alpha$	$HG^0 Z_\mu$	$-\frac{m_Z}{v} s_\alpha$
		$G^+ G^- \gamma_\mu$	ie

Table B.5: The Scalar-Scalar-Vector-Vector vertices and those coefficients.

$\phi_1 \phi_2 V_{1\mu} V_{2\nu}$ vertices	coefficient	$\phi_1 \phi_2 V_{1\mu} V_{2\nu}$ vertices	coefficient
$hhW_\mu^+ W_\nu^-$	$\frac{m_W^2}{v^2} c_\alpha^2$	$G^\pm G^0 W_\mu^\mp Z_\nu$	$\pm i \frac{2m_W m_Z}{v^2} s_W^2$
$HHW_\mu^+ W_\nu^-$	$\frac{m_W^2}{v^2} s_\alpha^2$	$G^\pm h W_\mu^\mp Z_\nu$	$-\frac{2m_W m_Z}{v^2} s_W^2 c_\alpha$
$G^0 G^0 W_\mu^+ W_\nu^-$	$\frac{m_W^2}{v^2}$	$G^\pm H W_\mu^\mp Z_\nu$	$-\frac{2m_W m_Z}{v^2} s_W^2 s_\alpha$
$G^+ G^+ W_\mu^+ W_\nu^-$	$\frac{2m_W^2}{v^2}$	$G^\pm h W_\mu^\mp \gamma_\nu$	$\frac{e m_W}{v} c_\alpha$
$hhZ_\mu Z_\nu$	$\frac{m_Z^2}{2v^2} c_\alpha^2$	$G^\pm H W_\mu^\mp \gamma_\nu$	$\frac{e m_W}{v} s_\alpha$
$HHZ_\mu Z_\nu$	$\frac{m_Z^2}{2v^2} s_\alpha^2$	$G^\pm G^0 W_\mu^\mp \gamma_\nu$	$\mp i \frac{e m_W}{v}$
$G^0 G^0 Z_\mu Z_\nu$	$\frac{m_Z^2}{2v^2}$	$G^+ G^- Z_\mu \gamma_\nu$	$2e \frac{m_Z}{v} c_{2W}$
$G^+ G^- Z_\mu Z_\nu$	$\frac{m_Z^2}{v^2} c_{2W}^2$	$G^+ G^- \gamma_\mu \gamma_\mu$	e^2
$hHW_\mu^+ W_\mu^-$	$\frac{2m_W^2}{v^2} s_\alpha c_\alpha$	$hHZ_\mu Z_\mu$	$\frac{m_Z^2}{v^2} s_\alpha c_\alpha$

Coefficients of the scalar self vertices $\lambda_{\phi_1\phi_2\phi_3}$ and $\lambda_{\phi_1\phi_2\phi_3\phi_4}$ are obtained as

$$\lambda_{hhh} = -\frac{c_\alpha^3}{2v}m_h^2 - s_\alpha^2(c_\alpha\lambda_{\Phi S}v - 4s_\alpha\lambda_S v_S - s_\alpha\mu_S), \tag{B.22}$$

$$\lambda_{hHH} = -(m_h^2 + 2m_H^2)\frac{c_\alpha s_\alpha^2}{2v} - \frac{\lambda_{\Phi S}v}{4}(c_\alpha + 3c_{3\alpha}) + 12s_\alpha c_\alpha^2\lambda_S v_S + 3s_\alpha c_\alpha^2\mu_S, \tag{B.23}$$

$$\lambda_{hhH} = -(2m_h^2 + m_H^2)\frac{s_\alpha c_\alpha^2}{2v} + \frac{s_\alpha\lambda_{\Phi S}v}{2}(1 + 3c_{2\alpha}) - 3s_\alpha^2 c_\alpha\mu_S - 6s_\alpha s_{2\alpha}\lambda_S v_S, \tag{B.24}$$

$$\lambda_{HHH} = -\frac{s_\alpha^3}{2v}m_H^2 - 4c_\alpha^3\lambda_S v_S - c_\alpha^3\mu_S - s_\alpha c_\alpha^2\lambda_{\Phi S}v, \tag{B.25}$$

$$\lambda_{hG^0G^0} = -\frac{m_h^2 c_\alpha}{2v}, \tag{B.26}$$

$$\lambda_{hG^+G^-} = -\frac{m_h^2 c_\alpha}{v}, \tag{B.27}$$

$$\lambda_{HG^0G^0} = -\frac{m_H^2 s_\alpha}{2v}, \tag{B.28}$$

$$\lambda_{HG^+G^-} = -\frac{m_H^2 s_\alpha}{v}, \tag{B.29}$$

$$\lambda_{hhhh} = -(c_\alpha^2 m_h^2 + s_\alpha^2 m_H^2)\frac{c_\alpha^4}{8v^2} - s_\alpha^4\lambda_S - \frac{s_{2\alpha}^2}{8}\lambda_{\Phi S}, \tag{B.30}$$

$$\lambda_{hhhH} = -\frac{c_\alpha^5 s_\alpha}{2v^2}m_h^2 - \frac{s_{2\alpha}^3}{16v^2}m_H^2 + 4c_\alpha s_\alpha^3\lambda_S + \frac{s_{4\alpha}}{4}\lambda_{\Phi S}, \tag{B.31}$$

$$\lambda_{hhHH} = -(c_\alpha^2 m_h^2 + s_\alpha^2 m_H^2)\frac{3s_\alpha^2 c_\alpha^2}{4v^2} - \frac{\lambda_{\Phi S}}{8}(1 + 3c_{4\alpha}), \tag{B.32}$$

$$\lambda_{hHHH} = 4\lambda_S c_\alpha^3 s_\alpha - \frac{m_H^2}{2v^2}c_\alpha s_\alpha^5 - \frac{m_h^2}{16v^2}s_{2\alpha}^3 - \frac{\lambda_{\Phi S}}{4}s_{4\alpha}, \tag{B.33}$$

$$\lambda_{hhG^+G^-} = -\frac{c_\alpha^4}{2v^2}m_h^2 - \frac{s_{2\alpha}^2}{8v^2}m_H^2 - s_\alpha^2\lambda_{\Phi S}, \tag{B.34}$$

$$\lambda_{hHG^+G^-} = -(c_\alpha^2 m_h^2 + s_\alpha^2 m_H^2)\frac{s_\alpha c_\alpha}{v^2} + 2s_\alpha c_\alpha\lambda_{\Phi S}, \tag{B.35}$$

$$\lambda_{HHG^+G^-} = -(4s_\alpha^4 m_H^2 + m_h^2 s_{2\alpha}^2)\frac{1}{8v^2} - c_\alpha^2\lambda_{\Phi S}, \tag{B.36}$$

$$\lambda_{hhG^0G^0} = -\frac{m_h^2}{2v^2}c_\alpha^4 - \frac{m_H^2}{16v^2}s_{2\alpha}^2 - \frac{\lambda_{\Phi S}}{2}s_\alpha^2, \tag{B.37}$$

$$\lambda_{hHG^0G^0} = -\frac{m_h^2}{2v^2}c_\alpha^3 s_\alpha - \frac{m_H^2}{2v^2}c_\alpha s_\alpha^3 + \lambda_{\Phi S}c_\alpha s_\alpha. \tag{B.38}$$

B.3 Feynman rule in the HTM

The coefficients of trilinear vertices $g_{\phi V_1 V_2}$ and $g^\mu_{\phi_1\phi_2 V}$, and those of quartic vertices $g_{\phi_1\phi_2 V_1 V_2}$ of the HTM are listed in Tab. B.6 and Tab. **??**.

Coefficients of the scalar three point vertices can be written in terms of the physical param-

Table B.6: The Higgs-gauge-gauge type vertices and those corresponding coefficients in the HTM.

Vertices	Coefficient	Vertices	Coefficient
$hW^+_\mu W^-_\nu$	$gm_W(c_\beta c_\alpha + \sqrt{2}s_\beta s_\alpha)g_{\mu\nu}$	$hZ_\mu Z_\nu$	$\frac{g_Z m_Z}{2}(c_{\beta'}c_\alpha + 2s_{\beta'}s_\alpha)g_{\mu\nu}$
$HW^+_\mu W^-_\nu$	$gm_W(-c_\beta s_\alpha + \sqrt{2}s_\beta c_\alpha)g_{\mu\nu}$	$HZ_\mu Z_\nu$	$\frac{g_Z m_Z}{2}(-c_{\beta'}s_\alpha + 2s_{\beta'}c_\alpha)g_{\mu\nu}$
$H^\pm W^\mp_\mu Z_\nu$	$-g_Z m_W s_\beta c_\beta g_{\mu\nu}$	$G^\pm W^\mp_\mu Z_\nu$	$-g_Z m_W\left(s^2_W + s^2_\beta\right)g_{\mu\nu}$
$H^{\pm\pm}W^\mp_\mu W^\mp_\nu$	$gm_W s_\beta g_{\mu\nu}$	$G^\pm W^\mp_\mu A_\nu$	$em_W g_{\mu\nu}$

Table B.7: The Higgs-ghost-anti ghost type vertices and those corresponding coefficients in the HTM.

Vertices	Coefficient	Vertices	Coefficient
$h\bar{c}^\pm c^\mp$	$-\frac{gm_W}{2}(c_\beta c_\alpha + \sqrt{2}s_\beta s_\alpha)$	$h\bar{c}_Z c_Z$	$-\frac{g_Z m_Z}{2}(c_{\beta'}c_\alpha + 2s_{\beta'}s_\alpha)$
$H\bar{c}^\pm c^\mp$	$-\frac{gm_W}{2}(-c_\beta s_\alpha + \sqrt{2}s_\beta c_\alpha)$	$H\bar{c}_Z c_Z$	$-\frac{g_Z m_Z}{2}(-c_{\beta'}s_\alpha + 2s_{\beta'}c_\alpha)$
$G^\pm\bar{c}_Z c^\mp$	$i\frac{g_Z m_W}{2}(1+s^2_\beta)$	$G^\pm\bar{c}^\mp c_Z$	$i\frac{g_Z m_W}{2}(-c_{2W}c^2_\beta + 2s^2_W s^2_\beta)$
$H^\pm\bar{c}_Z c^\mp$	$i\frac{g_Z m_W}{2}c_\beta s_\beta$	$H^\pm\bar{c}^\mp c_Z$	$i\frac{g_Z m_W}{2}c_\beta s_\beta(c_{2W} + 2s^2_W)$

eters as follows;

$$\lambda_{H^{++}H^{--}H} = \frac{2v_\phi}{v^2+2v^2_\Delta}\left[2m^2_{H^+}\left(1+\frac{2v^2_\Delta}{v^2}\right) - m^2_A\right]s_\alpha - \frac{1}{v_\Delta}\left[2m^2_{H^{++}} - 4m^2_{H^+}\frac{v^2_\phi}{v^2} + m^2_A\left(1-\frac{4v^2_\Delta}{v^2+2v^2_\Delta}\right) + m^2_H\right]c_\alpha, \tag{B.39}$$

$$\lambda_{H^{++}H^{--}h} = -\frac{2v_\phi}{v^2+2v^2_\Delta}\left[2m^2_{H^+}\left(1+\frac{2v^2_\Delta}{v^2}\right) - m^2_A\right]c_\alpha - \frac{1}{v_\Delta}\left[2m^2_{H^{++}} - 4m^2_{H^+}\frac{v^2_\phi}{v^2} + m^2_A\left(1-\frac{4v^2_\Delta}{v^2+2v^2_\Delta}\right) + m^2_h\right]s_\alpha, \tag{B.40}$$

$$\lambda_{H^+H^-H} = \frac{1}{v_\phi}\left[2m^2_{H^+}\frac{v^2_\phi}{v^2} + m^2_H\frac{2v^2_\Delta}{v^2}\right]s_\alpha - \frac{1}{v_\Delta}\left[4m^2_{H^+}\frac{v^2_\Delta}{v^2} - m^2_A\frac{v^2}{v^2+2v^2_\Delta} + m^2_H\frac{v^2_\phi}{v^2}\right]c_\alpha, \tag{B.41}$$

$$\lambda_{H^+H^-h} = -\frac{1}{v_\phi}\left(2m^2_{H^+}\frac{v^2_\phi}{v^2} + m^2_h\frac{2v^2_\Delta}{v^2}\right)c_\alpha - \frac{1}{v_\Delta}\left(4m^2_{H^+}\frac{v^2_\Delta}{v^2} - m^2_A\frac{v^2}{v^2+2v^2_\Delta} + m^2_h\frac{v^2_\phi}{v^2}\right)s_\alpha, \tag{B.42}$$

Table B.8: The Higgs-Higgs-gauge type vertices and those corresponding coefficients in the HTM.

Vertices	Coefficient	Vertices	Coefficient
$H^{\pm\pm}H^{\mp}W^{\mp}_{\mu}$	$\pm g c_{\beta}$	$H^{++}H^{--}A_{\mu}$	$2e$
$H^{\pm\pm}G^{\mp}W^{\mp}_{\mu}$	$\pm g s_{\beta}$	$H^{+}H^{-}A_{\mu}$	e
$H^{\pm}AW^{\mp}_{\mu}$	$-i\frac{g}{2}(s_{\beta'}s_{\beta}+\sqrt{2}c_{\beta'}c_{\beta})$	$G^{+}G^{-}A_{\mu}$	e
$H^{\pm}HW^{\mp}_{\mu}$	$\pm\frac{g}{2}(s_{\alpha}s_{\beta}+\sqrt{2}c_{\alpha}c_{\beta})$	$H^{++}H^{--}Z_{\mu}$	$g_Z(\hat{c}^2_W-\hat{s}^2_W)$
$H^{\pm}hW^{\mp}_{\mu}$	$\pm\frac{g}{2}(-c_{\alpha}s_{\beta}+\sqrt{2}s_{\alpha}c_{\beta})$	$H^{+}H^{-}Z_{\mu}$	$\frac{g_Z}{2}(\hat{c}^2_W-\hat{s}^2_W-c^2_{\beta})$
$H^{\pm}G^{0}W^{\mp}_{\mu}$	$-i\frac{g}{2}(-c_{\beta'}s_{\beta}+\sqrt{2}s_{\beta'}c_{\beta})$	$G^{+}G^{-}Z_{\mu}$	$\frac{g_Z}{2}(\hat{c}^2_W-\hat{s}^2_W-s^2_{\beta})$
$G^{\pm}AW^{\mp}_{\mu}$	$-i\frac{g}{2}(-s_{\beta'}c_{\beta}+\sqrt{2}c_{\beta'}s_{\beta})$	$H^{\pm}G^{\mp}Z_{\mu}$	$\mp\frac{g_Z}{4}s_{2\beta}$
$G^{\pm}HW^{\mp}_{\mu}$	$\pm\frac{g}{2}(-s_{\alpha}c_{\beta}+\sqrt{2}c_{\alpha}s_{\beta})$	AHZ_{μ}	$-i\frac{g_Z}{2}(2c_{\alpha}c_{\beta'}+s_{\alpha}s_{\beta'})$
$G^{\pm}hW^{\mp}_{\mu}$	$\pm\frac{g}{2}(c_{\alpha}c_{\beta}+\sqrt{2}s_{\alpha}s_{\beta})$	AhZ_{μ}	$-i\frac{g_Z}{2}(-c_{\alpha}s_{\beta'}+2s_{\alpha}c_{\beta'})$
$G^{\pm}G^{0}W^{\mp}_{\mu}$	$-i\frac{g}{2}(c_{\beta'}c_{\beta}+\sqrt{2}s_{\beta'}s_{\beta})$	$G^{0}HZ_{\mu}$	$-i\frac{g_Z}{2}(-c_{\beta'}s_{\alpha}+2c_{\alpha}s_{\beta'})$
		$G^{0}hZ_{\mu}$	$-i\frac{g_Z}{2}(c_{\alpha}c_{\beta'}+2s_{\alpha}s_{\beta'})$

$$\lambda_{H^+G^-A} = i\frac{\sqrt{2}(m^2_A - m^2_{H^+})}{\sqrt{v^2+2v^2_{\Delta}}}, \tag{B.43}$$

$$\lambda_{H^+G^-G^0} = -i\sqrt{\frac{2}{v^2+2v^2_{\Delta}}}\frac{v_{\Delta}v_{\phi}}{v^2}m^2_{H^+}, \tag{B.44}$$

$$\lambda_{H^+G^-H} = \frac{\sqrt{2}(m^2_{H^+} - m^2_H)}{v^2}(v_{\phi}c_{\alpha}+v_{\Delta}s_{\alpha}), \tag{B.45}$$

$$\lambda_{H^+G^-h} = -\frac{\sqrt{2}(m^2_{H^+} - m^2_h)}{v^2}(v_{\Delta}c_{\alpha}-v_{\phi}s_{\alpha}), \tag{B.46}$$

$$\lambda_{G^+G^-H} = \frac{m^2_H}{v^2}(-2v_{\Delta}c_{\alpha}+v_{\phi}s_{\alpha}), \tag{B.47}$$

$$\lambda_{G^+G^-h} = -\frac{m^2_h}{v^2}(v_{\phi}c_{\alpha}+2v_{\Delta}s_{\alpha}), \tag{B.48}$$

$$\begin{aligned}\lambda_{AAH} = {} & \frac{v^2}{v_{\phi}}\frac{1}{v^2+2v^2_{\Delta}}\left[m^2_A\left(1-\frac{2v^2_{\Delta}}{v^2}\right)+m^2_H\frac{2v^2_{\Delta}}{v^2}\right]s_{\alpha} \\ & +\frac{1}{2v_{\Delta}}\left[m^2_A\left(1-\frac{8v^2_{\Delta}}{v^2+2v^2_{\Delta}}\right)-m^2_H\left(1-\frac{4v^2_{\Delta}}{v^2+2v^2_{\Delta}}\right)\right]c_{\alpha},\end{aligned} \tag{B.49}$$

$$\begin{aligned}\lambda_{AAh} = {} & -\frac{v^2}{v_{\phi}}\frac{1}{v^2+2v^2_{\Delta}}\left[m^2_A\frac{v^2_{\phi}}{v^2}+m^2_h\frac{2v^2_{\Delta}}{v^2}\right]c_{\alpha} \\ & +\frac{1}{2v_{\Delta}}\left[m^2_A\left(1-\frac{8v^2_{\Delta}}{v^2+2v^2_{\Delta}}\right)-m^2_h\left(1-\frac{4v^2_{\Delta}}{v^2+2v^2_{\Delta}}\right)\right]s_{\alpha},\end{aligned} \tag{B.50}$$

Table B.9: The Higgs-Higgs-gauge-gauge type vertices and those corresponding coefficients in the HTM.

Vertices	Coefficient	Vertices	Coefficient
$H^{++}H^{--}W^+_\mu W^-_\nu$	g^2	$H^{++}H^{--}Z_\mu Z_\nu$	$g_Z^2(c_W^2-s_W^2)^2$
$H^+H^-W^+_\mu W^-_\nu$	$\frac{g^2}{4}(5+3c_{2\beta})$	$H^+H^-Z_\mu Z_\nu$	$\frac{g_Z^2}{8}\left(2+c_{4W}-4c_{2W}c_\beta^2+c_{2\beta}\right)$
$G^+G^-W^+_\mu W^-_\nu$	$\frac{g^2}{4}(5-3c_{2\beta})$	$G^+G^-Z_\mu Z_\nu$	$\frac{g_Z^2}{8}\left(2+c_{4W}-4c_{2W}s_\beta^2-c_{2\beta}\right)$
$HHW^+_\mu W^-_\nu$	$\frac{g^2}{8}(3+c_{2\alpha})$	$H^\pm G^\mp Z_\mu Z_\nu$	$\frac{g_Z^2}{8}s_{2\beta}(1-2c_{2W})$
$hhW^+_\mu W^-_\nu$	$\frac{g^2}{8}(3-c_{2\alpha})$	$AAZ_\mu Z_\nu$	$\frac{g_Z^2}{16}(5+3c_{2\beta'})$
$AAW^+_\mu W^-_\nu$	$\frac{g^2}{8}(3+c_{2\beta'})$	$G^0G^0Z_\mu Z_\nu$	$\frac{g_Z^2}{16}(5-3c_{2\beta'})$
$G^0G^0W^+_\mu W^-_\nu$	$\frac{g^2}{8}(3-c_{2\beta'})$	$AG^0Z_\mu Z_\nu$	$\frac{3g_Z^2}{8}s_{2\beta'}$
$H^\pm G^\mp W^+_\mu W^-_\nu$	$\frac{3}{4}g^2 s_{2\beta}$	$HHZ_\mu Z_\nu$	$\frac{g_Z^2}{16}(5+3c_{2\alpha})$
$AG^0W^+_\mu W^-_\nu$	$\frac{1}{4}g^2 s_{2\beta'}$	$hhZ_\mu Z_\nu$	$\frac{g_Z^2}{16}(5-3c_{2\alpha})$
$HhW^+_\mu W^-_\nu$	$\frac{1}{4}g^2 s_{2\alpha}$	$HhZ_\mu Z_\nu$	$\frac{3g_Z^2}{8}s_{2\alpha}$
$H^{++}H^{--}A_\mu Z_\nu$	$4eg_Z(\hat{c}_W^2-\hat{s}_W^2)$	$H^{++}H^{--}A_\mu A_\nu$	$4e^2$
$H^+H^-A_\mu Z_\nu$	$eg_Z(\hat{c}_W^2-\hat{s}_W^2-c_\beta^2)$	$H^+H^-A_\mu A_\nu$	e^2
$G^+G^-A_\mu Z_\nu$	$eg_Z(\hat{c}_W^2-\hat{s}_W^2-s_\beta^2)$	$G^+G^-A_\mu A_\nu$	e^2
$G^\pm hW^\mp_\mu Z_\nu$	$\frac{gg_Z}{2}[-c_\alpha c_\beta s_W^2+\sqrt{2}(c_W^2-2)s_\alpha s_\beta]$	$G^\pm hW^\mp_\mu A_\nu$	$\frac{ge}{2}(c_\alpha c_\beta+\sqrt{2}s_\alpha s_\beta)$
$H^\pm hW^\mp_\mu Z_\nu$	$\frac{gg_Z}{2}[c_\alpha s_\beta s_W^2+\sqrt{2}(c_W^2-2)s_\alpha c_\beta]$	$H^\pm hW^\mp_\mu A_\nu$	$\frac{ge}{2}(-c_\alpha s_\beta+\sqrt{2}s_\alpha c_\beta)$
$H^{\pm\pm}hW^\mp_\mu W^\mp_\nu$	$\frac{g^2}{\sqrt{2}}s_\alpha$		

$$\lambda_{AG^0H}=\frac{2(m_A^2-m_H^2)}{v^2+2v_\Delta^2}(v_\phi c_\alpha+v_\Delta s_\alpha), \tag{B.51}$$

$$\lambda_{AG^0h}=-\frac{2(m_A^2-m_h^2)}{v^2+2v_\Delta^2}(v_\Delta c_\alpha-v_\phi s_\alpha), \tag{B.52}$$

$$\lambda_{G^0G^0H}=\frac{m_H^2}{2(v^2+2v_\Delta^2)}(-4v_\Delta c_\alpha+v_\phi s_\alpha), \tag{B.53}$$

$$\lambda_{G^0G^0h}=-\frac{m_h^2}{2(v^2+2v_\Delta^2)}(v_\phi c_\alpha+4v_\Delta s_\alpha), \tag{B.54}$$

$$\lambda_{HHH}=-\frac{1}{8v_\Delta}\left(3c_\alpha+c_{3\alpha}-\frac{4v_\Delta}{v_\phi}s_\alpha^3\right)m_H^2+\frac{v_\phi c_\alpha^2}{2v_\Delta(v^2+2v_\Delta^2)}(v_\phi c_\alpha+2v_\Delta s_\alpha)m_A^2, \tag{B.55}$$

$$\lambda_{HHh}=-\frac{1}{2v_\Delta}\left(c_\alpha+\frac{v_\Delta}{v_\phi}s_\alpha\right)\left(m_H^2+\frac{m_h^2}{2}\right)s_{2\alpha}+\frac{v_\phi c_\alpha}{4(v^2+2v_\Delta^2)}\left(2-6c_{2\alpha}+\frac{3v_\phi}{v_\Delta}s_{2\alpha}\right)m_A^2, \tag{B.56}$$

$$\lambda_{Hhh} = -\frac{s_{2\alpha}}{2v_\Delta}\left(s_\alpha - \frac{v_\Delta}{v_\phi}c_\alpha\right)\left(m_h^2 + \frac{m_H^2}{2}\right) - \frac{v_\phi s_\alpha}{4(v^2+2v_\Delta^2)}\left(2 + 6c_{2\alpha} - \frac{3v_\phi}{v_\Delta}s_{2\alpha}\right)m_A^2, \quad \text{(B.57)}$$

$$\lambda_{hhh} = -\left(\frac{c_\alpha^3}{v_\phi} + \frac{s_\alpha^3}{v_\Delta}\right)\frac{m_h^2}{2} - \frac{s_\alpha^2}{v^2+2v_\Delta^2}\left(v_\phi c_\alpha - \frac{v_\phi^2}{2v_\Delta}s_\alpha\right)m_A^2. \quad \text{(B.58)}$$

Coefficients for the scalar four-point vertices can be written in terms of the physical parameters as follows;

$$\lambda_{H^{++}H^{--}AA} = \frac{1}{v_\Delta^2(v^2+2v_\Delta^2)}\Bigg[- v_\phi^2 m_{H^{++}}^2 + 2(v^2-4v_\Delta^2)m_{H^+}^2 + \frac{-v^4+4v^2v_\Delta^2+4v_\Delta^4}{2(v^2+2v_\Delta^2)}m_A^2 + \frac{1}{2}(2v_\Delta^2-v^2)(c_\alpha^2 m_H^2 + s_\alpha^2 m_h^2) + \frac{v_\Delta^3}{v_\phi}s_{2\alpha}(m_H^2-m_h^2)\Bigg], \quad \text{(B.59)}$$

$$\lambda_{H^{++}H^{--}AG^0} = \frac{1}{v_\Delta(v^2+2v_\Delta^2)}\Bigg[- 4v_\phi m_{H^{++}}^2 + \frac{8v_\phi}{v^2}(v^2-v_\Delta^2)m_{H^+}^2 - \frac{2v^2v_\phi}{v^2+2v_\Delta^2}m_A^2 - 2c_\alpha(v_\phi c_\alpha + v_\Delta s_\alpha)m_H^2 + (-2v_\phi s_\alpha^2 + v_\Delta s_{2\alpha})m_h^2\Bigg], \quad \text{(B.60)}$$

$$\lambda_{H^{++}H^{--}HH} = -\frac{1}{v_\Delta^2}\Bigg\{c_\alpha^2 m_{H^{++}}^2 + \left[\frac{v_\Delta^2}{v^2}(3+c_{2\alpha}) - (1+c_{2\alpha})\right]m_{H^+}^2 + \frac{1}{4}\frac{v^2(1+c_{2\alpha})-4v_\Delta^2}{v^2+2v_\Delta^2}m_A^2 + \frac{c_\alpha}{2}\left(c_\alpha^3 - \frac{v_\Delta}{v_\phi}s_\alpha^3\right)m_H^2 + \frac{c_\alpha s_\alpha^2}{2}\left(c_\alpha + \frac{v_\Delta}{v_\phi}s_\alpha\right)m_h^2\Bigg\}, \quad \text{(B.61)}$$

$$\lambda_{H^{++}H^{--}Hh} = -\frac{s_{2\alpha}}{v_\Delta^2}\Bigg[m_{H^{++}}^2 + 2\left(\frac{v_\Delta^2}{v^2}-1\right)m_{H^+}^2 + \frac{v^2}{2(v^2+2v_\Delta^2)}m_A^2 + \frac{1}{2}\left(c_\alpha^2 + \frac{v_\Delta}{2v_\phi}s_{2\alpha}\right)m_H^2 - \frac{1}{2}\left(\frac{v_\Delta}{2v_\phi}s_{2\alpha} - s_\alpha^2\right)m_h^2\Bigg], \quad \text{(B.62)}$$

$$\lambda_{H^{++}H^{--}hh} = \frac{1}{v_\Delta^2}\Bigg\{ - s_\alpha^2 m_{H^{++}}^2 + 2\left[\left(1-\frac{v_\Delta^2}{v^2}\right)s_\alpha^2 - \frac{v_\Delta^2}{v^2}\right]m_{H^+}^2 - \frac{v^2}{2(v^2+2v_\Delta^2)}\left(s_\alpha^2 - \frac{2v_\Delta^2}{v^2}\right)m_A^2 + \frac{c_\alpha^2 s_\alpha}{2}\left(\frac{v_\Delta}{v_\phi}c_\alpha - s_\alpha\right)m_H^2 - \frac{s_\alpha}{2}\left(s_\alpha^3 + \frac{v_\Delta}{v_\phi}c_\alpha^3\right)m_h^2\Bigg\}, \quad \text{(B.63)}$$

$$\lambda_{H^+H^-AA} = \frac{v^6-6v^4v_\Delta^2+16v_\Delta^6}{2v^2v_\Delta^2(v^2+2v_\Delta^2)^2}m_A^2 - \frac{v^6-6v^4v_\Delta^2+12v^2v_\Delta^4}{4v^2v_\Delta^2(v^4-4v_\Delta^4)}(m_H^2+m_h^2) - \frac{1}{4v^2v_\Delta^2(v^4-4v_\Delta^4)}[(v^6-6v^4v_\Delta^2+12v^2v_\Delta^4-16v_\Delta^6)c_{2\alpha} - 6v_\Delta^3v_\phi^3 s_{2\alpha}](m_H^2-m_h^2), \quad \text{(B.64)}$$

$$\lambda_{H^+H^-AG^0} = \frac{1}{v^2 v_\Delta v_\phi (v^2+2v_\Delta^2)}\Bigg\{ \frac{2(v^6-4v^4v_\Delta^2+8v_\Delta^6)}{v^2+2v_\Delta^2} m_A^2 + \left(-v^4+4v^2v_\Delta^2-2v_\Delta^4\right)(m_H^2+m_h^2) + \left[-(v^4-4v^2v_\Delta^2+6v_\Delta^4)c_{2\alpha} - v_\Delta v_\phi (v^2-4v_\Delta^2)s_{2\alpha}\right](m_H^2-m_h^2)\Bigg\}, \tag{B.65}$$

$$\lambda_{H^+H^-HH} = \frac{1}{2v^4}\left[-v^2-2v_\Delta^2+(v^2-6v_\Delta^2)c_{2\alpha}+4v_\Delta v_\phi s_{2\alpha}\right] m_{H^+}^2 + \frac{c_\alpha}{2v^2v_\Delta^2(v^2+2v_\Delta^2)}\left[(v^4-4v^2v_\Delta^2+8v_\Delta^4)c_\alpha - 8v_\Delta^3 v_\phi s_\alpha\right] m_A^2 + \frac{1}{16}\left(-\frac{8c_\alpha^4}{v_\Delta^2}+\frac{9+4c_{2\alpha}+3c_{4\alpha}}{v^2}+\frac{8c_\alpha s_\alpha^3}{v_\Delta v_\phi}-\frac{8s_\alpha^4}{v_\phi^2}+\frac{4v_\Delta s_{4\alpha}}{v^2 v_\phi}\right) m_H^2 + \frac{s_{2\alpha}}{8v^2 v_\Delta v_\phi^3}\left[-v^4+2v^2v_\Delta^2+(v^4-6v^2v_\Delta^2+8v_\Delta^4)c_{2\alpha}-\frac{v_\phi}{v_\Delta}(v^4-4v^2v_\Delta^2+6v_\Delta^4)s_{2\alpha}\right] m_h^2, \tag{B.66}$$

$$\lambda_{H^+H^-Hh} = \frac{1}{v^4}\left[-4v_\Delta v_\phi c_{2\alpha}+(v^2-6v_\Delta^2)s_{2\alpha}\right] m_{H^+}^2 + \frac{1}{2v^2v_\Delta^2(v^2+2v_\Delta^2)}\left[8v_\Delta^3 v_\phi c_{2\alpha}+(v^4-4v^2v_\Delta^2+8v_\Delta^4)s_{2\alpha}\right] m_A^2 - \frac{s_{2\alpha}}{4v^2v_\Delta^2v_\phi^2}\left(v^4-4v^2v_\Delta^2+2v_\Delta^4\right)(m_H^2+m_h^2) - \frac{s_{2\alpha}}{4v^2v_\Delta^2v_\phi^2}\left[(v^4-4v^2v_\Delta^2+6v_\Delta^4)c_{2\alpha}+\frac{v_\Delta}{v_\phi}(v^4-6v^2v_\Delta^2+8v_\Delta^4)s_{2\alpha}\right](m_H^2-m_h^2), \tag{B.67}$$

$$\lambda_{H^+H^-hh} = -\frac{1}{2v^2}\left[1+\frac{2v_\Delta^2}{v^2}+\left(1-\frac{6v_\Delta^2}{v^2}\right)c_{2\alpha}+\frac{4v_\Delta v_\phi}{v^2}s_{2\alpha}\right] m_{H^+}^2 + \frac{v^2 s_\alpha}{2v_\Delta^2(v^2+2v_\Delta^2)}\left[\frac{8v_\Delta^3 v_\phi}{v^4}c_\alpha+\left(1-\frac{4v_\Delta^2}{v^2}+\frac{8v_\Delta^4}{v^4}\right)s_\alpha\right] m_A^2 + \frac{v^2 s_{2\alpha}}{8v_\Delta v_\phi^3}\left[\frac{v_\phi^2}{v^2}+\left(1-\frac{6v_\Delta^2}{v^2}+\frac{8v_\Delta^4}{v^4}\right)c_{2\alpha}-\frac{v_\phi}{v_\Delta}\left(1-\frac{4v_\Delta^2}{v^2}+\frac{6v_\Delta^4}{v^4}\right)s_{2\alpha}\right] m_H^2 + \frac{1}{16}\left[-\frac{8c_\alpha^4}{v_\phi^2}-\frac{8s_\alpha}{v_\Delta^2}\left(\frac{v_\Delta}{v_\phi}c_\alpha^3+s_\alpha^3\right)+\frac{1}{v^2}\left(9-4c_{2\alpha}+3c_{4\alpha}+\frac{4v_\Delta}{v_\phi}s_{4\alpha}\right)\right] m_h^2, \tag{B.68}$$

$$\lambda_{H^+G^-hh} = \frac{1}{\sqrt{2}v^2}\Bigg\{\frac{1}{v^2}\left[v_\Delta v_\phi(1-3c_{2\alpha})+(v^2-4v_\Delta^2)s_{2\alpha}\right] m_{H^+}^2 + \frac{(v^2-4v_\Delta^2)s_\alpha}{v_\Delta v_\phi(v^2+2v_\Delta^2)}\left[v^2 s_\alpha - 2v_\Delta(v_\phi c_\alpha + v_\Delta s_\alpha)\right] m_A^2 + \frac{s_{2\alpha}}{4v_\Delta v_\phi}\left[2v_\Delta v_\phi c_{2\alpha}-(v^2-3v_\Delta^2)s_{2\alpha}\right] m_H^2 + \frac{1}{8v_\Delta v_\phi}\left[-3v^2+9v_\Delta^2+4(v^2-v_\Delta^2)c_{2\alpha}-(v^2-3v_\Delta^2)c_{4\alpha}-2v_\Delta v_\phi s_{4\alpha}\right] m_h^2\Bigg\}, \tag{B.69}$$

$$\lambda_{G^+G^-AA} = \frac{1}{v^2+2v_\Delta^2}\Bigg\{ -2m_{H^+}^2 + \frac{2v_\phi^2}{v^2}m_A^2 - \frac{1}{2}(m_H^2+m_h^2) + \frac{1}{4v^2}\left[-2(v^2-4v_\Delta^2)c_{2\alpha} + \frac{1}{v_\phi v_\Delta}(v^4-4v^2v_\Delta^2+12v_\Delta^4)s_{2\alpha}\right](m_H^2-m_h^2)\Bigg\}, \tag{B.70}$$

$$\lambda_{G^+G^-AG^0} = \frac{1}{v^2(v^2+2v_\Delta^2)}\Bigg\{ -4v_\Delta v_\phi(m_{H^+}^2-m_A^2) - v_\Delta v_\phi(m_H^2+m_h^2) + [-3v_\Delta v_\phi c_{2\alpha} + (v^2-4v_\Delta^2)s_{2\alpha}](m_H^2-m_h^2)\Bigg\}, \tag{B.71}$$

$$\lambda_{G^+G^-Hh} = \frac{1}{v^2}\Bigg\{ \frac{1}{v^2}\left[4v_\Delta v_\phi c_{2\alpha} - 2(v^2-3v_\Delta^2)s_{2\alpha}\right]m_{H^+}^2 + \frac{1}{v^2+2v_\Delta^2}\left[-4v_\Delta v_\phi c_{2\alpha} + 2v_\phi^2 s_{2\alpha}\right]m_A^2 - \frac{s_{2\alpha}}{4}(m_H^2+m_h^2) - \frac{s_{2\alpha}}{4}\left[3c_{2\alpha} - \frac{v^2-4v_\Delta^2}{v_\Delta v_\phi}s_{2\alpha}\right](m_H^2-m_h^2)\Bigg\}, \tag{B.72}$$

$$\lambda_{G^+G^-hh} = \frac{1}{v^2}\Bigg\{ \frac{1}{v^2}\left[-v^2+v_\Delta^2+(v^2-3v_\Delta^2)c_{2\alpha}+2v_\Delta v_\phi s_{2\alpha}\right]m_{H^+}^2 + \frac{2s_\alpha}{v^2+2v_\Delta^2}\left[v^2 s_\alpha - 2v_\Delta(v_\phi c_\alpha + v_\Delta s_\alpha)\right]m_A^2 + \frac{s_{2\alpha}}{8v_\Delta v_\phi}\left[v^2-(v^2-4v_\Delta^2)c_{2\alpha}-3v_\Delta v_\phi s_{2\alpha}\right]m_H^2 - \frac{1}{16}\left[9+\frac{8v^2c_\alpha s_\alpha^3}{v_\phi v_\Delta}+\left(-4c_{2\alpha}+3c_{4\alpha}+\frac{4v_\Delta}{v_\phi}s_{4\alpha}\right)\right]m_h^2\Bigg\}, \tag{B.73}$$

$$\lambda_{AAAA} = \frac{v^4-8v^2v_\Delta^2+12v_\Delta^4}{8v_\Delta^2(v^2+2v_\Delta^2)^2}m_A^2 - \frac{v^6-6v^4v_\Delta^2+12v^2v_\Delta^4+8v_\Delta^6}{16v_\Delta^2v_\phi^2(v^2+2v_\Delta^2)^2}(m_H^2+m_h^2) - \frac{1}{16v_\Delta^2v_\phi^2(v^2+2v_\Delta^2)^2}[(v^6-6v^4v_\Delta^2+12v^2v_\Delta^4-24v_\Delta^6)c_{2\alpha}-8v_\Delta^3v_\phi^3s_{2\alpha}](m_H^2-m_h^2), \tag{B.74}$$

$$\lambda_{AAAG^0} = \frac{1}{v_\Delta(v^2+2v_\Delta^2)^2}\Bigg\{(v^2-4v_\Delta^2)v_\phi m_A^2 + \frac{-v^4+4v^2v_\Delta^2}{2v_\phi}(m_H^2+m_h^2) + \frac{1}{2v_\phi}\left[-(v^4-4v^2v_\Delta^2+8v_\Delta^4)c_{2\alpha} - v_\Delta v_\phi(v^2-6v_\Delta^2)s_{2\alpha}\right](m_H^2-m_h^2)\Bigg\}, \lambda_{AAG^0G^0}$$
$$+ \frac{1}{4}\left[-12(v^2-3v_\Delta^2)c_{2\alpha} + \frac{1}{v_\phi v_\Delta}(v^4-20v^2v_\Delta^2+52v_\Delta^4)s_{2\alpha}\right](m_H^2-m_h^2)\Bigg\}, \tag{B.75}$$

$$\lambda_{AG^0G^0G^0} = \frac{1}{2(v^2+2v_\Delta^2)^2}\Bigg\{4v_\Delta v_\phi m_A^2 - 3v_\Delta v_\phi(m_H^2+m_h^2) + \left[-5v_\Delta v_\phi c_{2\alpha} + (v^2-6v_\Delta^2)s_{2\alpha}\right](m_H^2-m_h^2) \tag{B.76}$$

$$\lambda_{AAHH} = \frac{m_A^2}{8v_\Delta^2(v^2+2v_\Delta^2)^2}[v^4-6v^2v_\Delta^2+(v^4-2v^2v_\Delta^2-8v_\Delta^4)c_{2\alpha}]$$
$$-\frac{m_H^2}{32v_\Delta^2(v^4-4v_\Delta^4)}[2(v^4-4v^2v_\Delta^2+8v_\Delta^4)(1+c_{2\alpha}^2)+4v^2c_{2\alpha}(v^2-4v_\Delta^2)$$
$$-\frac{2v_\Delta}{v_\phi}(v^4-4v_\Delta^4)s_{2\alpha}+\frac{v_\Delta}{v_\phi}(v^4-8v^2v_\Delta^2+12v_\Delta^4)s_{4\alpha}]$$
$$-\frac{s_{2\alpha}m_h^2}{16v_\Delta v_\phi^3(v^2+2v_\Delta^2)}[v^4-4v_\Delta^4-(v^4-8v^2v_\Delta^2+12v_\Delta^4)c_{2\alpha}+\frac{v_\phi}{v_\Delta}(v^4-4v^2v_\Delta^2+8v_\Delta^4)s_{2\alpha}], \tag{B.77}$$

$$\lambda_{AAHh} = \frac{s_{2\alpha}}{4v_\Delta^2}\Bigg\{\frac{v^2-4v_\Delta^2}{v^2+2v_\Delta^2}m_A^2-\frac{v^2(v^2-4v_\Delta^2)}{2v_\phi^2(v^2+2v_\Delta^2)}(m_H^2+m_h^2)$$
$$-\frac{m_H^2-m_h^2}{2v_\phi^2(v^2+2v_\Delta^2)}\left[(v^4-4v^2v_\Delta^2+8v_\Delta^4)c_{2\alpha}+\frac{v_\Delta}{v_\phi}(v^4-8v^2v_\Delta^2+12v_\Delta^4)s_{2\alpha}\right]\Bigg\}, \tag{B.78}$$

$$\lambda_{AAhh} = \frac{v^4}{8v_\Delta^2(v^2+2v_\Delta^2)^2}\left[1-\frac{6v_\Delta^2}{v^2}-\left(1-\frac{2v_\Delta^2}{v^2}-\frac{8v_\Delta^4}{v^4}\right)c_{2\alpha}\right]m_A^2$$
$$+\frac{s_{2\alpha}v^4}{16v_\Delta v_\phi^3(v^2+2v_\Delta^2)}\left[1-\frac{4v_\Delta^4}{v^4}+\left(1-\frac{8v_\Delta^2}{v^2}+\frac{12v_\Delta^4}{v^4}\right)c_{2\alpha}-\frac{v_\phi}{v_\Delta}\left(1-\frac{4v_\Delta^2}{v^2}+\frac{8v_\Delta^4}{v^4}\right)s_{2\alpha}\right]m_H^2$$
$$-\frac{v^4}{16v_\Delta^2(v^4-4v_\Delta^4)}\Big[\left(1-\frac{4v_\Delta^2}{v^2}+\frac{8v_\Delta^4}{v^4}\right)(1+c_{2\alpha}^2)-2c_{2\alpha}\left(1-\frac{4v_\Delta^2}{v^2}\right)$$
$$+\frac{v_\Delta}{v_\phi}s_{2\alpha}\left(1-\frac{4v_\Delta^4}{v^4}\right)+\frac{v_\Delta}{v_\phi}\left(1-\frac{8v_\Delta^2}{v^2}+\frac{12v_\Delta^4}{v^4}\right)s_{2\alpha}c_{2\alpha}\Big]m_h^2, \tag{B.79}$$

$$\lambda_{AG^0HH} = \frac{1}{2v_\Delta v_\phi(v^2+2v_\Delta^2)}\Bigg\{\frac{v_\phi^4+(v^4-4v_\Delta^4)c_{2\alpha}}{v^2+2v_\Delta^2}m_A^2$$
$$+\frac{1}{4}\left[-3v^2+9v_\Delta^2+4(-v^2+v_\Delta^2)c_{2\alpha}-(v^2-3v_\Delta^2)c_{4\alpha}-2v_\Delta v_\phi s_{4\alpha}\right]m_H^2$$
$$+\frac{s_{2\alpha}}{2}\left[2v_\Delta v_\phi c_{2\alpha}-(v^2-3v_\Delta^2)s_{2\alpha}\right]m_h^2\Bigg\}, \tag{B.80}$$

$$\lambda_{AG^0hh} = \frac{1}{2v_\Delta v_\phi(v^2+2v_\Delta^2)}\Bigg\{\frac{v_\phi^4-(v^4-4v_\Delta^4)c_{2\alpha}}{v^2+2v_\Delta^2}m_A^2+\frac{s_{2\alpha}}{2}\left[2v_\Delta v_\phi c_{2\alpha}-(v^2-3v_\Delta^2)s_{2\alpha}\right]m_H^2$$
$$+\frac{1}{4}\left[-3v^2+9v_\Delta^2+4(v^2-v_\Delta^2)c_{2\alpha}-(v^2-3v_\Delta^2)c_{4\alpha}-2v_\Delta v_\phi s_{4\alpha}\right]m_h^2\Bigg\}, \tag{B.81}$$

$$\lambda_{G^0G^0Hh} = \frac{s_{2\alpha}}{2(v^2+2v_\Delta^2)}\left[m_A^2-\frac{3}{4}(m_H^2+m_h^2)-\frac{1}{4}\left(5c_{2\alpha}-\frac{v^2-6v_\Delta^2}{v_\phi v_\Delta}s_{2\alpha}\right)(m_H^2-m_h^2)\right], \tag{B.82}$$

$$\lambda_{G^0G^0hh} = \frac{1}{4(v^2+2v_\Delta^2)}\Bigg\{\frac{1}{v^2+2v_\Delta^2}\left[v^2-6v_\Delta^2-(v^2+2v_\Delta^2)c_{2\alpha}\right]m_A^2$$
$$+\frac{s_{2\alpha}}{4v_\Delta v_\phi}\left[v^2+2v_\Delta^2-(v^2-6v_\Delta^2)c_{2\alpha}-5v_\Delta v_\phi s_{2\alpha}\right]m_H^2$$
$$-\frac{1}{8v_\Delta v_\phi}\left[8v^2c_\alpha s_\alpha^3+v_\Delta v_\phi(15-12c_{2\alpha}+5c_{4\alpha})+v_\Delta^2(4s_{2\alpha}+6s_{4\alpha})\right]m_h^2\Bigg\}, \tag{B.83}$$

$$\begin{aligned}
\lambda_{HHHH} &= \frac{1}{8v_\Delta^2(v^2+2v_\Delta^2)}(v_\phi^2 c_\alpha^4 - v_\Delta^2 s_{2\alpha}^2)m_A^2 \\
&- \frac{1}{8v_\Delta^2 v_\phi^2}\left[v_\phi^2 c_\alpha^6 - \frac{2v^4 v_\Delta}{v_\phi(v^2+2v_\Delta^2)}c_\alpha^3 s_\alpha^3 + v_\Delta^2 s_\alpha^6 + \frac{v_\Delta^5}{v_\phi(v^2+2v_\Delta^2)}s_{2\alpha}^3\right]m_H^2 \\
&- \frac{s_{2\alpha}^2}{64v_\Delta^2 v_\phi^2}\left[v^2 - v_\Delta^2 + (v^2-3v_\Delta^2)c_{2\alpha} + 2v_\Delta v_\phi s_{2\alpha}\right]m_h^2, \qquad \text{(B.84)} \\
\lambda_{HHHh} &= \frac{s_{2\alpha}}{8v_\Delta^2}\Bigg\{\frac{v_\phi^2 + (v^2+2v_\Delta^2)c_{2\alpha}}{v^2+2v_\Delta^2}m_A^2 \\
&- \frac{1}{4v_\phi^2}\left[3v^2 - 9v_\Delta^2 + 4(v^2-v_\Delta^2)c_{2\alpha} + (v^2-3v_\Delta^2)c_{4\alpha} + 2v_\Delta v_\phi s_{4\alpha}\right]m_H^2 \\
&- \frac{s_{2\alpha}}{2v_\phi^2}[-2v_\Delta v_\phi c_{2\alpha} + (v^2-3v_\Delta^2)s_{2\alpha}]m_h^2\Bigg\}, \qquad \text{(B.85)} \\
\lambda_{HHhh} &= \frac{v^2}{32v_\Delta^2(v^2+2v_\Delta^2)}\left[3 - \frac{10v_\Delta^2}{v^2} - 3\left(1+\frac{2v_\Delta^2}{v^2}\right)c_{4\alpha}\right]m_A^2 \\
&+ \frac{v^2 s_{2\alpha}}{32v_\Delta v_\phi^3}\Bigg\{\left[1 - \frac{2v_\Delta^2}{v^2} + \frac{3v_\phi^2}{v^2}c_{4\alpha} + \left(-\frac{3v_\phi}{2v_\Delta} + \frac{9v_\Delta v_\phi}{2v^2}\right)s_{4\alpha}\right](m_H^2 - m_h^2) \\
&- \frac{3v_\phi}{v_\Delta}s_{2\alpha}\left(1 - \frac{v_\Delta^2}{v^2}\right)(m_H^2 + m_h^2)\Bigg\}, \qquad \text{(B.86)} \\
\lambda_{Hhhh} &= \frac{s_{2\alpha}v^2}{4v_\Delta^2(v^2+2v_\Delta^2)}\left(s_\alpha^2 - \frac{2v_\Delta^2}{v^2}c_\alpha^2\right)m_A^2 \\
&- \frac{s_{2\alpha}^2 v^2}{16v_\Delta^2 v_\phi^2}\left[\left(1 - \frac{3v_\Delta^2}{v^2}\right)s_{2\alpha} - \frac{2v_\Delta v_\phi}{v^2}c_{2\alpha}\right]m_H^2 \\
&- \frac{s_{2\alpha}v^2}{16v_\Delta^2 v_\phi^2}\left[(1+c_{2\alpha}^2)\left(1 - \frac{3v_\Delta^2}{v^2}\right) - 2\left(1 - \frac{v_\Delta^2}{v^2}\right)c_{2\alpha} + \frac{v_\Delta v_\phi}{v^2}s_{4\alpha}\right]m_h^2, \qquad \text{(B.87)} \\
\lambda_{hhhh} &= \frac{v^2}{8v_\Delta^2(v^2+2v_\Delta^2)}\left(\frac{v_\phi^2}{v^2}s_\alpha^4 - \frac{v_\Delta^2}{v^2}s_{2\alpha}^2\right)m_A^2 \\
&- \frac{s_{2\alpha}^2 v^2}{32v_\Delta^2 v_\phi^2}\left[s_\alpha^2\left(1 - \frac{v_\Delta^2}{v^2}\right) + \frac{v_\Delta^2}{v^2}c_{2\alpha} - \frac{v_\Delta v_\phi}{v^2}s_{2\alpha}\right]m_H^2 \\
&+ \frac{1}{16}\left[-\frac{2}{v_\phi^2}c_\alpha^6 - \frac{1}{v_\phi^3 v_\Delta}\left(\frac{v^2}{2} - v_\Delta^2\right)s_{2\alpha}^3 - \frac{2}{v_\Delta^2}s_\alpha^6\right]m_h^2. \qquad \text{(B.88)}
\end{aligned}$$

Appendix C

Loop functions

Passarino Veltman functions [111, 112] (A, B, C and D) are defined as following,

$$A(m_i) = \int \frac{d^{\bar{D}}k}{i\pi^2}\frac{1}{N_i}, \tag{C.1}$$

$$[B_0, B^\mu, B^{\mu\nu}](ij) = \int d^{\bar{D}}k i\pi^2 \frac{[1, k^\mu, k^{\mu\nu}]}{N_i N_j}, \tag{C.2}$$

$$[C_0, C^\mu, C^{\mu\nu}](ijk) = \int d^{\bar{D}}k i\pi^2 \frac{[1, k^\mu, k^{\mu\nu}]}{N_i N_j N_k}, \tag{C.3}$$

$$[D_0, D^\mu, D^{\mu\nu}](ijk) = \int d^{\bar{D}}k i\pi^2 \frac{[1, k^\mu, k^{\mu\nu}]}{N_i N_j N_k N_l}, \tag{C.4}$$

where $D = 4 - 2\epsilon$ and $d^{\bar{D}}k = \Gamma(1-\epsilon)(\pi\mu^2)^\epsilon d^D k$ and $\Gamma(1-\epsilon)$ is a gamma function. Factors of donominators are

$$N_1 = k^2 - m_1^2 + i\varepsilon, \tag{C.5}$$
$$N_2 = (k+p_1)^2 - m_2^2 + i\varepsilon, \tag{C.6}$$
$$N_3 = (k+p_1+p_2)^2 - m_3^2 + i\varepsilon, \tag{C.7}$$
$$N_2 = (k+p_1+p_2+p_3)^2 - m_4^2 + i\varepsilon, \tag{C.8}$$

where p_i is the momentum of the external particle i and m_j is the mass of the propagetor i. These vector/tensor functions are reducted to scalor functions as

$$B^\mu(12) = p_1^\mu B_1(12), \tag{C.9}$$
$$B^{\mu\nu}(12) = p_1^\mu p_1^\nu B_{21}(12) + g^{\mu\nu} B_{22}(12), \tag{C.10}$$

$$C^\mu(123) = p_1^\mu C_{11}(123) + p_2^\mu C_{12}(123), \tag{C.11}$$
$$C^{\mu\nu}(123) = p_1^\mu p_1^\nu C_{21}(123) + p_2^\mu p_2^\nu C_{22}(123) + (p_1^\mu p_2^\nu + p_2^\mu p_1^\nu) C_{23}(123) + g^{\mu\nu} C_{24}(123), \tag{C.12}$$

$$D^\mu(1234) = p_1^\mu D_{11}(1234) + p_2^\mu D_{12}(1234) + p_3^\mu D_{13}(1234), \tag{C.13}$$
$$D^{\mu\nu}(1234) = p_1^\mu p_1^\nu D_{21}(1234) + p_2^\mu p_2^\nu D_{22}(1234) + p_3^\mu p_3^\nu D_{23}(1234) + (p_1^\mu p_2^\nu + p_2^\mu p_1^\nu) D_{24}(1234)$$
$$+ (p_1^\mu p_3^\nu + p_3^\mu p_1^\nu) D_{25}(1234) + (p_2^\mu p_3^\nu + p_3^\mu p_2^\nu) D_{26}(1234) + g^{\mu\nu} D_{27}(1234). \tag{C.14}$$

Argiments of the scalar functions are following,

$$B_i(12) = B_i(p_1^2; m_1, m_2), \tag{C.15}$$
$$C_i(123) = C_i(p_1^2, p_2^2, q^2; m_1, m_2, m_3) \tag{C.16}$$
$$D_i(123) = D_i(p_1^2, p_2^2, p_3^2, (p_1+p_2+p_3)^2, (p_1+p_2)^2, (p_2+p_3)^2; m_1, m_2, m_3, m_4), \tag{C.17}$$

where $q = p_1 + p_2$.

C.1 A function

$A(m^2)$ function is expressed by

$$A[m^2] = m^2(1 - \ln m^2 + \mathrm{Div}), \tag{C.18}$$

where $\mathrm{Div} = \frac{1}{\epsilon} - \gamma_E + \ln\pi + \ln\mu^2$.

C.2 B function

C.2.1 B_0 function

B_0 function is expressed by

$$B_0[p_1^2; m_1, m_2] = \mathrm{Div} - \int dx \ln H, \tag{C.19}$$

where

$$H \equiv -x(1-x)p_1^2 + xm_1^2 + (1-x)m_2^2. \tag{C.20}$$

We show various approximate formulae of the B_0 function in various cases as follows.

- Large mass limit 1 ($m_1^2 = m_2^2 = m^2 \gg p^2$)

  $$B_0[0; m, m] = \mathrm{Div} - \ln m^2. \tag{C.21}$$

- Large mass limit 2 ($m_1^2 \neq m_2^2 \gg p^2$)

  $$B_0[0; m_1, m_2] = (\mathrm{Div} + 1) - \frac{1}{m_1^2 - m_2^2}\left(m_1^2 \ln m_1^2 - m_2^2 \ln m_2^2\right) \tag{C.22}$$

- Small mass limit 1 ($p_1^2 \gg m_1^2, m_2^2$)

  $$B_0[p_1^2; 0, 0] = \mathrm{Div} + 2 - \ln p_1^2. \tag{C.23}$$

- Small mass limit 2 ($p_1^2, m_2^2 \gg m_1^2$ or $p_1^2, m_1^2 \gg m_2^2$)

  $$B_0[p_1^2; m, 0] = B_0[p_1^2; 0, m] \tag{C.24}$$
  $$= \mathrm{Div} - \left\{-2 + 2i\pi + \ln p_1^2 - \left(-1 + \frac{m^2}{p_1^2}\ln\left(-1 + \frac{m^2}{p_1^2}\right) + \frac{m^2}{p_1^2}\ln\left(\frac{m^2}{p_1^2}\right)\right)\right\} \tag{C.25}$$

- Small mass limit 3 ($m_1^2 \gg m_2^2, p_1^2$ or $m_2^2 \gg m_1^2, p_1^2$)

  $$B_0[0; m, 0] = B_0[0; 0, m] = \mathrm{Div} - \ln m^2 + 1. \tag{C.26}$$

C.2.2 B_1 function

$B_1(12)$ function is expressed by

$$B_1[p^2; m_1, m_2] = -\frac{1}{2}\left(\frac{1}{\epsilon} + \ln\mu^2\right) + \int dx(1-x)\ln H. \tag{C.27}$$

Reduction form is

$$B_1[p_1^2; m_1, m_2] = \frac{1}{2p_1^2}\left(A[m_1] - A[m_2] - f_1[p_1, m_1, m_2]B_0[p_1^2; m_1, m_2]\right). \tag{C.28}$$

We show various approximate formulae of the B_1 function in various cases as follows.

- Large mass limit 1 ($m_1^2 = m_2^2 = m^2 \gg p_1^2$)

$$B_1[0; m, m] = -\frac{1}{2}\mathrm{Div} + \frac{1}{2}\ln m^2. \tag{C.29}$$

- Large mass limit 2 ($m_1^2 \neq m_2^2 \gg p_1^2$)

$$B_1[0; m_1, m_2] = -\frac{1}{2}\mathrm{Div} - \left(\frac{1}{2} + \frac{m_1^2+m_2^2}{4(m_1^2-m_2^2)} - \frac{1}{2}\ln m_2^2 - \frac{m_1^4}{2(m_1^2-m_2^2)^2}\ln\frac{m_1^2}{m_2^2}\right). \tag{C.30}$$

- Large mass limit 2 ($m_1^2 \gg m_2^2, p_1^2$)

$$B_1[0; m, 0] = -\frac{1}{2}\mathrm{Div} + \frac{1}{2}\ln m^2 - \frac{3}{4}. \tag{C.31}$$

- Large mass limit 2 ($m_2^2, \gg m_1^2, p_1^2$)

$$B_1[0; 0, m] = -\frac{1}{2}\mathrm{Div} + \frac{1}{2}\ln m^2 - \frac{1}{4}. \tag{C.32}$$

- Small mass limit 1 ($p_1^2 \gg m_1^2, m_2^2$)

$$B_1[p_1^2; 0, 0] = -\frac{1}{2}\mathrm{Div} + \frac{1}{2}\left(-2 + \ln(-p_1^2)\right). \tag{C.33}$$

- Small mass limit 2 ($p_1^2, m_1^2 \gg m_2$)

$$B_1[p_1^2; m, 0] = -\frac{1}{2}\mathrm{Div} + \left(-1 - \frac{m^2}{2p_1^2} + \frac{m^4}{2p_1^4}\ln m^2 + \frac{p_1^4 - m^4}{2p_1^4}\ln(p_1^2 - m^2)\right) + i\pi\left(1 - \frac{m^4}{2p_1^4}\right). \tag{C.34}$$

- Small mass limit 2 ($p_1^2, m_2^2 \gg m_1^2$)

$$B_1[p_1^2; 0, m] = -\frac{1}{2}\mathrm{Div} + \frac{(-2p_1^2 + m^2)(p_1^2 - m^2\ln m^2) + (p_1^2 - m^2)^2\ln(-p_1^2 + m^2)}{2p_1^4}. \tag{C.35}$$

C.2.3 B_{21} and B_{22} function

B_{21} and B_{22} functions are expressed by,

$$B_{21}[p^2; m_1, m_2] = \frac{1}{3}\left(\frac{1}{\epsilon} + \ln\mu^2\right) - \int dx(1-x)^2 \ln H, \tag{C.36}$$

$$B_{22}[p^2; m_1, m_2] = \frac{1}{4}\left(\frac{1}{\epsilon} + \ln\mu^2 + 1\right)\left(m_1^2 + m_2^2 - \frac{1}{3}p^2\right) - \frac{1}{2}\int dx H \ln H. \tag{C.37}$$

We show various approximate formulae of the B_{21} and B_{22} functions in various cases as follows.

- Large mass limit 1 ($m_1^2 = m_2^2 \equiv m^2 \gg p_1^2$)

$$B_{21}[0; m, m] = \frac{1}{3}\mathrm{Div} - \frac{1}{3}\ln m^2. \tag{C.38}$$

- Small mass limit 1 ($p_1^2 \gg m_1^2, m_2^2$)

$$B_{21}[p_1^2; 0, 0] = \frac{1}{3}\mathrm{Div} + \frac{1}{18}\left(13 - 6\ln(-p_1^2)\right). \tag{C.39}$$

- Large mass limit 1 ($m_1^2 = m_2^2 \equiv m^2 \gg p_1^2$)

$$B_{22}[0; m, m] = -\frac{p_1^2}{4}\mathrm{Div} + \frac{1}{2}m^2(1 + \mathrm{Div} - \ln m^2). \tag{C.40}$$

- Small mass limit 1 ($p_1^2 \gg m_1^2, m_2^2$)

$$B_{22}[p_1^2; 0, 0] = \frac{p_2^2}{4}\left(-\frac{p_1^2}{3}\mathrm{Div} + \frac{p_1^2}{9}(-8 + 3\ln p_1^2 + 3i\pi)\right). \tag{C.41}$$

C.3 C function

C.3.1 C_0 function

$C_0(123)$ function is expressed by,

$$C_0(123) = -\int_0^1 \int_0^{1-x} dxdy \frac{1}{G}, \tag{C.42}$$

where

$$G \equiv xm_1^2 + ym_2^2 + (1-x-y)m_3^2 - (1-x)^2 p_1^2 - (1-x-y)^2 p_2^2 - (1-x-y)(p_1+p_2)^2. \tag{C.43}$$

We show various approximate formulae of the C_0 function in various cases as follows.

- Large mass limit ($m_1^2 = m_2^2 = m_3^2 = m^2 \gg p_1^2, p_2^2, q^2$)

$$C_0[0, 0, 0; m, m, m] = -\frac{1}{2m^2}. \tag{C.44}$$

- Large mass limit ($m_1^2 = m_3^2, m_2^2 \gg p_1^2, p_2^2, q^2$)

$$C_0[0, 0, 0; m_1, m_2, m_1] = -\frac{1}{m_1^2 - m_2^2} + \frac{m_2^2}{(m_1^2 - m_2^2)^2}\ln\frac{m_1^2}{m_2^2}. \tag{C.45}$$

C.3.2 C_{11} function

C_{11} and C_{12} functions are expressed by,

$$C_{11}(123) = \int_0^1 \int_0^{1-x} dxdy \frac{1-x}{G}, \tag{C.46}$$

$$C_{12}(123) = \int_0^1 \int_0^{1-x} dxdy \frac{1-x-y}{G}. \tag{C.47}$$

We show various approximate formulae of the C_{11} and C_{12} function in various cases as follows.

- Large mass limit $(m_1^2 = m_2^2 = m_3^3 = m^2 \gg p_1^2, p_2^2, q^2)$

$$C_{11}[0,0,0;m,m,m] = \frac{1}{3m^2}. \tag{C.48}$$

- Large mass limit $(m_1^2 = m_3^3, m_2^2 \gg p_1^2, p_2^2, q^2)$

$$C_{11}[0,0,0;m_1,m_2,m_1] = \frac{1}{2(m_1^2-m_2^2)} + \frac{m_1^2+m_2^2}{4(m_1^2-m_2^2)^2} - \frac{m_2^2(2m_1^2-m_2^2)}{2(m_1^2-m_2^2)^3} \ln \frac{m_1^2}{m_2^2}. \tag{C.49}$$

- Large mass limit $(m_1^2 = m_2^2 = m_3^3 = m^2 \gg p_1^2, p_2^2, q^2)$

$$C_{12}[0,0,0;m,m,m] = \frac{1}{6m^2}. \tag{C.50}$$

- Large mass limit $(m_1^2 = m_3^3, m_2^2 \gg p_1^2, p_2^2, q^2)$

$$C_{12}[0,0,0;m_1,m_2,m_1] = \frac{1}{2(m_1^2-m_2^2)} - \frac{m_1^2+m_2^2}{4(m_1^2-m_2^2)^2} + \frac{m_2^4}{2(m_1^2-m_2^2)^3} \ln \frac{m_1^2}{m_2^2}. \tag{C.51}$$

C.3.3 C_{21} function

$C_{21}(123)$, $C_{22}(123)$, $C_{23}(123)$ and $C_{24}(123)$ functions are expressed by,

$$C_{21}(123) = -\int_0^1 \int_0^{1-x} dxdy \frac{(1-x)^2}{G}, \tag{C.52}$$

$$C_{22}(123) = -\int_0^1 \int_0^{1-x} dxdy \frac{(1-x-y)^2}{G}, \tag{C.53}$$

$$C_{23}(123) = -\int_0^1 \int_0^{1-x} dxdy \frac{(1-x)(1-x-y)}{G}, \tag{C.54}$$

$$C_{24}(123) = \frac{1}{4}\mathrm{Div} - \frac{1}{2}\int_0^1 \int_0^{1-x} dxdy \ln G. \tag{C.55}$$

We show various approximate formulae of the C_{2i} functions in various cases as follows.

- Large mass limit $(m_1^2 = m_2^2 = m_3^3 = m^2 \gg p_1^2, p_2^2, q^2)$

$$C_{21}[0,0,0;m,m,m] = -\frac{1}{4m^2}. \tag{C.56}$$

- Large mass limit $(m_1^2 = m_3^3, m_2^2 \gg p_1^2, p_2^2, q^2)$

$$C_{21}[0,0,0;m_1,m_2,m_1] = \tag{C.57}$$

$$-\frac{m_1^2}{2(m_1^2-m_2^2)^2} - \frac{m_1^6-m_2^6}{9(m_1^2-m_2^2)^4} + \frac{m_1^2 m_2^2}{(m_1^2-m_2^2)^3}\ln\frac{m_1^2}{m_2^2} + \frac{m_2^6}{3(m_1^2-m_2^2)^4}\ln\frac{m_1^2}{m_2^2}. \tag{C.58}$$

- Large mass limit $(m_1^2 = m_2^2 = m_3^3 = m^2 \gg p_1^2, p_2^2, q^2)$

$$C_{22}[0,0,0;m,m,m] = -\frac{1}{12m^2}. \tag{C.59}$$

- Large mass limit $(m_1^2 = m_3^3, m_2^2 \gg p_1^2, p_2^2, q^2)$

$$C_{22}[0,0,0;m_1,m_2,m_1] = \frac{1}{18(m_1^2-m_2^2)^4}\left(-2m_1^6 + 9m_1^4 m_2^2 - 18m_1^2 m_2^4 + 11m_2^6 + 6m_2^6\ln\frac{m_1^2}{m_2^2}\right). \tag{C.60}$$

- Large mass limit $(m_1^2 = m_2^2 = m_3^3 = m^2 \gg p_1^2, p_2^2, q^2)$

$$C_{23}[0,0,0;m,m,m] = -\frac{1}{8m^2}. \tag{C.61}$$

- Large mass limit $(m_1^2 = m_3^3, m_2^2 \gg p_1^2, p_2^2, q^2)$

$$C_{23}[0,0,0;m_1,m_2,m_1] = \frac{1}{36(m_1^2-m_2^2)^4}\Big(-7m_1^6 + 36m_1^4 m_2^2 - 45m_1^2 m_2^4 + 16m_2^6 + 12m_2^6\ln\frac{m_1^2}{m_2^2} - 18m_1^2 m_2^4\ln\frac{m_1^2}{m_2^2}\Big). \tag{C.62}$$

- Large mass limit $(m_1^2 = m_2^2 = m_3^3 = m^2 \gg p_1^2, p_2^2, q^2)$

$$C_{24}[0,0,0;m,m,m] = \frac{1}{4}\mathrm{Div} - \frac{1}{4}\ln m^2. \tag{C.63}$$

- Large mass limit $(m_1^2 = m_3^3, m_2^2 \gg p_1^2, p_2^2, q^2)$

$$C_{24}[0,0,0;m_1,m_2,m_1] = \frac{1}{4}\mathrm{Div} + \frac{1}{4} - \frac{(m_1^2+m_2^2)}{8(m_1^2-m_2^2)} - \frac{1}{4}\ln m^2 + \frac{m_2^4}{4(m_1^2-m_2^2)^2}\ln\frac{m_1^2}{m_2^2}. \tag{C.64}$$

Appendix D

1PI diagrams

In this section, we give one-loop fermion, vector boson and scalar boson contributions to the one, two and three point functions by using Passarino-Veltman functions [111] whose notation is same as those defined in Ref. [112]. We calculate 1PI diagrams in the 't Hooft-Feynman gauge so that the masses of Numbu-Goldstone bosons $m_{G^\pm}$ and m_{G^0} and those of Fadeev-Popov ghosts $m_{c^\pm}$, m_{c^0} and m_{c^γ} are the same as corresponding masses of the gauge bosons. We write 1PI diagram contributions separately for fermion loop contributions and boson loop contributions which are expressed by index F and B, respectively.

D.1 1PI diagrams in the THDMs

D.1.1 One-point functions

The 1PI tadpole diagrams for h and H are calculated by

$$T^{\rm 1PI}_{h,F} = -\sum_f \frac{4m_f^2}{v} N_c^f \xi_h^f A(f), \tag{D.1}$$

$$T^{\rm 1PI}_{H,F} = -\sum_f \frac{4m_f^2}{v} N_c^f \xi_H^f A(f), \tag{D.2}$$

$$\begin{aligned} T^{\rm 1PI}_{h,B} = {} & s_{\beta-\alpha}\left[3gm_W A(W) + \frac{3}{2}g_Z m_Z A(Z) - 2gm_W^3 - g_Z m_Z^3\right] \\ & - \lambda_{H^+H^-h}A(H^\pm) - \lambda_{AAh}A(A) - \lambda_{HHh}A(H) - 3\lambda_{hhh}A(h) \\ & - \lambda_{G^+G^-h}A(G^\pm) - \lambda_{G^0G^0h}A(G^0), \end{aligned} \tag{D.3}$$

$$\begin{aligned} T^{\rm 1PI}_{H,B} = {} & c_{\beta-\alpha}\left[3gm_W A(W) + \frac{3}{2}g_Z m_Z A(Z) - 2gm_W^3 - g_Z m_Z^3\right] \\ & - \lambda_{H^+H^-H}A(H^\pm) - \lambda_{AAH}A(A) - 3\lambda_{HHH}A(H) - \lambda_{Hhh}A(h) \\ & - \lambda_{G^+G^-H}A(G^\pm) - \lambda_{G^0G^0H}A(G^0). \end{aligned} \tag{D.4}$$

D.1.2 Two-point functions

The 1PI diagram contributions to the scalar boson two point functions are calculated as

$$16\pi^2\Pi^{\rm 1PI}_{hh}(p^2)_F = -\sum_f \frac{4m_f^2 N_c^f}{v^2}(\xi_h^f)^2\left[A(f)+\left(2m_f^2-\frac{p^2}{2}\right)B_0(p^2;f,f)\right], \tag{D.5}$$

$$16\pi^2\Pi^{\rm 1PI}_{HH}(p^2)_F = -\sum_f \frac{4m_f^2 N_c^f}{v^2}(\xi_H^f)^2\left[A(f)+\left(2m_f^2-\frac{p^2}{2}\right)B_0(p^2;f,f)\right], \tag{D.6}$$

$$16\pi^2\Pi^{\rm 1PI}_{Hh}(p^2)_F = -\sum_f \frac{4m_f^2 N_c^f}{v^2}\xi_h^f\xi_H^f\left[A(f)+\left(2m_f^2-\frac{p^2}{2}\right)B_0(p^2;f,f)\right], \tag{D.7}$$

$$16\pi^2\Pi^{\rm 1PI}_{AA}(p^2)_F = -\sum_f \frac{4m_f^2 N_c^f}{v^2}\xi_f^2\left[A(f)-\frac{p^2}{2}B_0(p^2;f,f)\right], \tag{D.8}$$

$$16\pi^2\Pi^{\rm 1PI}_{AG}(p^2)_F = -\sum_f \frac{4m_f^2 N_c^f}{v^2}\xi_f\left[A(f)-\frac{p^2}{2}B_0(p^2;f,f)\right], \tag{D.9}$$

$$\begin{aligned}
16\pi^2\Pi^{\rm 1PI}_{hh}(p^2)_B &= g^2\sin^2(\beta-\alpha)(3m_W^2-p^2)B_0(p^2;W,W)+\frac{g^2}{2}\left[4-\sin^2(\beta-\alpha)\right]A(W)\\
&+\frac{g_Z^2}{2}\sin^2(\beta-\alpha)(3m_Z^2-p^2)B_0(p^2;Z,Z)+\frac{g_Z^2}{4}\left[4-\sin^2(\beta-\alpha)\right]A(Z)\\
&-\frac{g^2}{2}\cos^2(\beta-\alpha)\left[2A(W)-A(H^\pm)+(2m_{H^\pm}^2-m_W^2+2p^2)B_0(p^2;W,H^\pm)\right]\\
&-\frac{g_Z^2}{4}\cos^2(\beta-\alpha)\left[2A(Z)-A(A)+(2m_A^2-m_Z^2+2p^2)B_0(p^2;Z,A)\right]\\
&-\left[\sin^2(\beta-\alpha)+1/2\right](2g^2m_W^2+g_Z^2m_Z^2)\\
&-2\lambda_{H^+H^-hh}A(H^\pm)-2\lambda_{AAhh}A(A)-2\lambda_{HHhh}A(H)-12\lambda_{hhhh}A(h)\\
&-2\lambda_{G^+G^-hh}A(G^\pm)-2\lambda_{G^0G^0hh}A(G^0)\\
&+\lambda^2_{H^+H^-h}B_0(p^2;H^\pm,H^\pm)+\lambda^2_{G^+G^-h}B_0(p^2;G^\pm,G^\pm)+2\lambda^2_{H^+G^-h}B_0(p^2;H^\pm,G^\pm)\\
&+2\lambda^2_{AAh}B_0(p^2;A,A)+2\lambda^2_{G^0G^0h}B_0(p^2;G^0,G^0)+\lambda^2_{AG^0h}B_0(p^2;A,G^0)\\
&+2\lambda^2_{HHh}B_0(p^2;H,H)+18\lambda^2_{hhh}B_0(p^2;h,h)+4\lambda^2_{Hhh}B_0(p^2;h,H),
\end{aligned} \tag{D.10}$$

$$\begin{aligned}
16\pi^2\Pi^{\rm 1PI}_{HH}(p^2)_B &= g^2\cos^2(\beta-\alpha)(3m_W^2-p^2)B_0(p^2;W,W)+\frac{g^2}{2}[4-\cos^2(\beta-\alpha)]A(W)\\
&+\frac{g_Z^2}{2}\cos^2(\beta-\alpha)(3m_Z^2-p^2)B_0(p^2;Z,Z)+\frac{g_Z^2}{4}\left[4-\cos^2(\beta-\alpha)\right]A(Z)\\
&-\frac{g^2}{2}\sin^2(\beta-\alpha)\left[2A(W)-A(H^\pm)+(2m_{H^\pm}^2-m_W^2+2p^2)B_0(p^2;W,H^\pm)\right]\\
&-\frac{g_Z^2}{4}\sin^2(\beta-\alpha)\left[2A(Z)-A(A)+(2m_A^2-m_Z^2+2p^2)B_0(p^2;Z,A)\right]\\
&-\left[\cos^2(\beta-\alpha)+1/2\right](2g^2m_W^2+g_Z^2m_Z^2)\\
&-2\lambda_{H^+H^-HH}A(H^\pm)-2\lambda_{AAHH}A(A)-12\lambda_{HHHH}A(H)-2\lambda_{HHhh}A(h)\\
&-2\lambda_{G^+G^-HH}A(G^\pm)-2\lambda_{G^0G^0HH}A(G^0)\\
&+\lambda^2_{H^+H^-H}B_0(p^2;H^\pm,H^\pm)+\lambda^2_{G^+G^-H}B_0(p^2;G^\pm,G^\pm)+2\lambda^2_{H^+G^-H}B_0(p^2;H^\pm,G^\pm)\\
&+2\lambda^2_{AAH}B_0(p^2;A,A)+2\lambda^2_{G^0G^0H}B_0(p^2;G^0,G^0)+\lambda^2_{AG^0H}B_0(p^2;A,G^0)\\
&+18\lambda^2_{HHH}B_0(p^2;H,H)+2\lambda^2_{Hhh}B_0(p^2;h,h)+4\lambda^2_{HHh}B_0(p^2;h,H),
\end{aligned} \tag{D.11}$$

$$
\begin{aligned}
16\pi^2\Pi^{\rm 1PI}_{Hh}(p^2)_B &= s_{\beta-\alpha}c_{\beta-\alpha} \\
&\times \Big\{ g^2(3m_W^2-p^2)B_0(p^2;W,W) - \frac{g^2}{2}A(W) \\
&+ \frac{g_Z^2}{2}(3m_Z^2-p^2)B_0(p^2;Z,Z) - \frac{g_Z^2}{4}A(Z) \\
&+ \frac{g^2}{2}[2A(W) - A(H^\pm) + (2m_{H^\pm}^2 - m_W^2 + 2p^2)B_0(p^2;W,H^\pm)] \\
&+ \frac{g_Z^2}{4}[2A(Z) - A(A) + (2m_A^2 - m_Z^2 + 2p^2)B_0(p^2;Z,A)] - (2g^2m_W^2 + g_Z^2m_Z^2)\Big\} \\
&- \lambda_{H^+H^-Hh}A(H^\pm) - \lambda_{AAHh}A(A) - 3\lambda_{HHHh}A(H) - 3\lambda_{Hhhh}A(h) \\
&- \lambda_{G^+G^-Hh}A(G^\pm) - \lambda_{G^0G^0Hh}A(G^0) \\
&+ \lambda_{H^+H^-h}\lambda_{H^+H^-H}B_0(p^2;H^\pm,H^\pm) + \lambda_{G^+G^-h}\lambda_{G^+G^-H}B_0(p^2;G^\pm,G^\pm) \\
&+ 2\lambda_{H^+G^-h}\lambda_{H^+G^-H}B_0(p^2;H^\pm,G^\pm) \\
&+ 2\lambda_{AAh}\lambda_{AAH}B_0(p^2;A,A) + 2\lambda_{hG^0G^0}\lambda_{G^0G^0H}B_0(p^2;G^0,G^0) \\
&+ \lambda_{AG^0h}\lambda_{AG^0H}B_0(p^2;A,G^0) + 6\lambda_{HHh}\lambda_{HHH}B_0(p^2;H,H) \\
&+ 6\lambda_{hhh}\lambda_{Hhh}B_0(p^2;h,h) + 4\lambda_{Hhh}\lambda_{HHh}B_0(p^2;H,h), \qquad \text{(D.12)}
\end{aligned}
$$

$$
\begin{aligned}
16\pi^2\Pi^{\rm 1PI}_{AA}(p^2)_B &= 2g^2A(W) + g_Z^2A(Z) - \frac{1}{2}(2g^2m_W^2 + g_Z^2m_Z^2) \\
&- \frac{g^2}{2}\left[2A(W) - A(H^\pm) + (2m_{H^\pm}^2 - m_W^2 + 2p^2)B_0(p^2;W,H^\pm)\right] \\
&- \frac{g_Z^2}{4}\cos^2(\beta-\alpha)\left[2A(Z) - A(h) + (2m_h^2 - m_Z^2 + 2p^2)B_0(p^2;Z,h)\right] \\
&- \frac{g_Z^2}{4}\sin^2(\beta-\alpha)\left[2A(Z) - A(H) + (2m_H^2 - m_Z^2 + 2p^2)B_0(p^2;Z,H)\right], \\
&- 2\lambda_{H^+H^-AA}A(H^\pm) - 12\lambda_{AAAA}A(A) - 2\lambda_{AAHH}A(H) - 2\lambda_{AAhh}A(h) \\
&- 2\lambda_{G^+G^-AA}A(G^\pm) - 2\lambda_{AAG^0G^0}A(G^0) \\
&+ 2|\lambda_{H^+G^-A}|^2B_0(p^2;H^\pm,G^\pm) + 4\lambda_{AAh}^2B_0(p^2;A,h) \\
&+ 4\lambda_{AAH}^2B_0(p^2;A,H) + \lambda_{AG^0h}^2B_0(p^2;h,G^0) + \lambda_{AG^0H}^2B_0(p^2;H,G^0), \qquad \text{(D.13)}
\end{aligned}
$$

$$
\begin{aligned}
16\pi^2\Pi^{\rm 1PI}_{AG}(p^2)_B &= s_{\beta-\alpha}c_{\beta-\alpha} \\
&\times \Big\{ \frac{g_Z^2}{4}\left[2A(Z) - A(H) + (2m_H^2 - m_Z^2 + 2p^2)B_0(p^2;Z,H)\right] \\
&- \frac{g_Z^2}{4}[2A(Z) - A(h) + (2m_h^2 - m_Z^2 + 2p^2)B_0(p^2;Z,h)]\Big\} \\
&- \lambda_{H^+H^-AG^0}A(H^\pm) - 3\lambda_{AAAG^0}A(A) - \lambda_{AG^0HH}A(H) - \lambda_{AG^0hh}A(h) \\
&- \lambda_{G^+G^-AG^0}A(G^\pm) - 3\lambda_{AG^0G^0G^0}A(G^0) \\
&+ 2\lambda_{AAh}\lambda_{AG^0h}B_0(p^2;A,h) + 2\lambda_{AAH}\lambda_{AG^0H}B_0(p^2;A,H) \\
&+ 2\lambda_{AG^0h}\lambda_{G^0G^0h}B_0(p^2;G^0,h) + 2\lambda_{AG^0H}\lambda_{G^0G^0H}B_0(p^2;G^0,H). \qquad \text{(D.14)}
\end{aligned}
$$

The 1PI diagram contributions to the gauge boson two point functions are calculated as

$$16\pi^2\Pi^{\rm 1PI}_{WW}(p^2)_F = \sum_{f,f'} g^2 N_c^f \Big(2p^2 B_3 - B_4\Big)(p^2; f, f'), \tag{D.15}$$

$$16\pi^2\Pi^{\rm 1PI}_{\gamma\gamma}(p^2)_F = \sum_{f} 8e^2 Q_f^2 N_c^f p^2 B_3(p^2; f, f), \tag{D.16}$$

$$16\pi^2\Pi^{\rm 1PI}_{Z\gamma}(p^2)_F = \sum_{f} e g_Z N_c^f \Big[2p^2(2I_f Q_f - 4s_W^2 Q_f^2)B_3\Big](p^2; f, f), \tag{D.17}$$

$$16\pi^2\Pi^{\rm 1PI}_{ZZ}(p^2)_F = \sum_{f} g_Z^2 N_c^f \Big[2p^2(4s_W^4 Q_f^2 - 4s_W^2 Q_f I_f + 2I_f^2)B_3 - 2I_f^2 f^2 B_0\Big](p^2; f, f), \tag{D.18}$$

$$\begin{aligned}
16\pi^2\Pi^{\rm 1PI}_{WW}(p^2)_B = g^2\Bigg\{ & \frac{1}{4}B_5(p^2; A, H^\pm) + \frac{1}{4}\sin^2(\beta-\alpha)B_5(p^2; H, H^\pm) \\
& + \frac{1}{4}\cos^2(\beta-\alpha)B_5(p^2; h, H^\pm) \\
& + \sin^2(\beta-\alpha)\left(m_W^2 B_0 + \frac{1}{4}B_5\right)(p^2; h, W) \\
& + \cos^2(\beta-\alpha)\left(m_W^2 B_0 + \frac{1}{4}B_5\right)(p^2; H, W) \\
& + \left[\left(\frac{1}{4} + 2c_W^2\right)B_5 + (m_W^2 - 4s_W^2 m_W^2 + m_Z^2 - 8p^2 c_W^2)B_0\right](p^2; Z, W) \\
& + 2s_W^2\Big[B_5 + (2m_W^2 - 4p^2)B_0\Big](p^2; 0, W) - \frac{2}{3}p^2\Bigg\},
\end{aligned} \tag{D.19}$$

$$16\pi^2\Pi^{\rm 1PI}_{\gamma\gamma}(p^2)_B = e^2 B_5(p^2; H^\pm, H^\pm) - e^2 p^2\left[12B_3 + 5B_0(p^2; W, W) + \frac{2}{3}\right], \tag{D.20}$$

$$\begin{aligned}
16\pi^2\Pi^{\rm 1PI}_{Z\gamma}(p^2)_B = & \frac{eg_Z}{2}B_5(p^2; H^\pm, H^\pm) - eg_Z p^2\left(10B_3 + \frac{11}{2}B_0 + \frac{2}{3}\right)(p^2; W, W) \\
& - \frac{s_W}{c_W}\Pi^{\rm 1PI}_{\gamma\gamma}(p^2)_B,
\end{aligned} \tag{D.21}$$

$$\begin{aligned}
16\pi^2\Pi^{\rm 1PI}_{ZZ}(p^2)_B = g_Z^2\Bigg\{ & \frac{1}{4}B_5(p^2; H^\pm, H^\pm) + \frac{1}{4}\sin^2(\beta-\alpha)B_5(p^2; H, A) \\
& + \frac{1}{4}\cos^2(\beta-\alpha)B_5(p^2; h, A)] \\
& + \sin^2(\beta-\alpha)\left(m_Z^2 B_0 + \frac{1}{4}B_5\right)(p^2; h, Z) \\
& + \cos^2(\beta-\alpha)\left(m_Z^2 B_0 + \frac{1}{4}B_5\right)(p^2; H, Z) \\
& + \Big[(2m_W^2 - \frac{23}{4}p^2)B_0 - 9p^2 B_3\Big](p^2; W, W) - \frac{2}{3}p^2\Bigg\} \\
& - \frac{2s_W}{c_W}\Pi^{\rm 1PI}_{Z\gamma}(p^2)_B - \frac{s_W^2}{c_W^2}\Pi^{\rm 1PI}_{\gamma\gamma}(p^2)_B,
\end{aligned} \tag{D.22}$$

where the fermion-loop contributions are the same as those in the SM.

The fermion two point functions can be decomposed into the following three parts

$$16\pi^2\Pi^{\rm 1PI}_{ff}(p^2) = \not{p}\Pi^{\rm 1PI}_{ff,V}(p^2) - \not{p}\gamma_5\Pi^{\rm 1PI}_{ff,A}(p^2) + m_f\Pi^{\rm 1PI}_{ff,S}(p^2). \tag{D.23}$$

Each part is caluclated as

$$\begin{aligned}
16\pi^2\Pi^{\rm 1PI}_{ff,V}(p^2) &= -e^2Q_f^2(2B_1+1)(p^2;f,\gamma) - g_Z^2(v_f^2+a_f^2)(2B_1+1)(p^2;f,Z)\\
&\quad - \frac{g^2}{4}(2B_1+1)(p^2;f',W)\\
&\quad - \frac{m_f^2}{v^2}\Big[(\xi_h^f)^2B_1(p^2;f,h) + (\xi_H^f)^2B_1(p^2;f,H) + \xi_f^2B_1(p^2;f,A) + B_1(p^2;f,G^0)\Big]\\
&\quad - \frac{m_f^2+m_{f'}^2}{v^2}B_1(p^2;f',G^\pm) - \frac{m_f^2\xi_f^2+m_{f'}^2\xi_{f'}^2}{v^2}B_1(p^2;f',H^\pm),\\
16\pi^2\Pi^{\rm 1PI}_{ff,A}(p^2) &= -2g_Z^2v_fa_f(2B_1+1)(p^2;f,Z) - \frac{g^2}{4}(2B_1+1)(p^2;f',W)\\
&\quad + \frac{m_f^2-m_{f'}^2}{v^2}B_1(p^2;f',G^\pm) + \frac{m_f^2\xi_f^2-m_{f'}^2\xi_{f'}^2}{v^2}B_1(p^2;f',H^\pm),\\
\Pi^{\rm 1PI}_{ff,S}(p^2) &= -2e^2Q_f^2(2B_0-1)(p^2;f,\gamma) - 2g_Z^2(v_f^2-a_f^2)(2B_0-1)(p^2;f,Z)\\
&\quad + \frac{m_f^2}{v^2}\Big[(\xi_h^f)^2B_0(p^2;f,h) + (\xi_H^f)^2B_0(p^2;f,H) - \xi_f^2B_0(p^2;f,A) - B_0(p^2;f,G^0)\Big]\\
&\quad - 2\frac{m_{f'}^2}{v^2}\left[B_0(p^2;f',G^\pm) + \xi_f\xi_{f'}B_0(p^2;f',H^\pm)\right],
\end{aligned} \tag{D.24}$$

where v_f and a_f are the coefficient of the vector coupling and axial vector coupling of $Zf\bar{f}$ vertex given as

$$v_f = \frac{I_f}{2} - s_W^2Q_f, \quad a_f = \frac{I_f}{2}. \tag{D.25}$$

D.1.3 Three-point functions

In this subsection, we give analytic expressions for the 1PI diagram contributions to the three point functions. The assignment for external momentum is taken in such a way that p_1 and (p_2) is the incoming momnetum of h (h), V (V) and f $(\bar{f})$ for the hhh, hVV and $hf\bar{f}$ vertices, respectively, and $q = p_1 + p_2$ is the outgoing momentum of h for all the above vertices.

First, the 1PI diagrams for the hhh coupling is calculated as

$$\begin{aligned}
16\pi^2\Gamma^{\rm 1PI}_{hhh}(p_1^2,p_2^2,q^2)_F &= -\sum_f \frac{8m_f^4N_c^f}{v^3}(\xi_h^f)^3\Big[B_0(p_1^2,f,f) + B_0(p_2^2,f,f) + B_0(q^2,f,f)\\
&\quad + (4m_f^2 - q^2 + p_1\cdot p_2)C_0(f,f,f)\Big],
\end{aligned} \tag{D.26}$$

$$
\begin{aligned}
16\pi^2\Gamma^{\rm 1PI}_{hhh}(p_1^2,p_2^2,q^2)_B &= \frac{g^3}{2}m_W^3 s^3_{\beta-\alpha}\Big[16C_0(W,W,W)-C_0(c^\pm,c^\pm,c^\pm)\Big]\\
&-\frac{g^3}{2}m_W s_{\beta-\alpha}\Big[s^2_{\beta-\alpha}C^{SVV}_{hhh}(G^\pm,W,W)+c^2_{\beta-\alpha}C^{SVV}_{hhh}(H^\pm,W,W)\Big]\\
&+\frac{g_Z^3}{4}m_Z^3 s^3_{\beta-\alpha}\Big[16C_0(Z,Z,Z)-C_0(c_Z,c_Z,c_Z)\Big]-\frac{g_Z^3 m_Z}{4}s_{\beta-\alpha}\Big[s^2_{\beta-\alpha}C^{SVV}_{hhh}(G^0,Z,Z)c^2_{\beta-\alpha}C^{SVV}_{hhh}(A,Z,Z)\Big]\\
&+\frac{g^2}{2}\lambda_{G^+G^-h}s^2_{\beta-\alpha}C^{VSS}_{hhh}(W,G^\pm,G^\pm)+\frac{g^2}{2}\lambda_{H^+H^-h}c^2_{\beta-\alpha}C^{VSS}_{hhh}(W,H^\pm,H^\pm)\\
&+\frac{g^2}{2}\lambda_{H^+G^-h}s_{\beta-\alpha}c_{\beta-\alpha}[C^{VSS}_{hhh}(W,G^\pm,H^\pm)+C^{VSS}_{hhh}(W,H^\pm,G^\pm)]\\
&+\frac{g_Z^2}{2}\lambda_{G^0G^0h}s^2_{\beta-\alpha}C^{VSS}_{hhh}(Z,G^0,G^0)+\frac{g_Z^2}{2}\lambda_{AAh}c^2_{\beta-\alpha}C^{VSS}_{hhh}(Z,A,A)\\
&+\frac{g_Z^2}{4}\lambda_{AG^0h}s_{\beta-\alpha}c_{\beta-\alpha}[C^{VSS}_{hhh}(Z,A,G^0)+C^{VSS}_{hhh}(Z,G^0,A)]\\
&+2g^3m_W s_{\beta-\alpha}[B_0(p_1^2,W,W)+B_0(p_2^2,W,W)+B_0(q^2,W,W)]-3g^3m_W s_{\beta-\alpha}\\
&+g_Z^3m_Z s_{\beta-\alpha}[B_0(p_1^2,Z,Z)+B_0(p_2^2,Z,Z)+B_0(q^2,Z,Z)]-\frac{3}{2}g_Z^3m_Z s_{\beta-\alpha}\\
&+2\lambda_{H^+H^-h}\lambda_{H^+H^-hh}[B_0(p_1^2,H^\pm,H^\pm)+B_0(p_2^2,H^\pm,H^\pm)+B_0(q^2,H^\pm,H^\pm)]\\
&+2\lambda_{hG^+G^-}\lambda_{hhG^+G^-}[B_0(p_1^2,G^\pm,G^\pm)+B_0(p_2^2,G^\pm,G^\pm)+B_0(q^2,G^\pm,G^\pm)]\\
&+4\lambda_{H^+G^-h}\lambda_{H^+G^-hh}[B_0(p_1^2,H^\pm,G^\pm)+B_0(p_2^2,H^\pm,G^\pm)+B_0(q^2,H^\pm,G^\pm)]\\
&+4\lambda_{AAh}\lambda_{AAhh}[B_0(p_1^2,A,A)+B_0(p_2^2,A,A)+B_0(q^2,A,A)]\\
&+4\lambda_{G^0G^0h}\lambda_{G^0G^0hh}[B_0(p_1^2,G^0,G^0)+B_0(p_2^2,G^0,G^0)+B_0(q^2,G^0,G^0)]\\
&+2\lambda_{AG^0h}\lambda_{AG^0hh}[B_0(p_1^2,A,G^0)+B_0(p_2^2,A,G^0)+B_0(q^2,A,G^0)]\\
&+4\lambda_{HHh}\lambda_{HHhh}[B_0(p_1^2,H,H)+B_0(p_2^2,H,H)+B_0(q^2,H,H)]\\
&+12\lambda_{Hhh}\lambda_{Hhhh}[B_0(p_1^2,h,H)+B_0(p_2^2,h,H)+B_0(q^2,h,H)]\\
&+72\lambda_{hhh}\lambda_{hhhh}[B_0(p_1^2,h,h)+B_0(p_2^2,h,h)+B_0(q^2,h,h)]\\
&-2\lambda^3_{H^+H^-h}C_0(H^\pm,H^\pm,H^\pm)-2\lambda^3_{G^+G^-h}C_0(G^\pm,G^\pm,G^\pm)-8\lambda^3_{G^0G^0h}C_0(G^0,G^0,G^0)\\
&-8\lambda^3_{AAh}C_0(A,A,A)-8\lambda^3_{HHh}C_0(H,H,H)-216\lambda^3_{hhh}C_0(h,h,h)\\
&-2\lambda_{H^+H^-h}\lambda^2_{H^+G^-h}[C_0(G^\pm,H^\pm,H^\pm)+C_0(H^\pm,G^\pm,H^\pm)+C_0(H^\pm,H^\pm,G^\pm)]\\
&-2\lambda_{G^+G^-h}\lambda^2_{H^+G^-h}[C_0(H^\pm,G^\pm,G^\pm)+C_0(G^\pm,H^\pm,W)+C_0(G^\pm,G^\pm,H^\pm)]\\
&-2\lambda_{AAh}\lambda^2_{AG^0h}[C_0(G^0,A,A)+C_0(A,G^0,A)+C_0(A,A,G^0)]\\
&-2\lambda_{G^0G^0h}\lambda^2_{AG^0h}[C_0(A,G^0,G^0)+C_0(G^0,A,G^0)+C_0(G^0,G^0,A)]\\
&-8\lambda_{HHh}\lambda^2_{Hhh}[C_0(h,H,H)+C_0(H,H,h)+C_0(H,h,H)]\\
&-24\lambda_{hhh}\lambda^2_{Hhh}[C_0(h,h,H)+C_0(H,h,h)+C_0(h,H,h)],
\end{aligned}
\tag{D.27}
$$

where

$$
\begin{aligned}
C^{SVV}_{hhh}(X,Y,Z) &\equiv \Big[p_1^2C_{21}+p_2^2C_{22}+2p_1p_2C_{23}+4C_{24}-\frac{1}{2}-(q+p_1)(p_1C_{11}+p_2C_{12})+qp_1C_0\Big](X,Y,Z)\\
&+\Big[p_1^2C_{21}+p_2^2C_{22}+2p_1p_2C_{23}+4C_{24}-\frac{1}{2}+(3p_1-p_2)(p_1C_{11}+p_2C_{12})+2p_1(p_1-p_2)C_0\Big](Z,X,Y)\\
&+\Big[p_1^2C_{21}+p_2^2C_{22}+2p_1p_2C_{23}+4C_{24}-\frac{1}{2}+(3p_1+4p_2)(p_1C_{11}+p_2C_{12})+2q(q+p_2)C_0\Big](Y,Z,X),
\end{aligned}
\tag{D.28}
$$

$$
\begin{aligned}
&C^{VSS}_{hhh}(X,Y,Z) \equiv \\
&\Big[p_1^2 C_{21} + p_2^2 C_{22} + 2p_1p_2 C_{23} + 4C_{24} - \frac{1}{2} + (4p_1 + 2p_2)(p_1 C_{11} + p_2 C_{12}) + 4p_1 \cdot q C_0\Big](X,Y,Z) \\
+ &\Big[p_1^2 C_{21} + p_2^2 C_{22} + 2p_1p_2 C_{23} + 4C_{24} - \frac{1}{2} + 2p_2(p_1 C_{11} + p_2 C_{12}) - p_1(p_1 + 2p_2) C_0\Big](Z,X,Y) \\
+ &\Big[p_1^2 C_{21} + p_2^2 C_{22} + 2p_1p_2 C_{23} + 4C_{24} - \frac{1}{2} - 2p_2(p_1 C_{11} + p_2 C_{12}) - q(p_1 - p_2) C_0\Big](Y,Z,X).
\end{aligned}
\tag{D.29}
$$

The $hf\bar{f}$ vertex can be decomposed into the following 8 form factors

$$
\begin{aligned}
&\Gamma^{\rm 1PI}_{hff}(p_1^2, p_2^2, q^2) = \\
&F^S_{hff} + \gamma_5 F^P_{hff} + \not{p}_1 F^{V1}_{hff} + \not{p}_2 F^{V2}_{hff} + \not{p}_1 \gamma_5 F^{A1}_{hff} + \not{p}_2 \gamma_5 F^{A2}_{hff} + \not{p}_1 \not{p}_2 F^T_{hff} + \not{p}_1 \not{p}_2 \gamma_5 F^{PT}_{hff}.
\end{aligned}
\tag{D.30}
$$

Each form factor can be calculated by

$$
\begin{aligned}
&16\pi^2 \left(\frac{m_f}{v}\right)^{-1} F^S_{hff} = -2g_Z^4 v^2 (v_f^2 - a_f^2) s_{\beta-\alpha} C_0(Z,f,Z) \\
&- 4\xi^f_h \Big\{ e^2 Q_f^2 [m_f^2 C_0 + p_1^2(C_{11} + C_{21}) + p_2^2(C_{12} + C_{22}) + p_1 \cdot p_2 (2C_{23} - C_0) + 4C_{24} - 1](f,\gamma,f) \\
&+ g_Z^2 (v_f^2 - a_f^2)[m_f^2 C_0 + p_1^2(C_{11} + C_{21}) + p_2^2(C_{12} + C_{22}) + p_1 \cdot p_2 (2C_{23} - C_0) + 4C_{24} - 1](f,Z,f) \Big\} \\
&+ \xi^f_h \frac{m_f^2}{v^2} \Big[(\xi^f_h)^2 C^{FSF}_{hff}(f,h,f) + (\xi^f_H)^2 C^{FSF}_{hff}(f,H,f) - C^{FSF}_{hff}(f,G^0,f) - \xi_f^2 C^{FSF}_{hff}(f,A,f) \Big] \\
&- \xi^{f'}_h \frac{2m_{f'}^2}{v^2} \Big[C^{FSF}_{hff}(f',G^\pm,f') + \xi_f \xi_{f'} C^{FSF}_{hff}(f',H^\pm,f') \Big] \\
&- \frac{m_f^2}{v} \Big\{ 6(\xi^f_h)^2 \lambda_{hhh} C_0(h,f,h) + 2(\xi^f_H)^2 \lambda_{HHh} C_0(H,f,H) + 2\xi^f_h \xi^f_H \lambda_{Hhh} [C_0(h,f,H) + C_0(H,f,h)] \\
&\qquad - 2\lambda_{G^0G^0h} C_0(G^0,f,G^0) - 2\xi_f^2 \lambda_{AAh} C_0(A,f,A) - \xi_f \lambda_{AG^0h} [C_0(A,f,G^0) + C_0(G^0,f,A)] \Big\} \\
&+ \frac{2m_{f'}^2}{v} \Big\{ \lambda_{G^+G^-h} C_0(G^\pm,f',G^\pm) + \xi_f \xi_{f'} \lambda_{H^+H^-h} C_0(H^\pm,f',H^\pm) \\
&\qquad + \frac{1}{2} \lambda_{H^+G^-h} (\xi_f + \xi_{f'}) [C_0(G^\pm,f',H^\pm) + C_0(H^\pm,f',G^\pm)] \Big\} \\
&- \frac{g^2}{4} s_{\beta-\alpha} \Big[C^{VFS}_{hff}(W,f',G^\pm) + C^{SFV}_{hff}(G^\pm,f',W) \Big] \\
&- \frac{g^2}{4} \xi_f c_{\beta-\alpha} \Big[C^{VFS}_{hff}(W,f',H^\pm) + C^{SFV}_{hff}(H^\pm,f',W) \Big] \\
&- \frac{g_Z^2}{8} s_{\beta-\alpha} \Big[C^{VFS}_{hff}(Z,f,G^0) + C^{SFV}_{hff}(G^0,f,Z) \Big] \\
&- \frac{g_Z^2}{8} \xi_f c_{\beta-\alpha} \Big[C^{VFS}_{hff}(Z,f,A) + C^{SFV}_{hff}(A,f,Z) \Big],
\end{aligned}
\tag{D.31}
$$

$$
\begin{aligned}
&16\pi^2\left(\frac{m_f}{v}\right)^{-1}F^P_{hff} = \lambda_{H^+G^-h}\frac{m^2_{f'}}{v}(\xi_{f'}-\xi_f)[C_0(G^\pm,f',H^\pm)-C_0(H^\pm,f',G^\pm)]\\
&-\frac{g^2}{4}s_{\beta-\alpha}\Big[C^{VFS}_{hff}(W,f',G^\pm)-C^{SFV}_{hff}(G^\pm,f',W)\Big]\\
&-\frac{g^2}{4}\xi_f c_{\beta-\alpha}\Big[C^{VFS}_{hff}(W,f',H^\pm)-C^{SFV}_{hff}(H^\pm,f',W)\Big]\\
&-g_Z^2 v_f I_f s_{\beta-\alpha}\Big[C^{VFS}_{hff}(Z,f,G^0)-C^{SFV}_{hff}(G^0,f,Z)\Big]\\
&-g_Z^2 v_f I_f \xi_f c_{\beta-\alpha}\Big[C^{VFS}_{hff}(Z,f,A)-C^{SFV}_{hff}(A,f,Z)\Big],
\end{aligned}
\tag{D.32}
$$

$$
\begin{aligned}
&16\pi^2 F^{V1}_{hff} = \frac{2m_f^2}{v}\xi^f_h\Big[g_Z^2(v_f^2+a_f^2)(C_0+2C_{11})(f,Z,f)+e^2Q_f^2(C_0+2C_{11})(f,\gamma,f)\Big]\\
&+g^2\frac{m^2_{f'}}{2v}\xi^{f'}_h(C_0+2C_{11})(f',W,f')\\
&-s_{\beta-\alpha}g_Z^4 v(v_f^2+a_f^2)(C_0+C_{11})(Z,f,Z)-s_{\beta-\alpha}\frac{g^4}{4}v(C_0+C_{11})(W,f',W)\\
&+\xi^f_h\frac{m_f^4}{v^3}\Big[(\xi^f_h)^2(C_0+2C_{11})(f,h,f)+(\xi^f_H)^2(C_0+2C_{11})(f,H,f)\\
&\qquad+(C_0+2C_{11})(f,G^0,f)+\xi_f^2(C_0+2C_{11})(f,A,f)\Big]\\
&+\frac{m^2_{f'}}{v^3}\xi^{f'}_h\Big[(m_f^2+m^2_{f'})(C_0+2C_{11})(f',G^\pm,f')+(m_f^2\xi_f^2+m^2_{f'}\xi^2_{f'})(C_0+2C_{11})(f',H^\pm,f')\Big]\\
&-\frac{m_f^2}{v^2}\Big\{6(\xi^f_h)^2\lambda_{hhh}(C_0+C_{11})(h,f,h)+2(\xi^f_H)^2\lambda_{HHh}(C_0+C_{11})(H,f,H)\\
&\qquad+2\xi^f_h\xi^f_H\lambda_{Hhh}[(C_0+C_{11})(H,f,h)+(C_0+C_{11})(h,f,H)]\\
&\qquad+2\lambda_{G^0G^0h}(C_0+C_{11})(G^0,f,G^0)+2\xi_f^2\lambda_{AAh}(C_0+C_{11})(A,f,A)\\
&\qquad+\xi_f\lambda_{AG^0h}[(C_0+C_{11})(A,f,G^0)+(C_0+C_{11})(G^0,f,A)]\Big\}\\
&-\frac{\lambda_{G^+G^-h}}{v^2}(m_f^2+m^2_{f'})(C_0+C_{11})(G^\pm,f',G^\pm)-\frac{\lambda_{H^+H^-h}}{v^2}(m_f^2\xi_f^2+m^2_{f'}\xi^2_{f'})(C_0+C_{11})(H^\pm,f',H^\pm)\\
&-\frac{\lambda_{H^+G^-h}}{v^2}(m_f^2\xi_f+m^2_{f'}\xi_{f'})[(C_0+C_{11})(G^\pm,f',H^\pm)+(C_0+C_{11})(H^\pm,f',G^\pm)]\\
&-g^2\frac{m^2_{f'}}{4v}\Big[s_{\beta-\alpha}(2C_0+C_{11})(W,f',G^\pm)+s_{\beta-\alpha}(-C_0+C_{11})(G^\pm,f',W)\\
&\qquad-\xi_{f'}c_{\beta-\alpha}(2C_0+C_{11})(W,f',H^\pm)-\xi_{f'}c_{\beta-\alpha}(-C_0+C_{11})(H^\pm,f',W)\Big]\\
&-g_Z^2\frac{m_f^2}{8v}\Big[s_{\beta-\alpha}(2C_0+C_{11})(Z,f,G^0)+s_{\beta-\alpha}(-C_0+C_{11})(G^0,f,Z)\\
&\qquad-\xi_f c_{\beta-\alpha}(2C_0+C_{11})(Z,f,A)-\xi_f c_{\beta-\alpha}(-C_0+C_{11})(A,f,Z)\Big],
\end{aligned}
\tag{D.33}
$$

$$
\begin{aligned}
16\pi^2 F^{V2}_{hff} &= \frac{2m_f^2}{v}\xi_h^f\Big[g_Z^2(v_f^2+a_f^2)(C_0+2C_{12})(f,Z,f)+e^2Q_f^2(C_0+2C_{12})(f,\gamma,f)\Big]\\
&+ g^2\frac{m_{f'}^2}{2v}\xi_h^{f'}(C_0+2C_{12})(f',W,f')\\
&- s_{\beta-\alpha}g_Z^4 v(v_f^2+a_f^2)C_{12}(Z,f,Z) - s_{\beta-\alpha}\frac{g^4}{4}vC_{12}(W,f',W)\\
&+ \xi_h^f\frac{m_f^4}{v^3}\Big[(\xi_h^f)^2(C_0+2C_{12})(f,h,f)+(\xi_H^f)^2(C_0+2C_{12})(f,H,f)\\
&\qquad + (C_0+2C_{12})(f,G^0,f)+\xi_f^2(C_0+2C_{12})(f,A,f)\Big]\\
&+ \xi_h^{f'}\frac{m_{f'}^2}{v^3}\Big[(m_f^2+m_{f'}^2)(C_0+2C_{12})(f',G^\pm,f')+(m_f^2\xi_f^2+m_{f'}^2\xi_{f'}^2)(C_0+2C_{12})(f',H^\pm,f')\Big]\\
&- \frac{m_f^2}{v^2}\Big\{6(\xi_h^f)^2\lambda_{hhh}C_{12}(h,f,h)+2(\xi_H^f)^2\lambda_{HHh}C_{12}(H,f,H)+2\xi_h^f\xi_H^f\lambda_{Hhh}[C_{12}(H,f,h)+C_{12}(h,f,H)]\\
&\qquad + 2\lambda_{G^0G^0h}C_{12}(G^0,f,G^0)+2\xi_f^2\lambda_{AAh}C_{12}(A,f,A)+2\xi_f\lambda_{AG^0h}[C_{12}(G^0,f,A)+C_{12}(A,f,G^0)]\Big\}\\
&- \frac{\lambda_{G^+G^-h}}{v^2}(m_f^2+m_{f'}^2)C_{12}(G^\pm,f',G^\pm) - \frac{\lambda_{H^+H^-h}}{v^2}(m_f^2\xi_f^2+m_{f'}^2\xi_{f'}^2)C_{12}(H^\pm,f',H^\pm)\\
&- \frac{\lambda_{H^+G^-h}}{v^2}(m_f^2\xi_f+m_{f'}^2\xi_{f'})[C_{12}(G^\pm,f',H^\pm)+C_{12}(H^\pm,f',G^\pm)]\\
&- \frac{g^2}{4}\frac{m_{f'}^2}{v}\Big[s_{\beta-\alpha}(2C_0+C_{12})(W,f',G^\pm)+s_{\beta-\alpha}(-C_0+C_{12})(G^\pm,f',W)\\
&\qquad - \xi_{f'}c_{\beta-\alpha}(2C_0+C_{12})(W,f',H^\pm)-\xi_{f'}c_{\beta-\alpha}(-C_0+C_{12})(H^\pm,f',W)\Big]\\
&- \frac{g_Z^2}{8}\frac{m_f^2}{v}\Big[s_{\beta-\alpha}(2C_0+C_{12})(Z,f,G^0)+s_{\beta-\alpha}(C_{12}-C_0)(G^0,f,Z)\\
&\qquad + \xi_f c_{\beta-\alpha}(2C_0+C_{12})(Z,f,A)+\xi_f c_{\beta-\alpha}(C_{12}-C_0)(A,f,Z)\Big],
\end{aligned}
\tag{D.34}
$$

$$
\begin{aligned}
16\pi^2 F^{A1}_{hff} &= -4g_Z^2 v_f a_f\frac{m_f^2}{v}\xi_h^f(C_0+2C_{11})(f,Z,f) - g^2\frac{m_{f'}^2}{2v}\xi_h^{f'}(C_0+2C_{11})(f',W,f')\\
&+ 2s_{\beta-\alpha}g_Z^4 v_f a_f v(C_0+C_{11})(Z,f,Z)+s_{\beta-\alpha}\frac{g^4}{4}v(C_0+C_{11})(W,f',W)\\
&+ \frac{m_{f'}^2}{v^3}\xi_h^{f'}\Big[(m_f^2-m_{f'}^2)(C_0+2C_{11})(f',G^\pm,f')+(m_f^2\xi_f^2-m_{f'}^2\xi_{f'}^2)(C_0+2C_{11})(f',H^\pm,f')\Big]\\
&- \frac{\lambda_{G^+G^-h}}{v^2}(m_f^2-m_{f'}^2)(C_0+C_{11})(G^\pm,f',G^\pm) - \frac{\lambda_{H^+H^-h}}{v^2}(m_f^2\xi_f^2-m_{f'}^2\xi_{f'}^2)(C_0+C_{11})(H^\pm,f',H^\pm)\\
&- \frac{\lambda_{H^+G^-h}}{v^2}(m_f^2\xi_f-m_{f'}^2\xi_{f'})[(C_0+C_{11})(G^\pm,f',H^\pm)+(C_0+C_{11})(H^\pm,f',G^\pm)]\\
&+ \frac{g^2}{4}\frac{m_{f'}^2}{v}\Big[s_{\beta-\alpha}(2C_0+C_{11})(W,f',G^\pm)+s_{\beta-\alpha}(-C_0+C_{11})(G^\pm,f',W)\\
&\qquad - \xi_{f'}c_{\beta-\alpha}(2C_0+C_{11})(W,f',H^\pm)-\xi_{f'}c_{\beta-\alpha}(-C_0+C_{11})(H^\pm,f',W)\Big]\\
&+ g_Z^2 I_f v_f\frac{m_f^2}{v}\Big[s_{\beta-\alpha}(2C_0+C_{11})(Z,f,G^0)+s_{\beta-\alpha}(-C_0+C_{11})(G^0,f,Z)\\
&\qquad + \xi_f c_{\beta-\alpha}(2C_0+C_{11})(Z,f,A)+\xi_f c_{\beta-\alpha}(-C_0+C_{11})(A,f,Z)\Big],
\end{aligned}
\tag{D.35}
$$

$$
\begin{aligned}
16\pi^2 F^{A2}_{hff} &= -4\xi^f_h g_Z^2 v_f a_f \frac{m_f^2}{v}(C_0+2C_{12})(f,Z,f) - \xi^{f'}_h g^2 \frac{m^2_{f'}}{2v}(C_0+2C_{12})(f',W,f') \\
&+ 2s_{\beta-\alpha} g_Z^4 v_f a_f v C_{12}(Z,f,Z) + s_{\beta-\alpha}\frac{g^4}{4} v C_{12}(W,f',W) \\
&+ \xi^{f'}_h \frac{m^2_{f'}}{v^3}\Big[(m_f^2-m^2_{f'})(C_0+2C_{12})(f',G^\pm,f') + (m_f^2\xi_f^2 - m^2_{f'}\xi^2_{f'})(C_0+2C_{12})(f',H^\pm,f')\Big] \\
&- \frac{\lambda_{G^+G^-h}}{v^2}(m_f^2-m^2_{f'})C_{12}(G^\pm,f',G^\pm) - \frac{\lambda_{H^+H^-h}}{v^2}(m_f^2\xi_f^2 - m^2_{f'}\xi^2_{f'})C_{12}(H^\pm,f',H^\pm) \\
&- \frac{\lambda_{H^+G^-h}}{v^2}(m_f^2\xi_f - m^2_{f'}\xi_{f'})[C_{12}(G^\pm,f',H^\pm) + C_{12}(H^\pm,f',G^\pm)] \\
&+ \frac{g^2}{4}\frac{m^2_{f'}}{v}\Big[s_{\beta-\alpha}(2C_0+C_{12})(W,f',G^\pm) + s_{\beta-\alpha}(-C_0+C_{12})(G^\pm,f',W) \\
&\qquad - \xi_{f'}c_{\beta-\alpha}(2C_0+C_{12})(W,f',H^\pm) - \xi_{f'}c_{\beta-\alpha}(-C_0+C_{12})(H^\pm,f',W)\Big] \\
&+ g_Z^2 I_f v_f \frac{m_f^2}{v}\Big[s_{\beta-\alpha}(2C_0+C_{12})(Z,f,G^0) + s_{\beta-\alpha}(-C_0+C_{12})(G^0,f,Z) \\
&\qquad + \xi_f c_{\beta-\alpha}(2C_0+C_{12})(Z,f,A) + \xi_f c_{\beta-\alpha}(-C_0+C_{12})(A,f,Z)\Big], \qquad \text{(D.36)}
\end{aligned}
$$

$$
\begin{aligned}
16\pi^2\left(\frac{m_f}{v}\right)^{-1} F^T_{hff} &= \xi^f_h \frac{m_f^2}{v^2}\Big[(\xi^f_h)^2(C_{11}-C_{12})(f,h,f) + (\xi^f_H)^2(C_{11}-C_{12})(f,H,f) \\
&- (C_{11}-C_{12})(f,G^0,f) - \xi_f^2(C_{11}-C_{12})(f,A,f)\Big] \\
&- \xi^{f'}_h \frac{2m^2_{f'}}{v^2}\Big[(C_{11}-C_{12})(f',G^\pm,f') + \xi_f\xi_{f'}(C_{11}-C_{12})(f',H^\pm,f')\Big] \\
&- \frac{g^2}{4}\Big[s_{\beta-\alpha}(-2C_0-2C_{11}+C_{12})(W,f',G^\pm) + s_{\beta-\alpha}(-C_0-C_{11}+2C_{12})(G^\pm,f',W) \\
&\qquad + \xi_f c_{\beta-\alpha}(-2C_0-2C_{11}+C_{12})(W,f',H^\pm) + \xi_f c_{\beta-\alpha}(-C_0-C_{11}+2C_{12})(H^\pm,f',W)\Big] \\
&- \frac{g_Z^2}{8}\Big[s_{\beta-\alpha}(-2C_0-2C_{11}+C_{12})(Z,f,G^0) + s_{\beta-\alpha}(-C_0-C_{11}+2C_{12})(G^0,f,Z) \\
&\qquad + \xi_f c_{\beta-\alpha}(-2C_0-2C_{11}+C_{12})(Z,f,A) + \xi_f c_{\beta-\alpha}(-C_0-C_{11}+2C_{12})(A,f,Z)\Big], \qquad \text{(D.37)}
\end{aligned}
$$

$$
\begin{aligned}
16\pi^2\left(\frac{m_f}{v}\right)^{-1} F^{PT}_{hff} &= \frac{g^2}{4}\Big[s_{\beta-\alpha}(2C_0+2C_{11}-C_{12})(W,f',G^\pm) - s_{\beta-\alpha}(C_0+C_{11}-2C_{12})(G^\pm,f',W) \\
&- \xi_f c_{\beta-\alpha}(-2C_0-2C_{11}+C_{12})(W,f',H^\pm) - \xi_f c_{\beta-\alpha}(C_0+C_{11}-2C_{12})(H^\pm,f',W)\Big] \\
&- g_Z^2 I_f v_f\Big[s_{\beta-\alpha}(-2C_0-2C_{11}+C_{12})(Z,f,G^0) + s_{\beta-\alpha}(C_0+C_{11}-2C_{12})(G^0,f,Z) \\
&+ \xi_f c_{\beta-\alpha}(-2C_0-2C_{11}+C_{12})(Z,f,A) + \xi_f c_{\beta-\alpha}(C_0+C_{11}-2C_{12})(A,f,Z)\Big], \qquad \text{(D.38)}
\end{aligned}
$$

where

$$
\begin{aligned}
&C^{FSF}_{hff}(X,Y,Z) \equiv \\
&[m_F^2 C_0 + p_1^2(C_{11}+C_{21}) + p_2^2(C_{12}+C_{22}) + 2p_1\cdot p_2(C_{12}+C_{23}) + 4C_{24}](X,Y,Z) - \frac{1}{2}, \\
&C^{VFS}_{hff}(X,Y,Z) \equiv \\
&[p_1^2(2C_0+3C_{11}+C_{21}) + p_2^2(2C_{12}+C_{22}) + 2p_1\cdot p_2(2C_0+2C_{11}+C_{12}+C_{23}) + 4C_{24}](X,Y,Z) - \frac{1}{2}, \\
&C^{SFV}_{hff}(X,Y,Z) \equiv [p_1^2(C_{21}-C_0) + p_2^2(C_{22}-C_{12}) + 2p_1\cdot p_2(C_{23}-C_{12}) + 4C_{24}](X,Y,Z) - \frac{1}{2}.
\end{aligned}
\tag{D.39}
$$

The 1PI diagram contributions to the form factors of the hZZ and hWW vertices which are defined in Eq. (7.73) are calculated as

$$
\begin{aligned}
&\Gamma^{1,1\mathrm{PI}}_{hZZ}(p_1^2,p_2^2,q^2)_F = \sum_f \frac{m_f^2 m_Z^2 N_c^f}{\pi^2 v^3}\Bigg\{(v_f^2+a_f^2)\Big[B_0(p_1^2,f,f) + B_0(p_2^2,f,f) + 2B_0(q^2,f,f) \\
&+ (4m_f^2 - p_1^2 - p_2^2)C_0(f,f,f) - 8C_{24}(f,f,f)\Big] \\
&- (v_f^2-a_f^2)\Big[B_0(p_2^2,f,f) + B_0(p_1^2,f,f) + (4m_f^2-q^2)C_0(f,f,f)\Big]\Bigg\},
\end{aligned}
\tag{D.40}
$$

$$
\begin{aligned}
&\Gamma^{2,1\mathrm{PI}}_{hZZ}(p_1^2,p_2^2,q^2)_F = -\sum_f \frac{2m_f^2 m_Z^4 N_c^f}{\pi^2 v^3} \\
&\Big[(v_f^2+a_f^2)(4C_{23}+3C_{12}+C_{11}+C_0) + (v_f^2-a_f^2)(C_{12}-C_{11})\Big](f,f,f),
\end{aligned}
\tag{D.41}
$$

$$
\Gamma^{3,1\mathrm{PI}}_{hZZ}(p_1^2,p_2^2,q^2)_F = \sum_f \frac{4m_f^2 m_Z^4 N_c^f}{\pi^2 v^3} v_f a_f (C_{11}+C_{12}+C_0)(f,f,f),
\tag{D.42}
$$

$$
\begin{aligned}
&\Gamma^{1,1\mathrm{PI}}_{hWW}(p_1^2,p_2^2,q^2)_F = \sum_{f,f'} \frac{m_W^2 m_f^2 N_c^f}{4\pi^2 v^3}\Bigg[\frac{1}{2}B_0(p_2^2,f,f') + B_0(q^2,f,f) + \frac{1}{2}B_0(p_1^2,f,f') \\
&- 4C_{24}(p_1^2,p_2^2,q^2,f,f',f) + \frac{1}{2}(2m_f^2+2m_{f'}^2-p_1^2-p_2^2)C_0(f,f',f)\Bigg] + (m_f \leftrightarrow m_{f'}),
\end{aligned}
\tag{D.43}
$$

$$
\Gamma^{2,1\mathrm{PI}}_{hWW}(p_1^2,p_2^2,q^2)_F = \frac{-m_W^4 m_f^2 N_c^f}{4\pi^2 v^3}(4C_{23}+3C_{12}+C_{11}+C_0)(f,f',f) + (m_f \leftrightarrow m_{f'}),
\tag{D.44}
$$

$$
\Gamma^{3,1\mathrm{PI}}_{hWW}(p_1^2,p_2^2,q^2)_F = \frac{-m_W^4 m_f^2 N_c^f}{4\pi^2 v^3}(C_{11}+C_{12}+C_0)(f,f',f) + (m_f \leftrightarrow m_{f'}),
\tag{D.45}
$$

$$
\begin{aligned}
&16\pi^2\Gamma^{1,1\mathrm{PI}}_{hZZ}(p_1^2,p_2^2,q^2)_B = 2g_Z^2\lambda_{G^+G^-h}m_W^2s_W^4C_0(G^\pm,W,G^\pm)\\
&+g^3m_Ws_{\beta-\alpha}\Big\{2c_W^2C^{VVV}_{hVV1}(W,W,W)-2c_W^2C_{24}(c^\pm,c^\pm,c^\pm)+s_W^2C^{SVV}_{hVV1}(G^\pm,W,W)+s_W^2C^{VVS}_{hVV1}(W,W,G^\pm)\\
&\qquad -2\frac{s_W^4}{c_W^2}m_W^2s_{\beta-\alpha}C_0(W,G^\pm,W)-(c_W^2-s_W^2)\frac{s_W^2}{c_W^2}[C_{24}(W,G^\pm,G^\pm)+C_{24}(G^\pm,G^\pm,W)]\Big\}\\
&+\frac{g_Z^3}{2}m_Zs_{\beta-\alpha}\Big\{-2m_Z^2\left[s_{\beta-\alpha}^2C_0(Z,h,Z)+c_{\beta-\alpha}^2C_0(Z,H,Z)\right]+s_{\beta-\alpha}^2[C_{24}(G^0,h,Z)+C_{24}(Z,h,G^0)]\\
&+c_{\beta-\alpha}^2\left[C_{24}(A,h,Z)+C_{24}(Z,h,A)+C_{24}(G^0,H,Z)+C_{24}(Z,H,G^0)-C_{24}(A,H,Z)-C_{24}(Z,H,A)\right]\Big\}\\
&+2g_Z^2m_Z^2\Big\{3\lambda_{hhh}s_{\beta-\alpha}^2C_0(h,Z,h)+\lambda_{HHh}c_{\beta-\alpha}^2C_0(H,Z,H)+\lambda_{Hhh}s_{\beta-\alpha}c_{\beta-\alpha}[C_0(H,Z,h)+C_0(h,Z,H)]\Big\}\\
&-2g_Z^2(c_W^2-s_W^2)^2\left[\lambda_{G^+G^-h}C_{24}(G^\pm,G^\pm,G^\pm)+\lambda_{H^+H^-h}C_{24}(H^\pm,H^\pm,H^\pm)\right]\\
&-2g_Z^2s_{\beta-\alpha}^2\Big[3\lambda_{hhh}C_{24}(h,G^0,h)+\lambda_{HHh}C_{24}(H,A,H)+\lambda_{GGh}C_{24}(G^0,h,G^0)+\lambda_{AAh}C_{24}(A,H,A)\Big]\\
&-2g_Z^2c_{\beta-\alpha}^2\Big[3\lambda_{hhh}C_{24}(h,A,h)+\lambda_{HHh}C_{24}(H,G^0,H)+\lambda_{AAh}C_{24}(A,h,A)+\lambda_{GGh}C_{24}(G^0,H,G^0)\Big]\\
&-2g_Z^2s_{\beta-\alpha}c_{\beta-\alpha}\lambda_{Hhh}[C_{24}(h,G^0,H)+C_{24}(H,G^0,h)-C_{24}(h,A,H)-C_{24}(H,A,h)]\\
&-2g_Z^2s_{\beta-\alpha}c_{\beta-\alpha}\lambda_{AGh}[C_{24}(A,h,G^0)+C_{24}(G^0,h,A)-C_{24}(A,H,G^0)-C_{24}(G^0,H,A)]\\
&+\frac{g_Z^2}{2}\lambda_{G^+G^-h}(c_W^2-s_W^2)^2B_0(q^2,G^\pm,G^\pm)+\frac{g_Z^2}{2}\lambda_{H^+H^-h}(c_W^2-s_W^2)^2B_0(q^2,H^\pm,H^\pm)\\
&+\frac{g_Z^2}{2}\lambda_{GGh}B_0(q^2,G^0,G^0)+\frac{g_Z^2}{2}\lambda_{AAh}B_0(q^2,A,A)+\frac{g_Z^2}{2}\lambda_{HHh}B_0(q^2,H,H)+\frac{3g_Z^2}{2}\lambda_{hhh}B_0(q^2,h,h)\\
&-g^3\frac{s_W^4}{c_W^2}m_Ws_{\beta-\alpha}[B_0(p_2^2,W,G^\pm)+B_0(p_1^2,G^\pm,W)]-\frac{g_Z^3}{2}m_Zs_{\beta-\alpha}[B_0(p_1^2,h,Z)+B_0(p_2^2,h,Z)]\\
&-6g^3c_W^2m_Ws_{\beta-\alpha}B_0(q^2,W,W)+4g^3c_W^2m_Ws_{\beta-\alpha},
\end{aligned}
\tag{D.46}
$$

$$
\begin{aligned}
&16\pi^2(g_Z^2m_Z^2)^{-1}\Gamma^{2,1\mathrm{PI}}_{hZZ}(p_1^2,p_2^2,q^2)_B = 2gm_Wc_W^4s_{\beta-\alpha}C^{VVV}_{hVV2}(W,W,W)-2gc_W^4m_Ws_{\beta-\alpha}C_{1223}(c^\pm,c^\pm,c^\pm)\\
&+gm_Ws_W^2c_W^2s_{\beta-\alpha}[C^{SVV}_{hVV2}(G^\pm,W,W)+C^{VVS}_{hVV2}(W,W,G^\pm)]\\
&-gm_W(c_W^2-s_W^2)s_W^2[C^{SSV}_{hVV2}(G^\pm,G^\pm,W)+C^{VSS}_{hVV2}(W,G^\pm,G^\pm)]\\
&+\frac{g_Z}{2}m_Z[C^{VSS}_{hVV2}(Z,h,G^0)+C^{VSS}_{hVV2}(G^0,h,Z)]\\
&+\frac{g_Z}{2}m_Zs_{\beta-\alpha}^3[C^{VSS}_{hVV2}(Z,h,G^0)+C^{SSV}_{hVV2}(G^0,h,Z)]\\
&+\frac{g_Z}{2}m_Zs_{\beta-\alpha}c_{\beta-\alpha}^2[C^{VSS}_{hVV2}(Z,h,A)+C^{VSS}_{hVV2}(Z,H,G^0)-C^{VSS}_{hVV2}(Z,H,A)\\
&\qquad +C^{SSV}_{hVV2}(A,h,Z)+C^{SSV}_{hVV2}(G^0,H,Z)-C^{SSV}_{hVV2}(A,H,Z)]\\
&-2(c_W^2-s_W^2)^2\left[\lambda_{G^+G^-h}C_{1223}(G^\pm,G^\pm,G^\pm)+\lambda_{H^+H^-h}C_{1223}(H^\pm,H^\pm,H^\pm)\right]\\
&-2s_{\beta-\alpha}^2\Big[3\lambda_{hhh}C_{1223}(h,G^0,h)+\lambda_{HHh}C_{1223}(H,A,H)+\lambda_{GGh}C_{1223}(G^0,h,G^0)+\lambda_{AAh}C_{1223}(A,H,A)\Big]\\
&-2c_{\beta-\alpha}^2\Big[3\lambda_{hhh}C_{1223}(h,A,h)+\lambda_{HHh}C_{1223}(H,G^0,H)+\lambda_{AAh}C_{1223}(A,h,A)+\lambda_{GGh}C_{1223}(G^0,H,G^0)\Big]\\
&-2s_{\beta-\alpha}c_{\beta-\alpha}\lambda_{Hhh}[C_{1223}(h,G^0,H)+C_{1223}(H,G^0,h)-C_{1223}(h,A,H)-C_{1223}(H,A,h)]\\
&-2s_{\beta-\alpha}c_{\beta-\alpha}\lambda_{AGh}[C_{1223}(A,h,G^0)+C_{1223}(G^0,h,A)-C_{1223}(A,H,G^0)-C_{1223}(G^0,H,A)],
\end{aligned}
\tag{D.47}
$$

$$
\Gamma^{3,1\mathrm{PI}}_{hZZ}(p_1^2,p_2^2,q^2)_B = 0, \tag{D.48}
$$

$$
\begin{aligned}
&16\pi^2\Gamma^{1,1\mathrm{PI}}_{hWW}(p_1^2,p_2^2,q^2)_B = \\
&g^3 m_W s_{\beta-\alpha}[C^{VVV}_{hVV1}(Z,W,Z) + c_W^2 C^{VVV}_{hVV1}(W,Z,W) + s_W^2 C^{VVV}_{hVV1}(W,\gamma,W) \\
&\qquad - C_{24}(c_Z,c^\pm,c_Z) - c_W^2 C_{24}(c^\pm,c_Z,c^\pm) - s_W^2 C_{24}(c^\pm,c_\gamma,c^\pm)] \\
&-\frac{g^3}{2} m_W s_W^2 s_{\beta-\alpha}[C^{SVV}_{hVV1}(G^\pm,Z,W) - C^{SVV}_{hVV1}(G^\pm,\gamma,W) + C^{VVS}_{hVV1}(W,Z,G^\pm) - C^{VVS}_{hVV1}(W,\gamma,G^\pm)] \\
&- g^3 m_W^3 \frac{s_W^4}{c_W^4} s_{\beta-\alpha} C_0(Z,G^\pm,Z) - g^3 m_W^3 s_{\beta-\alpha}^3 C_0(W,h,W) - g m_W^3 s_{\beta-\alpha} c_{\beta-\alpha}^2 C_0(W,H,W) \\
&+ g^2 \frac{s_W^4}{c_W^2} m_W^2 \lambda_{G^+G^-h} C_0(G^\pm,Z,G^\pm) + s_W^2 m_W^2 \lambda_{G^+G^-h} C_0(G^\pm,\gamma,G^\pm) \\
&+ 6g^2 \lambda_{hhh} m_W^2 s_{\beta-\alpha}^2 C_0(h,W,h) + 2g^2 \lambda_{HHh} m_W^2 c_{\beta-\alpha}^2 C_0(H,W,H) \\
&+ 2g^2 \lambda_{Hhh} m_W^2 c_{\beta-\alpha} s_{\beta-\alpha}[C_0(h,W,H) + C_0(H,W,h)] \\
&+ \frac{g^3}{2} m_W s_{\beta-\alpha}\Big\{ s_{\beta-\alpha}^2[C_{24}(W,h,G^\pm) + C_{24}(G^\pm,h,W)] \\
&\qquad + c_{\beta-\alpha}^2[C_{24}(W,H,G^\pm) + C_{24}(G^\pm,H,W) + C_{24}(W,h,H^\pm) + C_{24}(H^\pm,h,W) \\
&\qquad\qquad - C_{24}(W,H,H^\pm) - C_{24}(H^\pm,H,W)]\Big\} \\
&+ \frac{g^3}{2} m_W \frac{s_W^2}{c_W^2} s_{\beta-\alpha}[C_{24}(G^0,G^\pm,Z) + C_{24}(Z,G^\pm,G^0)] \\
&- g^2\Big[\lambda_{G^+G^-h} C_{24}(G^\pm,G^0,G^\pm) + \lambda_{H^+H^-h} C_{24}(H^\pm,A,H^\pm) \\
&\qquad + 2\lambda_{GGh} C_{24}(G^0,G^\pm,G^0) + 2\lambda_{AAh} C_{24}(A,H^\pm,A)\Big] \\
&- g^2 s_{\beta-\alpha}^2\Big[6\lambda_{hhh} C_{24}(h,G^\pm,h) + 2\lambda_{HHh} C_{24}(H,H^\pm,H) \\
&\qquad + \lambda_{G^+G^-h} C_{24}(G^\pm,h,G^\pm) + \lambda_{H^+H^-h} C_{24}(H^\pm,H,H^\pm)\Big] \\
&- g^2 c_{\beta-\alpha}^2\Big[6\lambda_{hhh} C_{24}(h,H^\pm,h) + 2\lambda_{HHh} C_{24}(H,G^\pm,H) \\
&\qquad + \lambda_{G^+G^-h} C_{24}(G^\pm,H,G^\pm) + \lambda_{H^+H^-h} C_{24}(H^\pm,h,H^\pm)\Big] \\
&- g^2 \lambda_{H^+G^-h} s_{\beta-\alpha} c_{\beta-\alpha}[C_{24}(G^\pm,h,H^\pm) + C_{24}(H^\pm,h,G^\pm) - C_{24}(G^\pm,H,H^\pm) - C_{24}(H^\pm,H,G^\pm)] \\
&- 2g^2 \lambda_{Hhh} s_{\beta-\alpha} c_{\beta-\alpha}[C_{24}(h,G^\pm,H) + C_{24}(H,G^\pm,h) - C_{24}(h,H^\pm,H) - C_{24}(H,H^\pm,h)] \\
&- g^3 m_W s_{\beta-\alpha}\Big[3B_0(q^2,W,W) + 3B_0(q^2,Z,Z) - 4\Big] \\
&+ \frac{g^2}{2}\lambda_{G^+G^-h} B_0(q^2,G^\pm,G^\pm) + \frac{g^2}{2}\lambda_{GGh} B_0(q^2,G^0,G^0) + \frac{3g^2}{2}\lambda_{hhh} B_0(q^2,h,h) \\
&+ \frac{g^2}{2}\lambda_{H^+H^-h} B_0(q^2,H^\pm,H^\pm) + \frac{g^2}{2}\lambda_{AAh} B_0(q^2,A,A) + \frac{g^2}{2}\lambda_{HHh} B_0(q^2,H,H) \\
&- \frac{g^3}{2} m_W s_{\beta-\alpha}\Big\{ B_0(p_1^2,W,h) + B_0(p_2^2,W,h) + \frac{s_W^4}{c_W^2}[B_0(p_1^2,Z,G^\pm) + B_0(p_2^2,Z,G^\pm)] \\
&\qquad + s_W^2[B_0(p_1^2,\gamma,G^\pm) + B_0(p_2^2,\gamma,G^\pm)]\Big\}, \qquad \text{(D.49)}
\end{aligned}
$$

$$
\begin{aligned}
&16\pi^2(g^2m_W^2)^{-1}\Gamma^{2,1\mathrm{PI}}_{hWW}(p_1^2,p_2^2,q^2)_B = \\
&gm_W s_{\beta-\alpha}\Big[C^{VVV}_{hVV2}(Z,W,Z)+c_W^2C^{VVV}_{hVV2}(W,Z,W)+s_W^2C^{VVV}_{hVV2}(W,\gamma,W) \\
&\qquad -C_{1223}(c_Z,c^\pm,c_Z)-c_W^2C_{1223}(c^\pm,c_Z,c^\pm)-s_W^2C_{1223}(c^\pm,c_\gamma,c^\pm)\Big] \\
&-\frac{g}{2}s_W^2m_Ws_{\beta-\alpha}[C^{SVV}_{hVV2}(G^\pm,Z,W)-C^{SVV}_{hVV2}(G^\pm,\gamma,W)+C^{VVS}_{hVV2}(W,Z,G^\pm)-C^{VVS}_{hVV2}(W,\gamma,G^\pm)] \\
&+\frac{g}{2}m_Ws_{\beta-\alpha}^3\Big[C^{VSS}_{hVV2}(W,h,G^\pm)+C^{SSV}_{hVV2}(G^\pm,h,W)\Big] \\
&+\frac{g}{2}m_Ws_{\beta-\alpha}c_{\beta-\alpha}^2\Big[C^{VSS}_{hVV2}(W,H,G^\pm)+C^{VSS}_{hVV2}(W,h,H^\pm)-C^{VSS}_{hVV2}(W,H,H^\pm) \\
&\qquad +C^{SSV}_{hVV2}(G^\pm,H,W)+C^{SSV}_{hVV2}(H^\pm,h,W)-C^{SSV}_{hVV2}(H^\pm,H,W)\Big] \\
&+\frac{g}{2}\frac{s_W^2}{c_W^2}m_Ws_{\beta-\alpha}^3\Big[C^{VSS}_{hVV2}(Z,G^\pm,G^0)+C^{SSV}_{hVV2}(G^0,G^\pm,Z)\Big] \\
&-\Big[\lambda_{G^+G^-h}C_{1223}(G^\pm,G^0,G^\pm)+\lambda_{H^+H^-h}C_{1223}(H^\pm,A,H^\pm) \\
&\qquad +2\lambda_{GGh}C_{1223}(G^0,G^\pm,G^0)+2\lambda_{AAh}C_{1223}(A,H^\pm,A)\Big] \\
&-s_{\beta-\alpha}^2\Big[6\lambda_{hhh}C_{1223}(h,G^\pm,h)+2\lambda_{HHh}C_{1223}(H,H^\pm,H) \\
&\qquad +\lambda_{G^+G^-h}C_{1223}(G^\pm,h,G^\pm)+\lambda_{H^+H^-h}C_{1223}(H^\pm,H,H^\pm)\Big] \\
&-c_{\beta-\alpha}^2\Big[6\lambda_{hhh}C_{1223}(h,H^\pm,h)+2\lambda_{HHh}C_{1223}(H,G^\pm,H) \\
&\qquad +\lambda_{G^+G^-h}C_{1223}(G^\pm,H,G^\pm)+\lambda_{H^+H^-h}C_{1223}(H^\pm,h,H^\pm)\Big] \\
&-\lambda_{H^+G^-h}s_{\beta-\alpha}c_{\beta-\alpha}[C_{1223}(G^\pm,h,H^\pm)+C_{1223}(H^\pm,h,G^\pm)-C_{1223}(G^\pm,H,H^\pm)-C_{1223}(H^\pm,H,G^\pm)] \\
&-2\lambda_{Hhh}s_{\beta-\alpha}c_{\beta-\alpha}[C_{1223}(h,G^\pm,H)+C_{1223}(H,G^\pm,h)-C_{1223}(h,H^\pm,H)-C_{1223}(H,H^\pm,h)],
\end{aligned}
\tag{D.50}
$$

$$
\Gamma^{3,1\mathrm{PI}}_{hWW}(p_1^2,p_2^2,q^2)_B = 0, \tag{D.51}
$$

where

$$
\begin{aligned}
&C^{VVV}_{hVV1}(X,Y,Z) \equiv \\
&\left[18C_{24}+p_1^2(2C_{21}+3C_{11}+C_0)+p_2^2(2C_{22}+C_{12})+p_1\cdot p_2(4C_{23}+3C_{12}+C_{11}-4C_0)\right](X,Y,Z)-3, \\
&C^{SVV}_{hVV1}(X,Y,Z) \equiv \\
&\left[3C_{24}+p_1^2(C_{21}-C_0)+p_2^2(C_{22}-2C_{12}+C_0)+2p_1\cdot p_2(C_{23}-C_{11})\right](X,Y,Z)-\frac{1}{2}, \\
&C^{VVS}_{hVV1}(X,Y,Z) \equiv \\
&\left[3C_{24}+p_1^2(C_{21}+4C_{11}+4C_0)+p_2^2(C_{22}+2C_{12})+2p_1\cdot p_2(C_{23}+2C_{12}+C_{11}+2C_0)\right](X,Y,Z)-\frac{1}{2}, \\
&C^{VVV}_{hVV2}(X,Y,Z) \equiv (10C_{23}+9C_{12}+C_{11}+5C_0)(X,Y,Z), \\
&C^{SVV}_{hVV2}(X,Y,Z) \equiv (4C_{11}-3C_{12}-C_{23})(X,Y,Z), \\
&C^{VVS}_{hVV2}(X,Y,Z) \equiv (2C_{11}-5C_{12}-2C_0-C_{23})(X,Y,Z), \\
&C^{VSS}_{hVV2}(X,Y,Z) \equiv (C_{23}+C_{12}+2C_{11}+2C_0)(X,Y,Z), \\
&C^{SSV}_{hVV2}(X,Y,Z) \equiv (C_{23}-C_{12})(X,Y,Z), \\
&C_{1223}(X,Y,Z) \equiv (C_{12}+C_{23})(X,Y,Z).
\end{aligned}
\tag{D.52}
$$

D.2 1PI diagrams in the HSM

D.2.1 One point functions

The 1PI tadpole contributions are calculated by

$$16\pi^2 T_h^{\mathrm{1PI},F} = -\sum_f 4\frac{m_f^2}{v} c_\alpha N_c^f A(m_f), \tag{D.53}$$

$$16\pi^2 T_H^{\mathrm{1PI},F} = -\sum_f 4\frac{m_f^2}{v} s_\alpha N_c^f A(m_f), \tag{D.54}$$

$$\begin{aligned} 16\pi^2 T_h^{\mathrm{1PI},B} &= -3\lambda_{hhh} A(m_h) - \lambda_{hHH} A(m_H) - \lambda_{hG^+G^-} A(m_{G^\pm}) - \lambda_{hG^0G^0} A(m_{G^0}) \\ &\quad - g m_W c_\alpha A(m_{c^\pm}) - \frac{g_Z m_Z}{2} c_\alpha A(m_{c^0}) + \frac{2m_W^2}{v} c_\alpha DA(m_W) + \frac{m_Z^2}{v} c_\alpha DA(m_Z), \end{aligned} \tag{D.55}$$

$$\begin{aligned} 16\pi^2 T_H^{\mathrm{1PI},B} &= -\lambda_{hhH} A(m_h) - 3\lambda_{HHH} A(m_H) - \lambda_{HG^+G^-} A(m_{G^+}) - \lambda_{Hzz} A(m_{G^0}) \\ &\quad - g m_W s_\alpha A(m_{c^\pm}) - \frac{g_Z m_Z}{2} s_\alpha A(m_{c^0}) + \frac{2m_W^2}{v} s_\alpha DA(m_W) + \frac{m_Z^2}{v} s_\alpha DA(m_Z), \end{aligned} \tag{D.56}$$

where $D = 4 - 2\epsilon$ and N_c^f indicates the color number of each particle.

D.2.2 Two point functions

The 1PI diagram contributions to the scalar boson two point functions are expressed as

$$16\pi^2 \Pi_{hh}^{\mathrm{1PI},F}[p^2] = -2\sum_f \left(\frac{m_f}{v} c_\alpha\right)^2 N_c^f \left\{2A(m_f) - (p^2 - 4m_f^2) B_0(p^2; m_f, m_f)\right\}, \tag{D.57}$$

$$16\pi^2 \Pi_{Hh}^{\mathrm{1PI},F}[p^2] = -2\sum_f \left(\frac{m_f}{v}\right)^2 c_\alpha s_\alpha N_c^f \left\{2A(m_f) - (p^2 - 4m_f^2) B_0(p^2; m_f, m_f)\right\}, \tag{D.58}$$

$$16\pi^2 \Pi_{HH}^{\mathrm{1PI},F}[p^2] = -2\sum_f \left(\frac{m_f}{v} s_\alpha\right)^2 N_c^f \left\{2A(m_f) - (p^2 - 4m_f^2) B_0(p^2; m_f, m_f)\right\}, \tag{D.59}$$

$$
\begin{aligned}
16\pi^2\Pi_{hh}^{1\mathrm{PI},B}[p^2] &= -2\lambda_{hhHH}A(m_H) - 12\lambda_{hhhh}A(m_h) - 2\lambda_{hhG^+G^-}A(m_{G^\pm}) \\
&\quad - 2\lambda_{hhG^0G^0}A(m_{G^0}) + 2\frac{m_W^2}{v^2}c_\alpha^2 DA(m_W) + \frac{m_Z^2}{v^2}c_\alpha^2 DA(m_Z) \\
&\quad + \lambda_{hG^+G^-}^2 B_0(p^2; m_{G^+}, m_{G^-}) + 2\lambda_{hHH}^2 B_0(p^2; m_H, m_H) \\
&\quad + 18\lambda_{hhh}^2 B_0(p^2; m_h, m_h) + 4\lambda_{hhH}^2 B_0(p^2; m_h, m_H) \\
&\quad + 2\lambda_{hG^0G^0}^2 B_0(p^2; m_{G^0}, m_{G^0}) + \frac{4m_W^4}{v^2}c_\alpha^2 DB_0(p^2; m_W, m_W) \\
&\quad + \frac{2m_Z^4}{v^2}c_\alpha^2 DB_0(p^2; m_Z, m_Z) \\
&\quad - \frac{2m_W^2}{v^2}c_\alpha^2\left\{2A(m_W) - A(m_{G^\pm}) + (2p^2 - m_W^2 + 2m_{G^\pm}^2)B_0(p^2; m_W, m_{G^\pm})\right\} \\
&\quad - \frac{m_Z^2}{v^2}c_\alpha^2\left\{2A(m_Z) - A(m_{G^0}) + (2p^2 - m_Z^2 + 2m_{G^0}^2)B_0(p^2; m_Z, m_{G^0})\right\} \\
&\quad - \frac{2m_W^4}{v^2}c_\alpha^2 B_0(p^2; m_{c^\pm}, m_{c^\pm}) - \frac{m_Z^4}{v^2}c_\alpha^2 B_0(p^2; m_{c^0}, m_{c^0}), \qquad \text{(D.60)} \\
16\pi^2\Pi_{Hh}^{1\mathrm{PI},B}[p^2] &= -\lambda_{hHG^+G^-}A(m_{G^\pm}) - 3\lambda_{hHHH}A(m_H) - 3\lambda_{hhhH}A(m_h) - \lambda_{hHG^0G^0}A(m_{G^0}) \\
&\quad + 4D\frac{m_W^2}{v^2}s_\alpha c_\alpha A(m_W^2) + 2D\frac{m_Z^2}{v^2}s_\alpha c_\alpha A(m_Z^2) \\
&\quad + \lambda_{hG^+G^-}\lambda_{HG^+G^-}B_0(p^2; m_{G^\pm}, m_{G^\pm}) + 6\lambda_{hHH}\lambda_{HHH}B_0(p^2; m_H, m_H) \\
&\quad + 4\lambda_{hhH}\lambda_{hHH}B_0(p^2; m_h, m_H) + 6\lambda_{hhh}\lambda_{hhH}B_0(p^2; m_h, m_h) \\
&\quad + 2\lambda_{hG^0G^0}\lambda_{HG^0G^0}B_0(p^2; m_{G^0}, m_{G^0}) \\
&\quad + \frac{4m_W^4}{v^2}s_\alpha c_\alpha DB_0(p^2; m_W, m_W) + \frac{2m_Z^4}{v^2}s_\alpha c_\alpha DB_0(p^2; m_Z, m_Z) \\
&\quad - \frac{2m_W^2}{v^2}s_\alpha c_\alpha\left\{2A(m_W) - A(m_{G^\pm}) + (2p^2 - m_W^2 + 2m_{G^\pm}^2)B_0(p^2; m_W, m_{G^\pm}))\right\} \\
&\quad - \frac{m_Z^2}{v^2}s_\alpha c_\alpha\left\{2A(m_Z) - A(m_{G^0}) + (2p^2 - m_Z^2 + 2m_{G^0}^2)B_0(p^2; m_Z, m_{G^0}))\right\} \\
&\quad - 2\frac{m_W^4}{v^2}s_\alpha c_\alpha B_0(p^2; m_{c^\pm}, m_{c^\pm}) - \frac{m_Z^4}{v^2}s_\alpha c_\alpha B_0(p^2; m_{c^0}, m_{c^0}), \qquad \text{(D.61)} \\
16\pi^2\Pi_{HH}^{1\mathrm{PI},B}[p^2] &= -12\lambda_{HHHH}A(m_H) - 2\lambda_{hhHH}A(m_h) - 2\lambda_{HHG^+G^-}A(m_{G^\pm}) \\
&\quad - 2\lambda_{HHG^0G^0}A(m_{G^0}) + 2\frac{m_W^2}{v^2}s_\alpha^2 DA(m_W) + \frac{m_Z^2}{v^2}s_\alpha^2 DA(m_Z) \\
&\quad + \lambda_{HG^+G^-}^2 B_0(p^2; m_{G^\pm}, m_{G^\pm}) + 18\lambda_{HHH}^2 B_0(p^2; m_H, m_H) \\
&\quad + 2\lambda_{hhH}^2 B_0(p^2; m_h, m_h) + 4\lambda_{hHH}^2 B_0(p^2; m_h, m_H) \\
&\quad + 2\lambda_{HG^0G^0}^2 B_0(p^2; m_{G^0}, m_{G^0}) + \frac{4m_W^4}{v^2}s_\alpha^2 DB_0(p^2; m_W, m_W) \\
&\quad + \frac{2m_Z^4}{v^2}s_\alpha^2 DB_0(p^2; m_Z, m_Z) \\
&\quad - \frac{2m_W^2}{v^2}s_\alpha^2\left\{2A(m_W) - A(m_{G^\pm}) + (2p^2 - m_W^2 + 2m_{G^\pm}^2)B_0(p^2; m_W, m_{G^\pm})\right\} \\
&\quad - \frac{m_Z^2}{v^2}s_\alpha^2\left\{2A(m_Z) - A(m_{G^0}) + (2p^2 - m_Z^2 + 2m_{G^0}^2)B_0(p^2; m_Z, m_{G^0})\right\} \\
&\quad - \frac{2m_W^4}{v^2}s_\alpha^2 B_0(p^2; m_{c^\pm}, m_{c^\pm}) - \frac{m_Z^4}{v^2}s_\alpha^2 B_0(p^2; m_{c^0}, m_{c^0}). \qquad \text{(D.62)}
\end{aligned}
$$

The fermion loop contributions to the gauge boson two point functions are calculated as

$$16\pi^2\Pi_{WW}^{\rm 1PI,F}[p^2] = \sum_f \frac{4m_W^2 N_c^f}{v^2}\left[-B_4 + 2p^2 B_3\right](p^2; m_f, m_{f'}), \tag{D.63}$$

$$16\pi^2\Pi_{ZZ}^{\rm 1PI,F}[p^2] = \sum_f \frac{4m_Z^2 N_c^f}{v^2}\left[2p^2(4s_W^4 Q_f^2 - 4s_W^2 Q_f I_f + 2I_f^2)B_3 - 2I_f^2 m_f^2 B_0\right](p^2; m_f, m_f), \tag{D.64}$$

$$16\pi^2\Pi_{\gamma Z}^{\rm 1PI,F}[p^2] = -\sum_f \frac{4em_Z N_c^f}{v} p^2(-4s_W^2 Q_f^2 + 2I_f Q_f)B_3(p^2; m_f, m_f), \tag{D.65}$$

$$16\pi^2\Pi_{\gamma\gamma}^{\rm 1PI,F}[p^2] = \sum_f 8e^2 N_c^f Q_f^2 p^2 B_3(p^2; m_f, m_f), \tag{D.66}$$

where $B_3(p^2; m_1, m_2) = -B_1(p^2; m_1, m_2) - B_{21}(p^2; m_1, m_2)$ and $B_4(p^2; m_1, m_2) = -m_1^2 B_1(p^2; m_2, m_1) - m_2^2 B_2(p^2; m_1, m_2)$ defined in Ref. [112] and Q_f is the electric charge of a fermion f. The boson loop contributions to the gauge boson two point functions are calculated as

$$\begin{aligned}
16\pi^2\Pi_{WW}^{\rm 1PI,B}[p^2] = \frac{m_W^2}{v^2}\Bigg[& s_\alpha^2 B_5(p^2, m_{G^\pm}, m_H) + 4s_\alpha^2 m_W^2 B_0(p^2, m_W, m_H) \\
& + 4c_\alpha^2 m_W^2 B_0(p^2; m_W, m_h) + c_\alpha^2 B_5(p^2; m_{G^\pm}, m_h) \\
& - 4\left\{(8c_W^2 p^2 - (1-4s_W^2)m_W^2 - m_Z^2)B_0 - (\frac{9}{4} - 2s_W^2)B_5\right\}(p^2; m_W, m_Z) \\
& - 4\left\{2s_W^2\Big[(4p^2 - 2m_W^2)B_0 - B_5\Big](p^2; m_W, m_\gamma) + \frac{2p^2}{3}\right\}\Bigg],
\end{aligned} \tag{D.67}$$

$$\begin{aligned}
16\pi^2\Pi_{ZZ}^{\rm 1PI,B}[p^2] = \frac{m_Z^2}{v^2}\Bigg[& s_\alpha^2 B_5(p^2, m_H, m_{G^0}) + 4s_\alpha^2 m_Z^2 B_0(p^2; m_Z, m_H) \\
& + 4c_\alpha^2 m_Z^2 B_0(p^2; m_Z, m_h) + c_\alpha^2 B_5(p^2; m_{G^0}, m_h) \\
& - 4\left[\left(\frac{23}{4}p^2 - 2m_W^2\right)B_0 + 9p^2 B_3\right](p^2; m_W, m_W) \\
& - 4\frac{2p^2}{3} + 8s_W^2 p^2\left[\frac{11}{2}B_0 + 10B_3\right](p^2; m_W, m_W) + \frac{16s_W^2 p^2}{3} \\
& - 4s_W^4 p^2\left[5B_0 + 12B_3\right](p^2; m_W, m_W) - \frac{8s_W^4 p^2}{3}\Bigg],
\end{aligned} \tag{D.68}$$

$$\begin{aligned}
16\pi^2\Pi_{\gamma Z}^{\rm 1PI,B}[p^2] = -\frac{2em_Z}{v}p^2\Bigg\{ & \left[\frac{11}{2}B_0 + 10B_3\right](p^2; m_W, m_W) \\
& - s_W^2\left[5B_0 + 12B_3\right](p^2; m_W, m_W) + \frac{2}{3}(1 - s_W^2)\Bigg\},
\end{aligned} \tag{D.69}$$

$$16\pi^2\Pi_{\gamma\gamma}^{\rm 1PI,B}[p^2] = -e^2 p^2\left\{(5B_0 + 12B_3)(p^2; m_W, m_W) + \frac{2}{3}\right\}, \tag{D.70}$$

where $B_5(p^2; m_1, m_2) = A(m_1) + A(m_2) - 4B_{22}(p^2; m_1, m_2)$ [112].

Next, we give one-loop contributions to fermion two point functions, which are composed of following three kind parts,

$$\Pi^{\rm 1PI}_{ff}[p^2] = m_f \Pi^{\rm 1PI}_{ff,S}[p^2] + \not{p}\Pi^{\rm 1PI}_{ff,V}[p^2] - \not{p}\gamma_5 \Pi^{\rm 1PI}_{ff,A}[p^2]. \tag{D.71}$$

They are calculated as

$$\begin{aligned}
16\pi^2 \Pi^{\rm 1PI}_{ff,S}[p^2] &= -2\frac{m_Z^2}{v^2}(v_f^2 - a_f^2)(2B_0[p^2; m_f, m_Z] - 1) - 2(Q_f e)^2(2B_0[p^2; m_f, m_\gamma] - 1) \\
&\quad + \frac{m_f^2}{v^2} c_\alpha^2 B_0[p^2; m_f, m_h] + \frac{m_f^2}{v^2} s_\alpha^2 B_0[p^2; m_f, m_H] \\
&\quad - \frac{m_f^2}{v^2} B_0[p^2; m_f, m_{G^0}] - 2\frac{m_{f'}^2}{v^2} B_0[p^2; m_f, m_{G^\pm}],
\end{aligned} \tag{D.72}$$

$$\begin{aligned}
16\pi^2 \Pi^{\rm 1PI}_{ff,V}[p^2] &= -\frac{m_W^2}{v^2}(2B_1[p^2; m_{f'}, m_W] + 1) - \frac{m_Z^2}{v^2}(v_f^2 + a_f^2)(2B_1[p^2; m_f, m_Z] + 1) \\
&\quad - (Q_f e)^2(2B_1[p^2; m_f, m_\gamma] + 1) - \frac{m_f^2}{v^2} c_\alpha^2 B_1[p^2; m_f, m_h] - \frac{m_f^2}{v^2} s_\alpha^2 B_1[p^2; m_f, m_H] \\
&\quad - \frac{m_f^2}{v^2} B_1[p^2; m_f, m_{G^0}] - \frac{m_{f'}^2 + m_f^2}{v^2} B_1[p^2; m_f, m_{G^\pm}],
\end{aligned} \tag{D.73}$$

$$\begin{aligned}
16\pi^2 \Pi^{\rm 1PI}_{ff,A}[p^2] &= -\frac{m_f^2 - m_{f'}^2}{v^2} B_1[p^2; m_f, m_{G^\pm}] + \frac{m_W^2}{v^2}(2B_1[p^2; m_{f'}, m_W] + 1) \\
&\quad + 2\frac{m_Z^2}{v^2} v_f a_f (2B_1[p^2; m_f, m_Z] + 1),
\end{aligned} \tag{D.74}$$

where $v_f = I_f - 2s_W^2 Q_f$, $a_f = I_f$ and I_f represents the third component of the isospin of a fermion f; i.e., $I_f = +1/2$ $(-1/2)$ for $f = u$ (d, e).

D.2.3 Three point functions

In this subsection, we use the simplified form for the three point function of the Passarino-Veltman as $C_i[X, Y, Z] \equiv C_i[p_1^2, p_2^2, q^2; m_X, m_Y, m_Z]$. The 1PI diagram contributions for each

form factor of the hZZ and the hWW couplings defined in Eq. (6.27) are calculated as

$$M^{\mathrm{1PI},F}_{hZZ,1}[p_1^2,p_2^2,q^2] = \sum_f \frac{32m_Z^2m_f^2N_c^f}{16\pi^2v^3}c_\alpha\times$$
$$\Big[\Big(\frac{1}{2}I_f^2 - I_fQ_fs_W^2 + Q_f^2s_W^4\Big)\big(2p_1^2C_{21}+2p_2^2C_{22}+4p_1\cdot p_2C_{23}+2(D-2)C_{24}$$
$$+(3p_1^2+p_1\cdot p_2)C_{11}+(3p_1\cdot p_2+p_2^2)C_{12}+(p_1^2+p_1\cdot p_2)C_0\big)$$
$$+(I_fQ_fs_W^2-Q_f^2s_W^4)\big(p_1^2C_{21}+p_2^2C_{22}+2p_1\cdot p_2C_{23}+DC_{24}$$
$$+m_f^2C_0+(p_1^2+p_1\cdot p_2)C_{11}+(p_1\cdot p_2+p_2^2)C_{12}\big)\Big][f,f,f], \tag{D.75}$$

$$M^{\mathrm{1PI},F}_{hZZ,2}[p_1^2,p_2^2,q^2] = \sum_f \frac{4m_Z^2m_f^2N_c^f}{16\pi^2v^3}c_\alpha\times$$
$$\Big[(v_f^2+a_f^2)\big(4C_{23}+C_{11}+3C_{12}+C_0\big)+(v_f^2+a_f^2)\big(C_{12}-C_{11}\big)\Big][f,f,f], \tag{D.76}$$

$$M^{\mathrm{1PI},F}_{hZZ,3}[p_1^2,p_2^2,q^2] = -\sum_f \frac{8m_Z^2m_f^2N_c^f}{16\pi^2v^3}c_\alpha v_f a_f[C_{11}+C_{12}+C_0][f,f,f], \tag{D.77}$$

$$M^{\mathrm{1PI},F}_{hWW,1}[p_1^2,p_2^2,q^2] = \sum_f \frac{4m_W^2m_f^2N_c^f}{16\pi^2v^3}c_\alpha\Big[2p_1^2C_{21}+2p_2^2C_{22}+4p_1\cdot p_2C_{23}+(2D-4)C_{24}$$
$$+(3p_1^2+p_1\cdot p_2)C_{11}+(3p_1\cdot p_2+p_2^2)C_{12}+(p_1^2+p_1\cdot p_2)C_0\big)\Big][f,f',f], \tag{D.78}$$

$$M^{\mathrm{1PI},F}_{hWW,2}[p_1^2,p_2^2,q^2] = -\sum_f \frac{4m_W^2m_f^2N_c^f}{16\pi^2v^3}c_\alpha\big[4C_{23}+C_{11}+3C_{12}+C_0\big][f,f',f], \tag{D.79}$$

$$M^{\mathrm{1PI},F}_{hWW,3}[p_1^2,p_2^2,q^2] = -\sum_f \frac{4m_W^2m_f^2N_c^f}{16\pi^2v^3}c_\alpha[C_{11}+C_{12}+C_0][f,f',f], \tag{D.80}$$

$$
\begin{aligned}
&(16\pi^2)M^{1\mathrm{PI},B}_{hZZ,1}[p_1^2,p_2^2,q^2] = -2g^3 m_W c_W^2 c_\alpha (D-1) B_0[q^2;m_W,m_W] \\
&- g g_Z^2 m_W s_W^4 c_\alpha (B_0[p_1^2;m_W,m_{G^\pm}] + B_0[p_2^2;m_W,m_{G^\pm}) \\
&- \frac{g_Z^3 m_Z}{2} c_\alpha \left\{ c_\alpha^2 (B_0[p_1^2;m_Z,m_h] + B_0[p_2^2;m_Z,m_h]) + s_\alpha^2 (B_0[p_1^2;m_Z,m_H] + B_0[p_2^2;m_Z,m_H]) \right\} \\
&+ \frac{g_Z^2}{2} (c_{2W})^2 \lambda_{hG^+G^-} B_0[q^2;m_{G^+},m_{G^+}] + \frac{3g_Z^2}{2} c_\alpha^2 \lambda_{hhh} B_0[q^2;m_h,m_h] \\
&+ g_Z^2 c_\alpha s_\alpha \lambda_{hhH} B_0[q^2;m_h,m_H] + \frac{g_Z^2}{2} s_\alpha^2 \lambda_{hHH} B_0[q^2;m_H,m_H] + \frac{g_Z^2}{2} \lambda_{hG^0G^0} B_0[q^2;m_{G^0},m_{G^0}] \\
&+ 2g^3 m_W c_W^2 c_\alpha C^{hVV,1}_{VVV}[W,W,W] - 2g_Z^2 g m_W^3 s_W^4 c_\alpha C_0[W,G^\pm,W] \\
&+ g^3 m_W s_W^2 c_\alpha \Big\{ (C^{hVV,1}_{VVS}[W,W,G^\pm] + C^{hVV,1}_{SVV}[G^\pm,W,W]) \\
&- \frac{c_{2W}}{c_W^2} (C_{24}[W,G^\pm,G^\pm] + C_{24}[G^\pm,G^\pm,W]) \Big\} - g_Z^3 m_Z^3 c_\alpha \{ c_\alpha^2 C_0[Z,h,Z] + s_\alpha^2 C_0[Z,H,Z] \} \\
&+ \frac{g_Z^3}{2} m_Z c_\alpha \big\{ c_\alpha^2 (C_{24}[Z,h,G^0] + C_{24}[G^0,h,Z]) + s_\alpha^2 (C_{24}[Z,H,G^0] + C_{24}[G^0,H,Z]) \big\} \\
&+ 2g_Z^2 m_Z^2 \{ 3c_\alpha^2 \lambda_{hhh} C_0[h,Z,h] + s_\alpha^2 \lambda_{hHH} C_0[H,Z,H] \} \\
&+ 2\lambda_{hhH} g_Z^2 m_Z^2 c_\alpha s_\alpha \{ C_0[h,Z,H] + C_0[H,Z,h] \} - 2g^3 m_W c_W^2 c_\alpha C_{24}[c^\pm,c^\pm,c^\pm] \\
&+ 2g_Z^2 m_W^2 s_W^4 \lambda_{hG^+G^-} (m_W^2 s_W^4 C_0[G^\pm,W,G^\pm] - (c_{2W})^2 C_{24}[G^\pm,G^\pm,G^\pm]) \\
&- 2g_Z^2 \big\{ 3\lambda_{hhh} c_\alpha^2 C_{24}[h,G^0,h] + \lambda_{hhH} c_\alpha s_\alpha (C_{24}[h,G^0,H] + C_{24}[H,G^0,h]) \\
&+ \lambda_{hHH} s_\alpha^2 C_{24}[H,G^0,H] + \lambda_{hG^0G^0} (c_\alpha^2 C_{24}[G^0,h,G^0] + s_\alpha^2 C_{24}[G^0,H,G^0]) \Big\}, \qquad \text{(D.81)}
\end{aligned}
$$

$$
\begin{aligned}
&(16\pi^2)M^{1\mathrm{PI},B}_{hWW,1}[p_1^2,p_2^2,q^2] = -g^3 m_W(D-1)\{c_\alpha B_0(p^2;W,W)+s_\alpha B_0(p^2;Z,Z)\}\\
&-\frac{g^3}{2}m_W c_\alpha\{c_\alpha^2(B_0[p_1^2;W,h]+B_0[p_2^2;W,h])+s_\alpha^2(B_0[p_1^2;W,H]+B_0[p_2^2;W,H])\}\\
&-\frac{g^3}{2}s_W^2 m_W c_\alpha\left\{\frac{s_W^2}{c_W^2}(B_0[p_1^2;Z,G^\pm]+B_0[p_2^2;Z,G^\pm])+(B_0[p_1^2;\gamma,G^\pm]+B_0[p_2^2;\gamma,G^\pm])\right\}\\
&+\frac{g^2}{2}\big\{\lambda_{hG^+G^-}B_0[p^2,G^\pm,G^\pm]+3\lambda_{hhh}c_\alpha^2 B_0[p^2;h,h]+\lambda_{hHH}s_\alpha^2 B_0[p^2;H,H]\\
&+2\lambda_{hhH}s_\alpha c_\alpha B_0[p^2;h,H]+\lambda_{hG^0G^0}B_0[p^2;G^0,G^0]\big\}\\
&+g^3 m_W c_W^2 c_\alpha C^{hVV,1}_{VVV}[W,Z,W]+e^2 g m_W c_\alpha C^{hVV,1}_{VVV}[W,\gamma,W]+g^3 m_W c_\alpha C^{hVV,1}_{VVV}[Z,W,Z]\\
&-\frac{g^3}{2}m_W s_W^2 c_\alpha C^{hVV,1}_{VVS}[W,Z,G^\pm]+\frac{eg^2}{2}m_W s_W c_\alpha C^{hVV,1}_{VVS}[W,\gamma,G^\pm]\\
&-g^3 m_W^3 c_\alpha\{c_\alpha^2 C_0[W,h,W]+s_\alpha^2 C_0[W,H,W]\}-g^2 g_Z m_Z^3 s_W^4 c_\alpha C_0[Z,G^+,Z]\\
&-\frac{g^3}{2}m_W s_W^2 c_\alpha(C^{hVV,1}_{SVV}[G^\pm,Z,W]-C^{hVV,1}_{SVV}[W,\gamma,G^\pm])\\
&+\frac{g^3}{2}m_W c_\alpha\left\{(c_\alpha^2 C_{24}[W,h,G^\pm]+s_\alpha^2 C_{24}[W,H,G^\pm])\}+\frac{s_W^2}{c_W^2}(C_{24}[Z,G^+,G^0]+C_{24}[G^0,G^\pm,Z])\right\}\\
&+g^2 m_W^2\left\{\lambda_{hG^+G^-}\frac{s_W^4}{c_W^2}C_0[G^\pm,Z,G^\pm]+\lambda_{hG^+G^-}s_W^2 C_0[G^\pm,\gamma,G^\pm]+6\lambda_{hhh}c_\alpha^2 C_0[h,W,h]\right\}\\
&+2\lambda_{hhH}g^2 m_W^2 c_\alpha s_\alpha(C_0[h,W,H]+C_0[H,W,h])+2\lambda_{hHH}g^2 m_W^2(s_\alpha)^2 C_0[H,W,H]\\
&+\frac{g^3}{2}m_W c_h\{s_\alpha^2 C_{24}[G^\pm,h,W]+c_\alpha^2 C_{24}[G^\pm,H,W]\}\\
&-g^3 m_W c_W^2 c_\alpha C_{24}(c^\pm,c^0,c^\pm)-e^2 g m_W s_\alpha C_{24}(c^\pm,c^\gamma,c^\pm)-g^3 m_W c_\alpha C_{24}(c^0,c^\pm,c^0)\\
&-\lambda_{hG^+G^-}g^2\{c_\alpha^2 C_{24}[G^\pm,h,G^\pm]+s_\alpha^2 C_{24}[G^\pm,H,G^\pm]+C_{24}[G^\pm,G^0,G^\pm]\}\\
&-6\lambda_{hhh}g^2 c_\alpha^2 C_{24}[h,G^\pm,h]-2\lambda_{hhH}g^2 c_\alpha s_\alpha(C_{24}[h,G^\pm,H]+C_{24}[H,G^\pm,h])\\
&-2\lambda_{hHH}g^2(s_\alpha)^2 C_{24}[H,G^\pm,H]-2\lambda_{hG^0G^0}g^2 C_{24}[G^0,G^\pm,G^0],
\end{aligned}
\tag{D.82}
$$

$$
\begin{aligned}
(16\pi^2)M^{1\mathrm{PI},B}_{hZZ,2}[p_1^2,p_2^2,q^2] &= g^3 m_W c_\alpha \big\{ 2c_W^2 C^{hVV,2}_{VVV}[W,W,W] + s_W^2 C^{hVV,2}_{VVS}[W,W,G^\pm] \\
&+ s_W^2(-C_{23}+2C_0)\big\}[G^\pm,W,W] - g^3 m_W \frac{s_W^2 c_{2W}}{c_W^2} c_\alpha \Big\{ C^{hVV,2}_{VSS}[W,G^\pm,G^\pm] + C_{23}[G^\pm,G^\pm,W] \Big\} \\
&- g_Z^3 m_Z c_\alpha \Big\{ s_W^2 c_{2W}(C^{hVV,2}_{VSS}[W,G^\pm,G^\pm] + C_{23}[G^\pm,G^\pm,W]) \\
&- c_\alpha^2 (C^{hVV,2}_{VSS}[Z,h,G^0] + C_{23}[G^0,h,Z]) \Big\} + \frac{g_Z^3}{2} m_Z c_\alpha s_\alpha^2 \Big\{ C^{hVV,2}_{VSS}[Z,H,G^0] + C_{23}[G^0,H,Z] \Big\} \\
&- 2g^3 m_W c_W^2 c_\alpha C_{12}[c^\pm,c^\pm,c^\pm] - 2g_Z^2 \Big\{ c_{2W}^2 \lambda_{hG^+G^-} C_{1223}[G^\pm,G^\pm,G^\pm] \\
&+ 3c_\alpha^2 \lambda_{hhh} C_{1223}[h,G^0,h] + c_\alpha s_\alpha \lambda_{hhH} \big\{ C_{1223}[h,G^0,H] + C_{1223}[H,G^0,h] \big\} \\
&+ s_\alpha^2 \lambda_{hHH} C_{1223}[H,G^0,H] + \lambda_{hG^0G^0} \big\{ c_\alpha^2 C_{1223}[G^0,h,G^0] + s_\alpha^2 C_{1223}[G^0,H,G^0] \big\} \Big\},
\end{aligned}
\tag{D.83}
$$

$$
\begin{aligned}
(16\pi^2)M^{1\mathrm{PI},B}_{hWW,2}[p_1^2,p_2^2,q^2] &= g^3 m_W c_\alpha \Big\{ c_W^2 C^{hVV,2}_{VVV}[W,Z,W] + s_W^2 C^{hVV,2}_{VVV}[W,\gamma,W] \\
&+ C^{hVV,2}_{VVV}[Z,W,Z] \Big\} - \frac{g^3}{2} m_W s_W^2 c_\alpha \Big\{ C^{hVV,2}_{VVS}[W,Z,G^\pm] + C^{hVV,2}_{VVS}[W,\gamma,G^\pm] \Big\} \\
&- \frac{g^3}{2} m_W s_W^2 c_\alpha \big\{ (-C_{23}+2C_0)[G^\pm,Z,W](-C_{23}+2C_0)[G^\pm,\gamma,W] \big\} \\
&+ \frac{g^3}{2} m_W c_\alpha \Big\{ c_\alpha^3 (C^{hVV,2}_{VSS}[W,h,G^\pm] + C_{23}[G^\pm,h,W]) + s_\alpha^2 (C^{hVV,2}_{VSS}[W,H,G^\pm] + C_{23}[G^\pm,H,W]) \\
&+ \frac{s_W^2}{c_W^2} (C^{hVV,2}_{VSS}[Z,G^\pm,G^0] + C_{23}[G^0,G^\pm,Z]) \Big\} \\
&- g^3 m_W c_\alpha \Big\{ c_W^2 C_{12}[c^\pm,c^0,c^\pm] + s_W^2 C_{12}[c^\pm,c^\gamma,c^\pm] + C_{12}[c^0,c^\pm,c^0] \Big\} \\
&- g^2 \lambda_{hG^+G^-} \big\{ c_\alpha^2 C_{1223}[G^\pm,h,G^\pm] + s_\alpha^2 C_{1223}[G^\pm,H,G^\pm] + C_{1223}[G^\pm,G^0,G^\pm] \big\} \\
&- 6g^2 \lambda_{hhh} c_\alpha^2 C_{1223}[h,G^\pm,h] - 2g^2 \lambda_{hHH} s_\alpha^2 C_{1223}[H,G^\pm,H] \\
&- 2g^2 \lambda_{hhH} c_\alpha s_\alpha \big\{ C_{1223}[h,G^\pm,H] + C_{1223}[H,G^\pm,h] \big\} - 2g^2 \lambda_{hG^0G^0} C_{1223}[G^0,G^\pm,G^0],
\end{aligned}
\tag{D.84}
$$

$$
M^{1\mathrm{PI},B}_{hZZ,3}[p_1^2,p_2^1,q^2] = M^{1\mathrm{PI},B}_{hWW,3}[p_1^2,p_2^2,q^2] = 0, \tag{D.85}
$$

where

$$C^{hVV,1}_{VVV}[X,Y,Z] = \big\{(6D-6)C_{24} + p_1^2(2C_{21}+3C_{11}+C_0) + p_2^2(2C_{22}+C_{12}) + p_1\cdot p_2(4C_{23}+3C_{12}+C_{11}-4C_0)\big\}[X,Y,Z], \tag{D.86}$$

$$C^{hVV,1}_{VVS}[X,Y,Z] = \big\{(D-1)C_{24} + p_1^2(C_{21}+4C_{11}+4C_0) + p_2^2(C_{22}+2C_{12}) + p_1\cdot p_2(2C_{23}+4C_{12}+2C_{11}+4C_0)\big\}[X,Y,Z], \tag{D.87}$$

$$C^{hVV,1}_{SVV}[X,Y,Z] = \big\{(D-1)C_{24} + p_1^2(C_{21}-C_0) + p_2^2(C_{22}-2C_{12}+C_0) + 2p_1\cdot p_2(C_{23}-C_{11})\big\}[X,Y,Z], \tag{D.88}$$

$$C^{hVV,2}_{VVV}[X,Y,Z] = [C_{11}+9C_{12}+10C_{23}+5C_0][X,Y,Z] \tag{D.89}$$

$$C^{hVV,2}_{VVS}[X,Y,Z] = [2C_{11}-5C_{12}-C_{23}-2C_0][X,Y,Z] \tag{D.90}$$

$$C^{hVV,2}_{VSS}[X,Y,Z] = [C_{1223}+2C_{11}+2C_0][X,Y,Z], \tag{D.91}$$

and $C_{1223} = C_{12} + C_{23}$.

We give 1PI diagram contributions to $hf\bar{f}$ couplings, which are composed of following seven form factors,

$$F^{\rm 1PI}_{hff}[p_1^2,p_2^2,q^2] = \Big\{F^{\rm 1PI}_{hff,S} + \gamma_5 F^{\rm 1PI}_{hff,P} + \not{p}_1 F^{\rm 1PI}_{hff,V1} + \not{p}_2 F^{\rm 1PI}_{hff,V2} + \not{p}_1\gamma_5 F^{\rm 1PI}_{hff,A1} + \not{p}_2\gamma_5 F^{\rm 1PI}_{hff,A2} + \not{p}_1\not{p}_2 F^{\rm 1PI}_{hff,T} + \not{p}_1\not{p}_2\gamma_5 F^{\rm 1PI}_{hff,TP}\Big\}[p_1^2,p_2^2,q^2]. \tag{D.92}$$

Each part is calculated as

$$\begin{aligned}
(16\pi^2)F^{\rm 1PI}_{hff,S}[p_1^2,p_2^2,q^2] &= -4c_\alpha\frac{m_f}{v}\left\{\frac{m_Z^2}{v^2}(v_f^2-a_f^2)C^{hff,S}_{FVF}[f,Z,f] + (Q_f e)^2 C^{hff,S}_{FVF}[f,Z,f]\right\} \\
&+ \frac{m_f^3}{v^3}c_\alpha\left\{c_\alpha^2 C^{hff,S}_{FSF}[f,h,f] + s_\alpha^2 C^{hff,S}_{FSF}[f,H,f] - c_\alpha C^{hff,S}_{FSF}[f,G^0,f]\right\} \\
&- 2c_\alpha\frac{m_f m_{f'}^2}{v^3}C^{hff,S}_{FSF}[f',G^\pm,f'] - 8c_\alpha\frac{m_Z^4}{v^3}m_f(v_f^2-a_f^2)C_0[Z,f,Z] \\
&- 2\frac{m_f^2}{v^2}\left\{3c_\alpha^2\lambda_{hhh}C_0[h,f,h] + s_\alpha^2\lambda_{hHH}C_0[H,f,H] + c_\alpha s_\alpha\lambda_{hhH}(C_0[h,f,H]+C_0[H,f,h])\right\} \\
&+ 2\frac{m_f^2}{v^2}\left\{\lambda_{hG^0G^0}\frac{m_f}{v}C_0[G^0,f,G^0] + \lambda_{hG^+G^-}\frac{m_{f'}}{v}C_0[G^\pm,f',G^\pm]\right\} \\
&- c_\alpha\frac{m_W^2 m_f}{v^3}(C^{hff,S}_{SFV}[G^\pm,f',W] + C^{hff,S}_{VFS}[W,f',G^\pm]) \\
&- c_\alpha\frac{m_Z^2 m_f}{2v^3}(C^{hff,S}_{SFV}[G^0,f,Z] + C^{hff,S}_{VFS}[Z,f,G^0]),
\end{aligned} \tag{D.93}$$

$$\begin{aligned}
F^{\rm 1PI}_{hff,P}[p_1^2,p_2^2,q^2] = -\frac{1}{16\pi^2}\frac{m_f}{v^2}c_\alpha\Big\{&m_W^2(C^{hff,T}_{VFS}[W,f',G^\pm] - C^{hff,T}_{SFV}[G^\pm,f',W]) \\
&+ 2I_f v_f m_Z^2(C^{hff,T}_{VFS}[Z,f,G^0] - C^{hff,T}_{SFV}[G^0,f,Z])\Big\},
\end{aligned} \tag{D.94}$$

$$
\begin{aligned}
(16\pi^2)F^{V1}_{hff}[p_1^2,p_2^2,q^2] &= \frac{m_f^4}{v^3}c_\alpha\big\{c_\alpha^2(C_0+2C_{11})[f,h,f]+s_\alpha^2(C_0+2C_{11})[f,H,f]\\
&+(C_0+2C_{11})[f,G^0,f]\big\}+\frac{m_{f'}^2}{v}c_\alpha\left(\frac{m_f^2}{v^2}+\frac{m_{f'}^2}{v^2}\right)\{C_0+2C_{11}\}[f',G^\pm,f']\\
&+2\frac{c_\alpha}{v^3}\left\{m_W^2m_{f'}^2(C_0+2C_{11})[f',W,f']+m_Z^2m_f^2(v_f^2+a_f^2)(C_0+2C_{11})[f,Z,f]\right\}\\
&+2(Q_fe)^2\frac{m_f^2}{v}c_\alpha\{C_0+2C_{11}\}[f,\gamma,f]+\lambda_{hG^+G^-}\left(\frac{m_f^2}{v^2}+\frac{m_{f'}^2}{v^2}\right)\{C_0+C_{11}\}[G^\pm,f',G^\pm]\\
&+2\frac{m_f^2}{v^2}\Big\{3\lambda_{hhh}c_\alpha^2(C_0+C_{11})[h,f,h]+\lambda_{hHH}s_\alpha^2(C_0+C_{11})[H,f,H]\\
&+\lambda_{hhH}s_\alpha c_\alpha(C_0+C_{11})\{[h,f,H]+[H,f,h]\}+2\lambda_{hG^0G^0}(C_0+C_{11})[G^0,f,G^0]\Big\}\\
&-4c_\alpha\frac{m_Z^4}{v^3}(v_f^2+a_f^2)\{C_0+C_{11}\}[Z,f,Z]-4c_\alpha\frac{m_W^4}{v^3}\{C_0+C_{11}\}[W,f',W]\\
&-c_\alpha\frac{m_W^2}{v^2}\frac{m_{f'}^2}{v}\left\{(2C_0+C_{11})[W,f',G^\pm]-(C_0-C_{11})[G^\pm,f',W]\right\}\\
&-2I_fc_\alpha\frac{m_Z^2}{v^2}\frac{m_f^2}{v}a_f\left\{(2C_0+C_{11})[Z,f,G^0]-(C_0-C_{11})[G^0,f,Z]\right\},
\end{aligned}
\tag{D.95}
$$

$$
\begin{aligned}
(16\pi^2)F^{\rm 1PI}_{hff,V2}[p_1^2,p_2^2,q^2] &= \frac{m_f^4}{v^3}c_\alpha\Big\{c_\alpha^2(C_0+2C_{12})[f,h,f]+s_\alpha^2(C_0+2C_{12})[f,H,f]\\
&+(C_0+2C_{12}[f,G^0,f]\Big\}+\frac{m_{f'}^2}{v}c_\alpha\left(\frac{m_f^2}{v^2}+\frac{m_{f'}^2}{v^2}\right)\{C_0+2C_{12}\}[f',G^\pm,f']\\
&+2\frac{c_\alpha}{v^3}\left\{m_W^2m_{f'}^2(C_0+2C_{12})[f',W,f']+m_Z^2m_f^2(v_f^2+a_f^2)(C_0+2C_{12})[f,Z,f]\right\}\\
&+2(Q_fe)^2\frac{m_f^2}{v}c_\alpha\{C_0+2C_{12}\}[f,\gamma,f]+\lambda_{hG^+G^-}\left(\frac{m_f^2}{v^2}+\frac{m_{f'}^2}{v^2}\right)C_{12}[G^\pm,f',G^\pm]\\
&+2\frac{m_f^2}{v^2}\Big\{3\lambda_{hhh}c_\alpha^2C_{12}[h,f,h]+\lambda_{hHH}s_\alpha^2C_{12}[H,f,H]+\lambda_{hG^0G^0}C_{12}[G^0,f,G^0]\\
&+\lambda_{hhH}s_\alpha c_\alpha(C_{12}[h,f,H]+[H,f,h])\Big\}-4\frac{c_\alpha}{v^3}\left\{m_Z^4(v_f^2+a_f^2)C_{12}[Z,f,Z]+m_W^4C_{12}[W,f',W]\right\}\\
&-c_\alpha\frac{m_W^2}{v^2}\frac{m_{f'}^2}{v}\left\{(2C_0+C_{12})[W,f',G^\pm]-(C_0-C_{12})[G^\pm,f',W]\right\}\\
&-2I_fc_\alpha\frac{m_Z^2}{v^2}\frac{m_f^2}{v}a_f\left\{(2C_0+C_{12})[Z,f,G^0]-(C_0-C_{12})[G^0,f,Z]\right\},
\end{aligned}
\tag{D.96}
$$

$$F^{\rm 1PI}_{hff,A1}[p_1^2,p_2^2,q^2] = \frac{1}{16\pi^2}\Bigg\{ 2c_\alpha \frac{m_W^2}{v^3}\left\{2m_W^2(C_0+C_{11})[W,f',W] - m_{f'}^2(C_0+2C_{11})[f',W,f']\right\}$$
$$+ 4c_\alpha \frac{m_Z^2}{v^3} v_f a_f \left\{2m_Z^2(c_0+C_{11})[Z,f,Z] - m_f^2(C_0+2C_{11})[f,Z,f]\right\}$$
$$+ c_\alpha \frac{m_W^2}{v^2}\frac{m_{f'}^2}{v}\left\{2C_0+C_{11}\right\}[W,f',G^+] - c_h \frac{m_W^2}{v^2}\frac{m_{f'}^2}{v}\left\{C_0-C_{11}\right\}[G^+,f',W]$$
$$+ c_\alpha \frac{m_W^2}{v^2}\frac{m_{f'}^2}{v}\left\{(2C_0+C_{11})[W,f',G^\pm] - (C_0-C_{11})[G^\pm,f',W]\right\}$$
$$+ c_\alpha I_f v_f \frac{m_Z^2}{v^2}\frac{m_f^2}{v}\left\{(2C_0+C_{11})[Z,f,G^0] - (C_0-C_{11})[G^0,f,Z]\right\}$$
$$+ \left(\frac{m_f^2}{v^2}-\frac{m_{f'}^2}{v^2}\right)\left\{\frac{m_{f'}^2}{v}c_\alpha(C_0+2C_{11})[f',G^\pm,f'] + \lambda_{hG^+G^-}(C_0+C_{11})[G^\pm,f',G^\pm]\right\}\Bigg\}, \qquad \text{(D.97)}$$

$$F^{\rm 1PI}_{hff,A2}[p_1^2,p_2^2,q^2] = \frac{1}{16\pi^2}\Bigg\{ 2c_\alpha \frac{m_W^2}{v^3}\left\{2m_W^2C_{12}[W,f',W] - m_{f'}^2(C_0+2C_{12})[f',W,f']\right\}$$
$$+ 4c_\alpha \frac{m_Z^2}{v^3} v_f a_f \left\{2m_Z^2C_{12}[Z,f,Z] - m_f^2(C_0+2C_{12})[f,Z,f]\right\}$$
$$+ c_\alpha \frac{m_W^2}{v^2}\frac{m_{f'}^2}{v}\left\{(2C_0+C_{12})[W,f',G^\pm] - (C_0-C_{12})[G^\pm,f',W]\right\}$$
$$+ 2I_f v_f^2 c_\alpha \frac{m_Z^2}{v^2}\frac{m_f^2}{v}\left\{(2C_0+C_{12})[Z,f,G^0] + (C_0-C_{12})[G^0,f,Z]\right\}$$
$$+ \left(\frac{m_f^2}{v^2}-\frac{m_{f'}^2}{v^2}\right)\left(\frac{m_{f'}^2}{v}c_\alpha(C_0+2C_{12})[f',G^\pm,f'] + \lambda_{hG^+G^-}C_{12}[G^\pm,f',G^\pm]\right)\Bigg\}, \qquad \text{(D.98)}$$

$$F^{\rm 1PI}_{hff,T}[p_1^2,p_2^2,q^2] = \frac{1}{16\pi^2}\Bigg\{ \frac{m_f^3}{v^3}c_\alpha\left\{c_\alpha^2(C_{11}-C_{12})[f,h,f] + s_\alpha^2(C_{11}-C_{12})[f,H,f]\right\}$$
$$\frac{m_f^2}{v^3}c_\alpha\left\{m_f(C_{11}-C_{12})[f,G^0,f] - 2m_{f'}(C_{11}-C_{12})[f',G^\pm,f']\right\}$$
$$+ c_\alpha \frac{m_W^2}{v^2}\frac{m_f}{v}\left\{(2C_0+2C_{11}-C_{12})[W,f',G^+](C_0+C_{11}-2C_{12})[G^+,f',W]\right\}$$
$$+ c_\alpha \frac{m_Z^2}{2v^2}\frac{m_f}{v}\left\{(2C_0+2C_{11}-C_{12})[Z,f,G^0] + (C_0+C_{11}-2C_{12})[G^0,f,Z]\right\}\Bigg\}, \qquad \text{(D.99)}$$

$$
\begin{aligned}
&F^{\rm 1PI}_{hff,TP}[p_1^2,p_2^2,q^2] \\
&= \frac{1}{16\pi^2}\Bigg\{ c_\alpha \frac{m_W^2}{v^2}\frac{m_f}{v}\Big\{(2C_0+2C_{11}-C_{12})[W,f',G^+]-(C_0+C_{11}-2C_{12})[G^+,f',W]\Big\} \\
&+ 2I_f v_f c_\alpha \frac{m_Z^2}{v^2}\frac{m_f}{v}\Big\{(2C_0+2C_{11}-C_{12})[Z,f,G^0]-(C_0+C_{11}-2C_{12})[G^0,f,Z]\Big\}\Bigg\}, \qquad \text{(D.100)}
\end{aligned}
$$

where

$$
\begin{aligned}
C^{hff,S}_{FVF}[X,Y,X] &= \{p_1^2(C_{11}+C_{21})+p_2^2(C_{12}+C_{22})+p_1\cdot p_2(C_{11}+C_{12}+2C_{23}) \\
&\quad + 4C_{24}-1+m_X^2C_0\}[X,Y,X], \qquad \text{(D.101)} \\
C^{hff,S}_{FSF}[X,Y,X] &= \{p_1^2(C_{11}+C_{21})+p_2^2(C_{12}+C_{22})+2p_1\cdot p_2(C_{12}+C_{23}) \\
&\quad + 4C_{24}-\frac{1}{2}+m_X^2C_0\}[X,Y,X], \qquad \text{(D.102)} \\
C^{hff,S}_{SFV}[X,Y,Z] &= \{p_1^2(C_{21}-C_0)+p_2^2(C_{22}-C_{12})+2p_1\cdot p_2(C_{23}-C_{12})+4C_{24}-\frac{1}{2}\}[X,Y,Z] \qquad \text{(D.103)} \\
C^{hff,S}_{VFS}[X,Y,Z] &= \{p_1^2(C_{21}+3C_{11}+2C_0)+p_2^2(C_{22}+2C_{12}) \\
&\quad + 2p_1\cdot p_2(C_{23}+C_{12}+2C_{11}+2C_0)+4C_{24}-\frac{1}{2}\}[X,Y,Z], \qquad \text{(D.104)} \\
C^{hff,T}_{VFS}[X,Y,Z] &= \big\{p_1^2(3C_{11}+2C_0+C_{21})+p_2^2(2C_{12}+C_{22}) \\
&\quad + 2p_1\cdot p_2(C_{12}+C_{23}+2C_{11}+2C_0)+DC_{24}\big\}[X,Y,Z], \qquad \text{(D.105)} \\
C^{hff,T}_{SFV}[X,Y,Z] &= \big\{p_1^2(C_{21}-C_0)+p_2^2(C_{22}-C_{12})+2p_1\cdot p_2(C_{23}-C_{12})+DC_{24}\big\}\,[X,Y,Z]. \qquad \text{(D.106)}
\end{aligned}
$$

D.2.4 1PI diagrams in the HTM

D.2.5 One-point functions

The 1PI diagram contributions to the one-point function are calculated by

$$
T^{\rm 1PI}_{h,F} = -\frac{4m_f^2N_c^f}{16\pi^2}\frac{c_\alpha}{v_\phi}A(m_f), \qquad \text{(D.107)}
$$

$$
T^{\rm 1PI}_{H,F} = +\frac{4m_f^2N_c^f}{16\pi^2}\frac{s_\alpha}{v_\phi}A(m_f), \qquad \text{(D.108)}
$$

$$T^{\rm 1PI}_{h,S} = -\frac{1}{16\pi^2}[\lambda_{H^{++}H^{--}h}A(m_{H^{++}}) + \lambda_{H^+H^-h}A(m_{H^+}) + \lambda_{AAh}A(m_A) + \lambda_{HHh}A(m_H) + 3\lambda_{hhh}A(m_h)], \tag{D.109}$$

$$T^{\rm 1PI}_{H,S} = -\frac{1}{16\pi^2}[\lambda_{H^{++}H^{--}H}A(m_{H^{++}}) + \lambda_{H^+H^-H}A(m_{H^+}) + \lambda_{AAH}A(m_A) + 3\lambda_{HHH}A(m_H) + \lambda_{Hhh}A(m_h)], \tag{D.110}$$

$$T^{\rm 1PI}_{h,V} = \frac{1}{16\pi^2}\Bigg[- \lambda_{G^+G^-h}A(m_{G^+}) - \lambda_{G^0G^0h}A(m_{G^0}) + gm_W(c_\beta c_\alpha + \sqrt{2}s_\beta s_\alpha)DA(m_W) + \frac{g_Z m_Z}{2}(c_{\beta'}c_\alpha + 2s_{\beta'}s_\alpha)DA(m_Z) - gm_W(c_\beta c_\alpha + \sqrt{2}s_\beta s_\alpha)A(m_{c^+}) - \frac{g_Z m_Z}{2}(c_{\beta'}c_\alpha + 2s_{\beta'}s_\alpha)A(m_{c_Z})\Bigg], \tag{D.111}$$

$$T^{\rm 1PI}_{H,V} = \frac{1}{16\pi^2}\Bigg[- \lambda_{G^+G^-H}A(m_{G^+}) - \lambda_{G^0G^0H}A(m_{G^0}) + gm_W(-c_\beta s_\alpha + \sqrt{2}s_\beta c_\alpha)DA(m_W) + \frac{g_Z m_Z}{2}(-c_{\beta'}s_\alpha + 2s_{\beta'}c_\alpha)DA(m_Z) - gm_W(-c_\beta s_\alpha + \sqrt{2}s_\beta c_\alpha)A(m_{c^+}) - \frac{g_Z m_Z}{2}(-c_{\beta'}s_\alpha + 2s_{\beta'}c_\alpha)A(m_{c_Z})\Bigg], \tag{D.112}$$

where m_{G^+} (m_{c^+}) and m_{G^0} (m_{c_Z}) are the masses of the NG bosons $G^\pm$ and G^0 (ghost fields $c^\pm$ and c_Z), respectively. In the 't Hooft-Feynman gauge, these masses are the same as the corresponding gauge boson masses, i.e., $m_{G^+} = m_{c^+} = m_W$ and $m_{G^0} = m_{c_Z} = m_Z$.

D.2.6 Two-point functions

The 1PI diagram contributions to the scalar boson two point functions are calculated as

$$\Pi^{\rm 1PI}_{hh}(p^2)_F = -\frac{4m_f^2 N_c^f}{16\pi^2}\frac{c_\alpha^2}{v_\phi^2}\left[A(m_f) + \left(2m_f^2 - \frac{p^2}{2}\right)B_0(p^2, m_f, m_f)\right], \tag{D.113}$$

$$\Pi^{\rm 1PI}_{HH}(p^2)_F = -\frac{4m_f^2 N_c^f}{16\pi^2}\frac{s_\alpha^2}{v_\phi^2}\left[A(m_f) + \left(2m_f^2 - \frac{p^2}{2}\right)B_0(p^2, m_f, m_f)\right], \tag{D.114}$$

$$\Pi^{\rm 1PI}_{Hh}(p^2)_F = \frac{4m_f^2 N_c^f}{16\pi^2}\frac{c_\alpha s_\alpha}{v_\phi^2}\left[A(m_f) + \left(2m_f^2 - \frac{p^2}{2}\right)B_0(p^2, m_f, m_f)\right], \tag{D.115}$$

$$\Pi^{\rm 1PI}_{AA}(p^2)_F = -\frac{4m_f^2 N_c^f}{16\pi^2}\frac{s_{\beta'}^2}{v_\phi^2}\left[A(m_f) - \frac{p^2}{2}B_0(p^2, m_f, m_f)\right], \tag{D.116}$$

$$\Pi^{\rm 1PI}_{AG}(p^2)_F = +\frac{2m_f^2 N_c^f}{16\pi^2}\frac{s_{2\beta'}}{v_\phi^2}\left[A(m_f) - \frac{p^2}{2}B_0(p^2, m_f, m_f)\right], \tag{D.117}$$

$$\Pi^{\rm 1PI}_{hh}(p^2)_S = \frac{1}{16\pi^2}[-2\lambda_{H^{++}H^{--}hh}A(m_{H^{++}}) - 2\lambda_{H^+H^-hh}A(m_{H^+})$$
$$- 2\lambda_{AAhh}A(m_A) - 2\lambda_{HHhh}A(m_H) + 12\lambda_{hhhh}A(m_h)$$
$$+ \lambda^2_{H^{++}H^{--}h}B_0(p^2, m_{H^{++}}, m_{H^{++}})$$
$$+ \lambda^2_{H^+H^-h}B_0(p^2, m_{H^+}, m_{H^+}) + \lambda^2_{G^+G^-h}B_0(p^2, m_{G^+}, m_{G^+}) + 2\lambda^2_{H^+G^-h}B_0(p^2, m_{H^+}, m_{G^+})$$
$$+ 2\lambda^2_{AAh}B_0(p^2, m_A, m_A) + 2\lambda^2_{G^0G^0h}B_0(p^2, m_{G^0}, m_{G^0}) + \lambda^2_{AG^0h}B_0(p^2, m_A, m_{G^0})$$
$$+ 2\lambda^2_{HHh}B_0(p^2, m_H, m_H) + 18\lambda^2_{hhh}B_0(p^2, m_h, m_h) + 4\lambda^2_{Hhh}B_0(p^2, m_h, m_H)], \tag{D.118}$$

$$\Pi^{\rm 1PI}_{HH}(p^2)_S = \frac{1}{16\pi^2}[-2\lambda_{H^{++}H^{--}HH}A(m_{H^{++}}) - 2\lambda_{H^+H^-HH}A(m_{H^+})$$
$$- 2\lambda_{HHAA}A(m_A) + 12\lambda_{HHHH}A(m_H) - 2\lambda_{HHhh}A(m_h)]$$
$$+ \lambda^2_{H^{++}H^{--}H}B_0(p^2, m_{H^{++}}, m_{H^{++}})$$
$$+ \lambda^2_{H^+H^-H}B_0(p^2, m_{H^+}, m_{H^+}) + \lambda^2_{G^+G^-H}B_0(p^2, m_{G^+}, m_{G^+}) + 2\lambda^2_{H^+G^-H}B_0(p^2, m_{H^+}, m_{G^+})$$
$$+ 2\lambda^2_{AAH}B_0(p^2, m_A, m_A) + 2\lambda^2_{G^0G^0H}B_0(p^2, m_{G^0}, m_{G^0}) + \lambda^2_{AG^0H}B_0(p^2, m_A, m_{G^0})$$
$$+ 18\lambda^2_{HHH}B_0(p^2, m_H, m_H) + 2\lambda^2_{Hhh}B_0(p^2, m_h, m_h) + 4\lambda^2_{HHh}B_0(p^2, m_h, m_H)], \tag{D.119}$$

$$\Pi^{\rm 1PI}_{Hh}(p^2)_S = \frac{1}{16\pi^2}[-\lambda_{H^{++}H^{--}Hh}A(m_{H^{++}}) - \lambda_{H^+H^-Hh}A(m_{H^+})$$
$$- \lambda_{AAHh}A(m_A) - 3\lambda_{HHHh}A(m_H) - 3\lambda_{Hhhh}A(m_h)$$
$$+ \lambda_{H^{++}H^{--}h}\lambda_{H^{++}H^{--}H}B_0(p^2, m_{H^{++}}, m_{H^{++}}) + \lambda_{H^+H^-h}\lambda_{H^+H^-H}B_0(p^2, m_{H^+}, m_{H^+})$$
$$+ \lambda_{G^+G^-h}\lambda_{G^+G^-H}B_0(p^2, m_{G^+}, m_{G^+}) + 2\lambda_{H^+G^-h}\lambda_{H^+G^-H}B_0(p^2, m_{H^+}, m_{G^+})$$
$$+ 2\lambda_{AAh}\lambda_{AAH}B_0(p^2, m_A, m_A) + 2\lambda_{hG^0G^0}\lambda_{G^0G^0H}B_0(p^2, m_{G^0}, m_{G^0})$$
$$+ \lambda_{AG^0h}\lambda_{AG^0H}B_0(p^2, m_A, m_{G^0}) + 6\lambda_{HHh}\lambda_{HHH}B_0(p^2, m_H, m_H)$$
$$+ 6\lambda_{hhh}\lambda_{Hhh}B_0(p^2, m_h, m_h) + 4\lambda_{Hhh}\lambda_{HHh}B_0(p^2, m_H, m_h)], \tag{D.120}$$

$$\Pi^{\rm 1PI}_{AA}(p^2)_S = -\frac{1}{16\pi^2}[2\lambda_{H^{++}H^{--}AA}A(m_{H^{++}}) + 2\lambda_{H^+H^-AA}A(m_{H^+})$$
$$+ 12\lambda_{AAAA}A(m_A) + 2\lambda_{AAHH}A(m_H) + 2\lambda_{AAhh}A(m_h)]$$
$$+ \frac{1}{16\pi^2}[2\lambda_{H^+G^-A}\lambda^*_{H^+G^-A}B_0(p^2, m_{H^+}, m_{G^+}) + 4\lambda^2_{AAh}B_0(p^2, m_A, m_h)$$
$$+ 4\lambda^2_{AAH}B_0(p^2, m_A, m_H) + \lambda^2_{AG^0h}B_0(p^2, m_h, m_{G^0}) + \lambda^2_{AG^0H}B_0(p^2, m_H, m_{G^0})], \tag{D.121}$$

$$\Pi^{\rm 1PI}_{AG}(p^2)_S = -\frac{1}{16\pi^2}[\lambda_{H^{++}H^{--}AG^0}A(m_{H^{++}}) + \lambda_{H^+H^-AG^0}A(m_{H^+})$$
$$+ 3\lambda_{AAAG^0}A(m_A) + \lambda_{AG^0HH}A(m_H) + \lambda_{AG^0hh}A(m_h)]$$
$$+ \frac{2}{16\pi^2}[\lambda_{H^+G^-A}\lambda^*_{H^+G^-G^0}B_0(p^2, m_{H^+}, m_{G^+})$$
$$+ \lambda_{AAh}\lambda_{AG^0h}B_0(p^2, m_A, m_h) + \lambda_{AAH}\lambda_{AG^0H}B_0(p^2, m_A, m_H)$$
$$+ \lambda_{AG^0h}\lambda_{G^0G^0h}B_0(p^2, m_{G^0}, m_h) + \lambda_{AG^0H}\lambda_{G^0G^0H}B_0(p^2, m_{G^0}, m_H), \tag{D.122}$$

$$\Pi^{\rm 1PI}_{H^+H^-}(p^2)_S = -\frac{1}{16\pi^2}[\lambda_{H^{++}H^{--}H^+H^-}A(m_{H^{++}}) + 4\lambda_{H^+H^-H^+H^-}A(m_{H^+})$$
$$+ \lambda_{H^+H^-AA}A(m_A) + \lambda_{H^+H^-HH}A(m_H) + \lambda_{H^+H^-hh}A(m_h)]$$
$$+ \frac{1}{16\pi^2}[4\lambda^2_{H^{++}H^-H^-}B_0(p^2, m_{H^{++}}, m_{H^+}) + \lambda^2_{H^{++}H^-G^-}B_0(p^2, m_{H^{++}}, m_{G^+})$$
$$+ \lambda^2_{H^+H^-H}B_0(p^2, m_{H^+}, m_H) + \lambda^2_{H^+H^-h}B_0(p^2, m_{H^+}, m_h)$$
$$+ \lambda^2_{H^+G^-H}B_0(p^2, m_H, m_{G^+}) + \lambda_{H^+G^-A}\lambda^*_{H^+G^-A}B_0(p^2, m_A, m_{G^+})$$
$$+ \lambda^2_{H^+G^-h}B_0(p^2, m_h, m_{G^+}) + \lambda_{H^+G^-G^0}\lambda^*_{H^+G^-G^0}B_0(p^2, m_{G^0}, m_{G^+})], \tag{D.123}$$

$$\Pi^{\rm 1PI}_{H^{++}H^{--}}(p^2)_S = -\frac{1}{16\pi^2}[4\lambda_{H^{++}H^{--}H^{++}H^{--}}A(m_{H^{++}}) + \lambda_{H^{++}H^{--}H^+H^-}A(m_{H^+})$$
$$+ \lambda_{H^{++}H^{--}AA}A(m_A) + \lambda_{H^{++}H^{--}HH}A(m_H) + \lambda_{H^{++}H^{--}hh}A(m_h)]$$
$$+ \frac{1}{16\pi^2}[2\lambda^2_{H^{++}H^-H^-}B_0(p^2, m_{H^+}, m_{H^+}) + 2\lambda^2_{H^{++}G^-G^-}B_0(p^2, m_{G^+}, m_{G^+})$$
$$+ \lambda^2_{H^{++}H^-G^-}B_0(p^2, m_{H^+}, m_{G^+})$$
$$+ \lambda^2_{H^{++}H^{--}H}B_0(p^2, m_{H^{++}}, m_H) + \lambda^2_{H^{++}H^{--}h}B_0(p^2, m_{H^{++}}, m_h)], \tag{D.124}$$

$$\Pi^{\rm 1PI}_{hh}(p^2)_V = \frac{1}{16\pi^2}\Bigg\{g^2m_W^2(c_\beta c_\alpha + \sqrt{2}s_\beta s_\alpha)^2DB_0(p^2, m_W, m_W) + \frac{g^2}{4}(3 - c_{2\alpha})DA(m_W)$$
$$- \frac{g^2}{2}(c_\alpha c_\beta + \sqrt{2}s_\alpha s_\beta)^2[2A(m_W) - A(m_{G^+}) + (2m^2_{G^+} - m^2_W + 2p^2)B_0(p^2, m_W, m_{G^+})]$$
$$- \frac{g^2}{2}(-c_\alpha s_\beta + \sqrt{2}s_\alpha c_\beta)^2[2A(m_W) - A(m_{H^+}) + (2m^2_{H^+} - m^2_W + 2p^2)B_0(p^2, m_W, m_{H^+})]$$
$$- 2\lambda_{G^+G^-hh}A(m_{G^+}) - \frac{g^2m_W^2}{2}(c_\beta c_\alpha + \sqrt{2}s_\beta s_\alpha)^2B_0(p^2, m_{c^+}, m_{c^+})$$
$$+ \frac{g_Z^2m_Z^2}{2}(c_{\beta'}c_\alpha + 2s_{\beta'}s_\alpha)^2DB_0(p^2, m_Z, m_Z) + \frac{g_Z^2}{8}(5 - 3c_{2\alpha})DA(m_Z)$$
$$- \frac{g_Z^2}{4}(c_\alpha c_{\beta'} + 2s_\alpha s_{\beta'})^2[2A(m_Z) - A(m_{G^0}) + (2m^2_{G^0} - m^2_Z + 2p^2)B_0(p^2, m_Z, m_{G^0})]$$
$$- \frac{g_Z^2}{4}(-c_\alpha s_{\beta'} + 2s_\alpha c_{\beta'})^2[2A(m_Z) - A(m_A) + (2m^2_A - m^2_Z + 2p^2)B_0(p^2, m_Z, m_A)]$$
$$- 2\lambda_{G^0G^0hh}A(m_{G^0}) - \frac{g_Z^2m_Z^2}{4}(c_{\beta'}c_\alpha + 2s_{\beta'}s_\alpha)^2B_0(p^2, m_{c_Z}, m_{c_Z})\Bigg\}, \tag{D.125}$$

$$\Pi^{\rm 1PI}_{HH}(p^2)_V = \frac{1}{16\pi^2}\Bigg\{ g^2 m_W^2(-c_\beta s_\alpha + \sqrt{2}s_\beta c_\alpha)^2 DB_0(p^2, m_W, m_W) + \frac{g^2}{4}(3+c_{2\alpha})DA(m_W)$$
$$- \frac{g^2}{2}(-s_\alpha c_\beta + \sqrt{2}c_\alpha s_\beta)^2[2A(m_W) - A(m_{G^+}) + (2m_{G^+}^2 - m_W^2 + 2p^2)B_0(p^2, m_W, m_{G^+})]$$
$$- \frac{g^2}{2}(s_\alpha s_\beta + \sqrt{2}c_\alpha c_\beta)^2[2A(m_W) - A(m_{H^+}) + (2m_{H^+}^2 - m_W^2 + 2p^2)B_0(p^2, m_W, m_{H^+})]$$
$$- 2\lambda_{G^+G^-HH}A(m_{G^+}) - \frac{g^2 m_W^2}{2}(-c_\beta s_\alpha + \sqrt{2}s_\beta c_\alpha)^2 B_0(p^2, m_{c^+}, m_{c^+})$$
$$+ \frac{g_Z^2 m_Z^2}{2}(-c_{\beta'} s_\alpha + 2s_{\beta'} c_\alpha)^2 DB_0(p^2, m_Z, m_Z) + \frac{g_Z^2}{8}(5+3c_{2\alpha})DA(m_Z)$$
$$- \frac{g_Z^2}{4}(-s_\alpha c_{\beta'} + 2c_\alpha s_{\beta'})^2[2A(m_Z) - A(m_{G^0}) + (2m_{G^0}^2 - m_Z^2 + 2p^2)B_0(p^2, m_Z, m_{G^0})]$$
$$- \frac{g_Z^2}{4}(2c_\alpha c_{\beta'} + s_\alpha s_{\beta'})^2[2A(m_Z) - A(m_A) + (2m_A^2 - m_Z^2 + 2p^2)B_0(p^2, m_Z, m_A)]$$
$$- 2\lambda_{G^0G^0HH}A(m_{G^0}) - \frac{g_Z^2 m_Z^2}{4}(-c_{\beta'} s_\alpha + 2s_{\beta'} c_\alpha)^2 B_0(p^2, m_{c_Z}, m_{c_Z})\Bigg\}, \tag{D.126}$$

$$\Pi^{\rm 1PI}_{Hh}(p^2)_V = \frac{1}{16\pi^2}\Bigg\{ g^2 m_W^2(c_\beta c_\alpha + \sqrt{2}s_\beta s_\alpha)(-c_\beta s_\alpha + \sqrt{2}s_\beta c_\alpha) DB_0(p^2, m_W, m_W) + \frac{g^2}{4}s_{2\alpha}DA(m_W)$$
$$- \frac{g^2}{2}(c_\alpha c_\beta + \sqrt{2}s_\alpha s_\beta)(-s_\alpha c_\beta + \sqrt{2}c_\alpha s_\beta)[2A(m_W) - A(m_{G^+}) + (2m_{G^+}^2 - m_W^2 + 2p^2)B_0(p^2, m_W, m_{G^+})]$$
$$- \frac{g^2}{2}(-c_\alpha s_\beta + \sqrt{2}s_\alpha c_\beta)(s_\alpha s_\beta + \sqrt{2}c_\alpha c_\beta)[2A(m_W) - A(m_{H^+}) + (2m_{H^+}^2 - m_W^2 + 2p^2)B_0(p^2, m_W, m_{H^+})]$$
$$- \lambda_{G^+G^-Hh}A(m_{G^+}) - \frac{g^2 m_W^2}{2}(c_\beta c_\alpha + \sqrt{2}s_\beta s_\alpha)(-c_\beta s_\alpha + \sqrt{2}s_\beta c_\alpha)B_0(p^2, m_{c^+}, m_{c^+})$$
$$+ \frac{g_Z^2 m_Z^2}{2}(c_{\beta'} c_\alpha + 2s_{\beta'} s_\alpha)(-c_{\beta'} s_\alpha + 2s_{\beta'} c_\alpha) DB_0(p^2, m_Z, m_Z) + \frac{3g_Z^2}{8}s_{2\alpha}DA(m_Z)$$
$$- \frac{g_Z^2}{4}(c_\alpha c_{\beta'} + 2s_\alpha s_{\beta'})(-s_\alpha c_{\beta'} + 2c_\alpha s_{\beta'})[2A(m_Z) - A(m_{G^0}) + (2m_{G^0}^2 - m_Z^2 + 2p^2)B_0(p^2, m_Z, m_{G^0})]$$
$$- \frac{g_Z^2}{4}(-c_\alpha s_{\beta'} + 2s_\alpha c_{\beta'})(s_\alpha s_{\beta'} + 2c_\alpha c_{\beta'})[2A(m_Z) - A(m_A) + (2m_A^2 - m_Z^2 + 2p^2)B_0(p^2, m_Z, m_A)]$$
$$- \lambda_{G^0G^0Hh}A(m_{G^0}) - \frac{g_Z^2 m_Z^2}{4}(c_{\beta'} c_\alpha + 2s_{\beta'} s_\alpha)(-c_{\beta'} s_\alpha + 2s_{\beta'} c_\alpha)B_0(p^2, m_{c_Z}, m_{c_Z})\Bigg\}, \tag{D.127}$$

$$\Pi^{\rm 1PI}_{AA}(p^2)_V = \frac{1}{16\pi^2}\Bigg\{ \frac{g^2}{4}(3+c_{2\beta'})DA(m_W) - 2\lambda_{G^+G^-AA}A(m_{G^+})$$
$$- \frac{g^2}{2}(-c_\beta s_{\beta'} + \sqrt{2}s_\beta c_{\beta'})^2[2A(m_W) - A(m_{G^+}) + (2m^2_{G^+} - m^2_W + 2p^2)B_0(p^2, m_W, m_{G^+})]$$
$$- \frac{g^2}{2}(s_\beta s_{\beta'} + \sqrt{2}c_\beta c_{\beta'})^2[2A(m_W) - A(m_{H^+}) + (2m^2_{H^+} - m^2_W + 2p^2)B_0(p^2, m_W, m_{H^+})]$$
$$+ \frac{g^2 m^2_W}{2}(-c_\beta s_{\beta'} + \sqrt{2}s_\beta c_{\beta'})^2 B_0(p^2, m_{c^+}, m_{c^+})$$
$$+ \frac{g^2_Z}{8}(5+3c_{2\beta'})DA(m_Z) - 2\lambda_{AAG^0G^0}A(m_{G^0})$$
$$- \frac{g^2_Z}{4}(-c_\alpha s_{\beta'} + 2s_\alpha c_{\beta'})^2[2A(m_Z) - A(m_h) + (2m^2_h - m^2_Z + 2p^2)B_0(p^2, m_Z, m_h)]$$
$$- \frac{g^2_Z}{4}(s_\alpha s_{\beta'} + 2c_\alpha c_{\beta'})^2[2A(m_Z) - A(m_H) + (2m^2_H - m^2_Z + 2p^2)B_0(p^2, m_Z, m_H)]\Bigg\}, \qquad \text{(D.128)}$$

$$\Pi^{\rm 1PI}_{AG}(p^2)_V = \frac{1}{16\pi^2}\Bigg\{ \frac{g^2}{4}s_{2\beta'}DA(m_W) + \frac{3}{8}g^2_Z s_{2\beta'}DA(m_Z)$$
$$- \frac{g^2}{2}(s_\beta s_{\beta'} + \sqrt{2}c_\beta c_{\beta'})(-s_\beta c_{\beta'} + \sqrt{2}c_\beta s_{\beta'})[2A(m_W) - A(m_{H^+}) + (2m^2_{H^+} - m^2_W + 2p^2)B_0(p^2, m_W, m_{H^+})$$
$$- \frac{g^2_Z}{4}(-c_\alpha s_{\beta'} + 2s_\alpha c_{\beta'})(c_\alpha c_{\beta'} + 2s_\alpha s_{\beta'})[2A(m_Z) - A(m_h) + (2m^2_h - m^2_Z + 2p^2)B_0(p^2, m_Z, m_h)]$$
$$- \frac{g^2_Z}{4}(2c_\alpha c_{\beta'} + s_\alpha s_{\beta'})(-s_\alpha c_{\beta'} + 2c_\alpha s_{\beta'})[2A(m_Z) - A(m_H) + (2m^2_H - m^2_Z + 2p^2)B_0(p^2, m_Z, m_H)]$$
$$- 3\lambda_{AG^0G^0G^0}A(m_{G^0}) - \lambda_{G^+G^-AG^0}A(m_{G^+})\Bigg\}. \qquad \text{(D.129)}$$

The 1PI diagram contributions to the gauge boson two point functions are calculated as follows. The fermion-loop contributions are

$$\Pi^{\rm 1PI}_{WW}(p^2)_F = \frac{g^2}{16\pi^2}N^f_c\Big[- B_4 + 2p^2 B_3\Big](p^2, m_f, m_{f'}), \qquad \text{(D.130)}$$
$$\Pi^{\rm 1PI}_{ZZ}(p^2)_F = \frac{g^2_Z}{16\pi^2}N^f_c\Big[2p^2(4s^4_W Q^2_f - 4s^2_W Q_f I_f + 2I^2_f)B_3 - 2I^2_f m^2_f B_0\Big](p^2, m_f, m_f), \qquad \text{(D.131)}$$
$$\Pi^{\rm 1PI}_{\gamma\gamma}(p^2)_F = \frac{e^2}{16\pi^2}N^f_c Q^2_f\Big[8p^2 B_3\Big](p^2, m_f, m_f), \qquad \text{(D.132)}$$
$$\Pi^{\rm 1PI}_{Z\gamma}(p^2)_F = -\frac{e g_Z}{16\pi^2}N^f_c\Big[2p^2(-4s^2_W Q^2_f + 2I_f Q_f)B_3\Big](p^2, m_f, m_f), \qquad \text{(D.133)}$$

where $B_3(p^2, m_1, m_2) = -B_1(p^2, m_1, m_2) - B_{21}(p^2, m_1, m_2)$ and $B_4(p^2, m_1, m_2) = -m^2_1 B_1(p^2, m_2, m_1) - m^2_2 B_1(p^2, m_1, m_2)$ [**?**].

The scalar-boson loop contirbutions are

$$\Pi^{\rm 1PI}_{WW}(p^2)_S = \frac{1}{16\pi^2}\frac{g^2}{4}\Big[4c_\beta^2 B_5(p^2,m_{H^{++}},m_{H^+}) + 4s_\beta^2 B_5(p^2,m_{H^{++}},m_{G^+})$$
$$+ (c_\alpha s_\beta - \sqrt{2}s_\alpha c_\beta)^2 B_5(p^2,m_{H^+},m_h) + (c_\alpha c_\beta + \sqrt{2}s_\alpha s_\beta)^2 B_5(p^2,m_{G^+},m_h)$$
$$+ (s_\alpha s_\beta + \sqrt{2}c_\alpha c_\beta)^2 B_5(p^2,m_{H^+},m_H) + (s_\alpha c_\beta - \sqrt{2}c_\alpha s_\beta)^2 B_5(p^2,m_{G^+},m_H)$$
$$+ (s_{\beta'} s_\beta + \sqrt{2}c_{\beta'} c_\beta)^2 B_5(p^2,m_{H^+},m_A) + (s_{\beta'} c_\beta - \sqrt{2}c_{\beta'} s_\beta)^2 B_5(p^2,m_{G^+},m_A)$$
$$+ (-c_{\beta'} s_\beta + \sqrt{2}s_{\beta'} c_\beta)^2 B_5(p^2,m_{H^+},m_Z) + (c_{\beta'} c_\beta + \sqrt{2}s_{\beta'} s_\beta)^2 B_5(p^2,m_{G^+},m_{G^0})\Big], \quad \text{(D.134)}$$

$$\Pi^{\rm 1PI}_{ZZ}(p^2)_S = \frac{1}{16\pi^2}\frac{g_Z^2}{4}\Big[4(c_W^2 - s_W^2)^2 B_5(p^2,m_{H^{++}},m_{H^{++}}) + (c_W^2 - s_W^2 - c_\beta^2)^2 B_5(p^2,m_{H^+},m_{H^+})$$
$$+ (c_W^2 - s_W^2 - s_\beta^2)^2 B_5(p^2,m_{G^+},m_{G^+}) + 2s_\beta^2 c_\beta^2 B_5(p^2,m_{H^+},m_{G^+})$$
$$+ (2c_\alpha c_{\beta'} + s_\alpha s_{\beta'})^2 B_5(p^2,m_H,m_A) + (2s_\alpha c_{\beta'} - c_\alpha s_{\beta'})^2 B_5(p^2,m_h,m_A)$$
$$+ (s_\alpha c_{\beta'} - 2c_\alpha s_{\beta'})^2 B_5(p^2,m_H,m_{G^0}) + (c_\alpha c_{\beta'} + 2s_\alpha s_{\beta'})^2 B_5(p^2,m_h,m_{G^0})\Big], \quad \text{(D.135)}$$

$$\Pi^{\rm 1PI}_{\gamma\gamma}(p^2)_S = \frac{e^2}{16\pi^2}\Big[4B_5(p^2,m_{H^{++}},m_{H^{++}}) + B_5(p^2,m_{H^+},m_{H^+}) + B_5(p^2,m_{G^+},m_{G^+})\Big], \quad \text{(D.136)}$$

$$\Pi^{\rm 1PI}_{Z\gamma}(p^2)_S = -\frac{eg_Z}{16\pi^2}\Big[2(c_W^2 - s_W^2)B_5(p^2,m_{H^{++}},m_{H^{++}})$$
$$+ \frac{1}{2}(c_W^2 - s_W^2 - c_\beta^2)B_5(p^2,m_{H^+},m_{H^+}) + \frac{1}{2}(c_W^2 - s_W^2 - s_{\beta_\pm}^2)B_5(p^2,m_{G^+},m_{G^+})\Big], \quad \text{(D.137)}$$

where $B_5(p^2,m_1,m_2) = A(m_1) + A(m_2) - 4B_{22}(p^2,m_1,m_2)$ [**?**]. The gauge boson loop contributions are

$$\overline{\Pi}^{\rm 1PI}_{WW}(p^2)_V = \Pi^{\rm 1PI}_{WW}(p^2)_V - \frac{4g^2}{16\pi^2}(p^2 - m_W^2)[c_W^2 B_0(p^2,m_Z,m_W) + s_W^2 B_0(p^2,0,m_W)],$$
$$\overline{\Pi}^{\rm 1PI}_{ZZ}(p^2)_V = \Pi^{\rm 1PI}_{ZZ}(p^2)_V - \frac{4g_Z^2}{16\pi^2}c_W^4(p^2 - m_Z^2)B_0(p^2,m_W,m_W),$$
$$\overline{\Pi}^{\rm 1PI}_{\gamma\gamma}(p^2)_V = \Pi^{\rm 1PI}_{\gamma\gamma}(p^2)_V - \frac{4e^2}{16\pi^2}p^2 B_0(p^2,m_W,m_W),$$
$$\overline{\Pi}^{\rm 1PI}_{Z\gamma}(p^2)_V = \Pi^{\rm 1PI}_{Z\gamma}(p^2)_V + \frac{4eg_Z}{16\pi^2}c_W^2\left(p^2 - \frac{1}{2}m_Z^2\right)B_0(p^2,m_W,m_W), \quad \text{(D.138)}$$

where $\overline{\Pi}^{\rm 1PI}_{XY}(p^2)_V$ functions are the gauge invariant two point functions while $\Pi^{\rm 1PI}_{XY}(p^2)_V$ functions are the amplitude calculated in the 't Hooft-Feynman gauge. The second term of the right-hand side in Eq. (D.138) corresponds to the pinch-terms [**?**] which are introduced to maintain the gauge invariance of the gauge boson two point functions. The $\Pi^{\rm 1PI}_{XY}(p^2)_V$ functions are

calculated as

$$\Pi^{\rm 1PI}_{WW}(p^2)_V = \frac{g^2}{16\pi^2}\Bigg\{ m_W^2\Big[\Big(c_\beta c_\alpha + \sqrt{2}s_\beta s_\alpha\Big)^2 B_0(p^2,m_h,m_W) + \Big(c_\beta s_\alpha - \sqrt{2}s_\beta c_\alpha\Big)^2 B_0(p^2,m_H,m_W)$$
$$+ 4s_\beta^2 B_0(p^2,m_{H^{++}},m_W) + \frac{c_\beta^2 s_\beta^2}{c_W^2}B_0(p^2,m_{H^+},m_Z) + s_W^2 B_0(p^2,m_{G^+},0) + \frac{(s_W^2+s_\beta^2)^2}{c_W^2}B_0(p^2,m_{G^+},m_Z)\Big]$$
$$- c_W^2\left[(6D-8)B_{22} + p^2(2B_{21}+2B_1+5B_0)\right](p^2,m_Z,m_W) + (D-1)\left[c_W^2 A(m_Z) + A(m_W)\right]$$
$$- s_W^2\left[(6D-8)B_{22} + p^2(2B_{21}+2B_1+5B_0)\right](p^2,0,m_W)\Bigg\}, \tag{D.139}$$

$$\Pi^{\rm 1PI}_{ZZ}(p^2)_V = \frac{g_Z^2}{16\pi^2}\Bigg\{ m_Z^2\Big[(c_{\beta'}c_\alpha + 2s_{\beta'}s_\alpha)^2 B_0(p^2,m_h,m_Z) + (c_{\beta'}s_\alpha - 2s_{\beta'}c_\alpha)^2 B_0(p^2,m_H,m_Z)\Big]$$
$$+ m_W^2\Big[2c_\beta^2 s_\beta^2 B_0(p^2,m_{H^+},m_W) + 2\left(s_W^2+s_\beta^2\right)^2 B_0(p^2,m_{G^+},m_W)\Big]$$
$$- c_W^4\left[(6D-8)B_{22} + p^2(2B_{21}+2B_1+5B_0)\right](p^2,m_W,m_W) + 2(D-1)c_W^4 A(m_W)\Bigg\}, \tag{D.140}$$

$$\Pi^{\rm 1PI}_{\gamma\gamma}(p^2)_V = -\frac{e^2}{16\pi^2}\Big[(6D-8)B_{22}(p^2,m_W,m_W) + p^2(2B_{21}+2B_1+5B_0)(p^2,m_W,m_W)$$
$$- 2(D-1)A(m_W) - 2m_W^2 B_0(p^2,m_{G^+},m_W)\Big], \tag{D.141}$$

$$\Pi^{\rm 1PI}_{Z\gamma}(p^2)_V = +\frac{eg_Z}{16\pi^2}\Big[c_W^2(6D-8)B_{22}(p^2,m_W,m_W) + c_W^2 p^2(2B_{21}+2B_1+5B_0)(p^2,m_W,m_W)$$
$$- 2c_W^2(D-1)A(m_W) + 2m_W^2(s_W^2+s_\beta^2)B_0(p^2,m_{G^+},m_W)\Big]. \tag{D.142}$$

D.2.7 Three-point functions

In this subsection, we use the shortened notation for the three-point function of the Passarino-Veltman function as $C_i(m_1,m_2,m_3) \equiv C_i(p_1^2,p_2^2,q^2,m_1,m_2,m_3)$. The 1PI diagram contributions to the hhh vertex can be expressed as a function of the incoming momenta p_1 and p_2 and the outgoing momentum $q = p_1 + p_2$ as

$$\Gamma^{\rm 1PI}_{hhh}(p_1^2,p_2^2,q^2)_F = -\frac{8m_f^4 N_c^f}{16\pi^2}\frac{c_\alpha^3}{v_\phi^3}\Big[B_0(p_1^2,m_f,m_f) + B_0(p_2^2,m_f,m_f) + B_0(q^2,m_f,m_f)$$
$$+ (4m_f^2 - q^2 + p_1\cdot p_2)C_0(m_f,m_f,m_f)\Big], \tag{D.143}$$

$$
\begin{aligned}
&\Gamma^{\rm 1PI}_{hhh}(p_1^2,p_2^2,q^2)_S = \frac{1}{16\pi^2}\Big\{ \\
&+2\lambda_{H^{++}H^{--}h}\lambda_{H^{++}H^{--}hh}[B_0(p_1^2,m_{H^{++}},m_{H^{++}})+B_0(p_2^2,m_{H^{++}},m_{H^{++}})+B_0(q^2,m_{H^{++}},m_{H^{++}})] \\
&+2\lambda_{H^{+}H^{-}h}\lambda_{H^{+}H^{-}hh}[B_0(p_1^2,m_{H^{+}},m_{H^{+}})+B_0(p_2^2,m_{H^{+}},m_{H^{+}})+B_0(q^2,m_{H^{+}},m_{H^{+}})] \\
&+2\lambda_{hG^+G^-}\lambda_{hhG^+G^-}[B_0(p_1^2,m_W,m_W)+B_0(p_2^2,m_W,m_W)+B_0(q^2,m_W,m_W)] \\
&+4\lambda_{H^+G^-h}\lambda_{H^+G^-hh}[B_0(p_1^2,m_{H^+},m_W)+B_0(p_2^2,m_{H^+},m_W)+B_0(q^2,m_{H^+},m_W)] \\
&+4\lambda_{AAh}\lambda_{AAhh}[B_0(p_1^2,m_A,m_A)+B_0(p_2^2,m_A,m_A)+B_0(q^2,m_A,m_A)] \\
&+4\lambda_{G^0G^0h}\lambda_{G^0G^0hh}[B_0(p_1^2,m_Z,m_Z)+B_0(p_2^2,m_Z,m_Z)+B_0(q^2,m_Z,m_Z)] \\
&+2\lambda_{AG^0h}\lambda_{AG^0hh}[B_0(p_1^2,m_A,m_Z)+B_0(p_2^2,m_A,m_Z)+B_0(q^2,m_A,m_Z)] \\
&+4\lambda_{HHh}\lambda_{HHhh}[B_0(p_1^2,m_H,m_H)+B_0(p_2^2,m_H,m_H)+B_0(q^2,m_H,m_H)] \\
&+12\lambda_{Hhh}\lambda_{Hhhh}[B_0(p_1^2,m_h,m_H)+B_0(p_2^2,m_h,m_H)+B_0(q^2,m_h,m_H)] \\
&+72\lambda_{hhh}\lambda_{hhhh}[B_0(p_1^2,m_h,m_h)+B_0(p_2^2,m_h,m_h)+B_0(q^2,m_h,m_h)]\Big]\Big\} \\
&-\frac{1}{16\pi^2}\Big\{2\lambda^3_{H^{++}H^{--}h}C_0(m_{H^{++}},m_{H^{++}},m_{H^{++}})+2\lambda^3_{H^+H^-h}C_0(m_{H^+},m_{H^+},m_{H^+}) \\
&+2\lambda^3_{G^+G^-h}C_0(m_W,m_W,m_W)+8\lambda^3_{G^0G^0h}C_0(m_Z,m_Z,m_Z) \\
&+8\lambda^3_{AAh}C_0(m_A,m_A,m_A)+8\lambda^3_{HHh}C_0(m_H,m_H,m_H)+216\lambda^3_{hhh}C_0(m_h,m_h,m_h) \\
&+2\lambda_{H^+H^-h}\lambda^2_{H^+G^-h}[C_0(m_{G^+},m_{H^+},m_{H^+})+C_0(m_{H^+},m_W,m_{H^+})+C_0(m_{H^+},m_{H^+},m_W)] \\
&+2\lambda_{G^+G^-h}\lambda^2_{H^+G^-h}[C_0(m_{H^+},m_W,m_W)+C_0(m_{G^+},m_{H^+},m_W)+C_0(m_W,m_W,m_{H^+})] \\
&+2\lambda_{AAh}\lambda^2_{AG^0h}[C_0(m_Z,m_A,m_A)+C_0(m_A,m_Z,m_A)+C_0(m_A,m_A,m_Z)] \\
&+2\lambda_{G^0G^0h}\lambda^2_{AG^0h}[C_0(m_A,m_Z,m_Z)+C_0(m_Z,m_A,m_Z)+C_0(m_Z,m_Z,m_A)] \\
&+8\lambda_{HHh}\lambda^2_{Hhh}[C_0(m_h,m_H,m_H)+C_0(m_H,m_H,m_h)+C_0(m_H,m_h,m_H)] \\
&+24\lambda_{hhh}\lambda^2_{Hhh}[C_0(m_h,m_h,m_H)+C_0(m_H,m_h,m_h)+C_0(m_h,m_H,m_h)]\Big\}, \qquad \text{(D.144)}
\end{aligned}
$$

$$\Gamma^{\rm 1PI}_{hhh}(p_1^2,p_2^2,q^2)_V = \frac{1}{16\pi^2}\Bigg[$$
$$+\frac{3g^3}{4}m_W(c_\beta c_\alpha+\sqrt{2}s_\beta s_\alpha)(3-c_{2\alpha})DB_0(q^2,m_W,m_W)+2g^3m_W^3(c_\beta c_\alpha+\sqrt{2}s_\beta s_\alpha)^3DC_0(m_W,m_W,m_W)$$
$$-\frac{g^3}{2}m_W(c_\beta c_\alpha+\sqrt{2}s_\beta s_\alpha)^3C^{hhh}_{SVV}(m_{G^+},m_W,m_W)$$
$$-\frac{g^3}{2}m_W(c_\beta c_\alpha+\sqrt{2}s_\beta s_\alpha)(-s_\beta c_\alpha+\sqrt{2}c_\beta s_\alpha)^2C^{hhh}_{SVV}(m_{H^+},m_W,m_W)$$
$$+\frac{g^2}{2}\lambda_{G^+G^-h}(c_\beta c_\alpha+\sqrt{2}s_\beta s_\alpha)^2C^{hhh}_{VSS}(m_W,m_{G^+},m_{G^+})$$
$$+\frac{g^2}{2}\lambda_{H^+H^-h}(-s_\beta c_\alpha+\sqrt{2}c_\beta s_\alpha)^2C^{hhh}_{VSS}(m_W,m_{H^+},m_{H^+})$$
$$+\frac{g^2}{2}\lambda_{H^+G^-h}(c_\beta c_\alpha+\sqrt{2}s_\beta s_\alpha)(-s_\beta c_\alpha+\sqrt{2}c_\beta s_\alpha)[C^{hhh}_{VSS}(m_W,m_{G^+},m_{H^+})+C_{VSS}(m_W,m_{H^+},m_{G^+})]$$
$$-\frac{g^3m_W^3}{2}(c_\beta c_\alpha+\sqrt{2}s_\beta s_\alpha)^3C_0(m_{c^+},m_{c^+},m_{c^+})$$
$$+\frac{3g_Z^3m_Z}{8}(c_{\beta'}c_\alpha+2s_{\beta'}s_\alpha)(5-3c_{2\alpha})DB_0(q^2,m_Z,m_Z)+g_Z^3m_Z^3(c_{\beta'}c_\alpha+2s_{\beta'}s_\alpha)^3DC_0(m_Z,m_Z,m_Z)$$
$$-\frac{g_Z^3m_Z}{4}(c_{\beta'}c_\alpha+2s_{\beta'}s_\alpha)^3C^{hhh}_{SVV}(m_{G^0},m_Z,m_Z)$$
$$-\frac{g_Z^3m_Z}{4}(c_{\beta'}c_\alpha+2s_{\beta'}s_\alpha)(-s_{\beta'}c_\alpha+2c_{\beta'}s_\alpha)^2C^{hhh}_{SVV}(m_A,m_Z,m_Z)$$
$$+\frac{g_Z^2}{2}\lambda_{G^0G^0h}(c_{\beta'}c_\alpha+2s_{\beta'}s_\alpha)^2C^{hhh}_{VSS}(m_Z,m_{G^0},m_{G^0})+\frac{g_Z^2}{2}\lambda_{AAh}(-s_{\beta'}c_\alpha+2c_{\beta'}s_\alpha)^2C^{hhh}_{VSS}(m_Z,m_A,m_A)$$
$$+\frac{g_Z^2}{4}\lambda_{AG^0h}(c_{\beta'}c_\alpha+2s_{\beta'}s_\alpha)(-s_{\beta'}c_\alpha+2c_{\beta'}s_\alpha)[C^{hhh}_{VSS}(m_Z,m_A,m_{G^0})+C^{hhh}_{VSS}(m_Z,m_{G^0},m_A)]$$
$$-\frac{g_Z^3m_Z^3}{4}(c_{\beta'}c_\alpha+2s_{\beta'}s_\alpha)^3C_0(m_{c_Z},m_{c_Z},m_{c_Z})\Bigg], \tag{D.145}$$

where we define

$$C^{hhh}_{SVV}(m_1,m_2,m_3)\equiv$$
$$\Big[p_1^2C_{21}+p_2^2C_{22}+2p_1p_2C_{23}+DC_{24}-(q+p_1)(p_1C_{11}+p_2C_{12})+qp_1C_0\Big](m_1,m_2,m_3)$$
$$+\Big[p_1^2C_{21}+p_2^2C_{22}+2p_1p_2C_{23}+DC_{24}+(3p_1-p_2)(p_1C_{11}+p_2C_{12})+2p_1(p_1-p_2)C_0\Big](m_3,m_1,m_2)$$
$$+\Big[p_1^2C_{21}+p_2^2C_{22}+2p_1p_2C_{23}+DC_{24}+(3p_1+4p_2)(p_1C_{11}+p_2C_{12})+2q(q+p_2)C_0\Big](m_2,m_3,m_1), \tag{D.146}$$

$$C^{hhh}_{VSS}(m_V,m_S,m_S)\equiv$$
$$\Big[p_1^2C_{21}+p_2^2C_{22}+2p_1p_2C_{23}+DC_{24}+(4p_1+2p_2)(p_1C_{11}+p_2C_{12})+4p_1\cdot qC_0\Big](m_V,m_S,m_S)$$
$$+\Big[p_1^2C_{21}+p_2^2C_{22}+2p_1p_2C_{23}+DC_{24}+2p_2(p_1C_{11}+p_2C_{12})-p_1(p_1+2p_2)C_0\Big](m_S,m_V,m_S)$$
$$+\Big[p_1^2C_{21}+p_2^2C_{22}+2p_1p_2C_{23}+DC_{24}-2p_2(p_1C_{11}+p_2C_{12})-q(p_1-p_2)C_0\Big](m_S,m_S,m_V). \tag{D.147}$$

The 1PI diagram contributions to the form factors of the hZZ and hWW vertices which are defined in Eq. (7.73) are calculated as

$$M^{hZZ}_{1,1\mathrm{PI}}(p_1^2,p_2^2,q^2)_F = -\frac{32m_f^2m_Z^2N_c^f c_\alpha}{v_\phi(v^2+2v_\Delta^2)}\frac{1}{16\pi^2}\Bigg\{-\frac{1}{4}(I_f^2-2s_W^2I_fQ_f+2s_W^4Q_f^2)$$
$$\Big[B_0(p_1^2,m_f,m_f)+B_0(p_2^2,m_f,m_f)+2B_0(q^2,m_f,m_f)$$
$$+\frac{s_W^2}{2}(-I_fQ_f+s_W^2Q_f^2)\Big[B_0(p_2^2,m_f,m_f)+B_0(p_1^2,m_f,m_f)+(4m_f^2-q^2)C_0(m_f,m_f,m_f)\Big]\Bigg\}, \tag{D.148}$$

$$M^{hZZ}_{2,1\mathrm{PI}}(p_1^2,p_2^2,q^2)_F = -\frac{32m_f^2m_Z^4N_c^f c_\alpha}{v_\phi(v^2+2v_\Delta^2)}\frac{1}{16\pi^2}$$
$$\times\Big[\frac{1}{2}(I_f^2-2s_W^2I_fQ_f+2s_W^4Q_f^2)\Big(4C_{23}+3C_{12}+C_{11}+C_0\Big)+s_W^2(-I_fQ_f+s_W^2Q_f^2)\Big(C_{12}-C_{11}\Big)\Big]$$
$$(m_f,m_f,m_f), \tag{D.149}$$

$$M^{hZZ}_{3,1\mathrm{PI}}(p_1^2,p_2^2,q^2)_F = -\frac{32m_f^2m_Z^4N_c^f c_\alpha}{v_\phi(v^2+2v_\Delta^2)}\frac{1}{16\pi^2}\frac{I_f}{2}(-I_f+2s_W^2Q_f)(C_{11}+C_{12}+C_0)(m_f,m_f,m_f), \tag{D.150}$$

$$M^{hWW}_{1,1\mathrm{PI}}(p_1^2,p_2^2,q^2)_F = \frac{4m_W^2m_t^2N_c^f c_\alpha}{v_\phi v^2}\frac{1}{16\pi^2}\Bigg[\frac{1}{2}B_0(p_2^2,m_t,m_b)+B_0(q^2,m_t,m_t)+\frac{1}{2}B_0(p_1^2,m_t,m_b)$$
$$-4C_{24}(p_1^2,p_2^2,q^2,m_t,m_b,m_t)+\frac{1}{2}(2m_t^2+2m_b^2-p_1^2-p_2^2)C_0(m_t,m_b,m_t)\Bigg]+(m_t\leftrightarrow m_b), \tag{D.151}$$

$$M^{hWW}_{2,1\mathrm{PI}}(p_1^2,p_2^2,q^2)_F = \frac{-4m_W^4m_t^2N_c^f c_\alpha}{v_\phi v^2}\frac{1}{16\pi^2}\left(4C_{23}+3C_{12}+C_{11}+C_0\right)(m_t,m_b,m_t)+(m_t\leftrightarrow m_b), \tag{D.152}$$

$$M^{hWW}_{3,1\mathrm{PI}}(p_1^2,p_2^2,q^2)_F = \frac{-4m_W^4m_t^2N_c^f c_\alpha}{v_\phi v^2}\frac{1}{16\pi^2}\left(C_{11}+C_{12}+C_0\right)(m_t,m_b,m_t)+(m_t\leftrightarrow m_b). \tag{D.153}$$

$$
\begin{aligned}
M^{hZZ}_{1,1\mathrm{PI}}(p_1^2,p_2^2,q^2)_S = &-\frac{16m_Z^2}{v^2+2v_\Delta^2}\frac{1}{16\pi^2}\Bigg\{2\lambda_{H^{++}H^{--}h}(c_W^2-s_W^2)^2C_{24}(m_{H^{++}},m_{H^{++}},m_{H^{++}})\\
&+\frac{1}{2}\lambda_{H^+H^-h}(c_W^2-s_W^2-c_\beta^2)^2C_{24}(m_{H^+},m_{H^+},m_{H^+})\\
&+\frac{1}{8}\lambda_{H^+H^-h}s_{2\beta}^2C_{24}(m_{H^+},m_{G^+},m_{H^+})+\frac{1}{8}\lambda_{G^+G^-h}s_{2\beta}^2C_{24}(m_{G^+},m_{H^+},m_{G^+})\\
&-\frac{1}{4}\lambda_{H^+G^-h}s_{2\beta}(c_W^2-s_W^2-c_\beta^2)[C_{24}(m_{H^+},m_{H^+},m_{G^+})+C_{24}(m_{G^+},m_{H^+},m_{H^+})]\\
&-\frac{1}{4}\lambda_{H^+G^-h}s_{2\beta}(c_W^2-s_W^2-s_\beta^2)[C_{24}(m_{H^+},m_{G^+},m_{G^+})+C_{24}(m_{G^+},m_{G^+},m_{H^+})]\\
&+\frac{1}{2}\lambda_{G^+G^-h}(c_W^2-s_W^2-s_\beta^2)^2C_{24}(m_{G^+},m_{G^+},m_{G^+})\\
&+\frac{1}{2}\lambda_{AAh}(2c_\alpha c_{\beta'}+s_\alpha s_{\beta'})^2C_{24}(m_A,m_H,m_A)+\frac{1}{2}\lambda_{AAh}(c_\alpha s_{\beta'}-2s_\alpha c_{\beta'})^2C_{24}(m_A,m_h,m_A)\\
&+\frac{1}{2}\lambda_{HHh}(2c_\alpha c_{\beta'}+s_\alpha s_{\beta'})^2C_{24}(m_H,m_A,m_H)+\frac{3}{2}\lambda_{hhh}(c_\alpha s_{\beta'}-2s_\alpha c_{\beta'})^2C_{24}(m_h,m_A,m_h)\\
&-\frac{1}{2}\lambda_{Hhh}(2c_\alpha c_{\beta'}+s_\alpha s_{\beta'})(c_\alpha s_{\beta'}-2s_\alpha c_{\beta'})\left[C_{24}(m_H,m_A,m_h)+C_{24}(m_h,m_A,m_H)\right]\\
&-\frac{1}{4}\lambda_{AG^0h}(2c_\alpha c_{\beta'}+s_\alpha s_{\beta'})(s_\alpha c_{\beta'}-2c_\alpha s_{\beta'})\left[C_{24}(m_A,m_H,m_{G^0})+C_{24}(m_{G^0},m_H,m_A)\right]\\
&-\frac{1}{4}\lambda_{AG^0h}(c_\alpha s_{\beta'}-2s_\alpha c_{\beta'})(c_\alpha c_{\beta'}+2s_\alpha s_{\beta'})\left[C_{24}(m_A,m_h,m_{G^0})+C_{24}(m_{G^0},m_h,m_A)\right]\\
&+\frac{1}{2}\lambda_{G^0G^0h}(s_\alpha c_{\beta'}-2c_\alpha s_{\beta'})^2C_{24}(m_{G^0},m_H,m_{G^0})+\frac{1}{2}\lambda_{G^0G^0h}(c_\alpha c_{\beta'}+2s_\alpha s_{\beta'})^2C_{24}(m_{G^0},m_h,m_{G^0})\\
&+\frac{1}{2}\lambda_{HHh}(s_\alpha c_{\beta'}-2c_\alpha s_{\beta'})^2C_{24}(m_H,m_{G^0},m_H)+\frac{3}{2}\lambda_{hhh}(c_\alpha c_{\beta'}+2s_\alpha s_{\beta'})^2C_{24}(m_h,m_{G^0},m_h)\\
&-\frac{1}{2}\lambda_{Hhh}(s_\alpha c_{\beta'}-2c_\alpha s_{\beta'})(c_\alpha c_{\beta'}+2s_\alpha s_{\beta'})\left[C_{24}(m_H,m_{G^0},m_h)+C_{24}(m_h,m_{G^0},m_H)\right]\Bigg\}\\
&+\frac{4m_Z^2}{v^2+2v_\Delta^2}\frac{1}{16\pi^2}\Bigg\{2\lambda_{H^{++}H^{--}h}(c_W^2-s_W^2)^2B_0(q^2,m_{H^{++}},m_{H^{++}})\\
&+\frac{1}{4}\lambda_{H^+H^-h}(2+c_{4W}-4c_{2W}c_\beta^2+c_{2\beta})B_0(q^2,m_{H^+},m_{H^+})\\
&+\frac{1}{4}\lambda_{G^+G^-h}(2+c_{4W}-4c_{2W}s_\beta^2-c_{2\beta})B_0(q^2,m_{G^+},m_{G^+})+\frac{1}{2}\lambda_{H^+G^-h}s_{2\beta}(1-2c_{2W})B_0(q^2,m_{H^+},m_{G^+})\\
&+\frac{1}{4}\lambda_{AAh}(5+3c_{2\beta'})B_0(q^2,m_A,m_A)+\frac{1}{4}\lambda_{G^0G^0h}(5-3c_{2\beta'})B_0(q^2,m_{G^0},m_{G^0})\\
&+\frac{1}{4}\lambda_{HHh}(5+3c_{2\alpha})B_0(q^2,m_H,m_H)+\frac{3}{4}\lambda_{hhh}(5-3c_{2\alpha})B_0(q^2,m_h,m_h)\\
&+\frac{3}{4}\lambda_{AG^0h}s_{2\beta'}B_0(q^2,m_A,m_{G^0})+\frac{3}{2}\lambda_{Hhh}s_{2\alpha}B_0(q^2,m_h,m_H)\Bigg\},
\end{aligned}
\tag{D.154}
$$

$$
\begin{aligned}
M^{hZZ}_{2,1\mathrm{PI}}(p_1^2,p_2^2,q^2)_S = -\frac{16m_Z^4}{v^2+2v_\Delta^2}\frac{1}{16\pi^2}\Bigg\{ & 2\lambda_{H^{++}H^{--}h}(c_W^2-s_W^2)^2 C_{1223}(m_{H^{++}},m_{H^{++}},m_{H^{++}}) \\
& + \frac{1}{2}\lambda_{H^+H^-h}(c_W^2-s_W^2-c_\beta^2)^2 C_{1223}(m_{H^+},m_{H^+},m_{H^+}) \\
& + \frac{1}{8}\lambda_{H^+H^-h}s_{2\beta}^2 C_{1223}(m_{H^+},m_W,m_{H^+}) + \frac{1}{8}\lambda_{G^+G^-h}s_{2\beta}^2 C_{1223}(m_W,m_{H^+},m_W) \\
& - \frac{1}{4}\lambda_{H^+G^-h}s_{2\beta}(c_W^2-s_W^2-c_\beta^2)[C_{1223}(m_{H^+},m_{H^+},m_W)+C_{1223}(m_W,m_{H^+},m_{H^+})] \\
& - \frac{1}{4}\lambda_{H^+G^-h}s_{2\beta}(c_W^2-s_W^2-s_\beta^2)[C_{1223}(m_{H^+},m_W,m_W)+C_{1223}(m_W,m_W,m_{H^+})] \\
& + \frac{1}{2}\lambda_{G^+G^-h}(c_W^2-s_W^2-s_\beta^2)^2 C_{1223}(m_W,m_W,m_W) \\
& + \frac{1}{2}\lambda_{AAh}(2c_\alpha c_{\beta'}+s_\alpha s_{\beta'})^2 C_{1223}(m_A,m_H,m_A) + \frac{1}{2}\lambda_{AAh}(c_\alpha s_{\beta'}-2s_\alpha c_{\beta'})^2 C_{1223}(m_A,m_h,m_A) \\
& + \frac{1}{2}\lambda_{HHh}(2c_\alpha c_{\beta'}+s_\alpha s_{\beta'})^2 C_{1223}(m_H,m_A,m_H) + \frac{3}{2}\lambda_{hhh}(c_\alpha s_{\beta'}-2s_\alpha c_{\beta'})^2 C_{1223}(m_h,m_A,m_h) \\
& - \frac{1}{2}\lambda_{Hhh}(2c_\alpha c_{\beta'}+s_\alpha s_{\beta'})(c_\alpha s_{\beta'}-2s_\alpha c_{\beta'})\,[C_{1223}(m_H,m_A,m_h)+C_{1223}(m_h,m_A,m_H)] \\
& - \frac{1}{4}\lambda_{AG^0h}(2c_\alpha c_{\beta'}+s_\alpha s_{\beta'})(s_\alpha c_{\beta'}-2c_\alpha s_{\beta'})\,[C_{1223}(m_A,m_H,m_Z)+C_{1223}(m_Z,m_H,m_A)] \\
& - \frac{1}{4}\lambda_{AG^0h}(c_\alpha s_{\beta'}-2s_\alpha c_{\beta'})(c_\alpha c_{\beta'}+2s_\alpha s_{\beta'})\,[C_{1223}(m_A,m_h,m_Z)+C_{1223}(m_Z,m_h,m_A)] \\
& + \frac{1}{2}\lambda_{G^0G^0h}(s_\alpha c_{\beta'}-2c_\alpha s_{\beta'})^2 C_{1223}(m_Z,m_H,m_Z) + \frac{1}{2}\lambda_{G^0G^0h}(c_\alpha c_{\beta'}+2s_\alpha s_{\beta'})^2 C_{1223}(m_Z,m_h,m_Z) \\
& + \frac{1}{2}\lambda_{HHh}(s_\alpha c_{\beta'}-2c_\alpha s_{\beta'})^2 C_{1223}(m_H,m_Z,m_H) + \frac{3}{2}\lambda_{hhh}(c_\alpha c_{\beta'}+2s_\alpha s_{\beta'})^2 C_{1223}(m_h,m_Z,m_h) \\
& - \frac{1}{2}\lambda_{Hhh}(s_\alpha c_{\beta'}-2c_\alpha s_{\beta'})(c_\alpha c_{\beta'}+2s_\alpha s_{\beta'})\,[C_{1223}(m_H,m_Z,m_h)+C_{1223}(m_h,m_Z,m_H)]\Bigg\},
\end{aligned}
\tag{D.155}
$$

$$
M^{hZZ}_{3,1\mathrm{PI}}(p_1^2,p_2^2,q^2)_S = 0, \tag{D.156}
$$

$$
\begin{aligned}
M^{hWW}_{1,1\mathrm{PI}}(p_1^2,p_2^2,q^2)_S = &-\frac{16m_W^2}{v^2}\frac{1}{16\pi^2}\Big\{\\
&+\lambda_{H^{++}H^{--}h}c_\beta^2 C_{24}(m_{H^{++}},m_{H^+},m_{H^{++}})+\lambda_{H^{++}H^{--}h}s_\beta^2 C_{24}(m_{H^{++}},m_{G^+},m_{H^{++}})\\
&+\lambda_{H^+H^-h}c_\beta^2 C_{24}(m_{H^+},m_{H^{++}},m_{H^+})+\lambda_{G^+G^-h}s_\beta^2 C_{24}(m_{G^+},m_{H^{++}},m_{G^+})\\
&+\lambda_{H^+G^-h}c_\beta s_\beta[C_{24}(m_{G^+},m_{H^{++}},m_{H^+})+C_{24}(m_{H^+},m_{H^{++}},m_{G^+})]\\
&+\frac{1}{2}\lambda_{AAh}\left[\left(s_\beta s_{\beta'}+\sqrt{2}c_\beta c_{\beta'}\right)^2 C_{24}(m_A,m_{H^+},m_A)+\left(-c_\beta s_{\beta'}+\sqrt{2}s_\beta c_{\beta'}\right)^2 C_{24}(m_A,m_{G^+},m_A)\right]\\
&+\frac{1}{2}\lambda_{G^0G^0h}\left[\left(-s_\beta c_{\beta'}+\sqrt{2}c_\beta s_{\beta'}\right)^2 C_{24}(m_{G^0},m_{H^+},m_{G^0})+\left(c_\beta c_{\beta'}+\sqrt{2}s_\beta s_{\beta'}\right)^2 C_{24}(m_{G^0},m_{G^+},m_{G^0})\right]\\
&+\frac{1}{4}\lambda_{AG^0h}\left(s_\beta s_{\beta'}+\sqrt{2}c_\beta c_{\beta'}\right)\left(-s_\beta c_{\beta'}+\sqrt{2}c_\beta s_{\beta'}\right)[C_{24}(m_A,m_{H^+},m_{G^0})+C_{24}(m_{G^0},m_{H^+},m_A)]\\
&+\frac{1}{4}\lambda_{AG^0h}\left(-c_\beta s_{\beta'}+\sqrt{2}s_\beta c_{\beta'}\right)\left(c_\beta c_{\beta'}+\sqrt{2}s_\beta s_{\beta'}\right)[C_{24}(m_A,m_{G^+},m_{G^0})+C_{24}(m_{G^0},m_{G^+},m_A)]\\
&+\frac{1}{2}\lambda_{HHh}\left[\left(s_\beta s_\alpha+\sqrt{2}c_\beta c_\alpha\right)^2 C_{24}(m_H,m_{H^+},m_H)+\left(-c_\beta s_\alpha+\sqrt{2}s_\beta c_\alpha\right)^2 C_{24}(m_H,m_{G^+},m_H)\right]\\
&+\frac{3}{2}\lambda_{hhh}\left[\left(-s_\beta c_\alpha+\sqrt{2}c_\beta s_\alpha\right)^2 C_{24}(m_h,m_{H^+},m_h)+\left(c_\beta c_\alpha+\sqrt{2}s_\beta s_\alpha\right)^2 C_{24}(m_h,m_{G^+},m_h)\right]\\
&+\frac{1}{2}\lambda_{Hhh}\left(s_\beta s_\alpha+\sqrt{2}c_\beta c_\alpha\right)\left(-s_\beta c_\alpha+\sqrt{2}c_\beta s_\alpha\right)[C_{24}(m_H,m_{H^+},m_h)+C_{24}(m_h,m_{H^+},m_H)]\\
&+\frac{1}{2}\lambda_{Hhh}\left(-c_\beta s_\alpha+\sqrt{2}s_\beta c_\alpha\right)\left(c_\beta c_\alpha+\sqrt{2}s_\beta s_\alpha\right)[C_{24}(m_H,m_{G^+},m_h)+C_{24}(m_h,m_{G^+},m_H)]\\
&+\frac{1}{4}\lambda_{H^+H^-h}\left[\left(s_\beta s_{\beta'}+\sqrt{2}c_\beta c_{\beta'}\right)^2 C_{24}(m_{H^+},m_A,m_{H^+})+\left(-s_\beta c_{\beta'}+\sqrt{2}c_\beta s_{\beta'}\right)^2 C_{24}(m_{H^+},m_{G^0},m_{H^+})\right]\\
&+\frac{1}{4}\lambda_{H^+H^-h}\left[\left(s_\beta s_\alpha+\sqrt{2}c_\beta c_\alpha\right)^2 C_{24}(m_{H^+},m_H,m_{H^+})+\left(-s_\beta c_\alpha+\sqrt{2}c_\beta s_\alpha\right)^2 C_{24}(m_{H^+},m_h,m_{H^+})\right]\\
&+\frac{1}{4}\lambda_{G^+G^-h}\left[\left(-c_\beta s_{\beta'}+\sqrt{2}s_\beta c_{\beta'}\right)^2 C_{24}(m_{G^+},m_A,m_{G^+})+\left(c_\beta c_{\beta'}+\sqrt{2}s_\beta s_{\beta'}\right)^2 C_{24}(m_{G^+},m_{G^0},m_{G^+})\right]\\
&+\frac{1}{4}\lambda_{G^+G^-h}\left[\left(-c_\beta s_\alpha+\sqrt{2}s_\beta c_\alpha\right)^2 C_{24}(m_{G^+},m_H,m_{G^+})+\left(c_\beta c_\alpha+\sqrt{2}s_\beta s_\alpha\right)^2 C_{24}(m_{G^+},m_h,m_{G^+})\right]\\
&+\frac{1}{4}\lambda_{H^+G^-h}(s_\beta s_{\beta'}+\sqrt{2}c_\beta c_{\beta'})(-c_\beta s_{\beta'}+\sqrt{2}s_\beta c_{\beta'})[C_{24}(m_{H^+},m_A,m_{G^+})+C_{24}(m_{G^+},m_A,m_{H^+})]\\
&+\frac{1}{4}\lambda_{H^+G^-h}(-s_\beta c_{\beta'}+\sqrt{2}c_\beta s_{\beta'})(c_\beta c_{\beta'}+\sqrt{2}s_\beta s_{\beta'})[C_{24}(m_{H^+},m_{G^0},m_{G^+})+C_{24}(m_{G^+},m_{G^0},m_{H^+})]\\
&+\frac{1}{4}\lambda_{H^+G^-h}(s_\beta s_\alpha+\sqrt{2}c_\beta c_\alpha)(-c_\beta s_\alpha+\sqrt{2}s_\beta c_\alpha)[C_{24}(m_{H^+},m_H,m_{G^+})+C_{24}(m_{G^+},m_H,m_{H^+})]\\
&+\frac{1}{4}\lambda_{H^+G^-h}(-s_\beta c_\alpha+\sqrt{2}c_\beta s_\alpha)(c_\beta c_\alpha+\sqrt{2}s_\beta s_\alpha)[C_{24}(m_{H^+},m_h,m_{G^+})+C_{24}(m_{G^+},m_h,m_{H^+})]\Big\}\\
&+\frac{4m_W^2}{v^2}\frac{1}{16\pi^2}\Big[\lambda_{H^{++}H^{--}h}B_0(q^2,m_{H^{++}},m_{H^{++}})+\lambda_{H^+H^-h}\frac{5+3c_{2\beta}}{4}B_0(q^2,m_{H^+},m_{H^+})\\
&+\lambda_{G^+G^-h}\frac{5-3c_{2\beta}}{4}B_0(q^2,m_{G^+},m_{G^+})+2\lambda_{H^+G^-h}\frac{3s_{2\beta}}{4}B_0(q^2,m_{H^+},m_{G^+})\\
&+2\lambda_{AAh}\frac{3+c_{2\beta'}}{8}B_0(q^2,m_A,m_A)+2\lambda_{G^0G^0h}\frac{3-c_{2\beta'}}{8}B_0(q^2,m_Z,m_Z)+\lambda_{AG^0h}\frac{s_{2\beta'}}{4}B_0(q^2,m_A,m_Z)\\
&+2\lambda_{HHh}\frac{3+c_{2\alpha}}{8}B_0(q^2,m_H,m_H)+6\lambda_{hhh}\frac{3-c_{2\alpha}}{8}B_0(q^2,m_h,m_h)+2\lambda_{Hhh}\frac{s_{2\alpha}}{4}B_0(q^2,m_H,m_h)\Big],
\end{aligned}
\tag{D.157}
$$

$$
\begin{aligned}
M^{hWW}_{2,1\mathrm{PI}}(p_1^2,p_2^2,q^2)_S = -\frac{16m_W^4}{v^2}\frac{1}{16\pi^2}\Bigg\{ \\
&+\lambda_{H^{++}H^{--}h}c_\beta^2 C_{1223}(m_{H^{++}},m_{H^+},m_{H^{++}}) + \lambda_{H^{++}H^{--}h}s_\beta^2 C_{1223}(m_{H^{++}},m_{G^+},m_{H^{++}}) \\
&+\lambda_{H^+H^-h}c_\beta^2 C_{1223}(m_{H^+},m_{H^{++}},m_{H^+}) + \lambda_{G^+G^-h}s_\beta^2 C_{1223}(m_{G^+},m_{H^{++}},m_{G^+}) \\
&+\lambda_{H^+G^-h}c_\beta s_\beta [C_{1223}(m_{G^+},m_{H^{++}},m_{H^+}) + C_{1223}(m_{H^+},m_{H^{++}},m_{G^+})] \\
&+\frac{1}{2}\lambda_{AAh}\left[\left(s_\beta s_{\beta'}+\sqrt{2}c_\beta c_{\beta'}\right)^2 C_{1223}(m_A,m_{H^+},m_A) + \left(-c_\beta s_{\beta'}+\sqrt{2}s_\beta c_{\beta'}\right)^2 C_{1223}(m_A,m_{G^+},m_A)\right] \\
&+\frac{1}{2}\lambda_{G^0G^0h}\left[\left(-s_\beta c_{\beta'}+\sqrt{2}c_\beta s_{\beta'}\right)^2 C_{1223}(m_{G^0},m_{H^+},m_{G^0}) + \left(c_\beta c_{\beta'}+\sqrt{2}s_\beta s_{\beta'}\right)^2 C_{1223}(m_{G^0},m_{G^+},m_{G^0})\right] \\
&+\frac{1}{4}\lambda_{AG^0h}\left(s_\beta s_{\beta'}+\sqrt{2}c_\beta c_{\beta'}\right)\left(-s_\beta c_{\beta'}+\sqrt{2}c_\beta s_{\beta'}\right)[C_{1223}(m_A,m_{H^+},m_{G^0}) + C_{1223}(m_{G^0},m_{H^+},m_A)] \\
&+\frac{1}{4}\lambda_{AG^0h}\left(-c_\beta s_{\beta'}+\sqrt{2}s_\beta c_{\beta'}\right)\left(c_\beta c_{\beta'}+\sqrt{2}s_\beta s_{\beta'}\right)[C_{1223}(m_A,m_{G^+},m_{G^0}) + C_{1223}(m_{G^0},m_{G^+},m_A)] \\
&+\frac{1}{2}\lambda_{HHh}\left[\left(s_\beta s_\alpha+\sqrt{2}c_\beta c_\alpha\right)^2 C_{1223}(m_H,m_{H^+},m_H) + \left(-c_\beta s_\alpha+\sqrt{2}s_\beta c_\alpha\right)^2 C_{1223}(m_H,m_{G^+},m_H)\right] \\
&+\frac{3}{2}\lambda_{hhh}\left[\left(-s_\beta c_\alpha+\sqrt{2}c_\beta s_\alpha\right)^2 C_{1223}(m_h,m_{H^+},m_h) + \left(c_\beta c_\alpha+\sqrt{2}s_\beta s_\alpha\right)^2 C_{1223}(m_h,m_{G^+},m_h)\right] \\
&+\frac{1}{2}\lambda_{Hhh}\left(s_\beta s_\alpha+\sqrt{2}c_\beta c_\alpha\right)\left(-s_\beta c_\alpha+\sqrt{2}c_\beta s_\alpha\right)[C_{1223}(m_H,m_{H^+},m_h) + C_{1223}(m_h,m_{H^+},m_H)] \\
&+\frac{1}{2}\lambda_{Hhh}\left(-c_\beta s_\alpha+\sqrt{2}s_\beta c_\alpha\right)\left(c_\beta c_\alpha+\sqrt{2}s_\beta s_\alpha\right)[C_{1223}(m_H,m_{G^+},m_h) + C_{1223}(m_h,m_{G^+},m_H)] \\
&+\frac{1}{4}\lambda_{H^+H^-h}\left[\left(s_\beta s_{\beta'}+\sqrt{2}c_\beta c_{\beta'}\right)^2 C_{1223}(m_{H^+},m_A,m_{H^+}) + \left(\sqrt{2}c_\beta s_{\beta'}-s_\beta c_{\beta'}\right)^2 C_{1223}(m_{H^+},m_{G^0},m_{H^+})\right] \\
&+\frac{1}{4}\lambda_{H^+H^-h}\left[\left(s_\beta s_\alpha+\sqrt{2}c_\beta c_\alpha\right)^2 C_{1223}(m_{H^+},m_H,m_{H^+}) + \left(-s_\beta c_\alpha+\sqrt{2}c_\beta s_\alpha\right)^2 C_{1223}(m_{H^+},m_h,m_{H^+})\right] \\
&+\frac{1}{4}\lambda_{G^+G^-h}\left[\left(-c_\beta s_{\beta'}+\sqrt{2}s_\beta c_{\beta'}\right)^2 C_{1223}(m_{G^+},m_A,m_{G^+}) + \left(c_\beta c_{\beta'}+\sqrt{2}s_\beta s_{\beta'}\right)^2 C_{1223}(m_{G^+},m_{G^0},m_{G^+})\right] \\
&+\frac{1}{4}\lambda_{G^+G^-h}\left[\left(-c_\beta s_\alpha+\sqrt{2}s_\beta c_\alpha\right)^2 C_{1223}(m_{G^+},m_H,m_{G^+}) + \left(c_\beta c_\alpha+\sqrt{2}s_\beta s_\alpha\right)^2 C_{1223}(m_{G^+},m_h,m_{G^+})\right] \\
&+\frac{1}{4}\lambda_{H^+G^-h}\left(s_\beta s_{\beta'}+\sqrt{2}c_\beta c_{\beta'}\right)\left(-c_\beta s_{\beta'}+\sqrt{2}s_\beta c_{\beta'}\right)[C_{1223}(m_{H^+},m_A,m_{G^+}) + C_{1223}(m_{G^+},m_A,m_{H^+})] \\
&+\frac{1}{4}\lambda_{H^+G^-h}\left(-s_\beta c_{\beta'}+\sqrt{2}c_\beta s_{\beta'}\right)\left(c_\beta c_{\beta'}+\sqrt{2}s_\beta s_{\beta'}\right)^2[C_{1223}(m_{H^+},m_{G^0},m_{G^+}) + C_{1223}(m_{G^+},m_{G^0},m_{H^+})] \\
&+\frac{1}{4}\lambda_{H^+G^-h}\left(s_\beta s_\alpha+\sqrt{2}c_\beta c_\alpha\right)\left(-c_\beta s_\alpha+\sqrt{2}s_\beta c_\alpha\right)[C_{1223}(m_{H^+},m_H,m_{G^+}) + C_{1223}(m_{G^+},m_H,m_{H^+})] \\
&+\frac{1}{4}\lambda_{H^+G^-h}\left(-s_\beta c_\alpha+\sqrt{2}c_\beta s_\alpha\right)\left(c_\beta c_\alpha+\sqrt{2}s_\beta s_\alpha\right)[C_{1223}(m_{H^+},m_h,m_{G^+}) + C_{1223}(m_{G^+},m_h,m_{H^+})]\Bigg\},
\end{aligned}
\tag{D.158}
$$

$$
M^{hWW(1\mathrm{PI})}_{3,1\mathrm{PI}}(p_1^2,p_2^2,q^2)_S = 0, \tag{D.159}
$$

$$
\begin{aligned}
M^{hZZ}_{1,1\mathrm{PI}}(p_1^2,p_2^2,q^2)_V = \frac{1}{16\pi^2}\Bigg\{ & 2g^3 m_W c_W^2 (c_\alpha c_\beta + \sqrt{2} s_\alpha s_\beta) C_{VVV}(m_W, m_W, m_W) \\
& + g^3 m_W (c_\alpha c_\beta + \sqrt{2} s_\alpha s_\beta)(s_W^2 + s_\beta^2) C^{hVV}_{SVV}(m_{G^+}, m_W, m_W) \\
& + g^3 m_W (-c_\alpha s_\beta + \sqrt{2} s_\alpha c_\beta) s_\beta c_\beta C^{hVV}_{SVV}(m_{H^+}, m_W, m_W) \\
& + g^3 m_W (c_\alpha c_\beta + \sqrt{2} s_\alpha s_\beta)(s_W^2 + s_\beta^2) C^{hVV}_{VVS}(m_W, m_W, m_{G^+}) \\
& + g^3 m_W (-c_\alpha s_\beta + \sqrt{2} s_\alpha c_\beta) s_\beta c_\beta C^{hVV}_{VVS}(m_W, m_W, m_{H^+}) \\
& - g g_Z^2 m_W (c_\alpha c_\beta + \sqrt{2} s_\alpha s_\beta)(c_W^2 - s_W^2 - s_\beta^2)(s_W^2 + s_\beta^2)[C_{24}(m_W, m_{G^+}, m_{G^+}) + C_{24}(m_{G^+}, m_{G^+}, m_W)] \\
& - g g_Z^2 m_W (-c_\alpha s_\beta + \sqrt{2} s_\alpha c_\beta)(c_W^2 - s_W^2 - c_\beta^2) s_\beta c_\beta [C_{24}(m_W, m_{H^+}, m_{H^+}) + C_{24}(m_{H^+}, m_{H^+}, m_W)] \\
& + g g_Z^2 m_W (c_\alpha c_\beta + \sqrt{2} s_\alpha s_\beta) s_\beta^2 c_\beta^2 [C_{24}(m_W, m_{H^+}, m_{G^+}) + C_{24}(m_{H^+}, m_{G^+}, m_W)] \\
& + g g_Z^2 m_W (-c_\alpha s_\beta + \sqrt{2} s_\alpha c_\beta) s_\beta c_\beta (s_W^2 + s_\beta^2)[C_{24}(m_W, m_{G^+}, m_{H^+}) + C_{24}(m_{G^+}, m_{H^+}, m_W)] \\
& - 2 g g_Z^2 (s_W^2 + s_\beta^2)^2 m_W^3 (c_\alpha c_\beta + \sqrt{2} s_\alpha s_\beta) C_0(m_W, m_{G^+}, m_W) \\
& - 2 g g_Z^2 s_\beta^2 c_\beta^2 m_W^3 (c_\alpha c_\beta + \sqrt{2} s_\alpha s_\beta) C_0(m_W, m_{H^+}, m_W) \\
& + 2 \lambda_{G^+G^-h} g_Z^2 m_W^2 (s_W^2 + s_\beta^2)^2 C_0(m_{G^+}, m_W, m_{G^+}) + 2 \lambda_{H^+H^-h} g_Z^2 m_W^2 s_\beta^2 c_\beta^2 C_0(m_{H^+}, m_W, m_{H^+}) \\
& + 2 \lambda_{H^+G^-h} g_Z^2 m_W^2 s_\beta c_\beta (s_W^2 + s_\beta^2)[C_0(m_{H^+}, m_W, m_{G^+}) + C_0(m_{G^+}, m_W, m_{H^+})] \\
& - 2 g^3 c_W^2 m_W (c_\alpha c_\beta + \sqrt{2} s_\alpha s_\beta) C_{24}(m_{c^+}, m_{c^+}, m_{c^+}) \\
& - g^3 c_W^2 m_W (c_\alpha c_\beta + \sqrt{2} s_\alpha s_\beta)(2D-2) B_0(q^2, m_W, m_W) \\
& + g g_Z^2 m_W [-c_\alpha c_\beta s_W^2 + \sqrt{2}(c_W^2 - 2) s_\alpha s_\beta](s_W^2 + s_\beta^2)[B_0(p_2^2, m_W, m_{G^+}) + B_0(p_1^2, m_{G^+}, m_W)] \\
& + g g_Z^2 m_W [c_\alpha s_\beta s_W^2 + \sqrt{2}(c_W^2 - 2) s_\alpha c_\beta] s_\beta c_\beta [B_0(p_2^2, m_W, m_{H^+}) + B_0(p_1^2, m_{H^+}, m_W)] \\
& + \frac{g_Z^3}{2} m_Z (c_\alpha c_{\beta'} + 2 s_\alpha s_{\beta'})^3 [C_{24}(m_Z, m_h, m_{G^0}) + C_{24}(m_{G^0}, m_h, m_Z)] \\
& + \frac{g_Z^3}{2} m_Z (c_\alpha c_{\beta'} + 2 s_\alpha s_{\beta'})(-c_\alpha s_{\beta'} + 2 s_\alpha c_{\beta'})^2 [C_{24}(m_Z, m_h, m_A) + C_{24}(m_A, m_h, m_Z)] \\
& + \frac{g_Z^3}{2} m_Z (c_\alpha c_{\beta'} + 2 s_\alpha s_{\beta'})(-s_\alpha c_{\beta'} + 2 c_\alpha s_{\beta'})^2 [C_{24}(m_Z, m_H, m_{G^0}) + C_{24}(m_{G^0}, m_H, m_Z)] \\
& + \frac{g_Z^3}{2} m_Z (-s_\alpha c_{\beta'} + 2 c_\alpha s_{\beta'})(2 c_\alpha c_{\beta'} + s_\alpha s_{\beta'})(-c_\alpha s_{\beta'} + 2 s_\alpha c_{\beta'})[C_{24}(m_Z, m_H, m_A) + C_{24}(m_A, m_H, m_Z)] \\
& - g_Z^3 m_Z^3 (c_\alpha c_{\beta'} + 2 s_\alpha s_{\beta'})^3 C_0(m_Z, m_h, m_Z) - g_Z^3 m_Z^3 (c_\alpha c_{\beta'} + 2 s_\alpha s_{\beta'})(-s_\alpha c_{\beta'} + 2 c_\alpha s_{\beta'})^2 C_0(m_Z, m_H, m_Z) \\
& + 6 \lambda_{hhh} g_Z^2 m_Z^2 (c_\alpha c_{\beta'} + 2 s_\alpha s_{\beta'})^2 C_0(m_h, m_Z, m_h) + 2 \lambda_{HHh} g_Z^2 m_Z^2 (-s_\alpha c_{\beta'} + 2 c_\alpha s_{\beta'})^2 C_0(m_H, m_Z, m_H) \\
& + 2 \lambda_{Hhh} g_Z^2 m_Z^2 (c_\alpha c_{\beta'} + 2 s_\alpha s_{\beta'})(-s_\alpha c_{\beta'} + 2 c_\alpha s_{\beta'})[C_0(m_h, m_Z, m_H) + C_0(m_H, m_Z, m_h)] \\
& - \frac{g_Z^3}{4} m_Z (5 - 3 c_{2\alpha})(c_\alpha c_{\beta'} + 2 s_\alpha s_{\beta'})[B_0(p_1^2, m_h, m_Z) + B_0(p_2^2, m_h, m_Z)] \\
& - \frac{3 g_Z^3}{4} m_Z s_{2\alpha} (-s_\alpha c_{\beta'} + 2 c_\alpha s_{\beta'})[B_0(p_1^2, m_H, m_Z) + B_0(p_2^2, m_H, m_Z)] \Bigg\}, \qquad \text{(D.160)}
\end{aligned}
$$

$$
\begin{aligned}
M^{hWW}_{1,1\mathrm{PI}}(p_1^2,p_2^2,q^2)_V = \frac{1}{16\pi^2}\Bigg\{ & g^3 c_W m_Z (c_\alpha c_{\beta'} + 2 s_\alpha s_{\beta'}) C_{VVV}(m_Z, m_W, m_Z) \\
& + g^3 m_W [c_W^2 (c_\alpha c_\beta + \sqrt{2} s_\alpha s_\beta) C_{VVV}(m_W, m_Z, m_W) + s_W^2 (c_\alpha c_\beta + \sqrt{2} s_\alpha s_\beta) C_{VVV}(m_W, 0, m_W)] \\
& - \frac{1}{2} g^3 m_W (c_\alpha c_\beta + \sqrt{2} s_\alpha s_\beta)[(s_W^2 + s_\beta^2) C^{hVV}_{SVV}(m_{G^+}, m_Z, m_W) - s_W^2 C^{hVV}_{SVV}(m_{G^+}, 0, m_W)] \\
& - \frac{1}{2} g^3 m_W (-c_\alpha s_\beta + \sqrt{2} s_\alpha c_\beta) s_\beta c_\beta C^{hVV}_{SVV}(m_{H^+}, m_Z, m_W) \\
& - \frac{1}{2} g^3 m_W (c_\alpha c_\beta + \sqrt{2} s_\alpha s_\beta)[(s_W^2 + s_\beta^2) C^{hVV}_{VVS}(m_W, m_Z, m_{G^+}) - s_W^2 C^{hVV}_{VVS}(m_W, 0, m_{G^+})] \\
& - \frac{1}{2} g^3 m_W (-c_\alpha s_\beta + \sqrt{2} s_\alpha c_\beta) s_\beta c_\beta C^{hVV}_{VVS}(m_W, m_Z, m_{H^+}) \\
& - 4 g^3 s_\beta^2 m_W^3 (c_\alpha c_\beta + \sqrt{2} s_\alpha s_\beta) C_0(m_W, m_{H^{++}}, m_W) - g_Z^3 m_W^3 (s_W^2 + s_\beta^2)^2 (c_\alpha c_{\beta'} + 2 s_\alpha s_{\beta'}) C_0(m_Z, m_{G^+}, m_Z) \\
& - g_Z^3 m_W^3 s_\beta^2 c_\beta^2 (c_\alpha c_{\beta'} + 2 s_\alpha s_{\beta'}) C_0(m_Z, m_{H^+}, m_Z) - g^3 m_W^3 (c_\alpha c_\beta + \sqrt{2} s_\alpha s_\beta)^3 C_0(m_W, m_h, m_W) \\
& - g^3 m_W^3 (c_\alpha c_\beta + \sqrt{2} s_\alpha s_\beta)(-s_\alpha c_\beta + \sqrt{2} c_\alpha s_\beta)^2 C_0(m_W, m_H, m_W) \\
& + 6 \lambda_{hhh} g^2 m_W^2 (c_\alpha c_\beta + \sqrt{2} s_\alpha s_\beta)^2 C_0(m_h, m_W, m_h) \\
& + 2 \lambda_{HHh} g^2 m_W^2 (-s_\alpha c_\beta + \sqrt{2} c_\alpha s_\beta)^2 C_0(m_H, m_W, m_H) \\
& + 2 \lambda_{Hhh} g^2 m_W^2 (c_\alpha c_\beta + \sqrt{2} s_\alpha s_\beta)(-s_\alpha c_\beta + \sqrt{2} c_\alpha s_\beta)[C_0(m_h, m_W, m_H) + C_0(m_H, m_W, m_h)] \\
& + 4 \lambda_{H^{++}H^{--}h} g^2 m_W^2 s_\beta^2 C_0(m_{H^{++}}, m_W, m_{H^{++}}) \\
& + \lambda_{G^+G^-h} g_Z^2 m_W^2 (s_W^2 + s_\beta^2)^2 C_0(m_{G^+}, m_Z, m_{G^+}) + \lambda_{hG^+G^-} g^2 s_W^2 m_W^2 C_0(m_{G^+}, 0, m_{G^+}) \\
& + \lambda_{H^+H^-h} g_Z^2 m_W^2 s_\beta^2 c_\beta^2 C_0(m_{H^+}, m_Z, m_{H^+}) \\
& + \lambda_{H^+G^-h} g_Z^2 m_W^2 s_\beta c_\beta (s_W^2 + s_\beta^2)[C_0(m_{H^+}, m_Z, m_{G^+}) + C_0(m_{G^+}, m_Z, m_{H^+})] \\
& + 2 g^3 m_W s_\beta^2 (c_\alpha c_\beta + \sqrt{2} s_\alpha s_\beta)[C_{24}(m_{G^+}, m_{H^{++}}, m_W) + C_{24}(m_W, m_{H^{++}}, m_{G^+})] \\
& + 2 g^3 m_W s_\beta c_\beta (-c_\alpha s_\beta + \sqrt{2} s_\alpha c_\beta)[C_{24}(m_{H^+}, m_{H^{++}}, m_W) + C_{24}(m_W, m_{H^{++}}, m_{H^+})] \\
& + \frac{1}{2} g^3 m_W (c_\alpha c_\beta + \sqrt{2} s_\alpha s_\beta)^3 [C_{24}(m_W, m_h, m_{G^+}) + C_{24}(m_{G^+}, m_h, m_W)] \\
& + \frac{1}{2} g^3 m_W (-s_\alpha c_\beta + \sqrt{2} c_\alpha s_\beta)^2 (c_\alpha c_\beta + \sqrt{2} s_\alpha s_\beta)[C_{24}(m_W, m_H, m_{G^+}) + C_{24}(m_{G^+}, m_H, m_W)] \\
& + \frac{1}{2} g^3 m_W (c_\alpha c_\beta + \sqrt{2} s_\alpha s_\beta)(-c_\alpha s_\beta + \sqrt{2} s_\alpha c_\beta)^2 [C_{24}(m_W, m_h, m_{H^+}) + C_{24}(m_{H^+}, m_h, m_W)] \\
& + \frac{1}{2} g^3 m_W (-s_\alpha c_\beta + \sqrt{2} c_\alpha s_\beta)(-c_\alpha s_\beta + \sqrt{2} s_\alpha c_\beta)(s_\alpha s_\beta + \sqrt{2} c_\alpha c_\beta)[C_{24}(m_W, m_H, m_{H^+}) + C_{24}(m_{H^+}, m_H, m_W)] \\
& + \frac{1}{2} g g_Z^2 m_W (s_W^2 + s_\beta^2)(c_\beta c_{\beta'} + \sqrt{2} s_\beta s_{\beta'})(c_\alpha c_{\beta'} + 2 s_\alpha s_{\beta'})[C_{24}(m_{G^0}, m_{G^+}, m_Z) + C_{24}(m_Z, m_{G^+}, m_{G^0})] \\
& + \frac{1}{2} g g_Z^2 m_W (s_W^2 + s_\beta^2)(-c_\beta s_{\beta'} + \sqrt{2} s_\beta c_{\beta'})(-c_\alpha s_{\beta'} + 2 s_\alpha c_{\beta'})[C_{24}(m_A, m_{G^+}, m_Z) + C_{24}(m_Z, m_{G^+}, m_A)] \\
& + \frac{1}{2} g g_Z^2 m_W s_\beta c_\beta (-s_\beta c_{\beta'} + \sqrt{2} c_\beta s_{\beta'})(c_\alpha c_{\beta'} + 2 s_\alpha s_{\beta'})[C_{24}(m_{G^0}, m_{H^+}, m_Z) + C_{24}(m_Z, m_{H^+}, m_{G^0})] \\
& + \frac{1}{2} g g_Z^2 m_W s_\beta c_\beta (s_\beta s_{\beta'} + \sqrt{2} c_\beta c_{\beta'})(-c_\alpha s_{\beta'} + 2 s_\alpha c_{\beta'})[C_{24}(m_A, m_{H^+}, m_Z) + C_{24}(m_Z, m_{H^+}, m_A)]
\end{aligned}
$$

$$
\begin{aligned}
&- g^3 c_W m_Z (c_\alpha c_{\beta'} + 2 s_\alpha s_{\beta'}) C_{24}(m_{c_Z}, m_{c^+}, m_{c_Z}) \\
&- g^3 c_W^2 m_W (c_\alpha c_\beta + \sqrt{2} s_\alpha s_\beta) C_{24}(m_{c^+}, m_{c_Z}, m_{c^+}) - g^3 s_W^2 m_W (c_\alpha c_\beta + \sqrt{2} s_\alpha s_\beta) C_{24}(m_{c^+}, m_{c_\gamma}, m_{c^+}) \\
&- g^3 m_W (c_\alpha c_\beta + \sqrt{2} s_\alpha s_\beta)(D-1) B_0(q^2, m_W, m_W) - g^3 c_W m_Z (c_\alpha c_{\beta'} + 2 s_\alpha s_{\beta'})(D-1) B_0(q^2, m_Z, m_Z) \\
&- \frac{4}{\sqrt{2}} g^3 m_W s_\alpha s_\beta [B_0(p_1^2, m_W, m_{H^{++}}) + B_0(p_2^2, m_W, m_{H^{++}})] \\
&- \frac{1}{4} g^3 (3 - c_{2\alpha}) m_W (c_\alpha c_\beta + \sqrt{2} s_\alpha s_\beta) [B_0(p_1^2, m_W, m_h) + B_0(p_2^2, m_W, m_h)] \\
&- \frac{1}{4} g^3 s_{2\alpha} m_W (-s_\alpha c_\beta + \sqrt{2} c_\alpha s_\beta) [B_0(p_1^2, m_W, m_H) + B_0(p_2^2, m_W, m_H)] \\
&- \frac{1}{2} g g_Z^2 m_W [c_\alpha c_\beta s_W^2 - \sqrt{2}(c_W^2 - 2) s_\alpha s_\beta](s_W^2 + s_\beta^2) [B_0(p_2^2, m_Z, m_{G^+}) + B_0(p_1^2, m_Z, m_{G^+})] \\
&+ \frac{1}{2} g g_Z^2 m_W [c_\alpha s_\beta s_W^2 + \sqrt{2}(c_W^2 - 2) s_\alpha c_\beta] s_\beta c_\beta [B_0(p_2^2, m_Z, m_{H^+}) + B_0(p_1^2, m_Z, m_{H^+})] \\
&- \frac{1}{2} g e^2 m_W (c_\alpha c_\beta + \sqrt{2} s_\alpha s_\beta) [B_0(p_2^2, 0, m_{G^+}) + B_0(p_1^2, 0, m_{G^+})] \Bigg\}, \qquad \text{(D.161)}
\end{aligned}
$$

where $C_{1223}(m_1, m_2, m_3) \equiv C_{12}(m_1, m_2, m_3) + C_{23}(m_1, m_2, m_3)$ and

$$
\begin{aligned}
&C_{VVV}^{hVV}(m_1, m_2, m_3) \equiv \\
&\left[6(D-1) C_{24} + p_1^2 (2C_{21} + 3C_{11} + C_0) + p_2^2 (2C_{22} + C_{12}) + p_1 \cdot p_2 (4C_{23} + 3C_{12} + C_{11} - 4C_0)\right] \\
&(m_1, m_2, m_3), \qquad \text{(D.162)} \\
&C_{SVV}^{hVV}(m_1, m_2, m_3) \equiv \\
&\left[(D-1) C_{24} + p_1^2 (C_{21} - C_0) + p_2^2 (C_{22} - 2C_{12} + C_0) + 2 p_1 \cdot p_2 (C_{23} - C_{11})\right] (m_1, m_2, m_3), \\
& \qquad \text{(D.163)} \\
&C_{VVS}^{hVV}(m_1, m_2, m_3) \equiv \\
&\left[(D-1) C_{24} + p_1^2 (C_{21} + 4C_{11} + 4C_0) + p_2^2 (C_{22} + 2C_{12}) + 2 p_1 \cdot p_2 (C_{23} + 2C_{12} + C_{11} + 2C_0)\right] \\
&(m_1, m_2, m_3). \qquad \text{(D.164)}
\end{aligned}
$$

Bibliography

[1] S. Schael *et al.* [ALEPH and DELPHI and L3 and OPAL and SLD and LEP Electroweak Working Group and SLD Electroweak Group and SLD Heavy Flavour Group Collaborations], Phys. Rept. **427**, 257 (2006)

[2] G. Aad *et al.* [ATLAS Collaboration], Phys. Lett. B **716**, 1 (2012).

[3] S. Chatrchyan *et al.* [CMS Collaboration], Phys. Lett. B **716**, 30 (2012).

[4] The ATLAS and CMS Collaborations, ATLAS-CONF-2015-044.

[5] ATLAS Collaboration, ATLAS-CONF-2014-009.

[6] V. Khachatryan *et al.* [CMS Collaboration], Eur. Phys. J. C **75**, no. 5, 212 (2015) doi:10.1140/epjc/s10052-015-3351-7 [arXiv:1412.8662 [hep-ex]].

[7] Y. Fukuda *et al.* [Super-Kamiokande Collaboration], Phys. Rev. Lett. **81**, 1562 (1998); R. Wendell *et al.* [Super-Kamiokande Collaboration], Phys. Rev. D **81**, 092004 (2010).

[8] Q. R. Ahmad *et al.* [SNO Collaboration], Phys. Rev. Lett. **89**, 011301 (2002).

[9] G. Hinshaw *et al.* [WMAP Collaboration], Astrophys. J. Suppl. 208, 19 (2013).

[10] P. A. R. Ade *et al.* [Planck Collaboration], Astron. Astrophys. **571**, A16 (2014).

[11] L. Evans and P. Bryant, JINST **3**, S08001 (2008).

[12] H. Baer *et al.*, arXiv:1306.6352 [hep-ph].

[13] D. M. Asner *et al.*, arXiv:1310.0763 [hep-ph].

[14] E. Accomando *et al.* [CLIC Physics Working Group Collaboration], hep-ph/0412251.

[15] M. Bicer *et al.* [TLEP Design Study Working Group Collaboration], JHEP **1401**, 164 (2014).

[16] G. Moortgat-Pick *et al.*, Eur. Phys. J. C **75**, no. 8, 371 (2015).

[17] G. Aad *et al.* [ATLAS Collaboration], Phys. Rev. D **90**, no. 5, 052004 (2014).

[18] CMS Collaboration, CMS-PAS-HIG-14-099.

[19] ATLAS Collaboration Summary plots from the ATLAS Higgs physics group 10/2014, https://atlas.web.cern.ch/Atlas/GROUPS/PHYSICS/CombinedSummaryPlots/HIGGS/. w

[20] G. Aad *et al.* [ATLAS Collaboration], Phys. Lett. B **726**, 88 (2013) [Phys. Lett. B **734**, 406 (2014)].

[21] D. B. Kaplan and H. Georgi, Phys. Lett. B **136**, 183 (1984).

[22] D. B. Kaplan, H. Georgi and S. Dimopoulos, Phys. Lett. B **136**, 187 (1984).

[23] H. Georgi, D. B. Kaplan and P. Galison, Phys. Lett. B **143**, 152 (1984).

[24] H. Georgi and D. B. Kaplan, Phys. Lett. B **145**, 216 (1984).

[25] M. J. Dugan, H. Georgi and D. B. Kaplan, Nucl. Phys. B **254**, 299 (1985).

[26] K. Agashe, R. Contino and A. Pomarol, Nucl. Phys. B **719**, 165 (2005).

[27] F. Zwicky, Helv. Phys. Acta **6**, 110 (1933).

[28] A. D. Sakharov, Pisma Zh. Eksp. Teor. Fiz. **5**, 32 (1967) [JETP Lett. **5**, 24 (1967)] [Sov. Phys. Usp. **34**, 392 (1991)] [Usp. Fiz. Nauk **161**, 61 (1991)].

[29] M. Fukugita and T. Yanagida, Phys. Lett. B **174**, 45 (1986).

[30] S. Davidson, E. Nardi and Y. Nir, Phys. Rept. **466**, 105 (2008).

[31] V. A. Kuzmin, V. A. Rubakov and M. E. Shaposhnikov, Phys. Lett. B **155**, 36 (1985).

[32] A. G. Cohen, D. B. Kaplan and A. E. Nelson, Ann. Rev. Nucl. Part. Sci. **43**, 27 (1993); K. Funakubo, Prog. Theor. Phys. **96**, 475 (1996).

[33] J. F. Gunion, H. E. Haber, G. L. Kane and S. Dawson, Front. Phys. **80**, 1 (2000).

[34] S. Kanemura, M. Kikuchi and K. Yagyu, Phys. Rev. D **88**, 015020 (2013).

[35] S. L. Glashow, J. Iliopoulos and L. Maiani, Phys. Rev. D **2**, 1285 (1970).

[36] S. L. Glashow and S. Weinberg, Phys. Rev. D **15**, 1958 (1977).

[37] E. A. Paschos, Phys. Rev. D **15**, 1966 (1977). doi:10.1103/PhysRevD.15.1966

[38] G. C. Branco, P. M. Ferreira, L. Lavoura, M. N. Rebelo, M. Sher and J. P. Silva, Phys. Rept. **516**, 1 (2012).

[39] T. D. Lee, Phys. Rev. D **8**, 1226 (1973). doi:10.1103/PhysRevD.8.1226

[40] K. A. Olive *et al.* [Particle Data Group Collaboration], Chin. Phys. C **38**, 090001 (2014).

[41] V. D. Barger, J. L. Hewett and R. J. N. Phillips, Phys. Rev. D **41**, 3421 (1990); Y. Grossman, Nucl. Phys. B **426**, 355 (1994).

[42] M. Aoki, S. Kanemura, K. Tsumura and K. Yagyu, Phys. Rev. D **80**, 015017 (2009).

[43] R. Schabinger and J. D. Wells, Phys. Rev. D **72**, 093007 (2005);
D. O'Connell, M. J. Ramsey-Musolf and M. B. Wise, Phys. Rev. D **75**, 037701 (2007);
V. Barger, P. Langacker, M. McCaskey, M. J. Ramsey-Musolf and G. Shaughnessy, Phys. Rev. D **77**, 035005 (2008);
C. Englert, T. Plehn, D. Zerwas and P. M. Zerwas, Phys. Lett. B **703**, 298 (2011);
C. Englert, T. Plehn, M. Rauch, D. Zerwas and P. M. Zerwas, Phys. Lett. B **707**, 512 (2012);
G. M. Pruna and T. Robens, Phys. Rev. D **88**, no. 11, 115012 (2013);
A. Falkowski, C. Gross and O. Lebedev, JHEP **1505**, 057 (2015).

[44] S. Khalil, J. Phys. G **35**, 055001 (2008).

[45] S. Iso, N. Okada and Y. Orikasa, Phys. Lett. B **676**, 81 (2009);
S. Iso, N. Okada and Y. Orikasa, Phys. Rev. D **80**, 115007 (2009).

[46] N. Okada and O. Seto, Phys. Rev. D **82**, 023507 (2010);
T. Basak and T. Mondal, Phys. Rev. D **89**, no. 6, 063527 (2014).

[47] K. Fuyuto and E. Senaha, Phys. Rev. D **90**, no. 1, 015015 (2014).

[48] R. Schabinger and J. D. Wells, Phys. Rev. D **72**, 093007 (2005);
V. Barger, P. Langacker, M. McCaskey, M. J. Ramsey-Musolf and G. Shaughnessy, Phys. Rev. D **77**, 035005 (2008).

[49] J. McDonald, Phys. Rev. D **50**, 3637 (1994);
C. P. Burgess, M. Pospelov and T. ter Veldhuis, Nucl. Phys. B **619**, 709 (2001).

[50] T. P. Cheng and L. F. Li, Phys. Rev. D **22**, 2860 (1980);
J. Schechter and J. W. F. Valle, Phys. Rev. D **22**, 2227 (1980);
G. Lazarides, Q. Shafi and C. Wetterich, Nucl. Phys. B **181**, 287 (1981);
R. N. Mohapatra and G. Senjanovic, Phys. Rev. D **23**, 165 (1981);
M. Magg and C. Wetterich, Phys. Lett. B **94**, 61 (1980).

[51] A. G. Akeroyd and H. Sugiyama, Phys. Rev. D **84**, 035010 (2011);
A. Melfo, M. Nemevsek, F. Nesti, G. Senjanovic and Y. Zhang, Phys. Rev. D **85**, 055018 (2012);
M. Aoki, S. Kanemura and K. Yagyu, Phys. Rev. D **85**, 055007 (2012);

[52] J. R. Ellis, M. K. Gaillard and D. V. Nanopoulos, Nucl. Phys. B **106**, 292 (1976);
J. Hisano and K. Tsumura, Phys. Rev. D **87**, 053004 (2013).

[53] H. Georgi and M. Machacek, Nucl. Phys. B **262**, 463 (1985);
M. S. Chanowitz and M. Golden, Phys. Lett. B **165**, 105 (1985).

[54] J. A. Grifols and A. Mendez, Phys. Rev. D **22**, 1725 (1980).

[55] A. Mendez and A. Pomarol, Nucl. Phys. B **349**, 369 (1991);
M. Capdequi Peyranere, H. E. Haber and P. Irulegui, Phys. Rev. D **44**, 191 (1991);
S. Kanemura, Phys. Rev. D **61**, 095001 (2000).

[56] [ATLAS Collaboration], arXiv:1307.7292 [hep-ex].

[57] S. Kanemura, K. Tsumura, K. Yagyu and H. Yokoya, Phys. Rev. D **90**, 075001 (2014)

[58] S. Kanemura, M. Kikuchi and K. Yagyu, Phys. Lett. B **731**, 27 (2014).

[59] S. Kanemura, M. Kikuchi and K. Yagyu, Nucl. Phys. B **896**, 80 (2015).

[60] S. Kanemura, M. Kikuchi and K. Yagyu, arXiv:1511.06211 [hep-ph].

[61] M. Aoki, S. Kanemura, M. Kikuchi and K. Yagyu, Phys. Lett. B **714**, 279 (2012).

[62] M. Aoki, S. Kanemura, M. Kikuchi and K. Yagyu, Phys. Rev. D **87**, no. 1, 015012 (2013).

[63] M. Kobayashi and T. Maskawa, Prog. Theor. Phys. **49**, 652 (1973).

[64] B. W. Lee, C. Quigg and H. B. Thacker, Phys. Rev. D **16**, 1519 (1977).

[65] L. Maiani, G. Parisi and R. Petronzio, Nucl. Phys. B **136**, 115 (1978);
N. Cabibbo, L. Maiani, G. Parisi and R. Petronzio, Nucl. Phys. B **158**, 295 (1979);
R. F. Dashen and H. Neuberger, Phys. Rev. Lett. **50**, 1897 (1983);
D. J. E. Callaway, Nucl. Phys. B **233**, 189 (1984);
M. A. B. Beg, C. Panagiotakopoulos and A. Sirlin, Phys. Rev. Lett. **52**, 883 (1984).

[66] H. Komatsu, Prog. Theor. Phys. **67**, 1177 (1982).

[67] K. Inoue, A. Kakuto, H. Komatsu and S. Takeshita, Prog. Theor. Phys. **67**, 1889 (1982).

[68] S. Chatrchyan *et al.* [CMS Collaboration], JHEP **1212**, 105 (2012).

[69] W. F. L. Hollik, Fortsch. Phys. **38**, 165 (1990);
W. Hollik, Adv. Ser. Direct. High Energy Phys. **14**, 37 (1995).

[70] S. Kanemura, Y. Okada, E. Senaha and C.-P. Yuan, Phys. Rev. D **70**, 115002 (2004).

[71] S. Kanemura, T. Kubota and E. Takasugi, Phys. Lett. B **313**, 155 (1993).

[72] A. G. Akeroyd, A. Arhrib and E. M. Naimi, Phys. Lett. B **490**, 119 (2000).

[73] I. F. Ginzburg and I. P. Ivanov, Phys. Rev. D **72**, 115010 (2005).

[74] S. Kanemura and K. Yagyu, Phys. Lett. B **751**, 289 (2015).

[75] N. G. Deshpande and E. Ma, Phys. Rev. D **18**, 2574 (1978).

[76] M. Sher, Phys. Rept. **179**, 273 (1989);
S. Nie and M. Sher, Phys. Lett. B **449**, 89 (1999).

[77] S. Kanemura, T. Kasai and Y. Okada, Phys. Lett. B **471**, 182 (1999).

[78] S. Kanemura, H. Yokoya and Y. J. Zheng, Nucl. Phys. B **886**, 524 (2014).

[79] M. E. Peskin and T. Takeuchi, Phys. Rev. Lett. **65**, 964 (1990).

[80] D. Toussaint, Phys. Rev. D **18**, 1626 (1978).

[81] S. Kanemura, Y. Okada, H. Taniguchi and K. Tsumura, Phys. Lett. B **704**, 303 (2011).

[82] S. Schael *et al.* [ALEPH and DELPHI and L3 and OPAL and LEP Working Group for Higgs Boson Searches Collaborations], Eur. Phys. J. C **47**, 547 (2006).

[83] G. Aad *et al.* [ATLAS Collaboration], JHEP **1503**, 088 (2015).

[84] V. Khachatryan *et al.* [CMS Collaboration], JHEP **1511**, 018 (2015).

[85] CMS Collaboration [CMS Collaboration], CMS-PAS-HIG-13-021.

[86] [ATLAS Collaboration], ATLAS-CONF-2013-027.

[87] T. Enomoto and R. Watanabe, arXiv:1511.05066 [hep-ph].

[88] J. R. Espinosa, T. Konstandin and F. Riva, Nucl. Phys. B **854**, 592 (2012).

[89] C. Y. Chen, S. Dawson and I. M. Lewis, Phys. Rev. D **91**, no. 3, 035015 (2015).

[90] G. Cynolter, E. Lendvai and G. Pocsik, Acta Phys. Polon. B **36**, 827 (2005).

[91] D. Löpez-Val and T. Robens, Phys. Rev. D **90**, 114018 (2014).

[92] T. Robens and T. Stefaniak, Eur. Phys. J. C **75**, 104 (2015).

[93] A. Arhrib, R. Benbrik, M. Chabab, G. Moultaka, M. C. Peyranere, L. Rahili and J. Ramadan, Phys. Rev. D **84**, 095005 (2011).

[94] M. Aoki and S. Kanemura, Phys. Rev. D **77**, no. 9, 095009 (2008) [Phys. Rev. D **89**, no. 5, 059902 (2014)].

[95] F. del Aguila and J. A. Aguilar-Saavedra, Nucl. Phys. B **813**, 22 (2009);
A. G. Akeroyd and C. W. Chiang, Phys. Rev. D **80**, 113010 (2009);
A. G. Akeroyd, C. W. Chiang and N. Gaur, JHEP **1011**, 005 (2010).

[96] G. Aad *et al.* [ATLAS Collaboration], JHEP **1503**, 041 (2015).

[97] S. Kanemura, M. Kikuchi, K. Yagyu and H. Yokoya, Phys. Rev. D **90**, no. 11, 115018 (2014);
S. Kanemura, M. Kikuchi, H. Yokoya and K. Yagyu, PTEP **2015**, 051B02 (2015).

[98] A. Djouadi, H. E. Haber and P. M. Zerwas, Phys. Lett. B **375**, 203 (1996);
J. F. Gunion *et al.*, Phys. Rev. D **38**, 3444 (1988);
S. Kanemura, S. Moretti and K. Odagiri, JHEP **0102**, 011 (2001);
S. Kanemura, H. Yokoya and Y. J. Zheng, Nucl. Phys. B **898**, 286 (2015)

[99] K. A. Olive *et al.* [Particle Data Group Collaboration], Chin. Phys. C **38**, 090001 (2014).

[100] S. Dawson *et al.*, arXiv:1310.8361 [hep-ex].

[101] A. Freitas and D. Stockinger, Phys. Rev. D **66**, 095014 (2002).

[102] A. Arhrib, M. Capdequi Peyranere, W. Hollik and S. Penaranda, Phys. Lett. B **579**, 361 (2004).

[103] I. F. Ginzburg, M. Krawczyk and P. Osland, Nucl. Instrum. Meth. A **472**, 149 (2001);
N. Bernal, D. Lopez-Val and J. Sola, Phys. Lett. B **677**, 39 (2009);
P. Posch, Phys. Lett. B **696**, 447 (2011);
D. Lopez-Val and J. Sola, Phys. Lett. B **702**, 246 (2011);
P. M. Ferreira, R. Santos, M. Sher and J. P. Silva, Phys. Rev. D **85**, 077703 (2012);
P. M. Ferreira, R. Santos, M. Sher and J. P. Silva, Phys. Rev. D **85**, 035020 (2012);
A. Arhrib, R. Benbrik and N. Gaur, Phys. Rev. D **85**, 095021 (2012);
G. Bhattacharyya, D. Das, P. B. Pal and M. N. Rebelo, JHEP **1310**, 081 (2013).

[104] A. Arhrib, M. Capdequi Peyranere, W. Hollik and S. Penaranda, Phys. Lett. B **579**, 361 (2004);
G. Bhattacharyya and D. Das, Phys. Rev. D **91**, no. 1, 015005 (2015).

[105] F. Wilczek, Phys. Rev. Lett. **39**, 1304 (1977);
H. M. Georgi, S. L. Glashow, M. E. Machacek and D. V. Nanopoulos, Phys. Rev. Lett. **40**, 692 (1978);
J. R. Ellis, M. K. Gaillard, D. V. Nanopoulos and C. T. Sachrajda, Phys. Lett. B **83**, 339 (1979);
T. G. Rizzo, Phys. Rev. D **22**, 178 (1980) [Addendum-ibid. D **22**, 1824 (1980)].

[106] S. Kanemura, Nuovo Cim. C **037**, no. 02, 113 (2014);
M. Kakizaki, S. Kanemura, H. Taniguchi and T. Yamashita, Phys. Rev. D **89**, no. 7, 075013 (2014);
S. Kanemura, K. Kaneta, N. Machida and T. Shindou, Phys. Rev. D **91**, 115016 (2015);
K. Fujii *et al.*, arXiv:1506.05992 [hep-ex].

[107] C. McNeile, C. T. H. Davies, E. Follana, K. Hornbostel and G. P. Lepage, Phys. Rev. D **82**, 034512 (2010).

[108] G. P. Lepage, P. B. Mackenzie and M. E. Peskin, arXiv:1404.0319 [hep-ph].

[109] S. Kanemura, M. Kikuchi and K. Yagyu, in preparation.

[110] T. Hahn and M. Perez-Victoria, Comput. Phys. Commun. **118**, 153 (1999).

[111] G. Passarino and M. J. G. Veltman, Nucl. Phys. B **160**, 151 (1979).

[112] K. Hagiwara, S. Matsumoto, D. Haidt and C. S. Kim, Z. Phys. C **64**, 559 (1994) [Z. Phys. C **68**, 352 (1995)].